Thermocleavable π-Conjugated Polymers - Synthesis and photovoltaic applications

Risø-PhD-Report

Martin Helgesen
Risø-PhD-54(EN)
October 2009

Risø DTU
National Laboratory for Sustainable Energy

Thermocleavable π-Conjugated Polymers

Synthesis and photovoltaic applications

Ph.D. Thesis

Martin Helgesen

Submitted October 2009

Risø National Laboratory, Technical University of Denmark

and

Faculty of Pharmaceutical Sciences, University of Copenhagen

Author: Martin Helgesen

Title: Thermocleavable π-Conjugated Polymers – Synthesis and photovoltaic applications

Division: The Solar Energy Division

Publication date:
October 2009

Report number:
Risø-PhD-54 (EN)

Academic advisors:

Professor Frederik C. Krebs
Risø National Laboratory
Technical University of Denmark

Professor Mikael Begtrup
Faculty of Pharmaceutical Sciences
University of Copenhagen

ISBN: 978-87-550-3786-1

Information Service Department
Risø National Laboratory for
Sustainable Energy
Technical University of Denmark
P.O.Box 49
DK-4000 Roskilde
Denmark
Telephone +45 46774005
bibl@risoe.dtu.dk
Fax +45 46774013
www.risoe.dtu.dk

Preface

This Ph.D. thesis presents the main results of my work carried out at Risø National Laboratory, Technical University of Denmark during the period October 2006 to October 2009, as a part of the Danish research program to obtain a Ph.D. degree. The work was financed by the Danish Strategic Research Council (DSF) with supervision by Senior Scientist Frederic C. Krebs (Risø-DTU) and Professor Mikael Begtrup (University of Copenhagen). Part of the work was carried at Eindhoven University of Technology (TU/e), The Netherlands with supervision by Professor René A. J. Janssen. The thesis is based on five papers which have been authored/co-authored during this project. I must admit that I did not have the time to fully complete all the tasks I had set for myself within the time available. This seems to be the general case in almost all Ph.D. projects, especially those concerning organic synthesis as this did. During my project, I have had the opportunity to work in a lot of different fields (i.e. polymer design, synthesis, device building, characterization), and for that I am very thankful.

First and foremost, I would like to thank my supervisor Frederik C. Krebs for his optimism and believe in me and this project. Due to your encouragement, enthusiasm and a lot of drive it has been a pleasure to work in your group. I thank Mikael Begtrup my supervisor at the University of Copenhagen for his commitment, always ready to give insightful advice and discuss synthetic problems. I would also like to thank Mikkel Jørgensen whose office always have been open when you wanted to discuss scientific problems of any kind.

Special thanks to the people in the Solar Cell Group: Frederik, Mikkel, Ole, Jan, Roar, Suren, Mette, Peter, Torben, Eva, Christian, Kion, Kim, Thomas, Jens, Jon. It has been a pleasure working with all of you during the last three years. I have enjoyed all the fruitful scientific discussions and especially enjoyed the parties, lunches, coffee breaks, funny emails and of course your friendship. For comments on my thesis I would like to thank Frederik and Mikkel.

I would also like to thank the rest of the people at the polymer department at Risø National Laboratory for being good colleagues. Special thanks to Ole Kristoffersen and Birgit Jensen for being able to help with almost everything.

My stay at Eindhoven University of Technology, in there Solar Cell Group, was a unique experience, both scientific (the collaboration lead to one paper) and personal. For giving me the opportunity to join his group I would especially like to thank Professor René A. J. Janssen. I would also like to thank the rest of the people in the Solar Cell Group for all there help and support during my stay; Arjan, Johan, Jan, Martin, Dominique, Bram, Marie-France, Noémie, Stefan, Martijn, Girish.

Finally, I would like to thank my family and friends for there support and understanding during the last three years. Special thanks to my girlfriend Jo Anna, I really appreciate everything you have done for me.

Abstract

Polymer solar cells (plastic solar cells) have seen remarkable improvements in recent years where power conversion efficiencies of up to 6% have been reported for small area devices. However in terms of stability polymer solar cells degrade during illumination and in the dark leading to operational lifetimes that are generally very poor. There has been a recent interest in the operational stability of devices and more importantly on the understanding of why devices and materials break down. This has lead to the discovery of a new class of materials that enable exceptionally long device lifetimes (>20000 hours). This Ph.D. thesis describes the synthesis, characterization and photovoltaic applications of these novel polymer materials. A key feature of these materials is that solubilizing thermocleavable alkyl ester side chains are introduced on the polymer backbone. The side chains make the polymer soluble in organic solvents and allow film formation via solution processing. Subsequently they can be removed by heating in a post-processing step forming a harder insoluble material with enhanced stability. These new thermocleavable materials can potentially offer higher chromophore density, higher level processing and improved stability in a solar cell device.

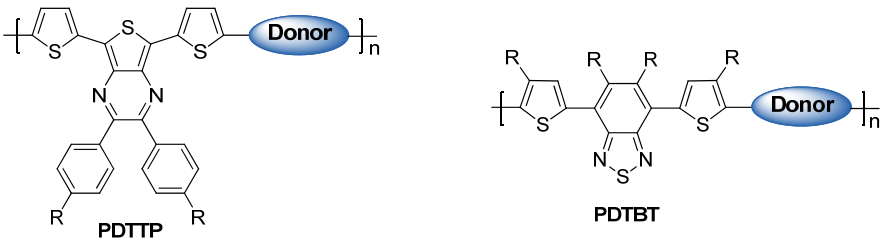

Polymer systems based on dithienylthienopyrazine (PDTTP)
and dithienylbenzothiadiazole (PDTBT)

The polymer systems that I chose to focus on is shown above. The PDTTP system has been designed to match the solar emission spectrum better with very low band gaps ranging from 1.17-1.37 eV (λ_{onset} ~1000 nm), depending on the donor unit. The extended absorption by the PDTTP system can potentially increase the photocurrent by absorbing more photons. Alkyl groups and ester groups can efficiently be incorporated on the benzene rings (R) to provide solubility and thermocleavability. The PDTBT system has been widely used in polymer/PCBM solar cells where high photovoltaic performance has been reported (~6%). I have developed

methods for the incorporation of alkoxy chains and thermocleavable ester groups on the benzothiadiazole and the thiophene units in an attempt to evolve the PDTBT system to a more advanced level. The synthesis and photovoltaic applications of the PDTTP and PDTBT systems is described in this thesis which is divided into five chapters. ***Chapter one*** gives an introduction to organic solar cells to explain the fundamental theory behind this project and ***Chapter two*** presents the basic properties of thermocleavable materials including their application in photovoltaics.

Since bulk heterojunction solar cells based on a polymer and PCBM are not directly compatible with the high temperatures required for elimination of the thermocleavable group one aim is to achieve as low a temperature of elimination as possible. ***Chapter three*** describes a thermal study of monomers and polymers bearing different thermocleavable ester groups to investigate the temperature of thermocleavage as a function of the choice of the alcohol. A series of different esters (primary, secondary and tertiary) of 13 monomers and 7 polymers based on diphenyldithienylthienopyrazine were synthesized and the temperature of elimination of the ester group was studied. The study also established whether the ester could be used efficiently as a solubilizing group that can be removed quantitatively by a simple thermal treatment. ***Chapter four*** describes the synthesis, characterization and solar cells of a series of thermocleavable low band gap polymers for solar cells. The polymers are based on dithienylthienopyrazine, bearing thermocleavable benzoate esters on the pyrazine ring, alternating with different donor segments. The effects of the different donor segments on the optical properties and photovoltaic performance of the polymers with and without thermocleavage is presented. The polymers were applied in bulk heterojunction solar cells together with PCBM where they gave a photoresponce up to 900 nm. The best cells had a power conversion efficiency of 1.2%. ***Chapter five*** presents some of the work that I carried out at Eindhoven University of Technology. It involves the synthesis of alkoxy substituted and unsubstituted 2,1,3-benzothiadiazoles copolymerized with substituted and unsubstituted thiophenes using both Stille and Yamamoto cross coupling reactions. One class of the materials bore thermally labile ester groups. The photovoltaic performance of the polymers were compared in bulk heterojunction solar cells together with PCBM which revealed that devices based on the thermocleavable polymers could match the conventional polymers in terms of performance. The best cells based on a thermocleavable material gave a power conversion efficiency of 1.9% which is one of the highest reported for these materials.

Resumé

Polymer solceller (plastik solceller) har oplevet mærkbare fremskridt de seneste år, hvor en effektivitet på op til 6% er blevet rapporteret for celler med små arealer. Med hensyn til stabilitet derimod nedbrydes polymer solceller under belysning og i mørke, hvilket generelt har ført til meget dårlige levetider. Der har dog været en øget interesse for stabiliteten af polymer solceller og forståelsen for hvorfor solceller og materialer nedbrydes. Dette har ført til opdagelsen af en ny klasse af materialer med udsædvanlig lange levetider (>20000 timer). Denne Ph.D. afhandling beskriver syntesen og karakteriseringen af disse nye polymer materialer, som har egenskaber, der kan give bedre kemisk stabilitet i polymer solceller. Et særligt aspekt er, at polymererne har inkorporeret termokløvbare sidekæder. Disse sidekæder gør polymererne opløselige i organiske solventer, hvilket gør det muligt at fremstille en tynd film fra opløsning. I et efterfølgende trin kan sidekæderne fjernes ved opvarmning, hvilket omdanner materialet til en hård uopløselig form, der giver meget mere stabile solceller. Disse nye termokløvbare materialer kan tilbyde højere kromofor densitet, avanceret film fremstilling og bedre stabilitet af polymer solceller.

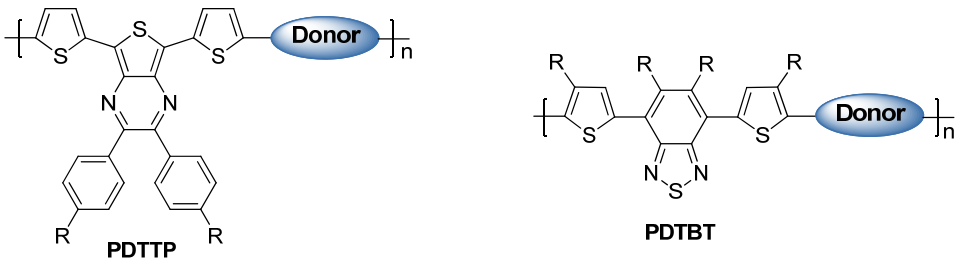

Polymer systemer baseret på dithienylthienopyrazin (PDTTP)
og dithienylbenzothiadiazol (PDTBT)

Polymererne som jeg valgte at fokusere på er vist ovenfor. PDTTP systemet har meget lave båndgab (1.17-1.37 eV), og er designet til at matche sol emission spektret bedre. Den udvidede absorption med PDTTP systemet kan potentielt forøge effektiviteten af en solcelle ved, at absorbere flere fotoner. Alkyl grupper og ester grupper kan effektivt inkorporeres på benzene ringene (R), og tilføre opløselighed og termokløvbarhed. PDTBT systemet er hyppigt blevet brugt i polymer/PCBM solceller, hvor høje ydeevner er blevet rapporteret (~6%). Jeg

har udviklet metoder til at inkorporere alkoxy kæder og termokløvbare ester grupper på benzothiadiazol og thiophen enheden i et forsøg på at udvikle PDTBT systemet. Syntesen og solcelle egenskaberne af PDTTP og PDTBT systemet er beskrevet i denne afhandling, som er opdelt i fem kapitler. Det første kapitel giver en introduktion til organiske og polymer solceller. Kapitel to omhandler emnet termokløvbare materialer og deres brug i solceller.

Et mål er at opnå en så lav temperatur som muligt for elimineringen af den termokløvbare sidekæde, fordi bulk heterojunction solceller baserede på en polymer og PCBM ikke er direkte forenelige med for høje temperaturer. Et studie af dette beskrives i kapitel tre for monomerer og polymerer med forskellige termokløvbare ester grupper. Forskellige estere (primære, sekundære og tertiære) af 13 monomerer og 7 polymerer baserede på diphenyldithienylthienopyrazin blev syntetiseret og elimineringstemperaturen af esteren blev undersøgt. Kapitel fire omhandler syntesen og karakteriseringen af en serie termokløvbare polymerer med lavt båndgab til brug i solceller. Polymererne er baseret på dithienylthienopyrazin forbundet med forskellige donor enheder. Effekten af de forskellige donor enheder, på polymerernes optiske egenskaber og ydeevne i en solcelle blev undersøgt. Polymererne blev anvendt i bulk heterojunction solceller sammen med PCBM, hvor de gav fotorespons op til 900 nm. De bedste solceller gav en effektivitet på op til 1.2%. Kapitel fem beskriver syntesen af alkoxysubstituerede og usubstituerede 2,1,3-benzothiadiazoler copolymeriserede med substituerede og usubstituerede thiophener. En klasse af materialerne bar termokløvbare ester grupper. Polymererne blev sammenlignet i bulk heterojunction solceller med PCBM, hvilket viste at cellerne baseret på termokløvbare polymerer, kunne måles med de konventionelle polymerer med hensyn til effektivitet. De bedste solceller baseret på termokløvbare polymerer gav en effektivitet på op til 1.9%, hvilket er en af de højeste effektiviteter, der er blevet rapporteret ved brug af disse materialer.

Table of Contents

CHAPTER 1
Introduction

1.1 Background 1

1.2 Polymer Solar cells 3

1.3 Device characteristics 8

1.4 State of the art materials 10

1.5 Stability of polymer solar cells 14

1.6 Aim and scope of the thesis 17

1.7 References 17

CHAPTER 2
Thermocleavable materials for higher level processing and stability of polymer solar cells

2.1 Introduction 23

2.2 Thermocleavable materials 24

2.3 Thermal patterning of polymer films 31

2.4 All solution processed tandem cells 33

2.5 Summary 36

2.6 References 37

CHAPTER 3
Thermal studies of monomers and polymers bearing different thermocleavable ester groups

3.1 Introduction 41

3.2 Synthesis 42

3.3 Thermal Behaviour 44

3.4 Photovoltaic performance 48

3.5 Stability Studies 51

3.6 Conclusion 53

3.7 Experimental section 54

3.8 References 61

CHAPTER 4
Photovoltaic performance of polymers based on dithienyl-thienopyrazines bearing thermocleavable benzoate esters

4.1 Introduction 64

4.2 Synthesis 65

4.3 Thermal Behaviour 67

4.4 Optical Properties 69

4.5 Photovoltaic performance 71

4.6 Morphology 73

4.7 Conclusion 74

4.8 Experimental section 75

4.9 References 81

CHAPTER 5
Substituted 2,1,3-benzothiadiazole- and thiophene-based polymers for solar cells – Introducing new thermocleavable precursors

5.1 Introduction 83

5.2 Synthesis 84

5.3 Thermal behaviour 87

5.4 Optical Properties 88

5.5 Photovoltaic performance 90

5.6 Morphology 95

5.7 Conclusion 96

5.8 Experimental section 96

5.9 References 107

APPENDIX 1 109
Attempted synthesis of a monomer based on 2,1,3-benzothiadiazole bearing thermocleavable alkyl ester groups at the 5- and 6-position

APPENDIX 2 113
List of publications

Chapter 1

Introduction

1.1 Background

The total world energy consumption in 2008 amounted to approximately 16 terawatts and the demand for energy is anticipated to increase in the near future. Because of continuous industrialization and growth of human population the level of energy consumption by the year 2050 is expected to be in the range 28-35 terawatts which is a challenge we cannot meet with the energy sources currently at hand. Most of our energy is derived from fossil fuels (coal, oil, gas) but the supply is finite and the energy derived from combustion of fossil fuels produce CO_2. The finite supply of fossil fuel sources and the negative long-term effects of CO_2 and other emission into our atmosphere call for the development of renewable energy resources. Providing energy from non-CO_2-emissive sources is required to prevent global warming that might induce irreversible climate changes.[1] Sunlight strikes the surface of earth with 165 thousand terawatt of power which corresponds to 1000 W/m^2 at the surface of the earth.[2] Thus harvesting energy directly from sunlight and converting it into electrical energy using photovoltaic (PV) technology is being increasingly recognized as part of the solution to the growing energy challenge and a fundamental factor of the future global renewable energy production.[3]

The photovoltaic effect, which is the conversion of absorbed solar photons directly into electrical energy, was first discovered in 1839 by the French physicist Edmond Becquerel. He found that a photocurrent emerged when platinum electrodes, covered with silver bromide or silver chloride, was illuminated in aqueous solution.[4] Commercialisation of the PV technology was not attempted until a century later where the first crystalline silicon p-n junction solar cell was developed in 1954 at Bell Laboratories.[5] The reported device could convert solar radiation into electrical power with an efficiency of 6%. In modern era solar technologies are currently dominated by wafer-size single-junction solar cells based on crystalline silicon that has reached efficiencies of up to 25%.[6] While the efficiency of such conventional solar cells is high, very expensive materials and energy consuming production techniques are required

which confines the technology to niches. Despite much effort in reducing the price of silicon based PVs, the technology still accounts for less than 0.1% of the total world energy production. Second generation photovoltaics are under active investigation in order to further reduce the cost of produced electricity. This is the so called thin film photovoltaic technology that includes cadmium sulphide (CdS), cadmium telluride (CdTe), chalcogenides such as copper indium diselenide (CIS) or copper indium gallium selenide (CIGS), amorphous and nanocrystalline silicon. Such inorganic semiconductor materials are more absorbing than crystalline silicon and can be processed into thin film directly onto large area substrates using techniques such as sputtering, physical vapour deposition, and plasma-enhanced chemical vapour deposition. The fabrication of low cost inorganic thin film solar cells with efficiencies ranging from 10-19% have been demonstrated in the laboratory[6] but the controlled manufacturing still remains a challenge and their commercial use is growing but not as widespread so far.

Simultaneously, over the past two decades, the development of organic semiconducting materials have advanced very rapidly, leading to the demonstration and optimization of a range of organic based solid state devices, including organic light-emitting diodes (OLEDs),[7] field-effect transistors (FETs),[8] photodiodes,[9] and photovoltaic cells. Although they are still in the development phase, organic photovoltaics appear as a likely low cost alternative to their more expensive inorganic counterpart. Organic PVs are particularly attractive because of their ease of processing, mechanical flexibility and potential for low cost fabrication of large area devices. In addition, their material properties can be substantially adapted by modifying their chemical structure, resulting in greater customization compared to traditional inorganic solar cells. The field of organic photovoltaics can be divided into three classes spanning small molecule,[9,10] dye-sensitized[11-13] and polymer based solar cells. Especially π-conjugated polymers in PVs are an attractive alternative to the traditional silicon-based solar cells because they are strong absorbers of visible light, in even <100 nm thin film devices, and can be deposited onto flexible substrates over large areas using wet-processing techniques such as spin-coating, printing or roll-to-roll coating.[14-27] This thesis will exclusively focus on polymer based solar cells.

1.2 Polymer Solar cells

Many reviews and special issues on the topic of organic solar cells have been published during the past 5 years[16,28-51] and the definitions are quite broad spanning all-polymer solar cells, polymer-fullerene solar cells, small molecule and hybrid solar cells. Polymer-fullerene solar cells based on composites of an electron-donating conjugated polymer and an electron-accepting fullerene has proven to be the most successful of them so far and is advancing rapidly towards commercial viability. Although the performance of polymer solar cells has increased steadily with power conversion efficiencies (PCEs) exceeding 6%[52-54] polymer PVs are still inferior when it comes to power conversion efficiency and stability compared to inorganic PVs. As can be seen in figure 1.1 the main advantage of organic PVs compared to inorganic PVs is the presumed very low production cost of large area devices. And since the lifetime and stability of organic PVs still improves the technology offers the possibility to compete with the inorganic PV market in a near future. However, to avoid being limited to a niche market, as seen for inorganic PVs, organic solar cells have to fulfil all requirements simultaneously, lifetime, efficiency and cost to a certain degree (figure 1.1).

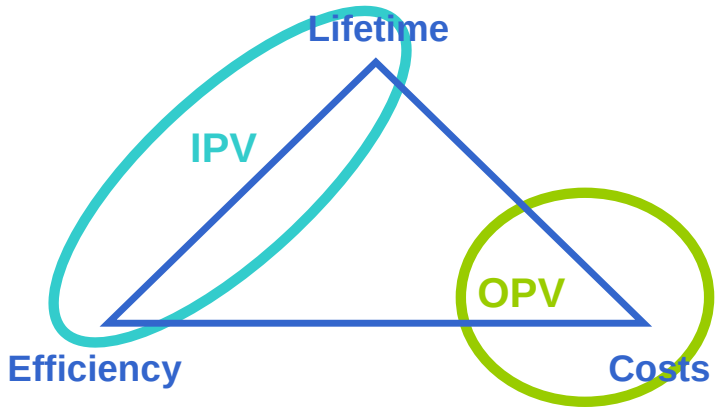

Figure 1.1. The critical triangle for photovoltaics. To be succesfull, a PV technology have to fulfil all requirements simultaneously, lifetime, efficiency and cost. OPVs have very low cost but still needs to improve the power conversion efficiency and lifetime to be successful. IPV: inorganic photovoltaic, OPV: organic photovoltaic.

The simplest conjugated polymer you can visualize is polyacetylene which is a hydrocarbon chain consisting of alternating single- and double-bonds (conjugation) based on sp^2-hybridized carbon atoms. This leads to a highly delocalized π-electron system with large

electronic polarizability which enables absorption within the visible region, due to π–π* transitions, and electrical charge transport. One of the earliest synthesis of polyacetylene was reported back in 1958[55] but the interest for this novel material was limited until 1977 where Shirakawa *et al.* discovered that polyacetylene can be made electrically conducting upon doping by exposure to iodine vapour.[56] Since then, intensive research in the use of conjugated polymers in modern electronics has led to the development of electronic applications like OLEDs, FETs and photovoltaics where the semiconducting characteristic of conjugated polymers is exploited. In the beginning PV devices based on polymers sandwiched between a transparent metal oxide and a metal electrode yielded limited PCEs that were typically well below 0.1%. Thus compared to inorganic semiconductors where absorption of light readily leads to free charge carriers upon excitation of electrons from the valence band to the conduction band (the two electronic bands are so close in energy that they practically form a continuum), the limiting aspect of organic semiconductors is the relatively low dielectric constant of organic materials which leads to a bound state of an electron and an imaginary particle called an electron hole (exciton)[57,58] as electrons are excited from the valence band to the conduction band. The energy difference between the two elctronic bands is also called the band gap. To achieve exciton dissociation into free charge carriers an electric field stronger than the coulombic barrier is needed. A major breakthrough came in 1986 where Tang introduced the bilayer heterojunction concept, in which two organic semiconductor layers with different workfunctions were sandwiched between the electrodes.[59] By using this donor–acceptor heterojunction concept, with a phtalocyanine derivative as a donor (*p*-type semiconductor) and a perylene derivative as an acceptor (*n*-type semiconductor) sandwiched between a glass substrate with indium oxide and a silver electrode, Tang reported a PCE of nearly 1%. The donor–acceptor approach[60-64] makes use of two electronic components that exhibit an energy offset in their molecular orbitals (Figure 1.2).

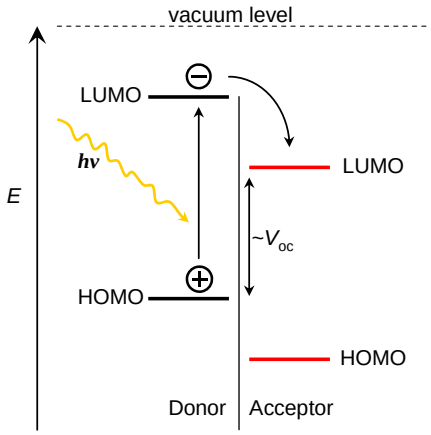

Figure 1.2. Energy-level diagram showing the HOMO and LUMO energies of two semiconductor materials. Upon light absorption in the donor material an electron is excited from the HOMO to the LUMO followed by photoinduced charge transfer to the LUMO of the acceptor.

When the energy levels are appropriately matched between the donor and acceptor material (HOMO-LUMO levels) absorption can lead to photoinduced charge transfer between the materials. Upon light absorption in the donor material an electron is excited from the HOMO (highest occupied molecular orbital) into the LUMO (lowest unoccupied molecular orbital). From this excited state the electron may be transferred into the LUMO of the acceptor resulting in free charge carriers. The driving force for this photoinduced charge transfer is the difference in ionization potential I_{D*} of the excited donor and the electron affinity E_A of the acceptor, minus the Coulomb correlations.[61] After the photoinduced charge transfer, the positively charged hole remains on the donor material whereas the electron is located on the acceptor material. Finally the free charge carriers need to be transported to the respective electrodes to create a photovoltaic effect. At this point the donor material serves to transport the holes while the electrons travel within the acceptor material. The charge carrier transport is driven by internal electric fields across the photoactive layer caused by the different work function electrodes for holes and electrons.

The efficiency of the bilayer heterojunction reported by Tang is limited by the exciton diffusion length, generally restricted to about 5–20 nm in organic materials,[65-67] as excitons formed at positions further away from the donor-acceptor interface than the exciton diffusion length have a lower probability of generating free charge carriers. If an exciton is not dissociated efficiently into its electron and hole within a timescale (~1 ns), it will recombine by emitting a photon or decay via thermalization. Efficient free charge carrier generation can

only occur at the donor-acceptor interface and ideally the heterojunction should be constructed in a manner such that the excitons are generated in the vicinity of the interface. The limitation of the bilayer approach was overcome with the development of the bulk heterojunction (BHJ),[60,64] where the photoactive layer consists of a intimately mixed blend of the donor and acceptor material, which indeed led to a major increase in generated free charge carriers upon light absorption. Ideally, a nanoscale interpenetrating bicontinous network of donor and acceptor materials are created within the entire photoactive layer, ensuring that every generated exciton can reach the donor-acceptor interface. At the same time the constructed bulk heterojunction should insure a direct or percolating pathway of the charge carriers to the respective electrodes in order to effectively transport and collect the charges.

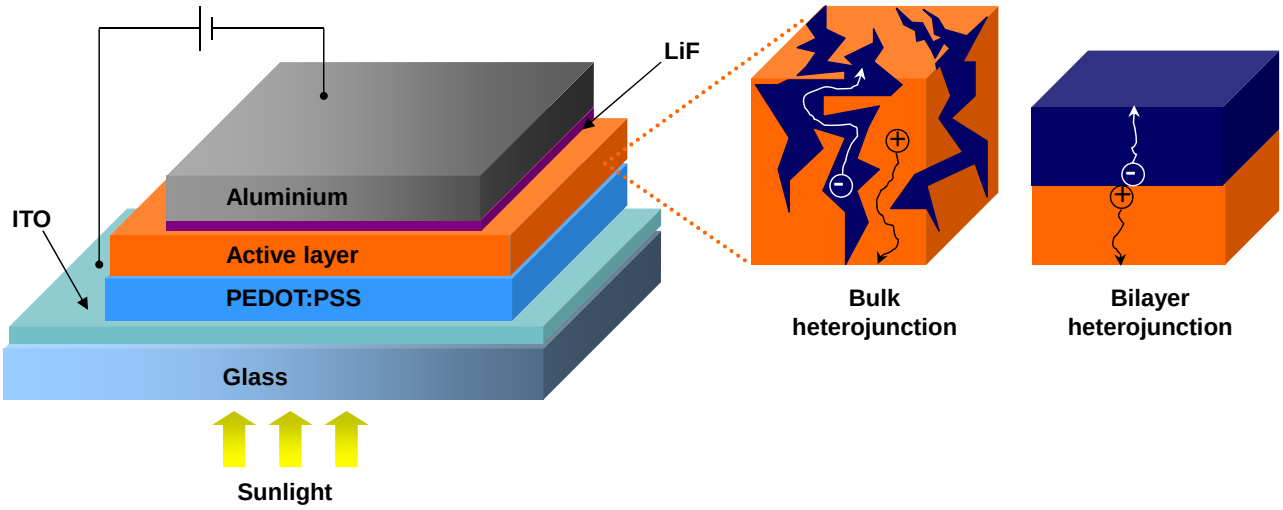

Figure 1.3. Typical device architecture of a bulk heterojunction polymer solar cell. A fragment of the active layer is also shown illustrating the interpenetrating network of the donor and acceptor material. The donor material serves to transport the positive charged holes while the negative charged electrons travel within the acceptor material. A bilayer heterojunction is also shown.

Today, most polymer solar cells are based on the bulk heterojunction concept first reported in 1995 by Yu *et al.*[64] The typical device architecture of a bulk heterojunction solar cell is depicted in Figure 1.3. First a layer of hole conducting poly(3,4-ethylenedioxythiophene)–poly-(styrenesulfonate) (PEDOT:PSS) is spin coated on a glass substrate coated with the transparent electrode indium-tin oxide (ITO). The PEDOT:PSS layer improves the surface roughness of the substrate and improves and stabilizes the electrical contact between ITO and the active layer. Subsequently, a mixture of the donor and acceptor material is spin coated

from a suitable organic solvent. During evaporation of the solvent a phase separation of the donor and acceptor material take place with the formation of an interpenetrating network within the photoactive layer. Finally a thin hole blocking layer of lithium fluoride (LiF) and a layer of aluminium (Al) is evaporated on top as the back electrode. The two components required in these devices for the photoactive layer are a soluble fullerene acceptor and a polymeric donor that can be processed in solution. Generally, π-conjugated polymers are electron rich materials that readily undergoes oxidation, have high HOMO levels and are typically hole conducting materials. However, organic materials with high electron affinity are much rarer.

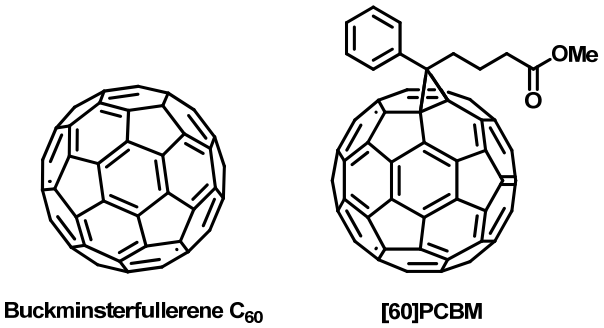

Figure 1.4. Molecular structure of buckminsterfullerene C_{60} and the soluble fullerene derivative [6,6]-phenyl C_{61} butyric acid methyl ester (PCBM).

Soluble buckminsterfullerene derivatives like PCBM (Figure 1.4) are at this time considered to be the most reasonable acceptors for organic solar cells for several reasons. First, they have an energetically deep-lying LUMO,[68] which provide the molecule with a very high electron affinity relative to the various potential organic donors. More importantly, conjugated polymer–fullerene blends are known to exhibit ultrafast photoinduced charge transfer (~45 fs) from the excited state of the polymer to the fullerene, with a back transfer that is orders of magnitude slower.[69] It is these essential properties together with very high electron mobility[70] and the ability to pack effectively in crystalline structures favourable to charge transport,[71] that have currently made soluble fullerene derivatives the most essential acceptor materials for bulk heterojunction solar cells. In devices based on blends of a conjugated polymer and [6,6]-phenyl C_{61} butyric acid methyl ester (PCBM) it is predominantly the polymer that absorbs light since PCBM has a very weak overlap with the solar emission spectrum. To harvest extra solar photons symmetrical C_{60} can be replaced by the oval egg-shaped C_{70} where low energy transitions become allowed, increasing light absorption.[72]

Organic solar cells based on polymer-fullerene blends represents the state of the art at present with efficiencies reaching 6% for single junction cells[53,54] and up to 6,5% with tandem cells,[52] while higher PCEs are possible from a theoretical point of view.[73-75]

1.3 Device characteristics

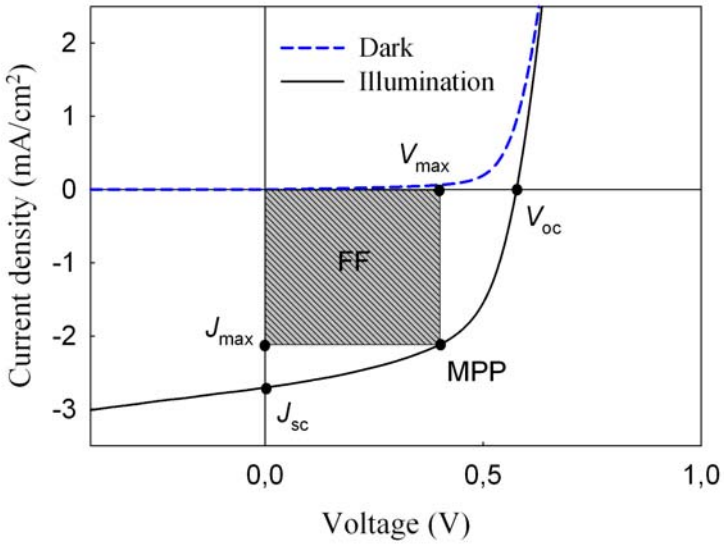

Figure 1.5. Current-voltage (*J-V*) curves of an organic solar cell in dark and under illumination. The characteristic intersections with the abscissa and the ordinate are the open circuit voltage (V_{OC}) and the short-circuit current density (J_{SC}) respectively. The maximum power point (MPP) is determined by the point where the product of voltage and current is maximized ($V_{max} \times J_{max}$). Division of MPP with $J_{SC} \times V_{OC}$ gives the fill factor, FF.

In Figure 1.5 the current-voltage (*J-V*) characteristics are shown for a solar cell in the dark and under illumination. In the dark there is almost no current flowing until external voltages larger than the open circuit voltage is applied. By allowing the device to short circuit under illumination the maximum current, which flow in the device when no voltage is applied, can be read at the intersection with the ordinate and is identified as the short circuit current density (J_{sc}). The maximum voltage the device can produce is called the open circuit voltage (V_{oc}) which can be read at the intersection with the abscissa under illumination. The V_{oc} is limited by the energy difference between the HOMO of the donor material and the LUMO of

the acceptor (figure 1.2). The V_{oc} of a conjugated polymer/PCBM solar cell can be estimated by:

$$V_{oc} = (-E_{LUMO}(A) - E_{HOMO}(D)) - 0.4V$$

where E_{HOMO}(D) is the oxidation potential of the polymer (donor), E_{LUMO}(A) is the reduction potential of PCBM and the value 0.4 V is the approximate voltage loss at the electrodes.[76,77] The maximum power the device can produce is characterised by the maximum power point (MPP) where the grey area in figure 1.5 is maximized. The maximum power point (MPP) is determined by:

$$MPP = V_{max} \times J_{max}$$

where V_{max} and J_{max} are the voltage and current at the MPP. The fill factor (FF) is the ratio between the MPP and the maximum theoretical power output:

$$FF = \frac{MPP}{V_{oc} \times J_{sc}} = \frac{V_{max} \times J_{max}}{V_{oc} \times J_{sc}}$$

The efficiency of the device can then be calculated by:

$$\eta = \frac{MPP}{P_{in}} = \frac{V_{oc} \times J_{sc} \times FF}{P_{in}}$$

where P_{in} is the incident light power. The incident photon to current efficiency (IPCE) is the ratio of the number of charge carriers collected at short circuit per incoming photon of a given energy shining on the device. The IPCE can be calculated by:

$$IPCE(\%) = \frac{J_{sc}}{e \times P_{Photons}} \times 100$$

where e is the elementary charge (1.602×10^{-19} C) and $P_{Photons}$ is the number of photons.

1.4 State of the art materials

Since the first report of photoinduced charge transfer from a conjugated polymer, 2-methoxy-5-(2-ethylhexyloxy)-polyphenylenevinylene (MEH-PPV), to a buckminsterfullerene (C_{60}) in 1992 by Sariciftci *et al.*,[61] the field of polymer–fullerene solar cells has been through a dynamic development. From a materials point of view the state-of-the-art in the field of organic photovoltaics is currently represented by bulk heterojunction solar cells based on poly(3-hexylthiophene) (P3HT) and the fullerenes [60]PCBM and [70]PCBM where efficiencies reported generally are in the 4-5% range[78-80] at present. To improve efficiencies further towards 10% new materials are needed because the P3HT:PCBM system is approaching optimal device performance. The main disadvantage of P3HT is the poor matching of its absorption spectrum with the solar emission spectrum. The band gap of P3HT is around 1.9 eV, limiting the absorbance to wavelengths below 650 nm. Since the photon flux reaching the surface of the earth from the sun has a maximum of approximately 1.8 eV (700 nm) P3HT is only able to harvest up to 22.4% (Figure 1.6) of the available solar photons.[30,43]

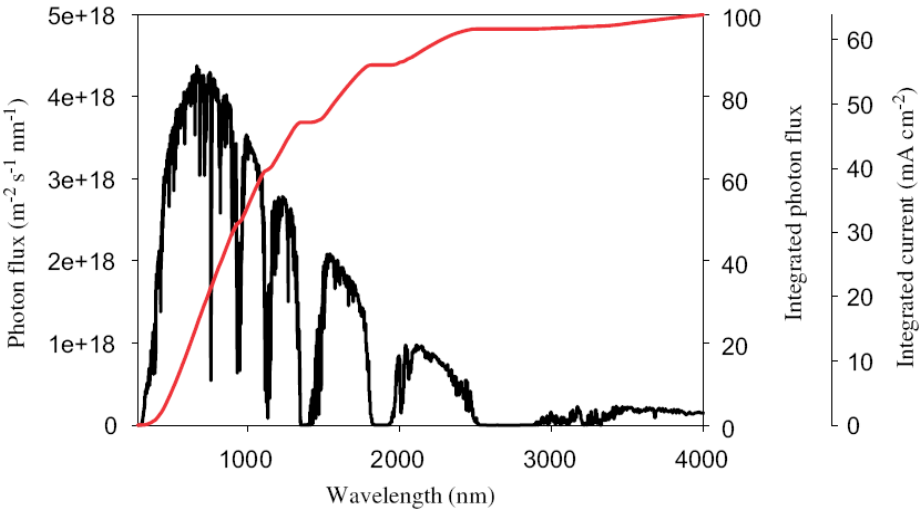

Figure 1.6. Photon flux from the sun (AM1.5) as a function of the wavelength. The percentage of the total photon flux and the corresponding maximum obtainable current density is displayed on the right y-axis.

Therefore, by decreasing the band gap of the active material it is possible to harvest a larger amount of the solar photons and thereby increase the power conversion efficiency. Absorption of light by a π-conjugated polymer involves the excitation of an electron from the

HOMO to the LUMO and hence the energy difference between the HOMO and LUMO, defined as the band gap, determines at which wavelength light is absorbed. Decreasing the band gap in conjugated polymers can generally be done in two ways. One is the approach used in polyisathianaphtalene (PITN) where the fused six-membered ring gains aromaticity and therefore stabilizes the quinoid form (Figure 1.7), resulting in a lower band gap (better overlap of π-orbitals in the repeating unit).[81]

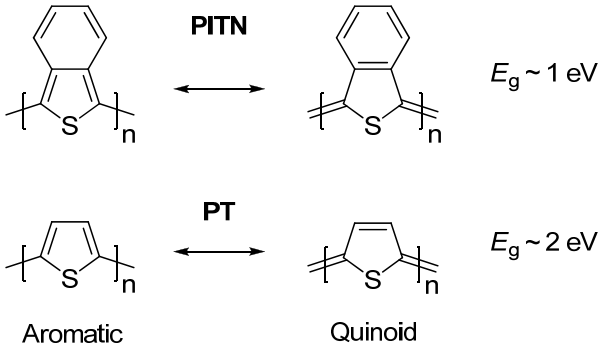

Figure 1.7. Aromatic and quinoidal form of polyisothianaphtalene (PITN) and polythiophene (PT).

Another method used to prepare low band gap polymers is the donor-acceptor approach where alternating electron-rich and electron-poor units are incorporated in the polymer backbone. Incorporating alternating donor and acceptor units can stabilize the quinoid form of a polymer since the alternation increases the double bond character between repeating units, by internal charge stabilization (D-A <–> D^+=A^-), resulting in a lower band gap.[81] The size of the band gap can be tuned by the strength of donor and acceptor units. New low band gap polymer:PCBM composites have already shown device efficiencies close to and even exceeding that of P3HT:PCBM with plenty of room for improvement.

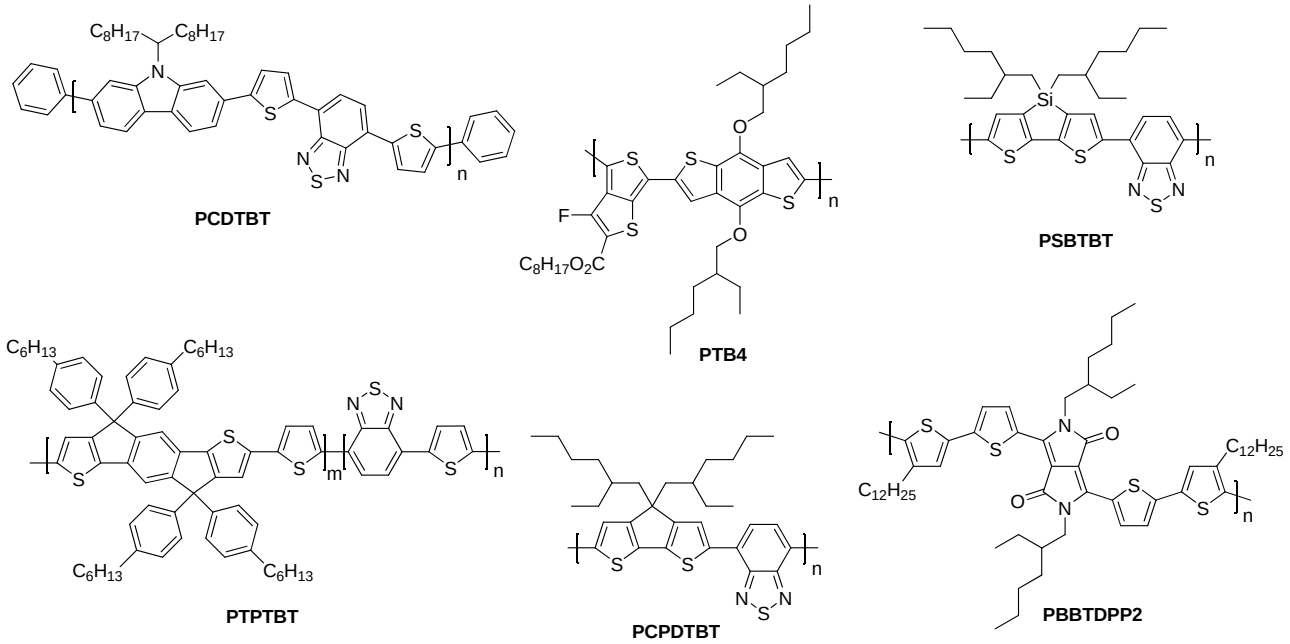

Figure 1.8. Novel donor materials used in polymer solar cells

Novel promising polymer materials are shown in figure 1.8 and there highest reported photovoltaic performance in blends with PCBM is listed in table 1.1. One of the most promising low band gap polymers to date is poly[2,6-(4,4-bis-(2-ethylhexyl)-4*H*-cyclopenta-[2,1-b;3,4-b′]-dithiophene)-*alt*-4,7-(2,1,3-benzothiadiazole)] (PCPDTBT) (Figure 1.8) that is based on a benzothiadiazole acceptor unit and the planar cyclopentadithiophene (CPDT) as the donor unit which gives it an optical band gap around 1.46 eV. Zhu *et al.* have reported power conversion efficiencies up to 3.5% for bulk heterojunction solar cells based on PCPDTBT and [70]PCBM with a maximum EQE of 38% around 700 nm and over 25% in the wavelength range between 400 and 800 nm.[82] Further optimizing of the processing conditions, by incorporating a few volume per cent of alkanedithiol in the solution used to process the films of PCPDTBT:[70]PCBM, improved the PCE up to 5.5% through altering the bulk heterojunction morphology better.[83] Upon optimization the short circuit current enhanced up to 16.2 mA/cm^2, which is among the highest reported to date. According to the electrooptical properties of PCPDTBT there is still room for improvement.[73-75] Silole derivatives of CPDT (PSBTBT, Figure 1.8) have also been synthesised showing a hole mobility of 3×10^{-3} cm^2/(V s) which is 3 times higher than that for PCPDTBT.[84] Efficiencies up to 5.1% have been reported for solar cells based on PSBTBT:[70]PCBM blends.

Table 1.1. Photovoltaic performance of some novel polymer materials in blends with PCBM

Polymer	Acceptor	E_g^{opt} (eV)	V_{oc} (V)	J_{sc} (mA/cm^2)	FF	η (%)	Ref.
PCDTBT	[70]PCBM	1.88	0.88	10.6	0.66	6.1	54
PTPTBT	[70]PCBM	1.70	0.80	10.1	0.53	4.3	85
PTB4	[60]PCBM	1.63	0.74	13.0	0.61	6.1[a]	53
PBBTDPP2	[70]PCBM	1.40	0.61	11.5	0.58	4.0	86
PCPDTBT	[70]PCBM	1.46	0.62	16.2	0.55	5.5[b]	83
PSBTBT	[70]PCBM	1.45	0.68	12.7	0.55	4.7[b]	84

[a] Value after spectral correction. [b] Average value.

Recently a power conversion efficiency of 6.1% was reported for a bulk heterojunction solar cell based on a blend of the polymer poly[*N*-9''-hepta-decanyl-2,7-carbazole-*alt*-5,5-(4',7'-di-2-thienyl-2',1',3'-benzothiadiazole) (PCDTBT, Figure 1.8) and [70]PCBM.[54] The PCDTBT:[70]PCBM solar cell demonstrate the best performance of any single junction polymer solar cell studied to date. PCDTBT (Figure 1.8) is based on a 4,7-dithienylbenzothiadiazole unit and a soluble carbazole unit that gives it a optical band gap around 1.88 eV. It should be pointed out that the high performance is not reached via reduction of the band gap, but through the deep HOMO level of the polymer, mainly fixed by the carbazole moiety, which leads to higher values for the open circuit voltage. The latest report of highly efficient polymer solar cells involve PTB4[53] (Figure 1.8) that is based on thieno[3,4-*b*]thiophene and benzodithiophene units resulting in a optical band gap around 1.63 eV. Fine tuning of the structure and electronic properties has been done by introducing electron-withdrawing fluorine to the thieno[3,4-*b*]thiophene unit, which reduce the HOMO energy level of the polymer. A power conversion efficiency of over 6% was achieved in solar cells based on fluorinated PTB4**:**[60]PCBM blends.

In summary, the photovoltaic performance for the selected novel polymer materials (Table 1.1) proves that the field of organic photovoltaics have a bright future. Although the performance of polymer solar cells has increased steadily, further improvements in efficiency are required for large scale commercialization. Aside from the power conversion efficiency, processing and stability are two other important aspects that have to be addressed with equal intensity for the success of polymer and organic solar cells. To combine all three parameters

into a useful material and device further research in device science and new materials is needed.

1.5 Stability of polymer solar cells

The lifetime of a PV device has been defined in many different ways e.g.: as the time it takes for the device to reach half (T_{50}) or 80% (T_{80}) of its initial efficiency or half its short circuit current value.[87] Long operational lifetimes of organic solar cell devices are essential for large scale commercialisation and the understanding/alleviation of the degradation phenomena are crucial for successful application of this new and promising technology. Polymer and organic solar cells degrade during illumination and in the dark leading to operational lifetimes that are generally very poor. This is in contrast to photovoltaics based on inorganic semiconductors such as silicon that have a lifetime of over 25 years. A few studies on the chemical degradation of polymer solar cells have been documented in the literature and they mainly focus on the role of oxygen, water and electrode material reactions with the active polymer layer (Figure 1.9).

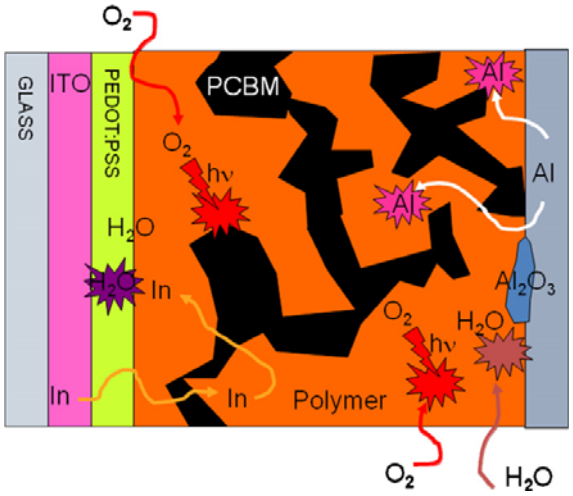

Figure 1.9. Cross section view of a solar cell with the many processes that conspire to degrade polymer solar cells, incl. diffusion of oxygen and water, diffusion of electrode materials, photooxidation and formation of Al_2O_3 at the electrode/active layer interface. Reprinted with permission from[35]. © 2008 Elsevier B.V.

By using time-of-flight secondary ion mass spectrometry (TOF-SIMS)[88] and isotopic labelling ($^{18}O_2$ and $H_2{}^{18}O$), the main finding is that oxygen and water diffuses into the various layers of the solar cell, reacts with the materials and thus degrade the solar cell and device

performance.[89-93] A striking finding was also that the electrode materials diffuse through the active layer and lead to further degradation.[89] Moreover, an insulating layer of Al_2O_3 can form at the interface between the aluminium electrode and the active layer. A thin layer has been reported to improve the interfacial charge transport, but if it gets too thick the charge transport will get worse.

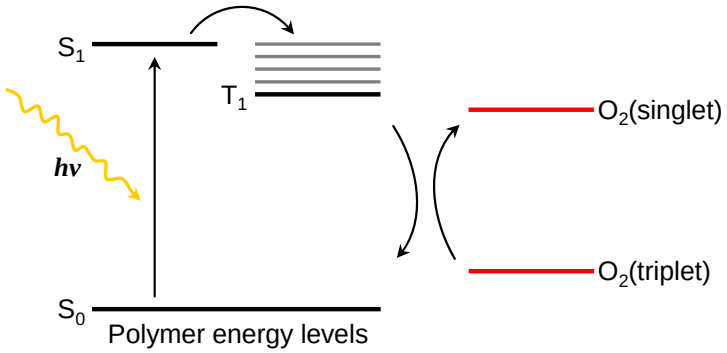

Figure 1.10. Energy-level diagram of a polymer and oxygen (O_2). The first excited state of the polymer (S_1) can cross over to the triplet state (T_1), which can then transfer the excitation to ground state oxygen (O_2 triplet), forming $^1O_2$.

Other degradation processes take place due to the fact that oxygen is readily activated by UV illumination in the presence of sensitizers such as conjugated organic materials. The previously popular PPV type polymers such as MEH-PPV and MDMO-PPV are in particular susceptible to photo-oxidation and are typically degraded significantly in a matter of minutes to hours under illumination.[94-96] The chemical degradation is initiated by the formation of singlet oxygen ($^1O_2$) by energy transfer from the photo-excited polymer to ground state oxygen molecules (Figure 1.10). The singlet oxygen can then react with the vinylene groups through a 2+2 cyclo-addition reaction forming an intermediate dioxetane (Figure 1.11) while other reactions are also possible. Finally the dioxetane can break down resulting in chain scission.

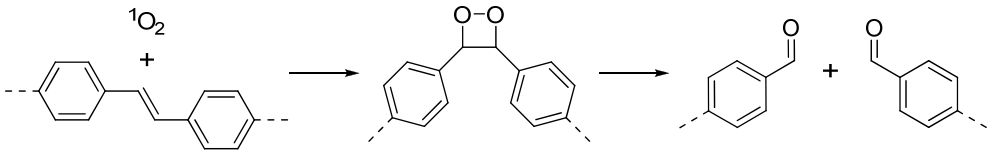

Figure 1.11. Reaction of the vinylene bond in a PPV polymer with $^1O_2$. $^1O_2$ adds to the vinylene bond forming an intermediate dioxetane followed by chain scission. The aldehyde products shown can react further with oxygen.

P3HT is significantly more stable, but devices based on this material are also susceptible to chemical degradation. The current state of the art employs morphologically stable bulk heterojunctions of regioregular P3HT as the donor material and PCBM as the acceptor material. Thermal annealing is used to produce and stabilize a nanoscale interpenetrating network with crystalline order resulting in stable device operation for 1000 hours under illumination in an inert atmosphere.[97] The reaction of P3HT with oxygen has not been investigated in any detail yet but it is known that poly(3-alkylthiophenes) form reversible charge transfer complexes with oxygen[98] (Figure 1.12a). Formation of $^1O_2$ by energy transfer from triplet states on P3HT appear unlikely due to the very low triplet energy level of this polymer, but $^1O_2$ may be formed on dissociation of the excited state of the charge transfer complex. The further reaction of oxygen with P3HT has not been investigated, but simple thiophenes are known to react with oxygen under illumination to form thioozonides, which undergo further degradation[99] (Figure 1.12b).

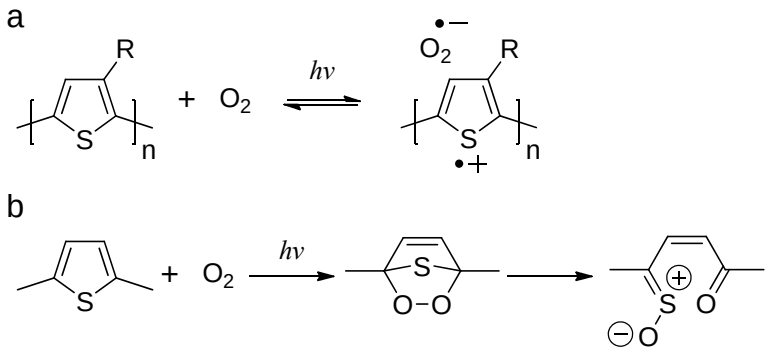

Figure 1.12. (a) Reversible formation of a charge transfer complex between poly(3-alkylthiophenes) and oxygen. R: alkyl group. (b) Reaction between 2,5-dimethylthiophene and oxygen forms a thio-ozonide intermediate that can then decompose to an S-oxide and other products.

In summary, concerning the fact that diffusion processes leads to degradation of polymer solar cells, it is ironic that all the synthetic effort spent towards making the polymer materials soluble and processable by attaching solubilizing side chains is also what makes them degrade quickly. More advanced materials are thus needed where solubility and processability is possible while making the devices. These properties should then be switched off in the final device such that diffusion phenomena are slowed down.

1.6 Aim and scope of the thesis

This project aims at developing the recent finding that a particular class of polymer materials leads to very stable devices when applied in polymer solar cells. The research in this thesis will focus on molecular design, synthesis and characterization of new π-conjugated polymer materials having properties for better chemical stability in polymer solar cells. A key feature of the materials is that solubilizing thermocleavable side chains are introduced on the polymer backbone. This novel type of material is soluble due to the solubilizing side chains and a thin film can thus be prepared from the conjugated polymer material. A subsequent thermal treatment allows for removal of the solubilizing side chains and an insoluble film of the desired material is thus left. The motivation for preparing materials with thermocleavable side chains are multifold and can be summarized as the possibility to prepare materials with a higher density of chromophores leading to device films with a better operational stability and a higher level of permissible processing conditions due to the insolubility of thermocleaved films in all solvents.

1.7 References

1. Solomon, S.; Plattner, G. K.; Knutti, R.; Friedlingstein, P. *Proc. Natl. Acad. Sci. U. S. A.* **2009,** *106* (6), 1704-1709.
2. Smalley, R. E. *MRS Bull.* **2005,** *30* (6), 412-417.
3. Lewis, N. S. *Science* **2007,** *315* (5813), 798-801.
4. Becquerel, A. E. *Comptes Rendus* **1839,** *9*, 561.
5. Chapin, D. M.; Fuller, C. S.; Pearson, G. L. *J. Appl. Phys.* **1954,** *25* (5), 676-677.
6. Green, M. A.; Emery, K.; Hishikawa, Y.; Warta, W. *Prog. Photovolt: Res. Appl.* **2009,** *17* (5), 320-326.
7. Friend, R. H.; Gymer, R. W.; Holmes, A. B.; Burroughes, J. H.; Marks, R. N.; Taliani, C.; Bradley, D. D. C.; Dos Santos, D. A.; Bredas, J. L.; Logdlund, M.; Salaneck, W. R. *Nature* **1999,** *397* (6715), 121-128.
8. Garnier, F.; Hajlaoui, R.; Yassar, A.; Srivastava, P. *Science* **1994,** *265* (5179), 1684-1686.

9. Peumans, P.; Yakimov, A.; Forrest, S. R. *J. Appl. Phys.* **2003,** *93* (7), 3693-3723.

10. Peumans, P.; Forrest, S. R. *Appl. Phys. Lett.* **2001,** *79* (1), 126-128.

11. Bai, Y.; Cao, Y.; Zhang, J.; Wang, M.; Li, R.; Wang, P.; Zakeeruddin, S. M.; Gratzel, M. *Nat Mater* **2008,** *7* (8), 626-630.

12. Wang, P.; Zakeeruddin, S. M.; Moser, J. E.; Nazeeruddin, M. K.; Sekiguchi, T.; Grätzel, M. *Nat. Mater.* **2003,** *2* (6), 402-407.

13. O'Regan, B.; Gratzel, M. *Nature* **1991,** *353* (6346), 737-740.

14. Blankenburg, L.; Schultheis, K.; Schache, H.; Sensfuss, S.; Schrodner, M. *Sol. Energy Mater. Sol. Cells* **2009,** *93* (4), 476-483.

15. Dennler, G.; Lungenschmied, C.; Neugebauer, H.; Sariciftci, N. S.; Labouret, A. *J. Mater. Res.* **2005,** *20* (12), 3224-3233.

16. Krebs, F. C. *Sol. Energy Mater. Sol. Cells* **2009,** *93* (4), 394-412.

17. Krebs, F. C.; Jørgensen, M.; Norrman, K.; Hagemann, O.; Alstrup, J.; Nielsen, T. D.; Fyenbo, J.; Larsen, K.; Kristensen, J. *Sol. Energy Mater. Sol. Cells* **2009,** *93* (4), 422-441.

18. Krebs, F. C. *Sol. Energy Mater. Sol. Cells* **2009,** *93* (4), 465-475.

19. Krebs, F. C.; Alstrup, J.; Spanggaard, H.; Larsen, K.; Kold, E. *Sol. Energy Mater. Sol. Cells* **2004,** *83* (2-3), 293-300.

20. Krebs, F. C.; Spanggaard, H.; Kjaer, T.; Biancardo, M.; Alstrup, J. *Mater. Sci. Eng. , B* **2007,** *138* (2), 106-111.

21. Krebs, F. C. *Sol. Energy Mater. Sol. Cells* **2009,** *93*, 1636-1641.

22. Krebs, F. C. *Org. Electron.* **2009,** *10*, 761-768.

23. Krebs, F. C.; Gevorgyan, S. A.; Alstrup, J. *J. Mater. Chem.* **2009,** *19*, 5442-5451.

24. Lungenschmied, C.; Dennler, G.; Neugebauer, H.; Sariciftci, S. N.; Glatthaar, M.; Meyer, T.; Meyer, A. *Sol. Energy Mater. Sol. Cells* **2007,** *91* (5), 379-384.

25. Niggemann, M.; Zimmermann, B.; Haschke, J.; Glatthaar, M.; Gombert, A. *Thin Solid Films* **2008,** *516* (20), 7181-7187.

26. Tipnis, R.; Bernkopf, J.; Jia, S.; Krieg, J.; Li, S.; Storch, M.; Laird, D. *Sol. Energy Mater. Sol. Cells* **2009,** *93* (4), 442-446.

27. Zimmermann, B.; Glatthaar, M.; Niggemann, M.; Riede, M. K.; Hinsch, A.; Gombert, A. *Sol. Energy Mater. Sol. Cells* **2007,** *91* (5), 374-378.

28. Brabec, C. J.; Hauch, J. A.; Schilinsky, P.; Waldauf, C. *MRS Bull.* **2005,** *30* (1), 50-52.

29. Brabec, C. J.; Durrant, J. R. *MRS Bull.* **2008,** *33* (7), 670-675.

30. Bundgaard, E.; Krebs, F. C. *Sol. Energy Mater. Sol. Cells* **2007,** *91* (11), 954-985.

31. Chen, L. M.; Hong, Z. R.; Li, G.; Yang, Y. *Adv. Mater.* **2009,** *21* (14-15), 1434-1449.

32. Coakley, K. M.; McGehee, M. D. *Chem. Mater.* **2004,** *16*, 4533-4542.

33. Coakley, K. M.; Liu, Y. X.; Goh, C.; McGehee, M. D. *MRS Bull.* **2005,** *30*, 37-40.

34. Dennler, G.; Scharber, M. C.; Brabec, C. J. *Adv. Mater.* **2009,** *21* (13), 1323-1338.

35. Jørgensen, M.; Norrman, K.; Krebs, F. C. *Sol. Energy Mater. Sol. Cells* **2008,** *92* (7), 686-714.

36. Gunes, S.; Neugebauer, H.; Sariciftci, N. S. *Chemical Reviews* **2007,** *107* (4), 1324-1338.

37. Günes, S.; Sariciftci, N. S. *Inorg. Chim. Acta* **2008,** *361* (3), 581-588.

38. Hoppe, H.; Sariciftci, N. S. *J. Mater. Res.* **2004,** *19* (7), 1924-1945.

39. Janssen, R. A. J.; Hummelen, J. C.; Saricifti, N. S. *MRS Bull.* **2005,** *30* (1), 33-36.

40. Kippelen, B.; Bredas, J. L. *Energy Environ. Sci.* **2009,** *2* (3), 251-261.

41. Krebs, F. C. *Sol. Energy Mater. Sol. Cells* **2004,** *83* (2-3).

42. Krebs, F. C. *Refocus* **2005,** *6* (3), 38-39.

43. Kroon, R.; Lenes, M.; Hummelen, J. C.; Blom, P. W. M.; de Boer, B. *Polym. Rev.* **2008,** *48* (3), 531-582.

44. Lloyd, M. T.; Anthony, J. E.; Malliaras, G. G. *Mater. Today* **2007,** *10*, 34-41.

45. Mayer, A. C.; Scully, S. R.; Hardin, B. E.; Rowell, M. W.; McGehee, M. D. *Mater. Today* **2007,** *10* (11), 28-33.

46. Rand, B. P.; Genoe, J.; Heremans, P.; Poortmans, J. *Prog. Photovolt: Res. Appl.* **2007,** *15* (8), 659-676.

47. Shaheen, S. E.; Ginley, D. S.; Jabbour, G. E. *MRS Bull.* **2005,** *30* (1), 10-19.

48. Shaheen, S. E.; Ginley, D. S.; Jabbour, G. E. *MRS Bull.* **2005,** *30* (Special Issue 1), 10-52.

49. Spanggaard, H.; Krebs, F. C. *Sol. Energy Mater. Sol. Cells* **2004,** *83* (2-3), 125-146.

50. Thompson, B. C.; Frechet, J. M. J. *Angew. Chem. Int. Ed.* **2008,** *47* (1), 58-77.

51. Winder, C.; Sariciftci, N. S. *J. Mater. Chem.* **2004,** *14* (7), 1077-1086.

52. Kim, J. Y.; Lee, K.; Coates, N. E.; Moses, D.; Nguyen, T. Q.; Dante, M.; Heeger, A. J. *Science* **2007,** *317* (5835), 222-225.

53. Liang, Y. Y.; Feng, D. Q.; Wu, Y.; Tsai, S. T.; Li, G.; Ray, C.; Yu, L. P. *J. Am. Chem. Soc.* **2009,** *131* (22), 7792-7799.

54. Park, S. H.; Roy, A.; Beaupre, S.; Cho, S.; Coates, N.; Moon, J. S.; Moses, D.; Leclerc, M.; Lee, K.; Heeger, A. J. *Nat. Photonics* **2009,** *3* (5), 297-302.

55. Natta, G.; Mazzanti, G.; Corradini, P. *Atti accad. nazl. Lincei Rend. Classe sci. fis. mat. e nat.* **1958,** *25*, 3-12.

56. Shirakawa, H.; Louis, E. J.; Macdiarmid, A. G.; Chiang, C. K.; Heeger, A. J. *J. Chem. Soc. , Chem. Commun.* **1977,** (16), 578-580.

57. Arkhipov, V. I.; Bassler, H. *Physica Status Solidi A-Applied Research* **2004,** *201* (6), 1152-1187.

58. Gregg, B. A.; Hanna, M. C. *J. Appl. Phys.* **2003,** *93* (6), 3605-3614.

59. Tang, C. W. *Appl. Phys. Lett.* **1986,** *48* (2), 183-185.

60. Halls, J. J. M.; Walsh, C. A.; Greenham, N. C.; Marseglia, E. A.; Friend, R. H.; Moratti, S. C.; Holmes, A. B. *Nature* **1995,** *376* (6540), 498-500.

61. Sariciftci, N. S.; Smilowitz, L.; Heeger, A. J.; Wudl, F. *Science* **1992,** *258* (5087), 1474-1476.

62. Sariciftci, N. S.; Braun, D.; Zhang, C.; Srdanov, V. I.; Heeger, A. J.; Stucky, G.; Wudl, F. *Appl. Phys. Lett.* **1993,** *62* (6), 585-587.

63. Yu, G.; Heeger, A. J. *J. Appl. Phys.* **1995,** *78* (7), 4510-4515.

64. Yu, G.; Gao, J.; Hummelen, J. C.; Wudl, F.; Heeger, A. J. *Science* **1995,** *270* (5243), 1789-1791.

65. Halls, J. J. M.; Pichler, K.; Friend, R. H.; Moratti, S. C.; Holmes, A. B. *Appl. Phys. Lett.* **1996,** *68* (22), 3120-3122.

66. Haugeneder, A.; Neges, M.; Kallinger, C.; Spirkl, W.; Lemmer, U.; Feldmann, J.; Scherf, U.; Harth, E.; Gugel, A.; Mullen, K. *Physical Review B* **1999,** *59* (23), 15346-15351.

67. Pettersson, L. A. A.; Roman, L. S.; Inganas, O. *J. Appl. Phys.* **1999,** *86* (1), 487-496.

68. Allemand, P. M.; Koch, A.; Wudl, F.; Rubin, Y.; Diederich, F.; Alvarez, M. M.; Anz, S. J.; Whetten, R. L. *J. Am. Chem. Soc.* **2002,** *113* (3), 1050-1051.

69. Brabec, C. J.; Zerza, G.; Cerullo, G.; De Silvestri, S.; Luzzati, S.; Hummelen, J. C.; Sariciftci, S. *Chem. Phys. Lett.* **2001,** *340* (3-4), 232-236.

70. Wobkenberg, P. H.; Bradley, D. D. C.; Kronholm, D.; Hummelen, J. C.; de Leeuw, D. M.; Cölle, M.; Anthopoulos, T. *Synth. Met.* **2008,** *158* (11), 468-472.

71. Rispens, M. T.; Meetsma, A.; Rittberger, R.; Brabec, C. J.; Sariciftci, N. S.; Hummelen, J. C. *Chem. Commun.* **2003,** (17), 2116-2118.

72. Wienk, M. M.; Kroon, J. M.; Verhees, W. J. H.; Knol, J.; Hummelen, J. C.; van Hal, P. A.; Janssen, R. A. J. *Angew. Chem. Int. Ed.* **2003,** *42* (29), 3371-3375.

73. Forrest, S. R. *MRS Bull.* **2005,** *30* (1), 28-32.

74. Koster, L. J. A.; Mihailetchi, V. D.; Blom, P. W. M. *Appl. Phys. Lett.* **2006,** *88* (9), 093511.

75. Scharber, M. C.; Wuhlbacher, D.; Koppe, M.; Denk, P.; Waldauf, C.; Heeger, A. J.; Brabec, C. L. *Adv. Mater.* **2006,** *18* (6), 789-794.

76. Gadisa, A.; Svensson, M.; Andersson, M. R.; Inganas, O. *Appl. Phys. Lett.* **2004,** *84* (9), 1609-1611.

77. Mihailetchi, V. D.; Blom, P. W. M.; Hummelen, J. C.; Rispens, M. T. *J. Appl. Phys.* **2003,** *94* (10), 6849-6854.

78. Ko, C. J.; Lin, Y. K.; Chen, F. C.; Chu, C. W. *Appl. Phys. Lett.* **2007,** *90* (6).

79. Li, G.; Shrotriya, V.; Huang, J. S.; Yao, Y.; Moriarty, T.; Emery, K.; Yang, Y. *Nat. Mater.* **2005,** *4* (11), 864-868.

80. Ma, W. L.; Yang, C. Y.; Gong, X.; Lee, K.; Heeger, A. J. *Adv. Funct. Mater.* **2005,** *15* (10), 1617-1622.

81. van Mullekom, H. A. M.; Vekemans, J. A. J. M.; Havinga, E. E.; Meijer, E. W. *Mater. Sci. Eng. , R* **2001,** *32* (1), 1-40.

82. Zhu, Z.; Waller, D.; Gaudiana, R.; Morana, M.; Muhlbacher, D.; Scharber, M.; Brabec, C. *Macromolecules* **2007,** *40* (6), 1981-1986.

83. Peet, J.; Kim, J. Y.; Coates, N. E.; Ma, W. L.; Moses, D.; Heeger, A. J.; Bazan, G. C. *Nat. Mater.* **2007,** *6* (7), 497-500.

84. Hou, J. H.; Chen, H. Y.; Zhang, S. Q.; Li, G.; Yang, Y. *J. Am. Chem. Soc.* **2008,** *130* (48), 16144-16145.

85. Yu, C. Y.; Chen, C. P.; Chan, S. H.; Hwang, G. W.; Ting, C. *Chem. Mater.* **2009,** *21* (14), 3262-3269.

86. Wienk, M. M.; Turbiez, M.; Gilot, J.; Janssen, R. A. J. *Adv. Mater.* **2008,** *20* (13), 2556-2560.

87. Alstrup, J.; Norrman, K.; Jørgensen, M.; Krebs, F. C. *Sol. Energy Mater. Sol. Cells* **2006,** *90* (17), 2777-2792.

88. Norrman, K.; Krebs, F. C. *Surf. Interface Anal.* **2004,** *36* (12), 1542-1549.

89. Krebs, F. C.; Norrman, K. *Prog. Photovolt: Res. Appl.* **2007,** *15* (8), 697-712.

90. Lira-Cantu, M.; Norrman, K.; Andreasen, J. W.; Krebs, F. C. *Chem. Mater.* **2006,** *18* (24), 5684-5690.

91. Norrman, K.; Alstrup, J.; Jørgensen, M.; Lira-Cantu, M.; Larsen, N. B.; Krebs, F. C. Three-dimensional chemical and physical analysis of the degradation mechanisms in organic photovoltaics. SPIE: San Diego, CA, USA, 2006; p 63340O.

92. Norrman, K.; Krebs, F. C. *Sol. Energy Mater. Sol. Cells* **2006,** *90* (2), 213-227.

93. Norrman, K.; Larsen, N. B.; Krebs, F. C. *Sol. Energy Mater. Sol. Cells* **2006,** *90* (17), 2793-2814.

94. Dam, N.; Scurlock, R. D.; Wang, B. J.; Ma, L. C.; Sundahl, M.; Ogilby, P. R. *Chem. Mater.* **1999,** *11* (5), 1302-1305.

95. Padinger, F.; Fromherz, T.; Denk, P.; Brabec, C. J.; Zettner, J.; Hierl, T.; Sariciftci, N. S. *Synth. Met.* **2001,** *121* (1-3), 1605-1606.

96. Scurlock, R. D.; Wang, B. J.; Ogilby, P. R.; Sheats, J. R.; Clough, R. L. *J. Am. Chem. Soc.* **1995,** *117* (41), 10194-10202.

97. Yang, X. N.; Loos, J.; Veenstra, S. C.; Verhees, W. J. H.; Wienk, M. M.; Kroon, J. M.; Michels, M. A. J.; Janssen, R. A. J. *Nano Lett.* **2005,** *5* (4), 579-583.

98. Abdou, M. S. A.; Orfino, F. P.; Son, Y.; Holdcroft, S. *J. Am. Chem. Soc.* **1997,** *119* (19), 4518-4524.

99. Matturro, M. G.; Reynolds, R. P.; Kastrup, R. V.; Pictroski, C. F. *J. Am. Chem. Soc.* **2002,** *108* (10), 2775-2776.

Chapter 2

Thermocleavable materials for higher level processing and stability of polymer solar cells

2.1 Introduction

This chapter gives an introduction to the properties of thermocleavable materials including their application in photovoltaics.

Traditionally conjugated materials were prepared by a thermocleavable precursor route whereby a soluble non-conjugated precursor was heated to provide the insoluble conjugated polymer film. The best known examples are the synthetic routes leading to native polyphenylenevinylene (PPV) and polyacetylene (PA) as exemplified by the Wessling route[1-4] and the Durham route[5-7] as shown in Figure 2.1.

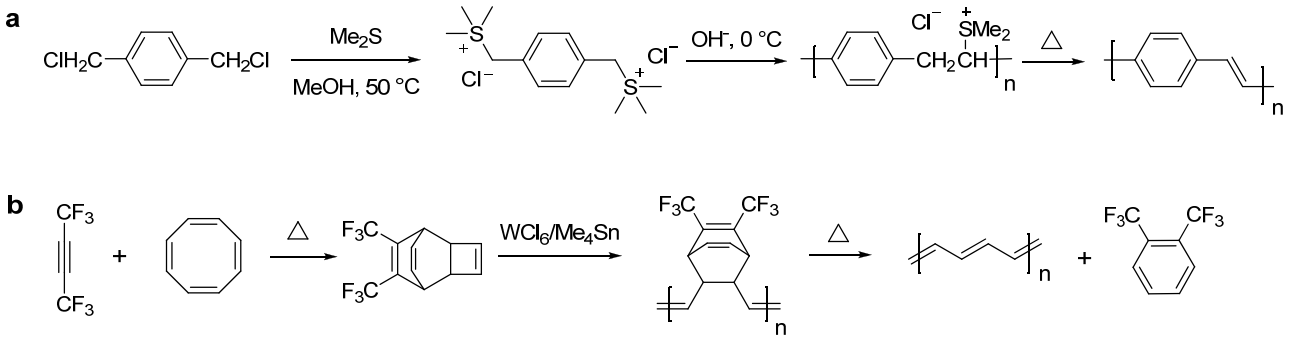

Figure 2.1. The Wessling (a) and the Durham (b) route to respectively PPV and PA.

Initially the potential of the precursor route was not realised and it was dismissed in the middle of the 1990s. It was then replaced by efficient routes to soluble conjugated materials and it is only recently that requirements for better operational stability and processing freedom has spawned new research in this area. Generally two approaches have been followed. The precursor route where the conjugation in the polymer film is formed upon thermocleavage after formation of a film based on the precursor polymer.[8-12] The other

approach is the thermocleavable sidechain route where the conjugated backbone is already present in the polymer film during formation but where the sidechains are removed upon the thermal treatment to give the unsubstituted conjugated polymer backbone.[13-26] Common to both approaches is that the final film is insoluble and the chromophore density is high. The main difference is that the thermocleavable sidechain film is functional as a photovoltaic device before being thermocleaved. One can view these materials as bringing an extra dimension into the optimisation scheme where the device film in addition to thermal annealing and solvent annealing can be altered chemically. Both precursor and thermocleavable side chain routes follow chemical reactions whereby a part of the material that constitute the formed film is removed, which typically amount to 30–50% of the polymer material by weight. The possibilities that thermocleavable materials have to offer warrant exploitation and certainly house the potential for bringing polymer solar cells to a more advanced level through materials design.

2.2 Thermocleavable materials

To make polymer materials solution processable, the introduction of solubilizing groups is required. This is normally achieved by attaching solubilizing side chains such as long alkyl chains onto the conjugated polymer backbone. However, typical nonconjugated solubilizing groups reduce the density of chromophores in the polymer and do not contribute to light harvesting and charge transport. Furthermore, the side chains make the material soft and allow for both morphological changes along with chemical transformations caused by diffusion of small molecules and constituents.[20,27-30] As a consequence, the softness provided by solubilizing chains has been linked to the instability of polymer solar cells, whereas more rigid systems have been demonstrated to give devices with a better stability.[19] From this point of view, it is of some interest to prepare polymer solar cells via solution processing where it is possible to remove the solubilizing side chains after the active layer has been deposited. Ideally the film forms a more rigid and stable morphology that leads to an increase in the glass transition temperature of the material and thus thermally stable devices.

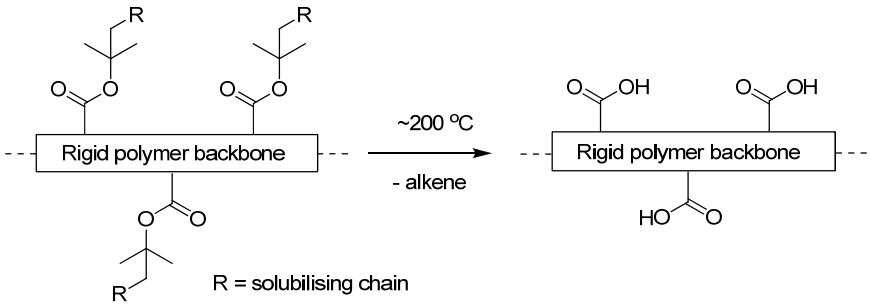

Figure 2.2. Thermocleavable ester groups attached to the polymer backbone. After a thermal treatment around 200 °C the solubilizing groups are eliminated

The application of thermocleavable materials fulfils this requirement. With thermocleavable materials you exploit the instability of a bond in the molecule where the labile bond functions as the linker between the solubilizing group and the active material. The most recent developments are the thermocleavable ester groups and the dithiocarbamate precursor route. With regard to the thermocleavable ester groups the solubilizing group is typically a branched alkyl chain attached to the active conjugated polymer backbone through an ester bond (Figure 2.2). When the polymer is heated this bond breaks, eliminating a volatile alkene and leaving the polymer component insoluble. The thermal treatment is an in-situ method to alter the physical and chemical properties such as solubility, hardness, hydrogen bonding, polarity, density and ionicity after the final device film has been prepared.

It has been demonstrated that bilayer heterojunction devices based on poly-3-(2-methylhexan-2-yl)-oxy-carbonylbithiophene (P3MHOCT) and C_{60} can provide very stable devices after thermal elimination of the solubilizing groups[19] which transforms P3MHOCT into the more rigid and insoluble poly-3-carboxydithiophene (P3CT). The improved stability of this system (P3CT:C_{60}) has been linked to the rigid nature of the film and cross-linking through a hydrogen-bonded network as shown in figure 2.3.[13]

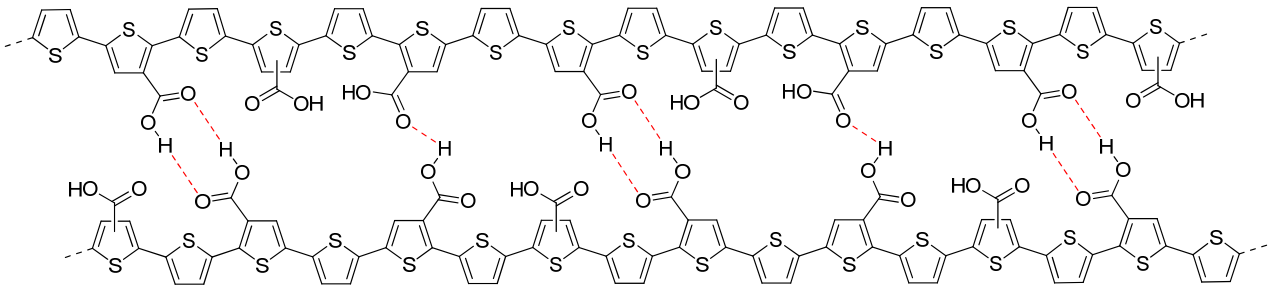

Figure 2.3. Proposed cross-linked structure of P3CT through a hydrogen-bonded network

P3MHOCT is readily soluble in common organic solvents and is easily processed into thin films with standard solution processing methods. Thermogravimetric data for P3MHOCT in the temperature range 25-475 °C shows two distinct weight loss mechanisms.[31] The first weight loss at ~200 °C accounts for the elimination of the ester group and the second weight loss at ~300 °C is decarboxylation (Figure 2.4). The thermal behaviour, where P3MHOCT transforms to P3CT that further converts to polythiophene (PT) at ~300 °C, was confirmed by ^{13}C labelling studies and solid-state NMR spectroscopy.

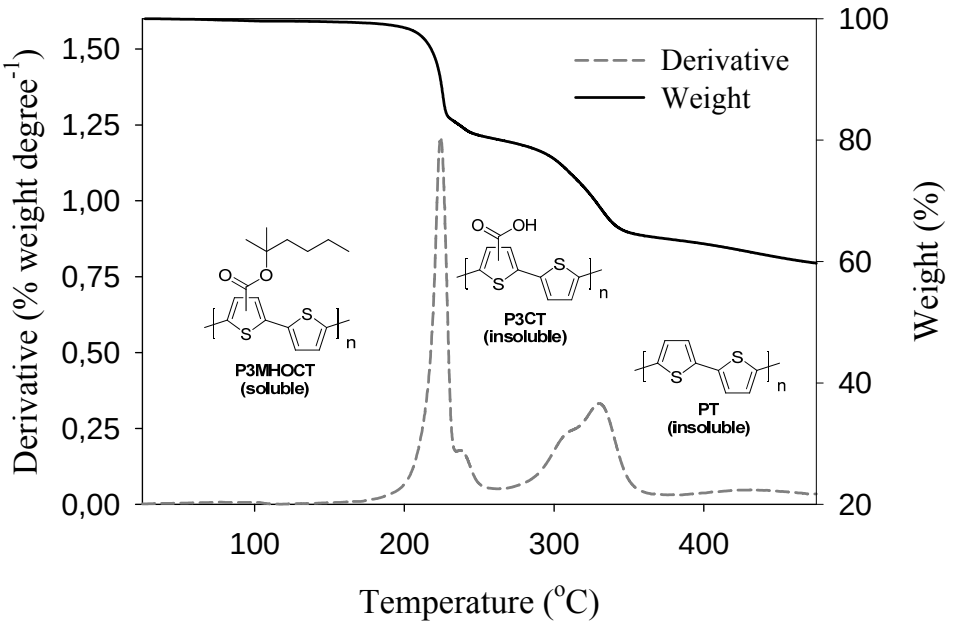

Figure 2.4. Thermogravimetric data for P3MHOCT in the temperature range 25-475 °C. P3MHOCT transforms to P3CT at ~200 °C that further converts to PT at ~300 °C.

This finding offers a route to native polythiophene (PT) by solution processing which has not been possible before. Photovoltaic performance of devices based on P3MHOCT:PCBM blends with different thermal treatments reveals some interesting results.[14] The power conversion efficiency of the devices at room temperature was in the range of 0.7 - 0.9 % and was found to decrease as the device film was annealed at temperatures below the cleavage temperature (~200 °C) of P3MHOCT. After the transformation to P3CT a broad minimum is reached with power conversion efficiencies in the range of 0.1-0.4%. When reaching the temperatures of the second transformation (~300 °C) from P3CT to PT, a dramatic increase in power conversion efficiency was observed. Up to 0.6% in the case of [60]PCBM and as high as 1.5% in the case of [70]PCBM as shown in figure 2.5b. Clearly the morphology is changing with the

chemical transformations and this is part of the explanation to the variable power conversion efficiency of this system. Another part of the explanation is the change in energy levels as the electron withdrawing carboxylic acid groups are removed from the conjugated polythiophene backbone. During the annealing, it is possible to observe the colour change of the sample from red to orange (conversion from P3MHOCT to P3CT) and then from orange to purple-red (conversion from P3CT to PT) (Figure 2.5a).

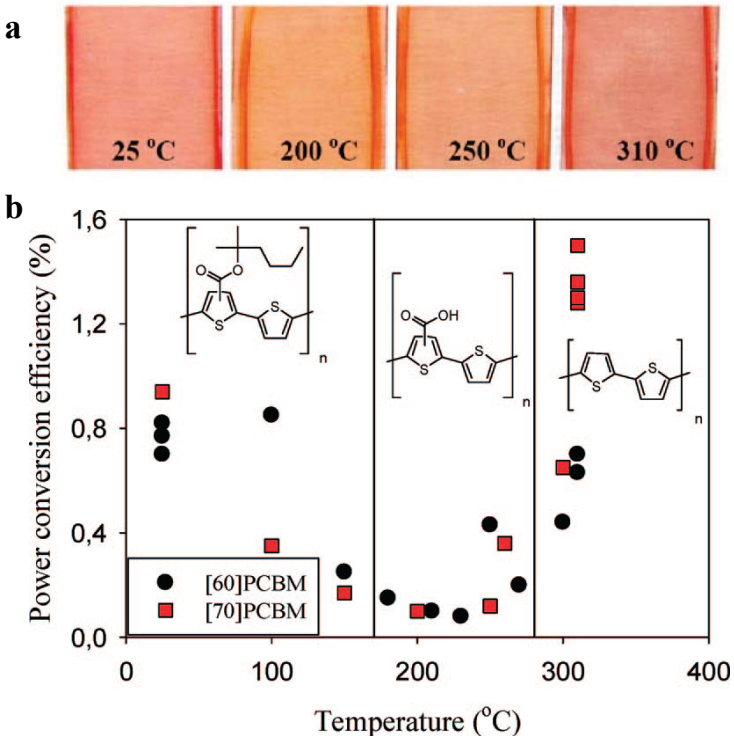

Figure 2.5. (a) A photograph showing the appearance of films based on P3MHOCT:[70]PCBM blends when heated to different temperatures. (b) Efficiency versus annealing temperature for bulk heterojunctions based on P3MHOCT and [60]PCBM or [70]PCBM. Reprinted with permission from[14]. © 2008 American Chemical Society.

The use of thermocleavable conjugated polymer materials in polymer solar cells have been relatively limited due to the low performance observed when preparing devices from them. The preparation of efficient devices from native polythiophene via a thermocleavable route should be seen as the first breakthrough in the use of thermocleavable materials for polymer solar cells.[14,31] The parameter space is enormous and the added complexity of thermocleavable materials (both their synthesis and processing into devices) combined with perhaps a poor starting point have resulted in a small investment in them in terms of research effort. The fact that efficiencies approaching 2% can be reached shows that it is not impossible

to prepare efficient polymer solar cell devices from thermocleavable materials and it is interesting to speculate how far thermocleavable materials could have been pushed pending the same investment of research effort that has gone into materials such as MEH-PPV or P3HT.

The use of thermocleavable P3MHOCT in thin film devices was first introduced by Liu *et al.*[24] The idea, besides improving the chromophore density, was to enable the interaction at the interface between the polymer and TiO_2 in a (FTO/TiO_2/P3CT/P3HT/Ag) photovoltaic cell (FTO = fluorine doped tin oxide). The device showed a 3-fold improvement in photocurrent compared to a reference cell without P3CT. Under illumination the FTO/TiO_2/ P3CT/P3HT/Ag cell had external quantum efficiency (EQE) of 12.6 % and a power conversion efficiency of 1.10 %, while the reference cell (FTO/TiO_2/P3HT/Ag) showed EQE of 4.2% and a power conversion efficiency of 0.69 %. The improvement in photocurrent/performance upon introduction of the P3CT layer may be related to a higher chromophore density after thermocleavage and the chelation of -COOH groups in P3CT to the TiO_2 may enhance the interfacial charge-transfer efficiency.

Other thermocleavable materials exploited as semiconductors are the dithiocarbamate precursors. Poly-(2,5-thienylene vinylene) (PTV) have been prepared via the dithiocarbamate precursor route which exploit the lability of the linking thiocarbamate bond in the molecule (Figure 2.6).[8-12] The solution processable non-conjugated precursor polymer is cleavable around 160 °C leaving a rigid conjugated polymer (PTV). Bulk-heterojunction solar cells based on blends of the precursor PTV and PCBM have demonstrated power conversion efficiencies of up to 0.76 % after the thermal treatment.[9]

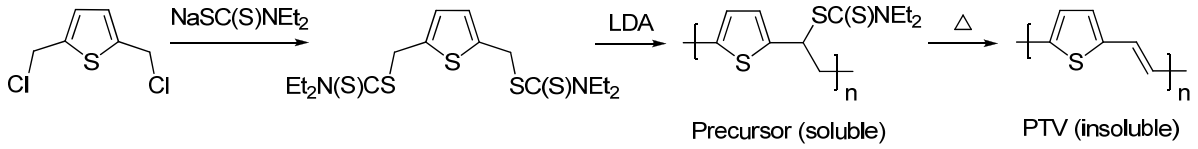

Figure 2.6. Preparation of PTV via the dithiocarbamate precursor route.

In terms of stability PTV is like PPV materials sensitive to oxygen due to the vinylene groups that are susceptible to photo-oxidation, though as mentioned above more rigid systems generally give devices with a better stability and therefore improved stability of PTV devices prepared with the dithiocarbamate precursor route can be expected.

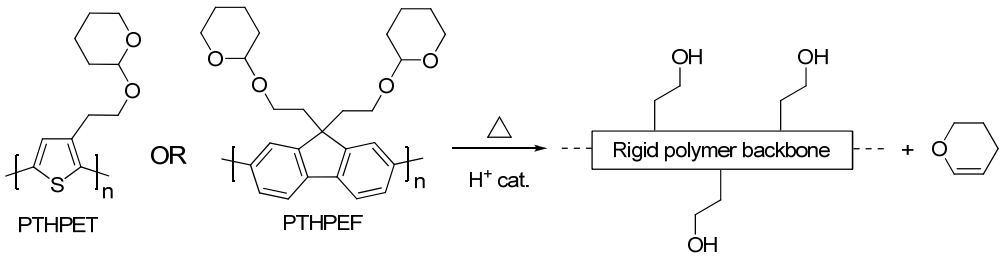

Figure 2.7. Thermocleavable polymers PTHPET and PTHPEF and acid-catalyzed elimination of dihydropyran from the polymer backbone.

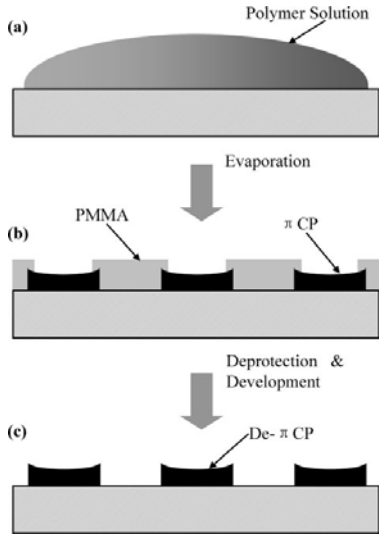

Figure 2.8. Schematic illustration of the formation of a well-ordered micro and nanometer-sized π-conjugated polymer features (PTHPET or PTHPEF) by **a)** solution casting, **b)** self-organization, and **c)** catalytic reaction and development. Reprinted with permission from[18]. © 2007 WILEY-VCH

The interpenetrating network of the donor and acceptor material is an extremely important factor in the construction of efficient bulk-heterojunction solar cells. A large donor-acceptor interface is required to ensure efficient exciton dissociation, while sufficient percolating pathways need to be present to allow efficient charge carrier transport to the electrodes. It is thus of interest to be capable of controlling the dimension of the domains in the interpenetrating network such that all domain boundaries are within the exciton diffusion range in the photoactive layer. Han *et al.* has demonstrated a novel procedure to create morphologically controlled nano/microscale patterns of π-conjugated polymers.[18] An Acidic mixture of polyfluorene or polythiophene bearing solubilizing thermocleavable tertrahydropyranyl (THP) groups (figure 2.7), and Poly(methyl methacrylate) (PMMA) is used for the active layer. After spin-coating on substrates phase separation is induced by the

chemical dissimilarity of the two polymers giving rise to a nano/microscale morphology. After an acid catalyzed thermal treatment where the THP groups are eliminated the insoluble conjugated polymer remains. Subsequently, PMMA is removed by treating the films with a chlorobenzene/hexane solution leaving patterns of conjugated polymer (figure 2.8).

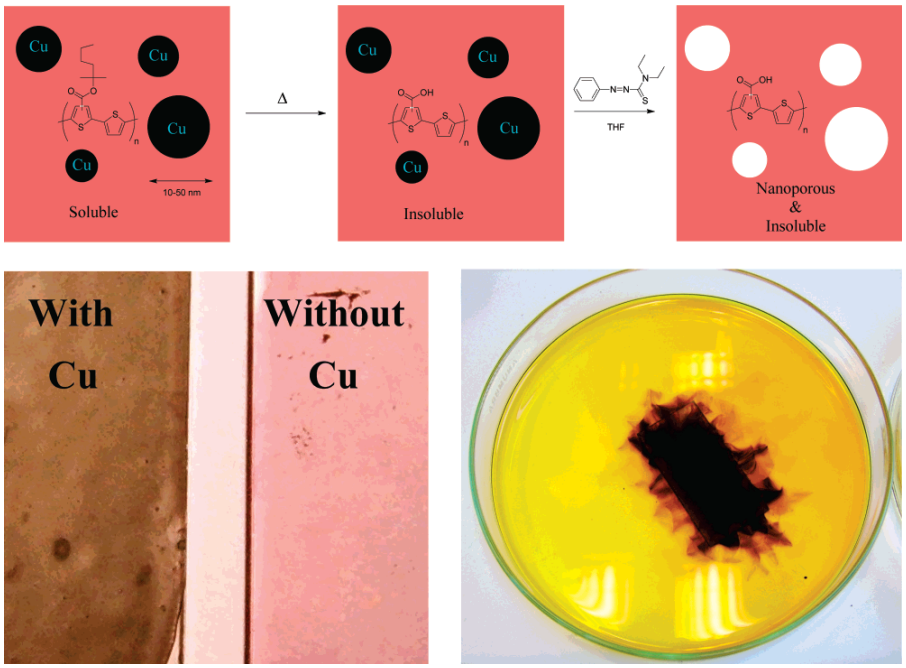

Figure 2.9. Reaction scheme for the process (**above**) and pictures of the films before and after removal of the copper nanoparticles. The film loaded with copper nanoparticles has a black appearance whereas the film where the copper nanoparticles have been removed has a red color (**lower left**). The dissolution step is also shown where a device slide (50 mm x 25 mm) is covered with a THF solution of azothioformamide. The dark color is due to the formation of the copper complex of azothioformamide (**lower right**). Reprinted with permission from[32]. © 2007 American Chemical Society

This method where a template is used to control the nanostructure of conjugated polymers has been exploited by Andreasen *et al*. in a solar cell context.[32] Instead of PMMA, copper nanoparticles with an average diameter of 32 nm were used as the template to nanostructure a conjugated polymer based on P3MHOCT. Mixtures of P3MHOCT and the copper nanoparticles are processed into thin films followed by a thermal treatment whereby the solubilizing side chains of the polymer were eliminated, leaving an insoluble film of conjugated P3CT with included copper nanoparticles. The copper nanoparticles could then be removed by treating the films with a THF solution of phenylazodiethylthioformamide

(copper-specific solubilizing agent[33,34]) leaving voids in place of the copper nanoparticles (Figure 2.9). Finally the voids in the dried nanoporous films were filled with PCBM by doctorblading forming a donor–acceptor bulk heterojunction. However, the nanostructures had little influence on the photovoltaic effect. The best device (active area of 3 cm^2) had an open-circuit voltage of 0.43 V, a short-circuit current of 0.19 mA/ cm^2, a fill factor of 27.4%, and a power conversion efficiency of 0.02% (0.1-0.4% for P3CT:[60]PCBM). These data are much lower than the state of the art and is ascribed to the low porosity of the films (<20%) and the large size of the PCBM domains. The ideal size of the PCBM domains should be of the order of 5-10 nm, and the porosity should be closer to 50% or more. This method may find importance in the modification of nanoscale morphologies for polymer solar cell devices if it could be advanced for incorporation of larger amounts of well-distributed smaller nanoparticles (5-10 nm) into the conjugated polymer film.

2.3 Thermal patterning of polymer films

Laser-induced thermal patterning is another technique to control the morphology of conjugated polymers. Gordon *et al.* has developed a method for direct thermal patterning of a thermocleavable π-conjugated polymer film containing a near-infrared (NIR) sensitive dye.[15] The NIR dye (figure 2.10) is incorporated directly into the polymer film by spin-coating a NIR dye/polymer blend on a substrate.

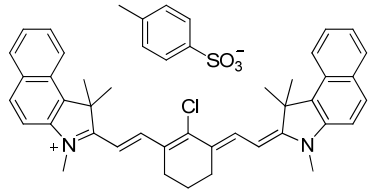

Figure 2.10. Near-infrared sensitive dye used by Gordon *et al.*

When the film is exposed to NIR light pulses from an 830 nm laser beam the dye absorbs the irradiation and converts the NIR photons into heat by internal conversion. The polymer (PTHPET, Figure 2.7) does not absorb the NIR light but the heat produced by the dye induces thermocleavage of the THP groups. Subsequently, the NIR dye is removed by rinsing the films with methanol followed by THF leaving patterned π-conjugated polymer (Figure 2.12a). The patterned π-conjugated polymer shows a significant reduction in the quantum yield,

compared to a pure PTHPET film, which is ascribed to either the presence of residual NIR dye remaining in the film after rinsing or/and coplanarization and chain aggregation after thermocleavage of the THP groups.

To overcome this problem novel strategies have been developed where the NIR dye is not incorporated into the film. Gordon *et al.* has described a bilayer approach,[16] wherein a NIR dye is contained in a film of poly(2-hydroxyethylmethacrylate) [p(HEMA)] spin-cast onto a thermocleavable *π*-conjugated polymer film of poly(9,9-dihexylfluorene-*alt*-2-(2-thiophen-3-ethoxy)tetrahydropyran)-*co*-(9,9-dihexylfluorene-*alt*-bithiophene) (PFT-TT) (Figure 2.11).

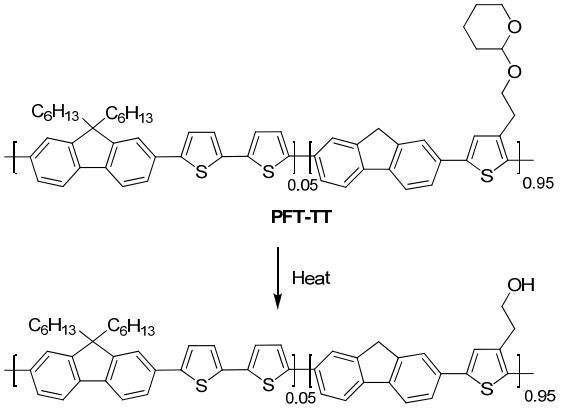

Figure 2.11. PFT-TT with thermocleavable THP groups

After exposure of the bilayer film to 830 nm NIR laser irradiation, the p(HEMA)/NIR dye layer is removed by rinsing with methanol. Subsequent treatment of the remaining film with a THF/Hexane solution removes non-cleaved PFT-TT (unexposed p(HEMA)/NIR dye regions) leaving patterned π-conjugated polymer (figure 2.12b). Using this bilayer film architecture the active conjugated polymer layer can be heated by exposure to NIR irradiation while minimizing deleterious mixing of the polymer with the NIR dye. Compared to the monolayer approach described above the π-conjugated polymer retains its photoluminescent properties showing quantum yields as high as 86% of the pristine polymer. The method is capable of imaging large surface areas, up to 1 m^2, at relatively high throughput and with micrometer size resolution, and thus could be valuable in the context of processing of thermocleavable polymers for solar cells.

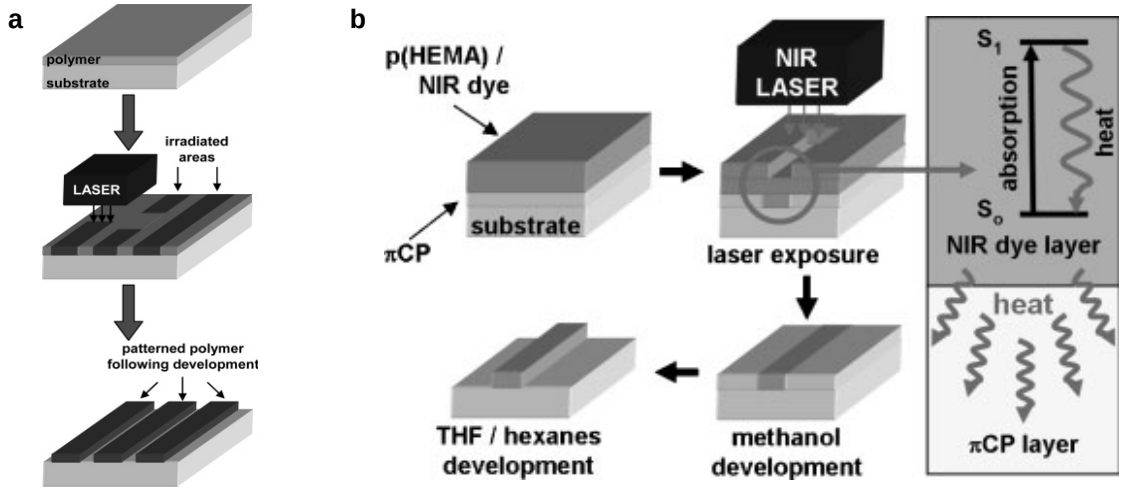

Figur 2.12. (a) Schematic diagram for the direct thermal patterning of a π-conjugated polymer using a NIR laser. (b) Bilayer approach to laser induced direct thermal patterning of a *π*-conjugated polymer. Reprinted with permission from[15]. © 2007 American Chemical Society

2.4 All solution processed tandem cells

One drawback of single junction polymer devices is their narrow absorption window compared to the solar cells based on inorganic semiconductors. A possible approach to efficiently harvest light at both short and long wavelengths is by stacking different band gap materials/devices on top of each other. This can be done by placing the cells in series giving devices known as tandem cells.[35-37] By stacking different band gap materials on top of each other the tandem cell should be able to exceed the maximum theoretical efficiency of a single junction solar cell because it increases the absorption of solar light and allows exploiting the photon energy more efficiently. When two cells (in a two terminal tandem cell) are connected in series the open-circuit voltage (V_{oc}) is the sum of the V_{oc}'s of the subcells, $V_{oc1} + V_{oc2} + V_{oc3...} = V_{oc\ (tandem)}$.

Figure 2.13a illustrates a typical organic tandem cell architecture comprising of two distinct active layers stacked on top of each other. Both of them are based on a donor–acceptor composition and the use of materials with different band gaps enables absorption of solar light over a wider spectral range. In order to prevent charge build-up within the cells a transparent intermediate layer is positioned between the two active layers. The intermediate layer ensures recombination of the electrons created in the first cell with the holes created in the second cell. In addition, it can act as a protective layer to support the bottom cell during

deposition of the top active layer. This can generally be accomplished with a thin inorganic layer.

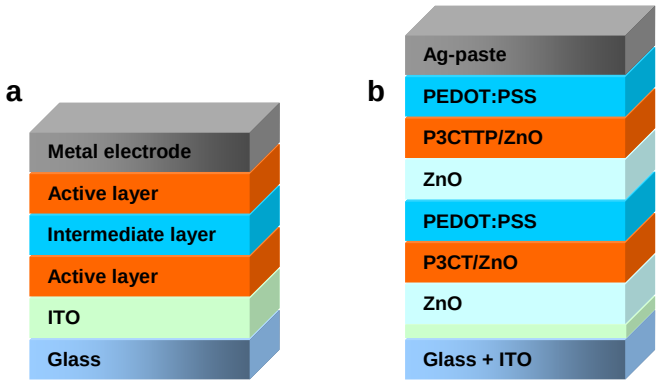

Figure 2.13. (a) Typical device setup for an organic tandem cell. (b) Tandem solar cell based on thermocleavable materials realized by Hagemann *et al.*

Several methods have been employed in the fabrication of tandem cells depending on the materials used for the active and the intermediate layer. The mode of preparation can be divided in three categories: all vacuum processing by evaporation of low molecular weight molecules, a combination of vacuum and solution processing and all solution processing. Due to the complexity of multilayer solution processing caused by interlayer mixing, the early reports of organic tandem cells are based on vacuum deposition of small molecules and they certainly show increased V_{oc} and efficiencies.[38-41] Also a combination of vacuum and solution processing is a fine approach where the solution processed underlying layer is not disturbed during subsequent vacuum processing.[42-44] However, from an industrial point of view, all solution processing without the use of vacuum where each layer is processed from solution is the most appealing because techniques like ink-jet printing, screen printing and roll-to-roll coating are less time and energy consuming and enable large scale organic solar cell production.

The approach has so far employed different solvents for the different layers that are orthogonal in the sense that the next solvent in the process is a poor one for the material in the previously deposited layer. The realization of a solvent combination that allows subsequent layers to be processed without affecting previously deposited layers has been reported by Gilot *et al.*[45] The challenging step is spin-coating of the intermediate layer which consist of a layer of zinc oxide nanoparticles spin-coated from acetone prior to a layer of pH

neutral PEDOT. The ZnO/PEDOT recombination layer was not affecting the underlying active layer of MDMO-PPV:PCBM and was also acting as a protective layer to support the bottom cell during spin-coating of the second active layer, from chlorobenzene, consisting of a P3HT:PCBM blend. One of the highest reported efficiencies to date (6.5%) was demonstrated with a solution-processed tandem cell[46] where the device showed a 38% performance improvement versus the best single device. For the bottom BHJ cell was used a blend of PCPDTBT and PCBM spin-coated from chlorobenzene and the top cell was made of blend of P3HT:[70]PCBM spin-coated from chloroform. For the intermediate layer the authors used a layer of TiO_x spin-coated from a TiO_x precursor solution (sol-gel chemistry)[47] prior to a layer of PEDOT. The TiO_x precursor hydrolyses to TiO_x during 1 hour in air (Figure 2.14) and the final TiO_x layer offers high mechanical stability to the tandem cell.

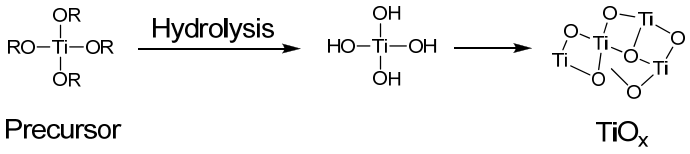

Figure 2.14. Preparation of the TiO_x layer

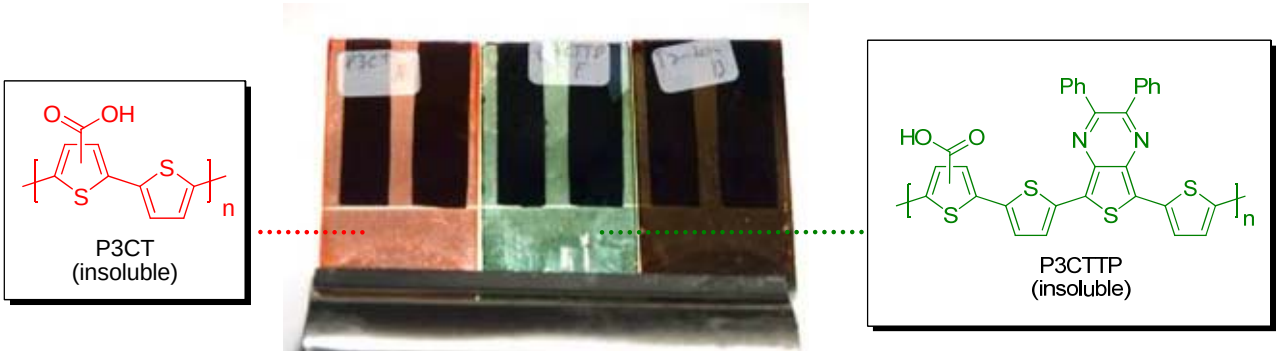

Figure 2.15. Photograph of the devices reported by Hagemann *et al.* Red colour: single junction of P3CT:ZnO. Green colour: single junction of P3CTTP:ZnO. Brown colour: tandem cell of P3CT:ZnO and P3CTTP:ZnO

An all solution processed tandem polymer solar cell based on thermocleavable materials (Figure 2.13b) has been reported by Hagemann *et al.*[17] Solution-processable precursors were used that allow for conversion to an insoluble state by a thermal treatment. A bulk heterojunction composite of P3MHOCT and ZnO was used for the bottom cell and a blend of the low band gap polymer poly-[(3'-(2,5,9-trimethyldecan-2-yl)-oxy-carbonyl)-

[2,2';5',2'']terthiophene-1,5''-diyl)-co-(2,3-diphenylthieno[3,4-b]pyrazine-5,7-diyl)] (P3TMDCTTP) and ZnO was used for the top cell. Straight after each film preparation a short thermal treatment eliminated the solubilizing group converting P3MHOCT to P3CT and P3TMDCTTP to P3CTTP (Figure 2.15). To separate the bottom cell from the top cell an intermediate layer of PEDOT:PSS and ZnO was used. Finally a solution processed silver electrode was deposited on top. The final tandem cell performed relatively poorly, mostly due to poor efficient single cells, but the approach does effectively solve the complications associated with solubility during application of subsequent layers. Due to an insoluble nature of the active materials after the thermal treatment there is no limit in the choice of solvents when processing the subsequent layers in the tandem cell and more research into this field appears worthwhile.

2.5 Summary

In summary, a short introduction was given to some of the thermocleavable materials described in the literature. The use of precursor or thermocleavable side chain routes results in a higher concentration of the photoactive participant in polymer solar cells. Heat treatment of the device film results in chemical reactions whereby part of the material that constitutes the original film is eliminated. Thus formed π-conjugated polymers have no solubilizing side chains and are insoluble in all solvents which induce enhanced stability towards degradation and furthermore allows for preparation of multilayer devices by all solution processing. Light cleavage by using a near-infrared (NIR) dye that is either incorporated in the polymer film or employed as a separate layer on top of the polymer is a sophisticated form of dealing with thermocleavable materials which allows for thermal patterning of polymer films.

2.6 References

1. Gagnon, D. R.; Capistran, J. D.; Karasz, F. E.; Lenz, R. W.; Antoun, S. *Polymer* **1987,** *28* (4), 567-573.

2. Garay, R. O.; Mayer, B.; Karasz, F. E.; Lenz, R. W. *J. Polym. Sci. , Part A: Polym. Chem.* **1995,** *33* (3), 525-531.

3. Lenz, R. W.; Han, C. C.; Stengersmith, J.; Karasz, F. E. *J. Polym. Sci. , Part A: Polym. Chem.* **1988,** *26* (12), 3241-3249.

4. Wessling, R. A. *J. Polym. Sci. Polym. Symp.* **1985,** (72), 55-66.

5. Bott, D. C.; Brown, C. S.; Chai, C. K.; Walker, N. S.; Feast, W. J.; Foot, P. J. S.; Calvert, P. D.; Billingham, N. C.; Friend, R. H. *Synth. Met.* **1986,** *14* (4), 245-269.

6. Feast, W. J.; Winter, J. N. *J. Chem. Soc. , Chem. Commun.* **1985,** (4), 202-203.

7. Furlani, A.; Napoletano, C.; Russo, M. V.; Feast, W. J. *Polym. Bull.* **1986,** *16* (4), 311-317.

8. Banishoeib, F.; Adriaensens, P.; Berson, S.; Guillerez, S.; Douheret, O.; Manca, J.; Fourier, S.; Cleij, T. J.; Lutsen, L.; Vanderzande, D. *Sol. Energy Mater. Sol. Cells* **2007,** *91* (11), 1026-1034.

9. Banishoeib, F.; Henckens, A.; Fourier, S.; Vanhooyland, G.; Breselge, M.; Manca, J.; Cleij, T. J.; Lutsen, L.; Vanderzande, D.; Nguyen, L. H.; Neugebauer, H.; Sariciftci, N. S. *Thin Solid Films* **2008,** *516* (12), 3978-3988.

10. Girotto, C.; Cheyns, D.; Aernouts, T.; Banishoeib, F.; Lutsen, L.; Cleij, T. J.; Vanderzande, D.; Genoe, J.; Poortman, J.; Heremans, P. *Org. Electron.* **2008,** *9* (5), 740-746.

11. Henckens, A.; Colladet, K.; Fourier, S.; Cleij, T. J.; Lutsen, L.; Gelan, J.; Vanderzande, D. *Macromolecules* **2005,** *38* (1), 19-26.

12. Nguyen, L. H.; Gunes, S.; Neugebauer, H.; Sariciftci, N. S.; Banishoeib, F.; Henckens, A.; Cleij, T.; Lutsen, L.; Vanderzande, D. *Sol. Energy Mater. Sol. Cells* **2006,** *90* (17), 2815-2828.

13. Bjerring, M.; Nielsen, J. S.; Siu, A.; Nielsen, N. C.; Krebs, F. C. *Sol. Energy Mater. Sol. Cells* **2008,** *92* (7), 772-784.

14. Gevorgyan, S. A.; Krebs, F. C. *Chem. Mater.* **2008,** *20* (13), 4386-4390.

15. Gordon, T. J.; Yu, J. F.; Yang, C.; Holdcroft, S. *Chem. Mater.* **2007,** *19* (9), 2155-2161.

16. Gordon, T. J.; Vamvounis, G.; Holdcroft, S. *Adv. Mater.* **2008,** *20* (13), 2486-2490.

17. Hagemann, O.; Bjerring, M.; Nielsen, N. C.; Krebs, F. C. *Sol. Energy Mater. Sol. Cells* **2008,** *92* (11), 1327-1335.

18. Han, X.; Chen, X. W.; Holdcroft, S. *Adv. Mater.* **2007,** *19* (13), 1697-1702.

19. Krebs, F. C.; Spanggaard, H. *Chem. Mater.* **2005,** *17* (21), 5235-5237.

20. Krebs, F. C.; Norrman, K. *Prog. Photovolt: Res. Appl.* **2007,** *15* (8), 697-712.

21. Krebs, F. C. *Sol. Energy Mater. Sol. Cells* **2008,** *92* (7), 715-726.

22. Krebs, F. C.; Thomann, Y.; Thomann, R.; Andreasen, J. W. *Nanotechnology* **2008,** *19* (42), 424013.

23. Krebs, F. C. Design and applications of polymer solar cells with lifetimes longer than 10000 hours. Kafafi, Z. H., Lane, P. A., Eds.; SPIE: San Diego, CA, USA, 2005; pp 59380Y-593811.

24. Liu, J. S.; Kadnikova, E. N.; Liu, Y. X.; McGehee, M. D.; Fréchet, J. M. J. *J. Am. Chem. Soc.* **2004,** *126* (31), 9486-9487.

25. Petersen, M. H.; Gevorgyan, S. A.; Krebs, F. C. *Macromolecules* **2008,** *41* (23), 8986-8994.

26. Yu, J. F.; Holdcroft, S. *Macromolecules* **2000,** *33* (14), 5073-5079.

27. Lira-Cantu, M.; Norrman, K.; Andreasen, J. W.; Krebs, F. C. *Chem. Mater.* **2006,** *18* (24), 5684-5690.

28. Norrman, K.; Alstrup, J.; Jørgensen, M.; Lira-Cantu, M.; Larsen, N. B.; Krebs, F. C. Three-dimensional chemical and physical analysis of the degradation mechanisms in organic photovoltaics. SPIE: San Diego, CA, USA, 2006; p U100-U111.

29. Norrman, K.; Krebs, F. C. *Sol. Energy Mater. Sol. Cells* **2006,** *90* (2), 213-227.

30. Norrman, K.; Larsen, N. B.; Krebs, F. C. *Sol. Energy Mater. Sol. Cells* **2006,** *90* (17), 2793-2814.

31. Bjerring, M.; Nielsen, J. S.; Nielsen, N. C.; Krebs, F. C. *Macromolecules* **2007,** *40* (16), 6012-6013.

32. Andreasen, J. W.; Jørgensen, M.; Krebs, F. C. *Macromolecules* **2007,** *40*, 7758-7762.

33. Nielsen, K. T.; Bechgaard, K.; Krebs, F. C. *Macromolecules* **2005,** *38* (3), 658-659.

34. Nielsen, K. T.; Bechgaard, K.; Krebs, F. C. *Synthesis* **2006,** (10), 1639-1644.

35. Ameri, T.; Dennler, G.; Lungenschmied, C.; Brabec, C. J. *Energy Environ. Sci.* **2009,** *2* (4), 347-363.

36. Hadipour, A.; de Boer, B.; Blom, P. W. M. *Org. Electron.* **2008,** *9* (5), 617-624.

37. Hadipour, A.; de Boer, B.; Blom, P. W. M. *Adv. Funct. Mater.* **2008,** *18* (2), 169-181.

38. Cheyns, D.; Gommans, H.; Odijk, M.; Poortmans, J.; Heremans, P. *Sol. Energy Mater. Sol. Cells* **2007,** *91* (5), 399-404.

39. Xue, J.; Uchida, S.; Rand, B. P.; Forrest, S. R. *Appl. Phys. Lett.* **2004,** *85* (23), 5757-5759.

40. Xue, J.; Uchida, S.; Rand, B. P.; Forrest, S. R. *Appl. Phys. Lett.* **2004,** *84* (16), 3013-3015.

41. Yakimov, A.; Forrest, S. R. *Appl. Phys. Lett.* **2002,** *80* (9), 1667.

42. Colsmann, A.; Junge, J.; Kayser, C.; Lemmer, U. *Appl. Phys. Lett.* **2006,** *89* (20), 203506-3.

43. Dennler, G.; Prall, H. J.; Koeppe, R.; Egginger, M.; Autengruber, R.; Sariciftci, N. S. *Appl. Phys. Lett.* **2006,** *89* (7), 073502-073503.

44. Hadipour, A.; de Boer, B.; Wildeman, J.; Kooistra, F. B.; Hummelen, J. C.; Turbiez, M. G. R.; Wienk, M. M.; Janssen, R. A. J.; Blom, P. W. M. *Adv. Funct. Mater.* **2006,** *16* (14), 1897-1903.

45. Gilot, J.; Wienk, M. M.; Janssen, R. A. J. *Appl. Phys. Lett.* **2007,** *90* (14), 143512-143513.

46. Kim, J. Y.; Lee, K.; Coates, N. E.; Moses, D.; Nguyen, T. Q.; Dante, M.; Heeger, A. J. *Science* **2007,** *317* (5835), 222-225.

47. Kim, J. Y.; Kim, S. H.; Lee, H. H.; Lee, K.; Ma, W. L.; Gong, X.; Heeger, A. J. *Adv. Mater.* **2006,** *18* (5), 572-576.

Chapter 3

Thermal studies of monomers and polymers bearing different thermocleavable ester groups*

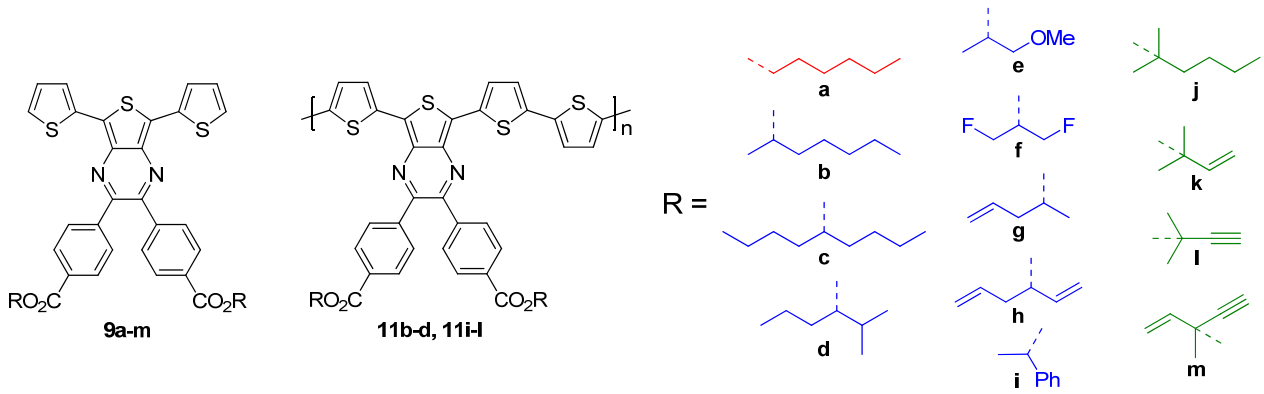

Figure 3.1. Monomers **9a-m** and polymers **11b-d**, **11i-l** based on dithienylthienopyrazines with thermocleavable benzoate esters (primary, secondary and tertiary) substituted on the pyrazine ring. R = (a) hexyl (b) 2-heptyl (c) 5-nonyl (d) 2-methyl-3-hexyl (e) 1-methoxy-2-propyl (f) 1,3-difluoro-2-propyl (g) 4-peten-2-yl (h) 1,5-hexadien-3-yl (i) 1-phenylethyl (j) 2-methyl-2-hexyl (k) 2-methyl-3-buten-2-yl (l) 2-methyl-3-butyn-2-yl (m) 3-methyl-1-penten-4-yn-3-yl

3.1 Introduction

The use of thermocleavable materials offers several advantages in the context of polymer solar cells. Most importantly the side chains that constitute a significant proportion of the final film are eliminated and ideally the final film comprises only the active component. Since bulk heterojunctions of polymer and PCBM are not directly compatible with the high temperatures acquired for elimination one aim is to achieve as low a temperature of elimination of the ester

* This work has been published: Helgesen Petersen M.; Gevorgyan, S. A.; Krebs, F. C. *Macromolecules* **2008,** *41* (23), 8986-8994.

group as possible. The purpose of the work presented in this chapter was to establish this, using the system shown in figure 3.1, in the context of choice of ester alcohol. Thermocleavable esters of monomers and polymers based on diphenyldithienylthieno-pyrazine were synthesized by incorporating carboxylic acid functionalities into the system followed by esterification. A series of 13 different ester groups (primary, secondary and tertiary) were prepared (Figure 3.1) and the temperature of elimination of the ester group was studied using thermogravimetric analysis (TGA) in conjunction with mass spectrometry of the carrier gas (TGA-MS). The photovoltaic performance of the soluble polymers in blends with PCBM is also presented together with stability studies in four different atmospheres.

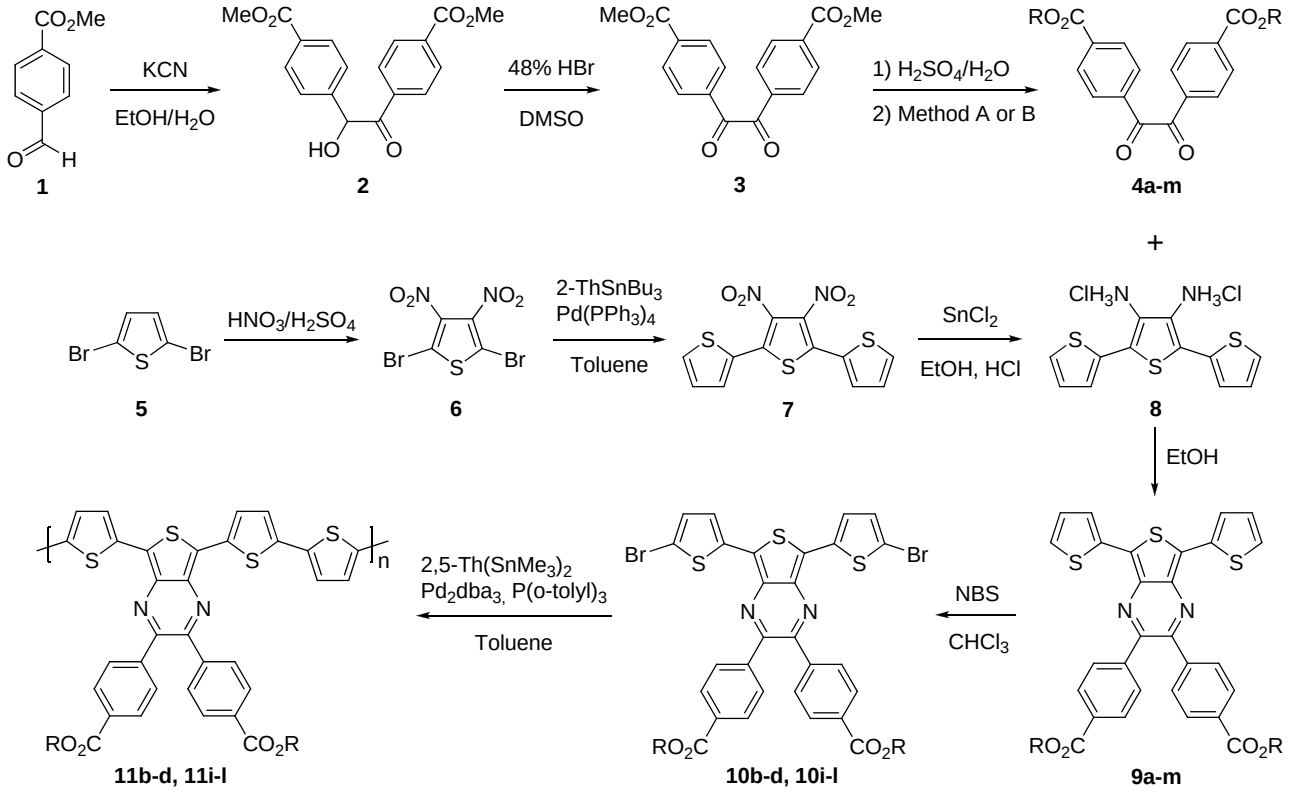

Sheme 3.1. Synthetic steps involved in the preparation of the monomers and polymers. Method A: ROH, 1,1′-carbonyldiimidazole, pyridine. Method B: ROH, DMAP, $Sc(OTf)_3$, *N,N*′-diisopropylcarbodiimide

3.2 Synthesis

The synthetic steps involved in the preparation of the dithienylthienopyrazines with thermocleavable esters are outlined in Scheme 3.1 while detailed synthetic procedures are

described in the experimental section (3.7). The benzils **4a**-**m** were prepared by a four step synthetic sequence employing a standard benzoin condensation of methyl 4-formylbenzoate (**1**) and potassium cyanide. The reaction was very fast and no heating was required. The benzoin **2**[1] was oxidized using 48% aqueous hydrobromic acid in dimethyl sulfoxide[2] affording the benzil **3**[3] that was then hydrolyzed in an aqueous acid to give the free acid 4,4'-bis(hydroxycarbonyl)benzil[4] followed by esterification. The esterifications of the primary and secondary esters **4a**-**i** employed 1,1′-carbonyldiimidazole as the acylating agent (method A) which turned out to work well with primary and secondary alcohols but not with tertiary alcohols. Tertiary esters are notoriously difficult to synthesize and a series of techniques were attempted. Transformation of the diacid, 4,4′-Bis(hydroxycarbonyl)benzil, into the diacid chloride followed by direct reaction with the tertiary alcohols (2-methyl-2-hexanol, 2-methyl-3-buten-2-ol, 2-methyl-3-butyn-2-ol, 3-methyl-1-penten-4-yn-3-ol) or by adding freshly precipitated AgCN[5] was ineffective. Other acylating agents such as 2,2′-dipyridyl disulfide/PPh_3,[6] 2-chloro-1-methylpyridinium iodide[7] and 2-chloro-3,5-dinitropyridine[8] all failed (0% product). The latter method, using 2-chloro-3,5-dinitropyridine, has proven useful for monoesterification albeit in low yield that makes its use impractical for diesterification. A procedure reported by Zhao *et al.*[9] turned out to work efficiently. The method employs a catalytic amount of scandium triflate in combination with *N*,*N*′-diisopropylcarbodiimide (DIPC) and 4-dimethylaminopyridine (DMAP) (method B). Very good yields of the tertiary diesters **4j**-**m** (78-81%) were obtained under mild conditions.

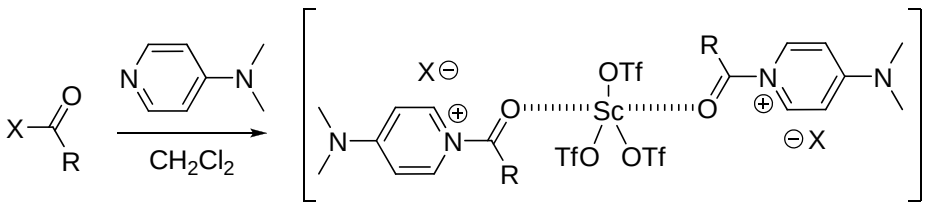

Figure 3.2. Possible intermediate

It has been suggested that the role of $Sc(OTf)_3$ in the esterification may be to coordinate with the initially formed carbonyl oxygen of the pyridinium intermediate, which could lead to the reactive species[9] shown in figure 3.2. I have also tested other transition metal salts (i.e. $HfCl_4$·2THF, $ZrCl_4$·2THF, $Y(OTf)_3$) as potential catalysts for the esterification where especially $HfCl_4$·2THF showed good catalytic effect (Table 3.1). Using $HfCl_4$·2THF in combination with

DIPC and DMAP gave yields of the tertiary diester **4j** in the range 60-70%. The reaction is slower but the lower cost of $HfCl_4$·2THF compared to $Sc(OTf)_3$ makes it a good alternative.

Table 3.1. Catalyst effect on the diesterification of 4,4'-bis(hydroxycarbonyl)benzil

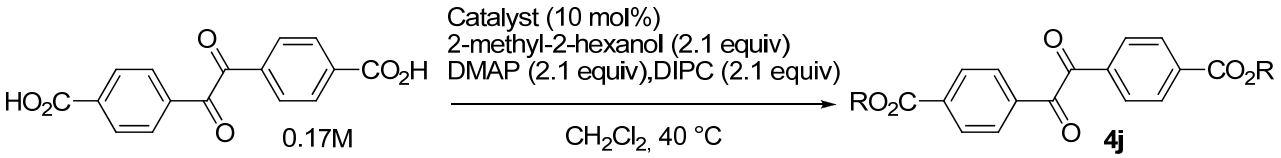

Entry	Catalyst	% yield[a] **4j** (20 h)	% yield[a] **4j** (40 h)
1	$Sc(OTf)_3$	70	76
2	$HfCl_4$·2THF	51	65
3	$ZrCl_4$·2THF	32	-
4	$Y(OTf)_3$	38	-

The detailed synthetic procedure is described in the experimental section. [a] isolated yield

The diamino precursor **8** was prepared by a known procedure[10] starting with nitration of 2,5-dibromothiophene (**5**).[11] Subsequently stille coupling of **6** with 2-tributylstannylthiophene followed by reduction of the nitro groups using $SnCl_2$[11] afforded **8**. Condensation of the benzils **4a**-**m** with **8** afforded the monomers **9a**-**m**. Finally the polymers were prepared by NBS bromination of the monomers **9b**-**d** and **9i**-**l** followed by Stille coupling polymerization with 2,5-bis(trimethylstannyl)thiophene giving **11b**-**d** and **11i**-**l** as dark green solids. The molecular weights for the polymers were in the 40000-70000 g/mol range and the polydispersity (PDI) was around 2.

3.3 Thermal Behaviour

The relative stability of the dithienylthienopyrazines with thermocleavable benzoate esters substituted on the pyrazine ring, **9a**-**m**, was investigated by thermogravimetric analysis (TGA) and thermogravimetric analysis in conjunction with mass spectrometry of the carrier gas (TGA-MS) in the temperature range 50-500 °C (Table 3.2). TGA is a type of testing that is performed on samples to determine changes in weight in relation to change in temperature. The thermogravimetric data in table 3.2 are consistent with earlier pyrolysis studies of esters.[12] As expected elimination of an alkene from the tertiary diesters **9j**-**l** take place at

lower temperatures than the secondary diesters **9b-i**. The primary diester **9a** eliminated with decomposition at a significantly higher temperature.

Table 3.2. List of TGA Data for **9a-m**, **11b-d, 11i-l**

R-group	Compound	Ester elimination (°C)	Weight loss (%)	
			Calculated	Found
	**9a**	410[a]	23.7	36
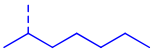	**9b**	333	26.7	25
	11b	329	24.0	25
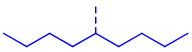	**9c**	325	31.8	34
	11c	325	28.9	28
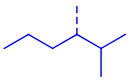	**9d**	332	26.7	25
	11d	325	24.0	24
	**9e**	360[a]	21.1	22
	**9f**[b]	-	22.4	-
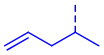	**9g**	326[a]	20.1	17
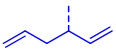	**9h**	300[a]	22.9	15
	**9i**	266	27.8	18
	11i	254	25.6	15
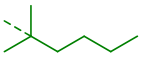	**9j**	225	26.7	26
	11j	225	24.0	21
	**9k**	197	20.1	18
	11k	206	18.0	8
	**9l**	246	19.7	10
	11l	-[c]	17.6	6
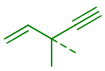	**9m**[b]	-	22.4	-

[a] Molecule decomposes at first inflection. [b] Insufficient TGA data. [c] Broad derivative peak with no maximum

The presence of an inductively (σ bond) electron withdrawing β substituent on the alcohol is known to slow down the rate of ester pyrolysis.[13] Methoxy substituted **9e** eliminate at 360 °C which is 35 °C higher than the elimination temperature of **9c** that bears a β alkyl substituent. A double bond substituent at the β carbon can reduce the elimination temperature moderately as observed by comparing **9g** with **9b** and **9d**. **9h** eliminates hexatriene at around 300 °C which is approximately 25 °C lower compared to **9c**. We ascribe this to an activation of the adjacent C_β-H bond that assist the elimination. The double bond substituents apparently

contribute to other reactions (weight losses) at the higher temperatures as **9g** and **9h** decompose at the elimination temperatures.

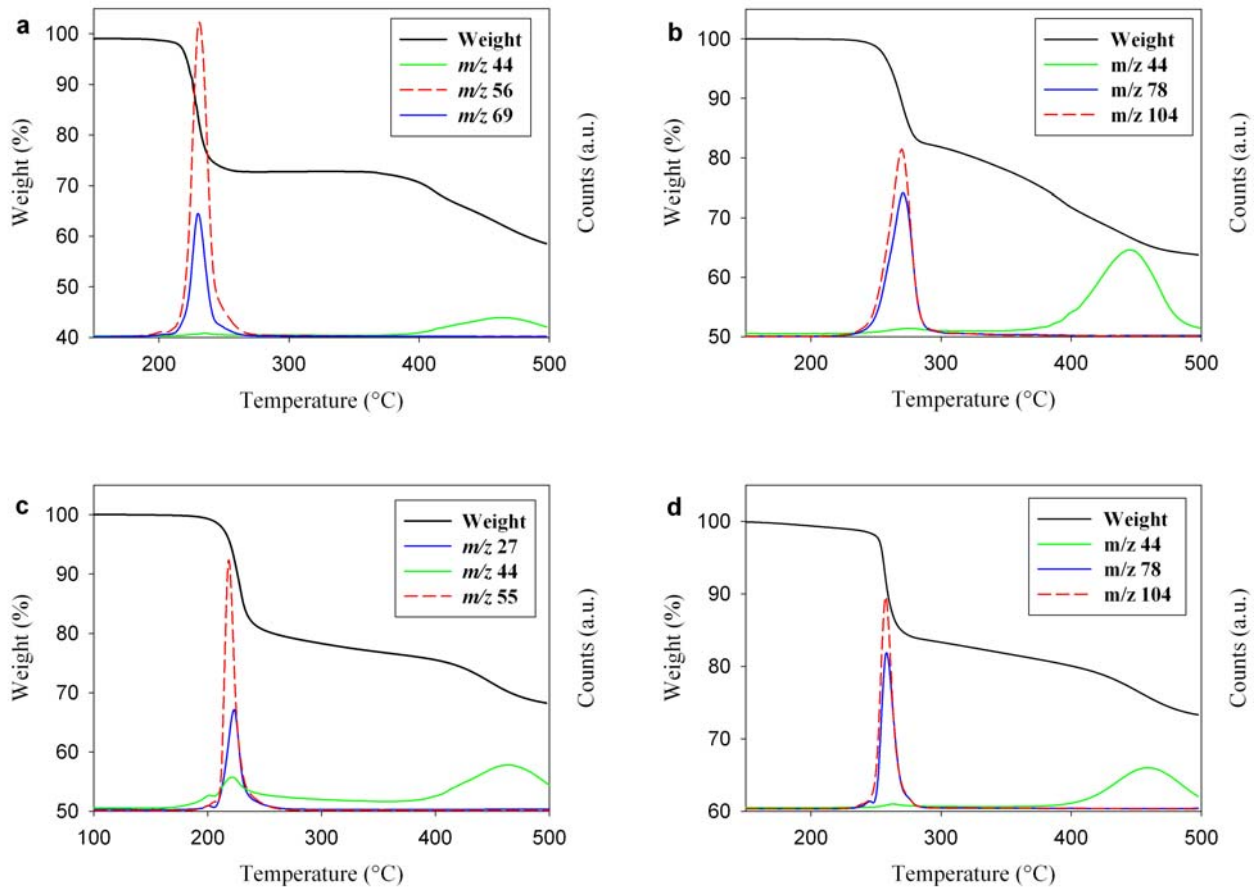

Figure 3.3. (a) TGA-MS of **9j**, (b) TGA-MS of **9i**, (c) TGA-MS of **11j**, and (d) TGA-MS of **11i**. The first inflection accounts for the ester elimination and the second weight loss around 400-500 °C is decomposition. The red and blue curves is the mass signals corresponding to loss of alkenes and the green curve corresponds to loss of carbon dioxide.

Furthermore, we observed that **9e**, **9h**, and **9m** showed a slight weight loss at low temperatures. We found no identifiable mass peaks corresponding to the solvent and also rule out the possibility for solvent loss as the samples were dried prior to analysis in a vacuum oven at 50 °C for 24 hours. It is possible that these materials are subject to chemical reactions in the solid state (ie. a Cope reaction for **9h** and **9m** or elimination of methanol for **9e**). We currently have no explanation for these observations other then it being an elimination reaction or an electrocyclic reaction followed by an elimination reaction giving fragments that

we did not observe in our mass spectra. **9i** has a 1-phenylethyl ester where the π-bonded substituent contributes to the activation of the adjacent C_{β}-H. It has a simple TGA curve where the first inflection is responsible for the elimination of styrene (Figure 3.3b). The phenyl substituent decrease the temperature for the first weight loss even further compared to **9g** and **9h.** The tertiary diesters **9j-l** eliminate in the temperature range 197-246 °C. **9k** eliminates at a lower temperature compared to **9j** (Figure 3.3a) which may arise from the double bond activation as described above. **9l** eliminate 14 °C higher compared to **9j** and we conclude that a triple bond is not as activating as the double bond in this position. The observed weight loss for the compounds **9g**, **9h**, **9i**, **6k**, and **9l** all show weight loss at the first inflection which is significantly lower than the calculated value.

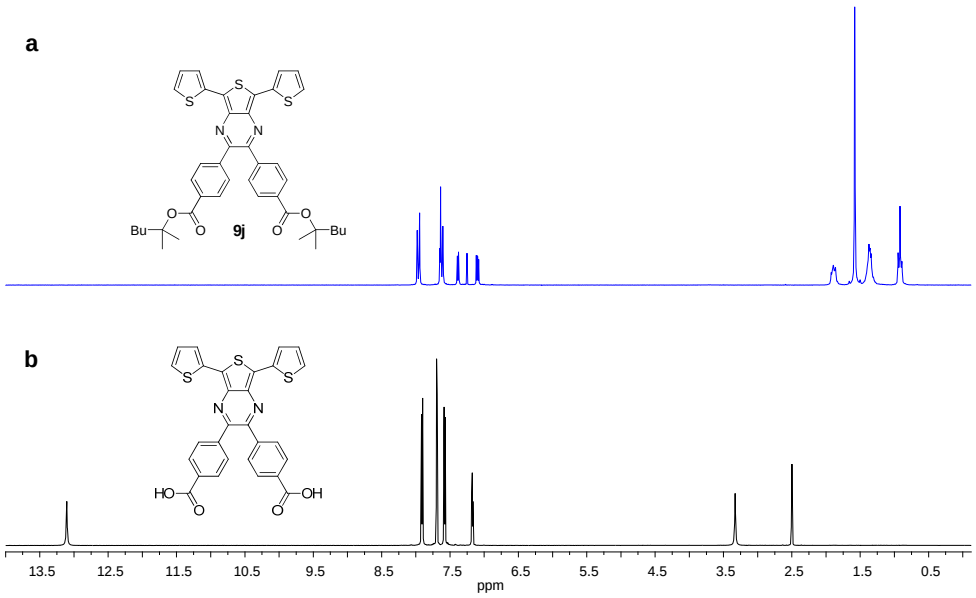

Figure 3.4. ^{1}H NMR spectra of 6j (a) from before ($CDCl_3$) and after (b) heating (DMSO-d_6) to 233 °C for 15 min under argon.

Since all these fragments have multiple unsaturations after the elimination we ascribe this to polymerization reactions of these materials in the matrix of the material or to cross-linking. Analysis of the materials after the first weight loss by NMR was used to establish whether the ester could be used efficiently as a solubilizing group that can be removed quantitatively by a simple thermal treatment. NMR analysis after heating compound **9a-m** at the temperature of the first weight loss for 15 min. under argon showed that compounds **9a**, **9e-h**, **9m** could not be used for the preparation of the diacid. While the esters may eliminate liberating an alkene

the materials also decompose at the given temperature. The ^{1}H NMR spectra of **9j** from before and after the pyrolysis clearly shows that the diester has been transformed into the diacid (Figure 3.4). Figure 3.4b shows no aliphatic protons and the protons from the carboxylic acid appear at 13.08 ppm

From the TGA-MS data it was possible to track evolution of various small molecules and fragments as a function of the temperature. As expected the signals for the observed fragments peak is in the same temperature range as the weight losses. The mass signals that we focused on were carbon dioxide and fragments for even and uneven alkenes. As shown earlier[14] for tertiary esters of polythiophene several weight loss mechanisms may be observed and the advantage of studying the monomer was that the effects of the polymer matrix on the weight loss mechanisms were possibly eliminated. The primary ester showed loss of both alkene and carbon dioxide starting at around 300 °C peaking at around 400 °C. For the secondary alkyl esters two loss mechanisms could be distinguished as elimination of the ester at the lower temperature (around 300 °C) and loss of carbon dioxide at a higher temperature (425 °C). The weight loss of the secondary alkyl esters corresponded well with the calculated loss while some decarboxylation was evident from a small mass peak of carbon dioxide during the first loss peak. The secondary esters with unsaturations, branching, fluorine and methoxy substituents showed more complex weight loss curves. It would seem that the only useful materials in this series are the simple secondary and tertiary esters. In terms of achieving a lower temperature for the thermocleavage this limits the choice to simple tertiary esters. The only secondary ester that works well is the ester with a phenyl group R to the alcohol and no other unsaturations. As discussed above the simplest secondary alcohol with an R-phenyl group gives styrene upon elimination and this gave an incomplete weight loss. While successfully achieving a lower temperature of elimination this alone does not grant usefulness. The elimination reaction also has to complete the weight loss and the polymer material that is the end product should be insoluble.

3.4 Photovoltaic performance

All of the polymer materials presented in Scheme 3.1 were intended for use in solar cell devices. Some of the polymer materials however were not very soluble and did not process well into films and the photovoltaic performance obtained for these were either not possible

to establish or very poor. Consequently only **11b**, **11c**, **11d**, and **11j** were studied in solar cells. Bulk heterojunction solar cells with an active area of 3 cm^2 were prepared on an indium tin oxide (ITO) covered glass substrate, using conventional device architecture. A thin layer of poly(3,4-ethylenedioxythiophene)–poly-(styrenesulfonate) (PEDOT-PSS) was spin coated on top of the ITO coating followed by spin coating of the active layer. The active layer contained a blend of the respective polymer and [60]PCBM. After spin coating of the active layer the devices were either processed directly into a solar cell by evaporation of aluminium as back electrode or subjected to a thermal treatment at the temperature of thermocleavage immediately before evaporation of the back electrode.

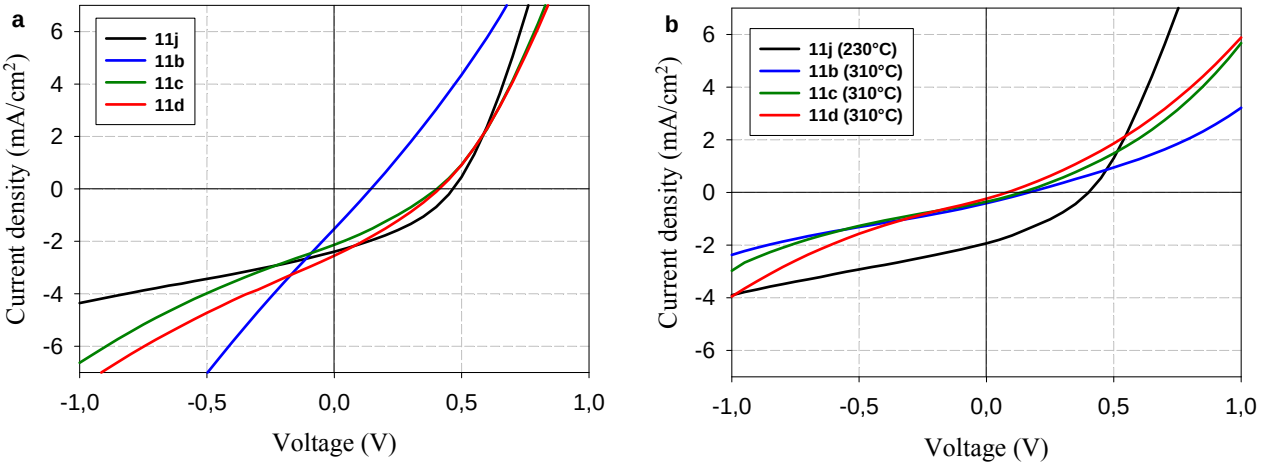

Figure 3.5. (a) *J-V* characteristics of the **11b**:PCBM, **11c**:PCBM, **11d**:PCBM and **11j**:PCBM solar cells measured under 100 mW/cm^2 white light before and (b) after a thermal treatment.

Table 3.3. Photovoltaic performance of devices based on blends of polymer and PCBM

Polymer	Cleaving Temp. (°C)*	J_{sc} (mA/cm^2)	V_{oc} (V)	FF	PCE (%)
11b	25	1.52	0.14	0.25	0.05
	310	0.41	0.16	0.26	0.017
11c	25	2.1	0.4	0.29	0.25
	310	0.36	0.14	0.27	0.013
11d	25	2.55	0.41	0.29	0.3
	310	0.24	0.08	0.26	0.005
11j	25	2.4	0.46	0.36	0.4
	230	1.94	0.4	0.33	0.25

*The duration of cleaving at 230 °C was 1 minute and at 310 °C was 10 minutes

The obtained current–voltage curves are presented in figure 3.5 which shows the current–voltage characteristics of the un-cleaved and cleaved **11b**:PCBM, **11c**:PCBM, **11d**:PCBM and **11j**:PCBM devices measured under 100 mW/cm^2 white light. A general observation was that the devices performed significantly worse after thermocleavage as indicated by a decrease in voltage and current (Table 3.3). The best performing material was **11j**, which show a decreased performance upon thermocleavage, but maintained a significant performance. It should be noted that polymer solar cells based on thermocleavable materials present additional complexity in terms of processing as compared to materials such as P3HT. In the case of P3HT heating of the device film leads to crystallization and changes in the morphology of the device film that significantly influences the device performance. In the case of thermocleavable materials these effects also take place, but in addition, the chemistry of the device film change and as the chemistry changes so do the processes relating to crystallization and changes in morphology. This has been observed in the case of P3MHOCT (see Chapter 2) where the chemistry of the device film can be processed into three distinct forms starting from the same device film. This allowed for the preparation of devices with a power conversion efficiency of up to 1.5%. This implies that not only the temperature of thermal annealing and the duration but also the speed of heating becomes influential. In the case of the polymers presented here the polymer esters are all chemically different materials and heating them to the temperature of thermocleavage gives, in principle, the same product polymer **12** (Figure 3.6).

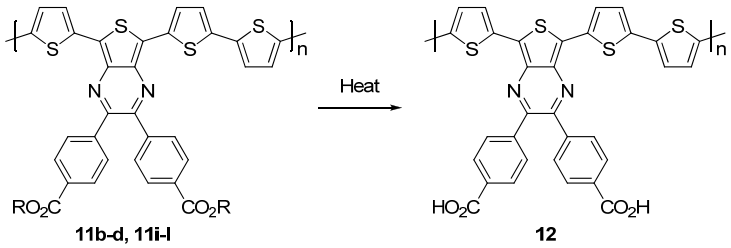

Figure 3.6. Thermocleavage of the polymer materials

The difference in device performance is thus not related to the molecule but rather how the final device film was obtained. Thus the same material can present different levels of performance depending on how it was processed. The chemistry of the side chains may influence the morphology before thermocleavage, and if the process of thermocleavage is faster than the changes in morphology upon heating, this may also allow for the preparation

of different final film morphologies. It has been shown that the morphology is stable in the final thermocleaved form when using a temperature of thermocleavage[15] below the glass transition temperature (T_g)* and the kinetics of the film formation in such a case is important. A final issue is the completion of the thermocleavage in the final film. It is likely that thermocleavage under a given set of conditions lead only to a partially cleaved film that then present chemistry corresponding to both the uncleaved and cleaved material to varying degrees.[16] Thus a detailed study of varying the degree of thermocleavage warrants further study. The drastic decrease of the performance for polymers **11b**, **11c** and **11d** is probably due to high cleaving temperature (310 °C) and long cleaving time (10 min), while thermocleavage of **11j** resulted in a minor decrease of performance. In the case of earlier reported cleaving of P3MHOCT (see Chapter 2) the performance dropped around 10-fold when cleaved to P3CT and then improved 15-fold when cleaved further to PT.[16]

3.5 Stability Studies

We chose to subject the best performing material **11j** to detailed stability studies. Polymer solar cells are inherently unstable under intense illumination and will degrade through a large number of coexisting paths. Some of the paths involve reactants such as water and oxygen from the atmosphere that will dominate the course of degradation if allowed to access the active layer during operation. Their efficient removal efficiently eliminates the associated degradation processes, and other slower processes become readily observable (ie. morphological changes, interlayer diffusion, reactions at interfaces, photochemistry). To get an overview of the stability of the polymer **11j** in relation to other known polymers and as a function of atmospheric reactants we performed two studies. One comparative study in an inert atmosphere and a study where devices were subjected to different atmospheres during continuous (uninterrupted) illumination. Figure 3.7 shows the degradation of devices prepared in the same manner employing respectively P3HT, PT, and **11j**. The performance of **11j** is inferior to both P3HT and PT while the photovoltaic parameters are much more stable in time. The P3HT device was annealed at 150 °C for 5 min after evaporation of the aluminum electrode. PT devices were prepared by heating P3MHOCT/PCBM films to 310 °C before evaporation of the aluminum electrode.

* The glass transition is the temperature where the polymer goes from a hard, glass like state to a rubber like state.

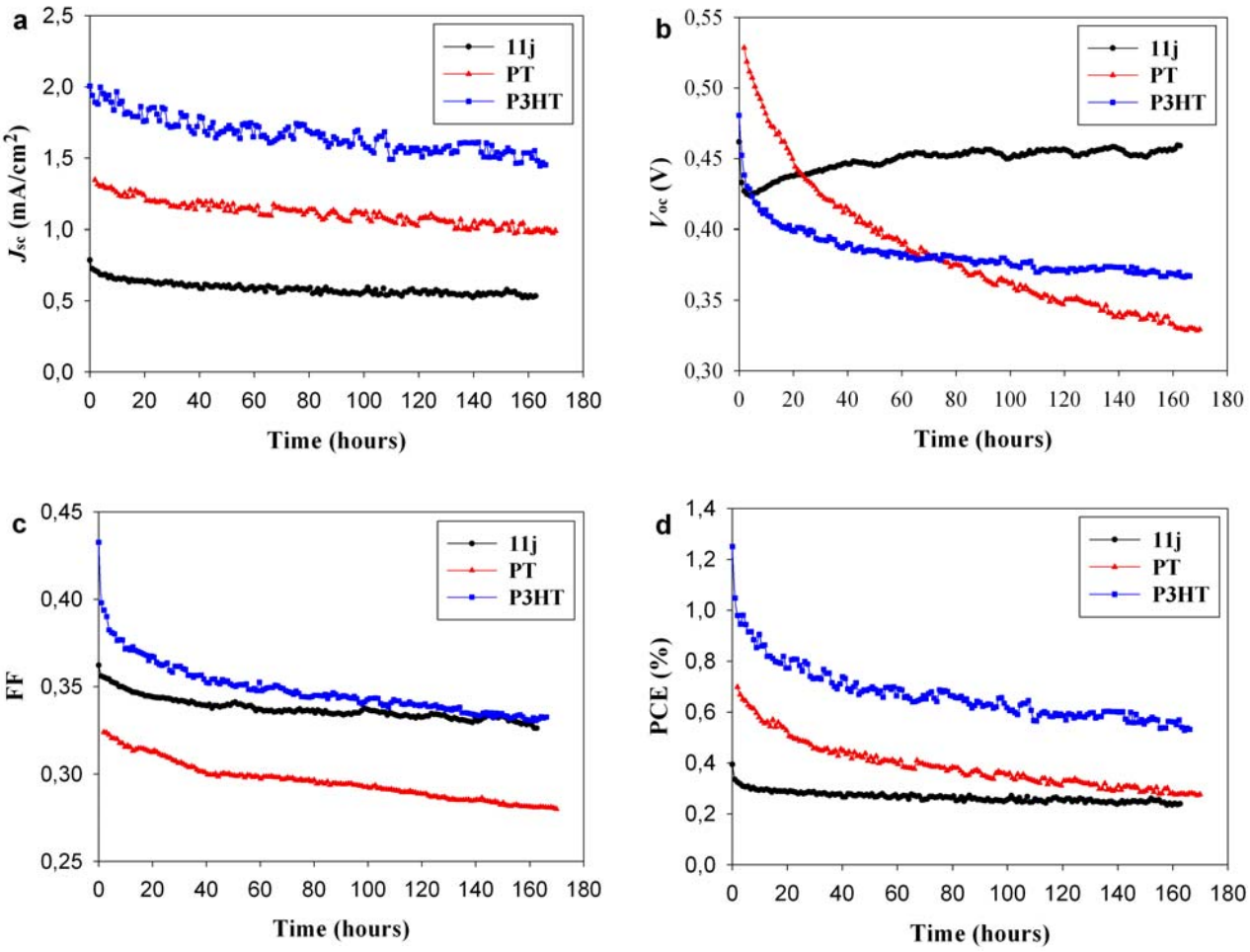

Figure 3.7. Comparison of the decay of the photovoltaic parameters for P3HT, PT, and **11j** polymers with a Glass/ITO/PEDOT:PSS/polymer:PCBM/Al device geometry in a nitrogen atmosphere (330 mW/cm^2, 30 °C, oxygen <2 ppm, water <2 ppm).

The decay in the photovoltaic parameters were not affected significantly by the thermocleavage at 230 °C and the stability of **11j** is thus concluded to be very good without cleavage while there are processing advantages of thermocleaved **11j**. Cleaving **11j** at a higher temperature (310 °C) reduced the photovoltaic performance drastically and the decay of V_{oc} and FF was much faster. When subjecting **11j** devices to four different atmospheres to establish the inherent stability in nitrogen and the effect of water and oxygen taken separately and finally in combination in the real atmosphere it was found that oxygen had little effect on the stability as shown in Figure 3.8. The interesting finding was that the presence of pure oxygen at high concentration (i.e., five times more than in the ambient atmosphere) does not seem to speed up degradation significantly so you could rate **11j** as stable toward oxygen under illumination. Humidity however was found to profoundly influence the stability leading

to rapid degradation that is complete within less than 20 hours whereas the absence of water leads to moderately stable operation.

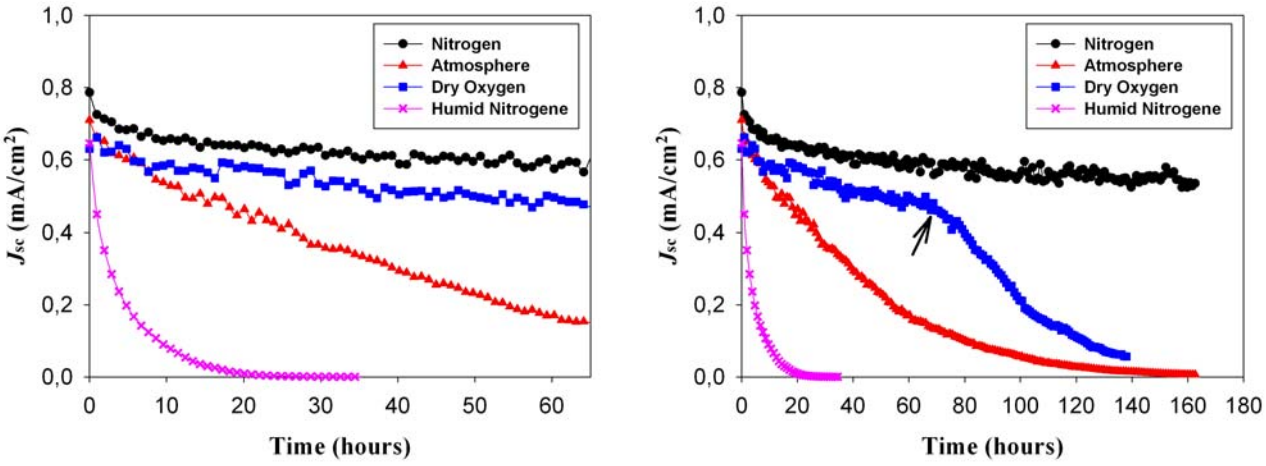

Figure 3.8. Decay of devices with configuration Glass/ITO/PEDOT:PSS/**8j**:PCBM/Al under conditions of: pure nitrogen atmosphere 99.999% (oxygen < 2 ppm, humidity < 2 ppm), dry oxygen atmosphere 99.5% (humidity < 2 ppm), ambient atmosphere (20 ± 5 % relative humidity), humid nitrogen 99.999% (oxygen < 2 ppm, 95 ± 5% relative humidity). The temperature was 30 ± 2 °C and the incident light intensity was 330 mW/cm^2 (left). The same experiment was repeated for a longer period of time while introducing ambient atmosphere after 70 hours (see arrow) thus reducing the oxygen level by a factor of 5 and increasing the humidity by a factor of 10 whereupon rapid degradation sets in thereafter (right).

3.6 Conclusion

In conclusion, the results from this work demonstrate that the application of esters as solubilizing groups that allow for removal by a simple thermal treatment is limited to simple secondary and tertiary esters where the alcohol is saturated in order to ensure that the alkene that is eliminated is removed efficiently without undesired side reactions. The lowest temperatures of elimination were found to be achieved when employing tertiary esters as expected. In contrast to the systems where the ester reside on a thiophene ring it was found that no decarboxylation takes place prior to decomposition, and it is thus not possible to access the native system without the carboxylic acid groups by a thermal treatment. It was showed that a monomer relevant to low band gap polymer systems could be prepared with solubilizing groups that allow for removal by a thermal treatment of around 200-225 °C. In addition the polymer materials from the monomers was synthesized and it was found that

only the polymers with secondary and tertiary esters are useful and the solubility requirements make the choice of side chain functionality limited. The best performing polymer in a bulk heterojunction solar cell was **11j** with J_{sc} = 2.4 mA/cm^2, V_{oc} = 0.46 V, FF = 0.36 and η = 0.4%. It shows a decreased performance upon thermocleavage, but maintained a significant performance. The operational stability of **11j** was found to be very good compared to model materials such as P3HT and PT. In addition polymer solar cells in a glass/ITO/PEDOT:PSS/**11j**:PCBM/Al device geometry were found to be very stable toward oxygen during operation. In pure oxygen the device decay was similar to inert conditions. This is in stark contrast to conjugated materials containing vinylene bonds that are very sensitive towards oxygen (see Chapter 2). The devices decayed rapidly in the presence of water (with and without oxygen present) and removal of water from this type of device gives devices with good stability.

3.7 Experimental section

^{1}H-NMR and ^{13}C-NMR spectra together with figures showing TGA and TGA-MS data are included in the Supporting Information.[17]

General methods. Molecular weights were determined using size exclusion chromatography in HPLC-grade chloroform against polystyrene standards on a KNAUER chromatograph with a refractive index detector and a diode array UV-vis detector. The samples were dried at 50 ^{o}C for 24 hours in a vacuum oven prior to analysis. Unless stated otherwise all reagents and solvents were obtained from Aldrich and used without further purification. Dichloromethane and pyridine were dried with molecular sieves (3 Å) and used directly without filtration or distillation. NBS was recrystallised from water and dried at 70 °C in vacuum. Evaporation was performed on a rotary evaporator at 40 °C. NMR spectra were obtained on 500 MHz or 250 MHz spectrometers. High resolution mass spectra were recorded on a tandem mass spectrometer. Melting points were determined on an electrothermal instrument and are uncorrected. The diamino precursor **8** was prepared as described in the literature.[10]

Thermal analysis. The sample holders were carefully weighed and the samples introduced followed by drying for 24 hours at 50 ˚C in vacuum. The thermogravimetric analysis was then carried out using heating rate of 10 ˚C min^{-1}. The carrier gas used was argon and the exhaust gasses were passed through a mass spectrometer allowing for the simultaneous acquisition of mass data. A series of masses relevant to the degradation process were specifically followed such as CO_2, alkyl chain fragments and fluorine when relevant (see supporting information for each material). TGA-MS was performed with a 30 seconds integration time for all the analyzed compounds at *m/z* 17, 18, 19, 25, 27, 28, 31, 33, 40, 41, 44, 45, 50, 51, 52, 53, 55, 56, 57, 58, 59, 66, 68, 69, 72, 77, 78, 80, 83, 84, 97, 98, 104, 111, 126. The elimination temperature has been read at the maximum of the derivative curve if possible. The weight loss (Found) has been read at the most abundant derivative peak (Weight (%)[peakstart] – Weight (%)[peakend]).

Polymer solar cell fabrication and analysis. Glass substrates with pre-etched 100 nm thick layer of ITO and a sheet resistivity of 8-12 Ω $square^{-1}$ purchased from LumTec were cleaned by consecutive ultrasonication in isopropanol and distilled water for 10 min each followed by drying immediately prior to use. A layer of PEDOT:PSS purchased from Aldrich as a 1.3 wt % aqueous solution was spin coated on top of ITO at a rotational speed of 2800 rpm and the slides were annealed at 160 ^{o}C for 5 min. Subsequently, the samples were transported into a glove box and the active layer was applied as a blend of the polymer and [60]PCBM in a 1:1 ratio (20 mg mL^{-1} in dichlorobenzene) by spin coating onto the glass/ITO/PEDOT:PSS substrates. The samples were then dried at room temperature (25 °C) or heated to the desired cleaving temperature (see table 3.2). An aluminum metal electrode was evaporated on top after the thermal annealing to complete the devices. The devices had an active area of 3 cm^2 and were tested for photovoltaic performance and stability. The photovoltaic performance was tested under a solar simulator (KHS575) where the irradiance and emission spectrum was checked carefully using an optical spectrum analyzer in conjunction with a precision radiometer from Eppley Laboratories. The spectrum during characterization of the solar cell efficiency was AM1.5G with an incident light power of 1000 W m^{-2}. The solar simulator is Class AAA from 400-800 nm, over the area of the cell and for the duration of the experiment. No corrections for mismatch were performed.

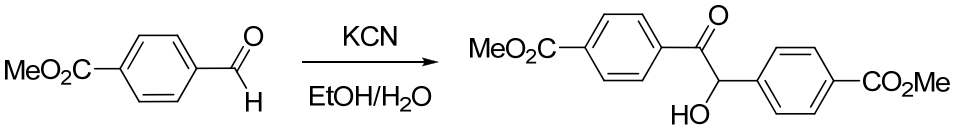

1 2

4,4'-bis(methyloxycarbonyl)benzoin (2). Methyl 4-formylbenzoate (**1**) (50 g, 305 mmol, 1 equiv) was stirred in 99 % ethanol (150 ml) and water (50 ml). Then potassium cyanide (6 g, 92.1 mmol, 0.3 equiv) was added and the reaction mixture was stirred at room temperature for 15 min. The product was filtered, washed with water (3 × 200 ml) and dried at 70 °C in vacuum. Yield: 48 g (48 %), light yellow solid. M_p = 140-141 °C. ^{1}H-NMR (DMSO-d$_6$): δ = 8.09 (d, 2H, J = 8.6 Hz), 8.00 (d, 2H, J = 8.6 Hz), 7.90 (d, 2H, J = 8.3 Hz), 7.55 (d, 2H, J = 8.3 Hz), 6.46 (s, 1H), 6.15 (s, 1H), 3.84 (s, 3H), 3.80 (s, 3H). ^{13}C-NMR (DMSO-d$_6$): δ = 199.0, 166.4, 165.9, 145.0, 138.8, 133.7, 129.7, 129.7, 129.6, 129.5, 127.9, 76.2, 52.9, 52.5.

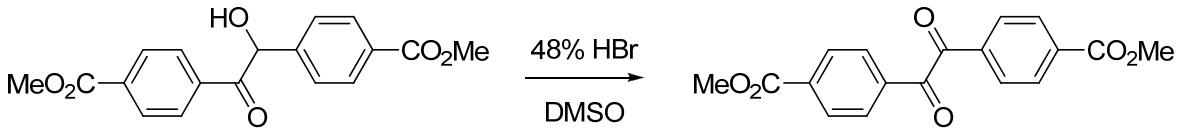

2 3

4,4'-bis(methyloxycarbonyl)benzil (3). To a stirred solution of **2** (74 g, 225 mmol) in DMSO (510 ml) was added slowly 105 ml 48 % aqueous hydrobromic acid. The solution was heated to 55 °C for 24 hours. Then 500 ml water was added and the product was filtered, washed with water (3 × 200 ml) and dried at 70 °C in vacuum. Yield: 72.5 g (99 %), yellow solid. M_p = 197-198 °C. ^{1}H-NMR ($CDCl_3$): δ = 8.19 (d, 4H, J = 7.5 Hz), 8.06 (d, 4H, J = 7.5 Hz), 3.97 (s, 6H). ^{13}C-NMR ($CDCl_3$): δ = 192.9, 165.8, 135.7, 135.5, 130.1, 129.9, 52.7.

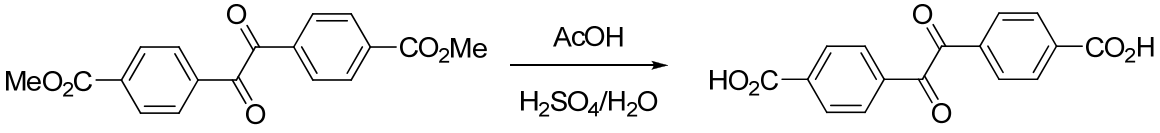

3

4,4'-bis(hydroxycarbonyl)benzil. 3 (5 g, 15.3 mmol) was mixed in acetic acid (350 ml) and a 4:1 H_2SO_4/H_2O solution (175 ml). The reaction mixture was heated to reflux and stirred for 10 hours. Then 250 ml water was added and the mixture was cooled on ice. After cooling the diacid was filtered, washed with water (3 × 20 ml) and dried at 70 °C in vacuum. Yield: 4.5 g (98 %), pale yellow solid. M_p > 300 °C. ^{1}H-NMR (DMSO-d$_6$): δ = 13.54 (s, 2H), 8.15 (d, 4H, J =

7.0 Hz), 8.08 (d, 4H, *J* = 7.0 Hz). ^{13}C-NMR (DMSO-d_6): δ = 193.8, 166.8, 136.9, 135.5, 130.5, 130.5.

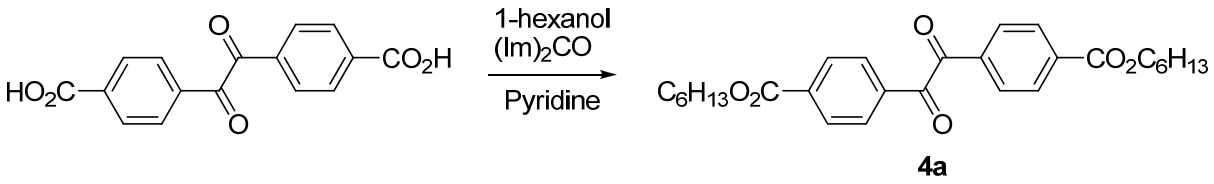

4a

General procedure for the preparation of primary and secondary diesters (Method A)

4,4'-bis(hexyloxycarbonyl)benzil (4a). The diacid 4,4'-bis(hydroxycarbonyl)benzil (500 mg, 1.68 mmol, 1 equiv) and 1,1´-carbonyldiimidazole (557 mg, 3.44 mmol, 2.05 equiv) was mixed in dry pyridine (5 ml) and stirred at 50 °C under argon for 1 hour. Then 1-hexanol (439 µl, 3.52 mmol, 2.1 equiv) was added and the reaction mixture was heated to reflux for 10 hours. After ended reaction pyridine was evaporated in vacuum. The residue was added saturated $NaHCO_3$ (30 ml) and extracted with ether (3 × 30 ml). The combined organic phase was dried ($MgSO_4$), filtered and concentrated in vacuum. Dry column chromatography (silica gel 15-40 µm, eluted with EtOAc/Heptane, gradient 1-5% EtOAc) afforded **4a**. Yield: 625 mg (80 %), yellow solid. M_p = 140-141 °C. ^{1}H-NMR ($CDCl_3$): δ = 8.18 (d, 4H, *J* = 8.5 Hz), 8.05 (d, 4H, *J* = 8.5 Hz), 4.36 (t, 4H, *J* = 6.7 Hz), 1.83-1.74 (m, 4H), 1.49-1.39 (m, 4H), 1.39-1.29 (m, 8H), 0.95-0.86 (m, 6H). ^{13}C-NMR ($CDCl_3$): δ = 192.9, 165.4, 135.9, 135.7, 130.1, 129.8, 65.9, 31.4, 28.6, 25.6, 22.5, 13.9. HRMS-FAB: *m/z* calcd. for $C_{28}H_{35}O_6$ $[M+H]^+$ 467.2434, found 467.2430.

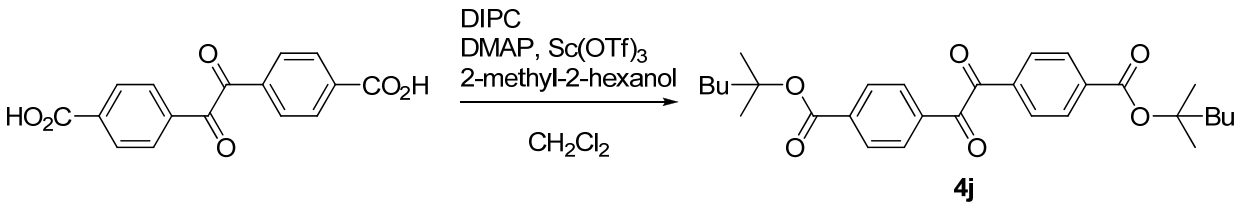

4j

General procedure for the preparation of tertiary diesters (Method B)

4,4'-bis(2-methylhexan-2-yloxycarbonyl)benzil (4j). A suspension of the diacid 4,4'-bis(hydroxycarbonyl)benzil (300 mg, 1.01 mmol, 1 equiv), DMAP (258 mg, 2.11 mmol, 2.1 equiv), scandium triflate (49.5 mg, 0,101 mmol, 0.1 equiv) and 2-methyl-2-hexanol (302 µl, 2.11 mmol, 2.1 equiv) in dry methylene chloride (5 ml) was stirred at room temperature under argon for 30 min. *N,N'*-diisopropylcarbodiimide (331 µl, 2.11 mmol, 2.1 equiv) was added and the reaction mixture was heated to reflux and stirred for 24 hours. After cooling to

room temperature the reaction mixture was concentrated on celite in vacuum. Dry column chromatography (silica gel 15-40 µm, eluted with EtOAc/Heptane, gradient 1-5% EtOAc) afforded **4j**. Yield: 388 mg (78 %), yellow oil. ^{1}H-NMR ($CDCl_3$): δ = 8.08 (d, 4H, J = 8.5 Hz), 7.99 (d, 4H, J = 8.5 Hz), 1.92-1.80 (m, 4H), 1.55 (s, 12H), 1.42-1.25 (m, 8H), 0.94-0.82 (m, 6H). ^{13}C-NMR ($CDCl_3$): δ = 193.1, 164.2, 137.5, 135.5, 129.9, 129.6, 84.4, 40.6, 26.1, 26.0, 22.9, 13.9. HRMS-FAB: *m/z* calcd. for $C_{30}H_{39}O_6$ $[M+H]^+$ 495.2747, found 495.2735.

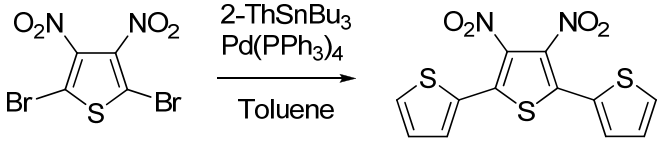

6 **7**

3',4'-Dinitro-2,2';5',2''-terthiophene (7). 2-Tributylstannylthiophene (5.8 g, 16 mmol) and 2,5-dibromo-3,4-dinitrothiophene (**6**) (2.6 g, 7.8 mmol) were mixed in toluene (20 mL) together with $Pd(PPh_3)_4$ (200 mg) and heated to reflux for 16 hours. Toluene was removed in vacuum to give a slurry. This was taken up in chloroform (ca. 200mL) and filtered through a layer of silica to remove a dark band. The silica was eluted with chloroform until the washings were almost colourless. The solvent was removed from the reddish liquid in vacuum and the remaining paste was mixed with heptane (50 mL) and filtered. The orange solid was washed with heptane and dried in vacuum. Yield: 2.45 g (92%), orange solid. ^{1}H-NMR ($CDCl_3$): δ = 7.62 (dd, J = 5.2 Hz, J = 1.1 Hz, 2H), 7.55 (dd, J = 3.6 Hz, J = 1.1 Hz, 2H), 7.18 (dd, J = 5.2 Hz, J = 3.6 Hz, 2H). ^{13}C-NMR ($CDCl_3$): δ = 133.9, 131.3, 131.1, 128.4, 128.0.

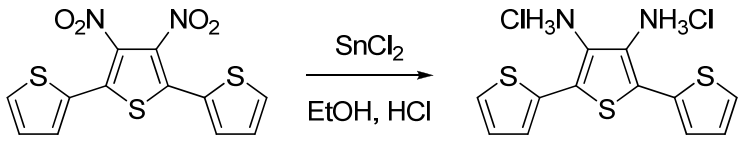

7 **8**

2,2';5',2''-terthiophene-3',4'-diaminium chloride (8). 7 (5 g, 14.8 mmol) and $SnCl_2$ (22.4 g, 118 mmol) was mixed in ethanol (60 ml) and concentrated HCl (25 ml). The reaction mixture was stirred at room temperature overnight. Ethanol was removed in vacuum and the remaining paste was filtered. The yellow/brown solid was washed extensively with water and dried at 70 °C in vacuum. Yield 4.5 g (87%). ^{1}H-NMR (CD_3OD) δ = 7.54 (dd, J = 5.2 Hz, J = 1.1 Hz, 2H), 7.29 (dd, J = 3.6 Hz, J = 1.1 Hz, 2H), 7.18 (dd, J = 5.2 Hz, J = 3.6 Hz, 2H), 4.95 (s, NH_x and

H_2O). ^{13}C-NMR (CD_3OD): δ = 132.3, 128.0, 126.54, 126.4, 126.3, 119.0. Anal. Calcd for C12H10N2S3: C, 51.77; H, 3.62; N, 10.06. Found: C, 51.93; H, 3.41; N, 10.01.

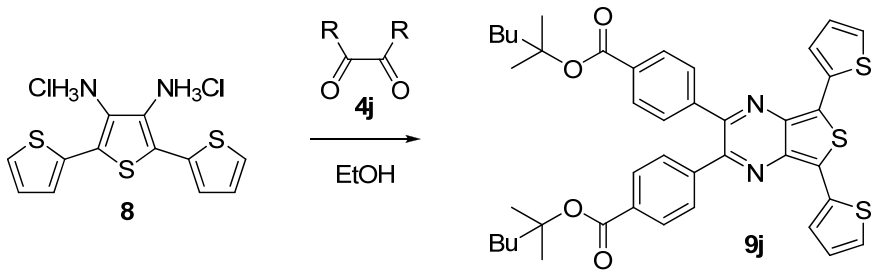

General procedure for the condensation bis(2-methylhexan-2-yl)-4,4'-(5,7-di(thiophen-2-yl)thieno-[3,4-*b*]pyrazine-2,3-diyl)-dibenzoate (9j). 4j (567 mg, 1.15 mmol, 1 equiv), **8** (444 mg, 1.26 mmol, 1.1 equiv) and triethylamine (3.44 mmol, 0.480 ml, 3 equiv) was mixed in 99 % ethanol (20 ml). The reaction mixture was heated to reflux and stirred for 15 hours. After ended reaction the mixture was cooled on ice followed by filtration of the product. The product was washed with 99 % ethanol (3 × 5 ml) and dried at 50 °C in vacuum. Yield: 730 mg (86 %), dark purple solid. M_p = 197-198 °C. ^{1}H-NMR ($CDCl_3$): δ = 7.97 (d, 4H, J = 8.3 Hz), 7.67-7.60 (m, 6H), 7.40 (dd, 2H, J = 5.1, 1.0 Hz), 7.11 (dd, 2H, J = 5.1, 3.7 Hz), 1.96-1.86 (m, 4H), 1.60 (s, 12H), 1.44-1.34 (m, 8H), 0.94 (t, 6H, J = 6.9, 6.9 Hz). ^{13}C-NMR ($CDCl_3$): δ = 165.0, 151.3, 142.6, 137.3, 134.5, 132.4, 129.8, 129.3, 127.3, 126.9, 125.6, 124.9, 83.7, 40.8, 26.2, 26.1, 23.0, 14.0. HRMS-FAB: *m/z* calcd. for $C_{42}H_{44}N_2O_4S_3$ $[M+H]^+$ 736.2463, found 736.2466.

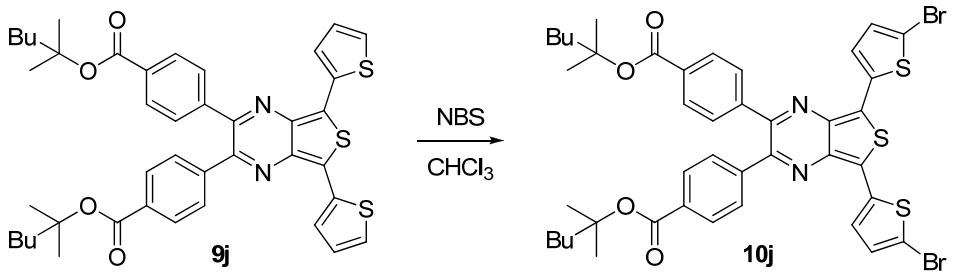

General procedure for the NBS bromination bis(2-methylhexan-2-yl)-4,4'-(5,7-bis(5-bromothiophen-2-yl)thieno[3,4-*b*]pyrazine-2,3-diyl)dibenzoate (10j). 9j (1 g, 1.36 mmol, 1 equiv) was dissolved in dry chloroform (70 ml). Then NBS (483 mg, 2.71 mmol, 2 equiv) was added slowly and the reaction mixture was stirred at room temperature in the dark for 20 min. After ended reaction the mixture was

washed with water (3 × 50 ml), dried ($MgSO_4$), filtered and concentrated in vacuum affording **10j**. Yield: 1.13 g (93 %), dark purple solid. M_p = 185-186 °C. ^{1}H-NMR ($CDCl_3$): δ = 7.98 (d, J = 8.4 Hz, 4H), 7.58 (d, J = 8.4 Hz, 4H), 7.22 (d, J = 4.0 Hz, 2H), 7.01 (d, J = 4.0 Hz, 2H), 1.97-1.87 (m, 4H), 1.61 (s, 12H), 1.46-1.33 (m, 8H), 0.94 (t, J = 7.0 Hz, 6H). ^{13}C-NMR ($CDCl_3$): δ = 165.1, 152.0, 142.1, 137.3, 135.6, 132.7, 129.9, 129.8, 129.3, 124.8, 124.3, 115.1, 83.8, 40.8, 26.2, 26.1, 23.0, 14.0. HRMS-FAB: *m/z* calcd. for $C_{42}H_{42}Br_2N_2O_4S_3$ [M]+ 892.0673, found 892.0670.

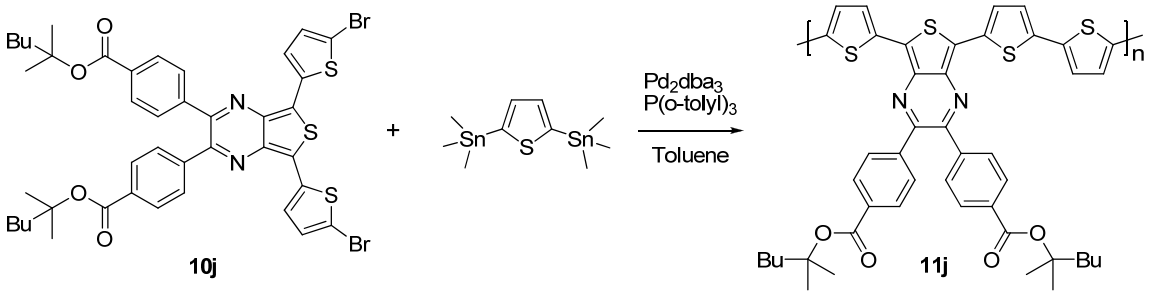

General procedure for the Stille coupling polymerisation

Poly(bis(2-methylhexan-2-yl)-4,4'-(5-(2,2'-bithiophen-5-yl)-7-(thiophen-2-yl)thieno-[3,4-b]pyrazine-2,3-diyl)dibenzoate) (11j). 10j (200 mg, 0.22 mmol, 1 equiv), 2,5-bis(trimethylstannyl)thiophene (92 mg, 0.22 mmol, 1 equiv), Pd_2dba_3 (20 mg, 0.022 mmol, 0.1 equiv) and tri-(o-tolyl)phosphine (54 mg, 0.18 mmol, 0.8 equiv) was dissolved in dry toluene (50 ml). The reaction mixture was heated to reflux for 24 hours under argon. Then the mixture was poured into 150 ml methanol and the polymer was allowed to precipitate. Finally the polymer **11j** was filtered and purified by Soxhlet extraction with methanol, hexane and chloroform. Yield: 670 mg (92 %), dark green solid. ^{1}H-NMR (CD_2Cl_2): δ = 8.18 – 6.37 (br, 14H), 2.30 – 0.45 (br, 30H). SEC ($CHCl_3$): M_w = 39400 g/mol, M_n = 20400, M_p = 17800, PDI = 1.9

3.8 References

1. Babu, S. A.; Yasuda, M.; Okabe, Y.; Shibata, I.; Baba, A. *Organic Letters* **2006,** *8* (14), 3029-3032.
2. Floyd, M. B.; Du, M. T.; Fabio, P. F.; Jacob, L. A.; Johnson, B. D. *J. Org. Chem.* **1985,** *50* (25), 5022-5027.
3. Shono, T.; Kise, N.; Nomura, R.; Yamanami, A. *Tetrahedron Lett.* **1993,** *34* (22), 3577-3580.
4. Armesto, D.; Horspool, W. M.; Ortiz, M. J.; Perez-Ossorio, R. *Synthesis* **1988,** *1988* (10), 799-801.
5. Takimoto, S.; Inanaga, J.; Katsuki, T.; Yamaguchi, M. *Bull. Chem. Soc. Jpn.* **1976,** *49* (8), 2335-2336.
6. Mukaiyama, T.; Matsueda, R.; Suzuki, M. *Tetrahedron Lett.* **1970,** (22), 1901-1904.
7. Mukaiyama, T.; Usui, M.; Shimada, E.; Saigo, K. *Chem. Lett.* **1975,** (10), 1045-1048.
8. Liu, J. S.; Kadnikova, E. N.; Liu, Y. X.; McGehee, M. D.; Fréchet, J. M. J. *J. Am. Chem. Soc.* **2004,** *126* (31), 9486-9487.
9. Zhao, H.; Pendri, A.; Greenwald, R. B. *J. Org. Chem.* **1998,** *63* (21), 7559-7562.
10. Petersen, M. H.; Hagemann, O.; Nielsen, K. T.; Jørgensen, M.; Krebs, F. C. *Sol. Energy Mater. Sol. Cells* **2007,** *91* (11), 996-1009.
11. Kenning, D. D.; Mitchell, K. A.; Calhoun, T. R.; Funfar, M. R.; Sattler, D. J.; Rasmussen, S. C. *J. Org. Chem.* **2002,** *67* (25), 9073-9076.
12. Houtman, J. P. W.; Vansteenis, J.; Heertjes, P. M. *Recueil des Travaux Chimiques des Pays-Bas-Journal of the Royal Netherlands Chemical Society* **1946,** *65* (10-1), 781-788.
13. Chuchani, G.; Martin, I.; Hernandez, J. A.; Rotinov, A.; Fraile, G.; Bigley, D. B. *J. Phys. Chem.* **1980,** *84* (9), 944-948.
14. Bjerring, M.; Nielsen, J. S.; Nielsen, N. C.; Krebs, F. C. *Macromolecules* **2007,** *40* (16), 6012-6013.
15. Andreasen, J. W.; Jørgensen, M.; Krebs, F. C. *Macromolecules* **2007,** *40*, 7758-7762.
16. Gevorgyan, S. A.; Krebs, F. C. *Chem. Mater.* **2008,** *20* (13), 4386-4390.
17. Petersen, M. H.; Gevorgyan, S. A.; Krebs, F. C. *Macromolecules* **2008,** *41* (23), 8986-8994.

Chapter 4

Photovoltaic performance of polymers based on dithienyl-thienopyrazines bearing thermocleavable benzoate esters*

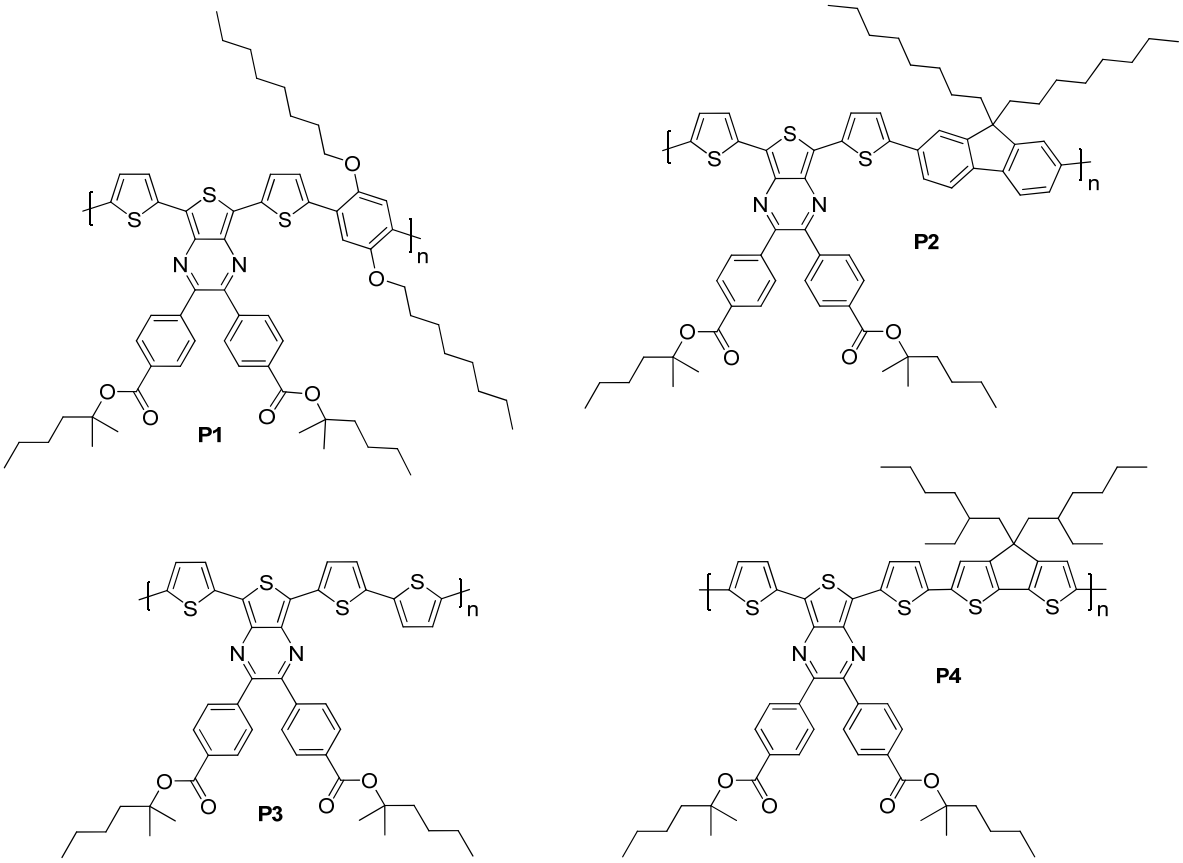

Figure 4.1. Low band gap polymers based on dithienylthienopyrazine alternating with different donor segments.

* This work has been published: Helgesen M.; Krebs, F. C. *Macromolecules* **2010,** *43,* 1253-1260

4.1 Introduction

Low band gap polymers are designed to match the solar emission spectrum better, which has a maximum in photon flux near 700 nm and an appreciable tail stretching into the infra-red region. The extended absorption by low band gap polymers can potentially increase the photocurrent by absorbing more photons. One approach to designing these materials is by use of alternating electron-rich (donor) and electron-poor (acceptor) units giving rise to a material with a low-energy absorption band that might be a charge transfer band. The absorption can be tuned by adjusting the donor–acceptor strengths, or HOMO-LUMO levels, respectively. For this purpose, polymers with alternating dithiophene and thienopyrazine units has been explored by several groups[1-3] who reports band gaps in the range 1.2–1.6 eV for this type of polymer. In our earlier work (see Appendix 2),[1] we explored the chemistry of the thienopyrazine type acceptor moiety to characterize the influence of the substituents and extended *p*-system on the absorption spectrum. Here we found that adding phenyl groups to the dithienylthienopyrazine system caused a red shift of the lowest energy absorption band with up to 50 nm, presumably due to the more extended conjugation.

In this chapter the synthesis, characterization and devices of a series of alternating thermoclevable copolymers for solar cells are presented. The materials are copolymers based on dithienylthienopyrazine, bearing thermocleavable benzoate esters on the pyrazine ring, alternating with different donor segments; dialkoxybenzene, fluorene, thiophene and cyclopentadithiophene (CPDT) (Figure 4.1). The effects of the different donor segments on the photovoltaic performance of the polymers in blends with [60]PCBM with and without thermal treatment is presented. The alkyl benzoate ester groups make the polymer soluble in organic solvents and allow for film formation. Subsequently they can be removed by heating in a post-processing step forming the free acid and a volatile alkene. These new thermocleavable low band gap materials can potentially offer better light harvesting, higher level processing and improved stability in a solar cell device.

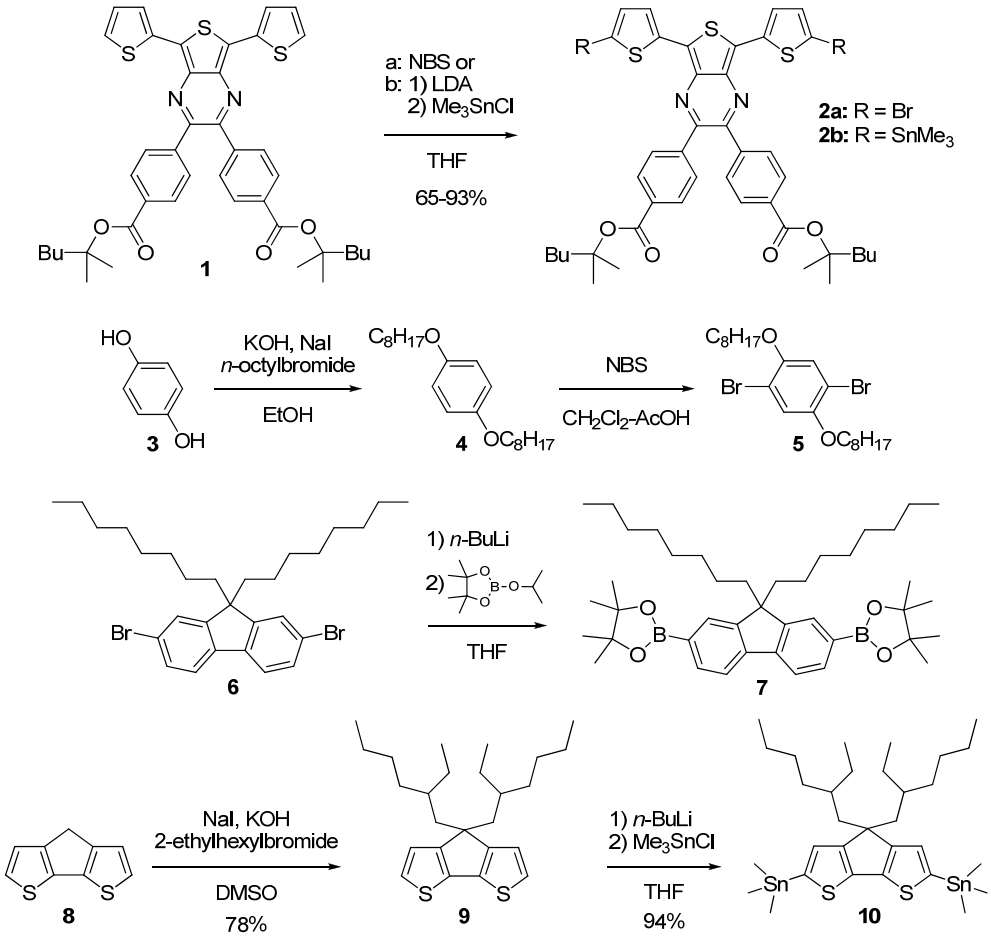

Scheme 4.1. Synthetic steps involved in the preparation of the monomers

4.2 Synthesis

The synthetic steps involved in the preparation of the monomers **2a**, **2b**, **5**, **7** and **10** are outlined in Scheme 4.1 while detailed synthetic procedures are described in the experimental section (4.8). Monomer **1** was functionalized by NBS bromination and by deprotonation using LDA followed by treatment with trimethyltin chloride. This afforded **2a**[4] and **2b**[5] to be used in Suzuki -and Stille-type copolymerizations. Deprotonation using *n*-buthyllithium (BuLi) did not work well since BuLi reacts with the pyrazine ring giving various by-products. The bromination was selective where only the dibrominated product was formed if 2 equivalents of NBS were added slowly. In our earlier work[1] (see Appendix 2) I explored a similar system where 4-alkylphenyl groups were incorporated instead of benzoate esters (Figure 4.2). Dibromination of the monomer shown in figure 4.2 turned out to be very challenging because the reaction proceeded very fast giving mixtures containing mono-, di- and tri-brominated

compounds. Thus extensive column chromatography was needed to separate all compounds and obtain the pure dibrominated compound. However, bromination of **1** does not show reduced selectivity since the electron attracting ester groups seems to improve the selectivity by reducing the reactivity towards electrophilic aromatic substitution on the outer thiophene rings.

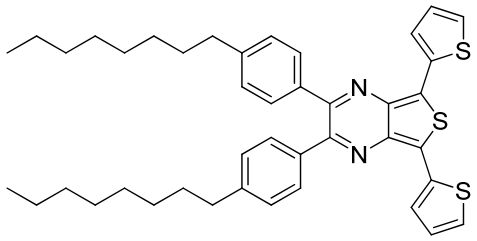

Figure 4.2. Dithienylthienopyrazine bearing 4-alkylphenyl groups on the pyrazine ring

According to a literature procedure,[6] monomer **5** can be synthesized in good yield starting with a standard alkylation of hydroquinone (**3**) followed by bromination of **4** with NBS. The diboronic acid pinacol ester **7** is prepared by lithiation of readily available 2,7-dibromo-9,9-dioctylfluorene (**6**) followed by addition of 2-isopropoxy-4,4,5,5-tetramethyl-1,3,2-dioxaborolane.[7] The synthetic route to **10**[8] initiates with a deprotonation of 4*H*-cyclopenta-[2,1-b:3,4-b']-dithiophene (**8**) and a subsequent alkylation which affords **9** in good yield. Deprotonation of **9** using *n*-buthyllithium followed by treatment with trimethyltin chloride affords monomer **10**. The synthesized stannyl compounds **2b** and **10** were very sensitive to acid (The stannyl group fall of) so they had to be purified under basic conditions by quickly passing them through a plug of basic aluminium oxide with a suitable eluent.

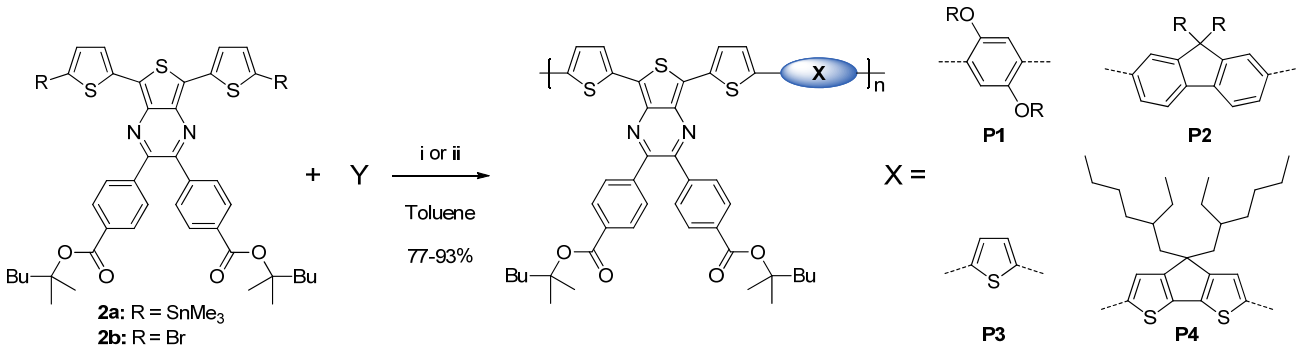

Scheme 4.2. Copolymerizations leading to the polymers **P1–4**. Y = **5**, **7**, **10** and 2,5-bis(trimethylstannyl)-thiophene. (i) Stille coupling using Pd_2dba_3 and tri-o-tolylphosphine. (ii) Suzuki coupling using Pd_2dba_3, tri-o-tolylphosphine and Cs_2CO_3.

Copolymerizations leading to the final polymers **P1–4** are presented in scheme 4.2. Copolymerisation of **2a** via Stille coupling, using the catalyst system Pd_2dba_3/tri-o-tolyl phosphine, with **5** gave polymer **P1** as a dark brown solid (M_w = 7 kg/mol, PDI = 1.9). Coupling of **2b** with **7** was performed with a Suzuki-type copolymerization reaction using Pd_2dba_3/tri-o-tolyl phosphine as a catalyst and cesium carbonate as a base. The polymer **P2** was afforded in 90% yield as a green solid with a molecular weight (M_w) of 42.3 kg/mol and a polydispersity (PDI) of 3. Using the same conditions as for the preparation of **P1**, copolymerisation of **2b** via Stille coupling with 2,5-bis(trimethylstannyl)thiophene and the cyclopentadithiophene **10** gave polymer **P3** and **P4** as dark green solids. All the polymers were isolated in good yields and are soluble in organic solvents such as chloroform and toluene at room temperature. The large variation in molecular weight, particularly between **P1** and **P4**, can be explained by a better solubility of **P4** but the steric nature of monomer **5** can also lead to deficient polymerization.

Table 4.1. GPC and spectroscopic data for polymers **P1-4**

	solution					film		
polymer	M_w (g/mol)	PDI	λ_{max} (nm)	λ_{onset} (nm)	E_g (eV)	λ_{max} (nm)	λ_{onset} (nm)	E_g (eV)
P1	7000	1.9	745	1015	1.22	845	1057	1.17
P2	42300	3.0	665	824	1.50	710	906	1.37
P3	39400	1.9	770	955	1.30	760	955	1.30
P4	363000	4.8	868	980	1.27	825	1002	1.24

4.3 Thermal Behaviour

The thermal behaviour of the thermocleavable polymers was investigated by Thermogravimetric analysis (TGA). The sample holders were carefully weighed and the samples introduced. TGA was then carried out using heating rate of 10 °C min^{-1}. TGA of **P1-4** are shown in figure 4.3 and indicates that the tertiary ester starts to eliminate around 200 °C in agreement with earlier results presented in chapter 3.[4] The second loss peak at ~400 °C

that corresponds to loss of CO_2[4] (not prior to decomposition) can only be observed for **P3** because a greater weight loss for **P1**, **P2** and **P4** is showing in the same temperature range. The observed value for this loss peak is ~20% which corresponds to loss of the alkyl chains on the donor units; dialkoxy benzene, fluorene and CPDT. The same precursor film prepared by standard solution processing of **P1–4** can give access to two chemically different thin films as shown in figure 4.4.

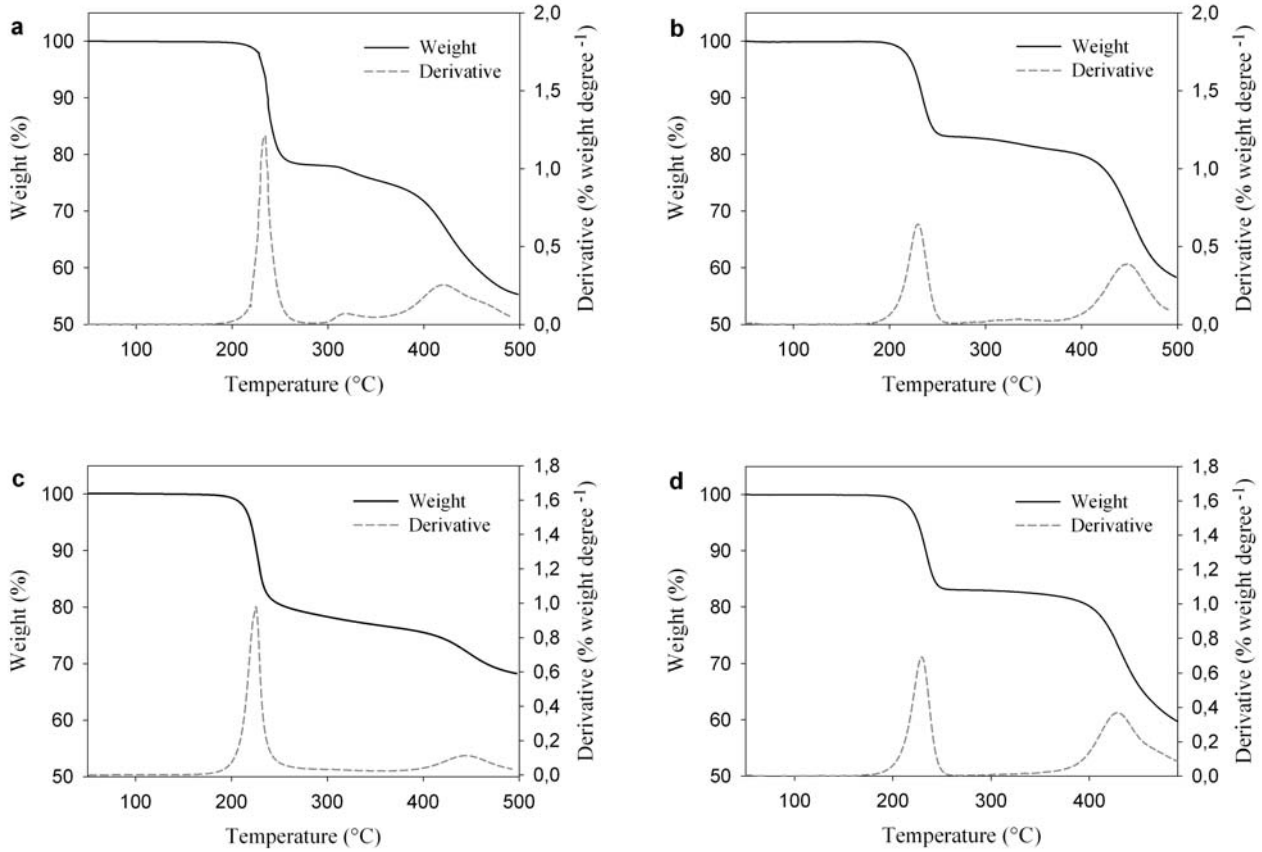

Figure 4.3. (a) TGA of **P1**, (b) TGA of **P2**, (c) TGA of **P3**, and (d) TGA of **P4** in the temperature range 50-500 °C. The data were recorded at 10 °C min^{-1} under an argon atmosphere. A derivative weight loss curve has been included to tell the point at which weight loss is most apparent.

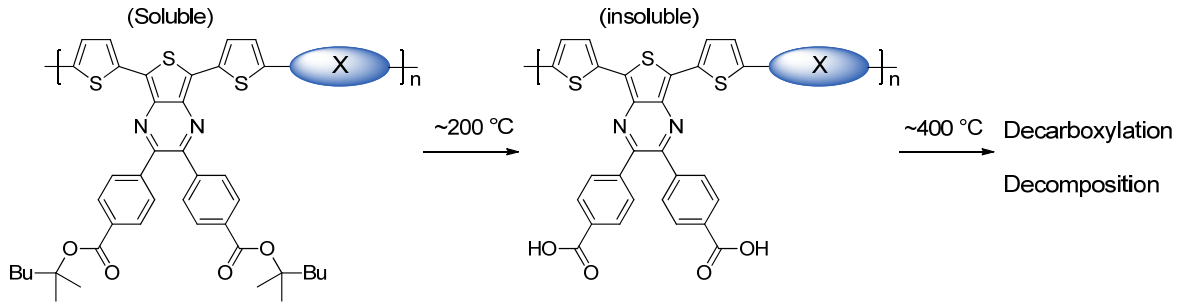

Figure 4.4. Possible chemical transitions of **P1–4**

4.4 Optical Properties

The absorption spectra for the polymers in chloroform solution are shown in figure 4.5a. The copolymers **P1–4** based on dithienylthienopyrazine does indeed show a considerable spectral coverage of the solar spectrum which is varied with the different donor units. The optical band gaps, defined by the onset of absorption, are ranging from 1.22-1.50 eV (Table 4.1). Partial aggregation of **P1** in solution gives it the lowest optical band gap with an onset at 1015 nm. **P2** has a somewhat higher band gap of 1.5 eV because of the decreased donor strength of the fluorine unit (high degree of aromaticity) which reduce conjugation in the polymer backbone.

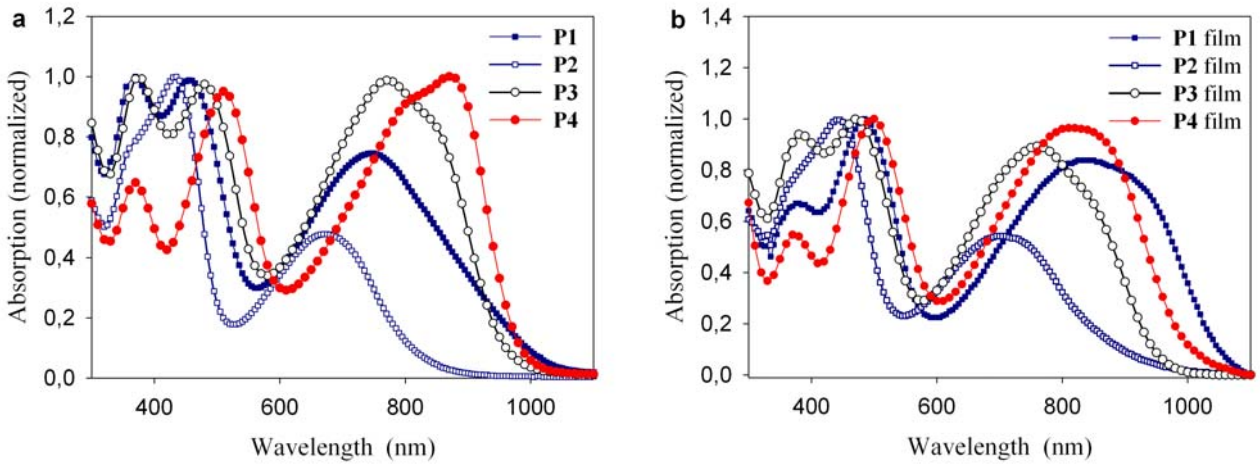

Figure 4.5. (a) UV-vis absorption spectra of the polymers **P1-4** in chloroform solution and (b) in thin film

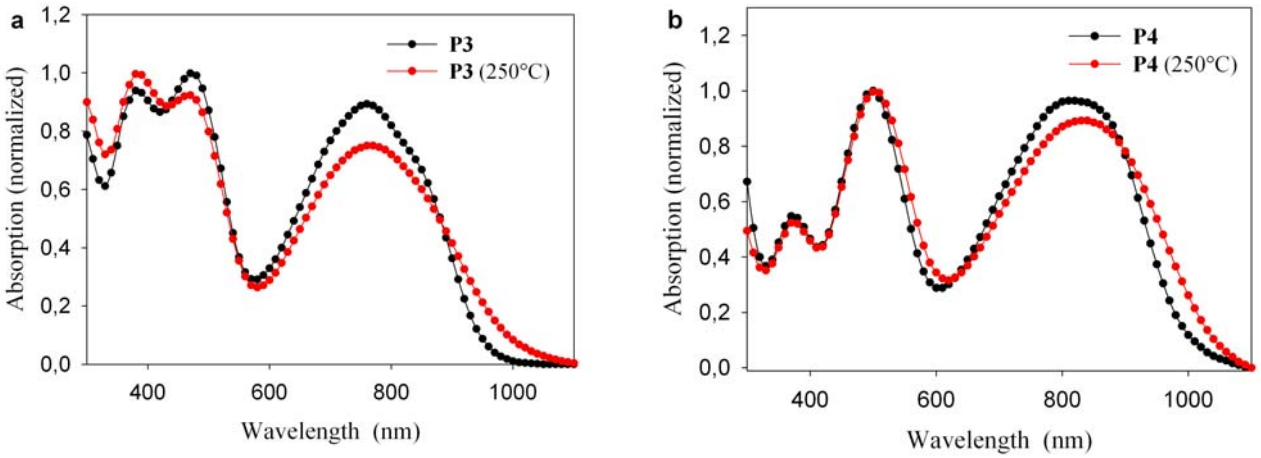

Figure 4.6. (a) UV-vis absorption spectra of **P3** and (b) **P4** in thin film before and after annealing for 1 min.

Three alternating thiophene units provide **P3** with a band gap of 1.3 eV in solution. Further extending the thiophene content by incorporating CPDT lowers the band gap to 1.27 eV (**P4**). Despite the improved donor character of the CPDT unit, caused by its planarity and electron donating alkyl chains, **P3** and **P4** has rather similar band gaps though the absorption maxima (λ_{max}) of **P3** is blue shifted compared to **P4**. The thin film absorption spectra for polymers **P1–4** are shown in figure 4.5b. The optical band gaps are ranging from 1.17-1.37 eV where only **P2** shows a significant decrease compared to in solution (table 4.1). The polymers **P1** and **P2** have absorption maxima in the range from 665-745 nm in chloroform solution, and these are red shifted further to 710-845 nm when in a solid film (table 4.1), indicating significant interchain association in the solid state. **P3** reveals a shoulder around 800 nm in solution and the same, but weaker, vibronic fine structure remains in the solid state. **P4** also reveals a shoulder in solution around 830 nm but in the solid state the absorption band has broadened, caused by intermolecular interactions, and the vibronic fine structure has disappeared. Upon annealing the films only **P3** and **P4** shows a significant change in the absorption spectra (Figure 4.6). Upon thermocleavage of the films by heating them at 250 °C for 1 min a colour change from olive green to a more brownish colour is observed. The associated changes in the absorption spectrum are a less intense low energy absorption band and a smaller band gap which is reduced to 1.23 eV for **P3** and 1.18 eV for **P4**. There may be several explanations for the lower absorption intensity. Firstly, the associated change in film thickness and, secondly the dielectric constant may lead to changes in the reflection phenomena that also contribute to the intensities in the observed absorption spectrum for a solid film in transmission

geometry. Thirdly, the intensity of absorption quite often decreases as the band gap is lowered. After the short thermal treatment the films maintained the optical quality and were insoluble in organic solvents.

4.5 Photovoltaic performance

Bulk heterojunction solar cells with an active area of 0.5 cm^2 were prepared on an indium tin oxide (ITO) covered glass substrate, using conventional device architecture. A thin layer of poly(3,4-ethylenedioxythiophene)–poly-(styrenesulfonate) (PEDOT-PSS) was spin coated on top of the ITO coating followed by spin coating of the active layer. The active layer contained a blend of the respective polymer and [60]PCBM. After spin coating of the active layer the devices were either processed directly into a solar cell by evaporation of aluminium as back electrode or subjected to a thermal treatment at the temperature of thermocleavage immediately before evaporation of the back electrode.

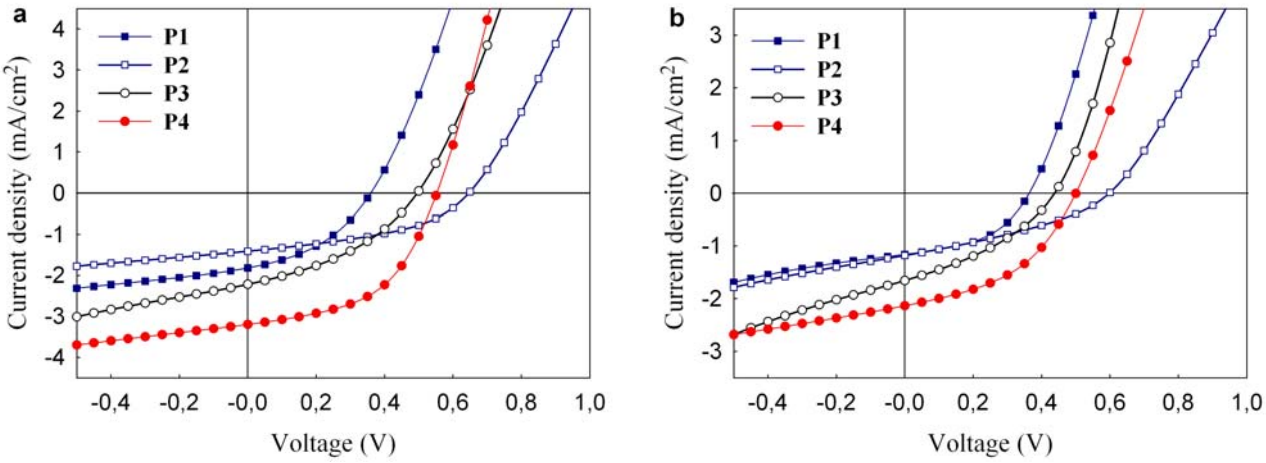

Figure 4.7. (a) *J-V* characteristics of the **P1**:PCBM, **P2**:PCBM, **P3**:PCBM and **P4**:PCBM solar cells measured under 74.3 mW/cm^2 white light before and (b) after a thermal treatment (see table 4.2).

The obtained current–voltage curves are presented in figure 4.7 which shows the current–voltage characteristics of the polymer:PCBM solar cells measured under 74.3 mW/cm^2 white light. The un-annealed devices based on **P1**, with the lowest band gap (1.15 eV), and PCBM had low open-circuit voltages (V_{oc}) of 0.36 V, moderate fill factors (FF) of 0.40 and current densities (J_{sc}) of 1.82 mA/cm^2. This resulted in power conversion efficiencies of up to 0.35%

(Table 4.2). Devices based on the fluorine coupled polymer **P2** and PCBM showed a somewhat higher V_{oc} up to 0.65 V (Figure 4.7a) as expected from earlier reports[3] with a similar system. **P2** provides a descent FF of 0.44 but the low current density (1.41 mA/cm^2) limits the performance to 0.54%. Changing the polymer backbone to be a complete thiophene segment raises the J_{sc} up to 2.22 mA/cm^2 for **P3**:PCBM devices. The V_{oc} was 0.5 V and together with a FF of 0.38 the devices had a PCE up to 0.57%. Solar cells based on **P4**:PCBM exhibits the best performance with the highest current density of 3.20 mA/cm^2 and a good fill factor of 0.51. Together with an open-circuit voltage of 0.55 V the power conversion efficiency sets to 1.21%. The somewhat higher J_{sc} obtained with **P4** is also reflected in the incident photon to current efficiency (IPCE) which reaches an average IPCE of 17% with a photoresponse up to 900 nm (Figure 4.8a). In contrast **P1–3** has an average IPCE in the range 7–8% but also extends up to 900 nm, except **P2** in agreement with the absorption spectra (Figure 4.5b). *J-V* curves of the polymer:PCBM solar cells after a thermal treatment is shown in figure 4.7b and a general observation is that the performance drops after the thermocleavage. Table 4.2 shows a large drop in the current density for all polymers after thermocleavage together with minor drops in the V_{oc} and FF. The drop in performance is also reflected in the IPCE which is lower at all wavelengths compared to the un-annealed devices (Figure 4.8b).

Table 4.2. Photovoltaic performance of devices based on blends of polymer and PCBM

polymer	polymer:PCBM (*w/w* ratio)	thermal treatment[a] (°C)	V_{oc} (V)	J_{sc} (mA/cm^2)	FF	η (%)
P1	1:2	-	0,36	1,82	0.40	0,35
P1	1:2	250	0,36	1,16	0.47	0,27
P2	1:3	-	0,65	1,41	0.44	0,54
P2	1:3	250	0,60	1,18	0.35	0,33
P3	1:4	-	0,5	2,22	0.38	0,57
P3	1:4	230	0,44	1,66	0.36	0,35
P4	1:3	-	0,55	3,20	0.51	1,21
P4	1:3	225	0,50	2,13	0.45	0,64

[a] heated for 30 seconds

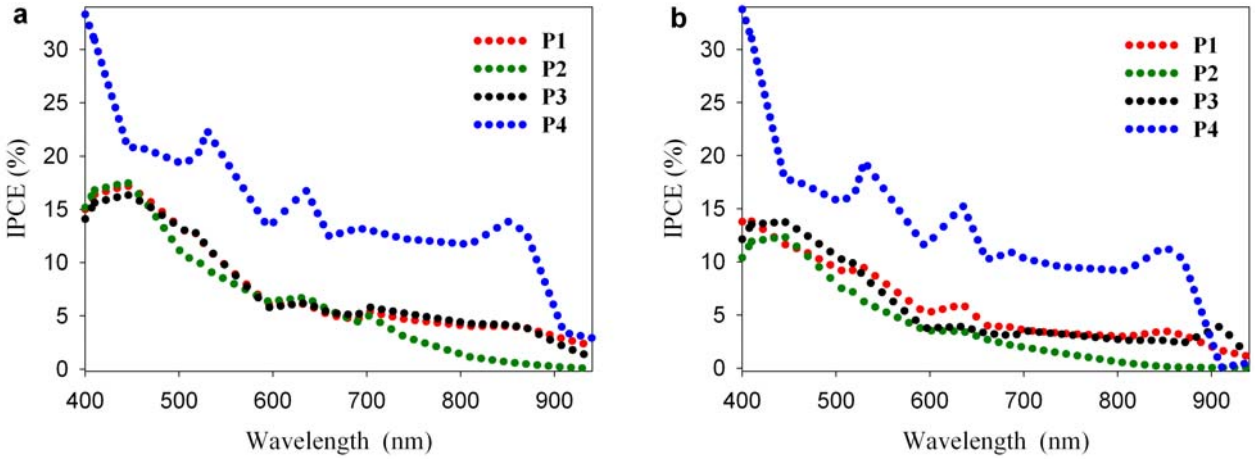

Figure 4.8. (a) IPCE of polymer:PCBM solar cells before and (b) after a thermal treatment.

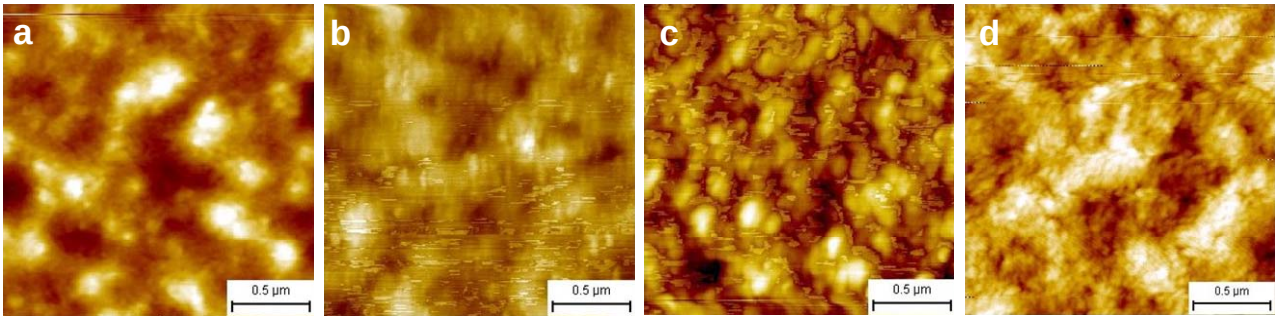

Figure 4.9. AFM topography images (2 µm × 2 µm) of solar cells based on blends of PCBM and (a) **P3** un-annealed, height scale is 20 nm (b) **P3** annealed at 230 °C, height scale is 15 nm (c) **P4** un-annealed, height scale is 15 nm (d) **P4** annealed at 225 °C, height scale is 15 nm.

4.6 Morphology

The **P3**:PCBM and **P4**:PCBM device films annealed at different temperatures, as measured by atomic force microscopy (AFM), are shown in figure 4.9. AFM reveals changes in the surface topography of the films and generally gives a good first insight into morphology of the active layer.[9] All films shows a significant roughness with a peak-to-valley difference around 15-20 nm. Comparing the films before (Figure 4.9a, 4.9c) and after annealing (Figure 4.9b, 4.9d) reveals that the domain sizes increases to features with dimensions larger than 100 nm which indicate extensive phase segregation of the polymer and PCBM upon annealing. The reduced current densities of the polymer:PCBM devices after thermocleavage might be a direct consequence of the changed morphology which is possibly limiting charge carrier generation

(reduced number of exitons reach the interface) and transport to the electrodes (insufficient percolating pathways).

4.7 Conclusion

A series of new thermocleavable low band gap polymers based on dithienylthienopyrazine, bearing thermocleavable benzoate esters on the pyrazine ring, alternating with different donor segments (incl. dialcoxybenzene, fluorene, thiophene and CPDT) have been synthesized. The solubilising benzoate ester groups are thermocleavable around 200 °C Where a volatile alkene is eliminated leaving the polymer component more rigid. Furthermore it was found that no decarboxylation takes place prior to decomposition at ~400 °C where a greater weight loss for **P1**, **P2** and **P4** is observed in the same temperature range which corresponds to loss of the alkyl chains on the donor units; dialkoxy benzene, fluorene and CPDT. The four polymers optical properties and photovoltaic performance in blends with PCBM have been investigated. In chloroform solution the polymers had optical band gaps ranging from 1.22-1.50 eV. The optical band gaps are lowered to 1.17-1.37 eV in thin film, showing a considerable spectral coverage of the solar emission spectrum. Furthermore polymer **P3** and **P4** showed a less intense low energy absorption band and a smaller band gap after annealing the film for 1 min. The best performing polymer in a bulk heterojunction solar cell was **P4** with J_{sc} = 3.20 mA/cm^2, V_{oc} = 0.55 V, FF = 0.51 and η = 1.21%. Devices generally performed worse after thermocleavage due to a drop in mainly the current density giving power conversion efficiencies up to 0.64% for **P4**:PCBM solar cells. The drop in performance after thermocleavage can be linked to extensive phase segregation of the polymer and PCBM as measured by AFM. We finally conclude that the interplay between temperature, morphology, and film chemistry needs to be understood before efficient thermocleavable materials can be optimally designed.

4.8 Experimental section

General methods. Molecular weights were determined using size exclusion chromatography in HPLC-grade chloroform against polystyrene standards on a KNAUER chromatograph with a refractive index detector and a diode array UV-vis detector. UV-vis absorption spectra were measured with a Perkin-Elmer Lambda 900 spectrometer. TGA experiments were performed with a dynamic heat rate (10 °C/min) under an Argon atmosphere (50 ml/min) in the temperature range 50-500 °C. AFM images were taken on a Nanos multimode AFM (Bruker). Unless stated otherwise all reagents and solvents were obtained from Aldrich and used without further purification. Dichloromethane, THF and toluene were dried with molecular sieves (3 Å) and used directly without filtration or distillation. NBS was recrystallised from water and dried at 70 °C in vacuum. Evaporation was performed on a rotary evaporator at 40 °C. NMR spectra were obtained on Bruker 500 MHz or 250 MHz spectrometers. Melting points were determined on an electrothermal instrument and are uncorrected. The samples were dried at 50 °C for 24 hours in a vacuum oven prior to analysis. **2a**,[4] **5**,[6] **7**[7] was prepared according to literature procedures and cyclopentadithiophene (**8**) was obtained from Astar Pharmaceuticals.

Polymer solar cell fabrication and analysis. Photovoltaic devices were made by spin coating PEDOT:PSS (Aldrich, 1.3 wt % aqueous solution) onto precleaned, patterned indium tin oxide (ITO) substrates (9-15 Ω per square) (LumTec) followed by annealing at 140 °C for 5 min. The active layer was deposited, in a glove box, by spin coating a blend of the polymer and [60]PCBM dissolved in *o*-dichlorobenzene (40 mg/ml). After a thermal treatment (see Table 4.2) the counter electrode of aluminium was deposited by vacuum evaporation at 2-3 × 10^{-6} mbar. The active area of the cells was 0.5 cm^2. *I-V* characteristics were measured under AM1.5G corresponding to 74.3 mW/cm^2 white light from a multi-wavelength high-power LED array using a Keithley 2400 source meter. IPCE spectra measurements were made on the same solar test platform[10] with the LED based illumination system.

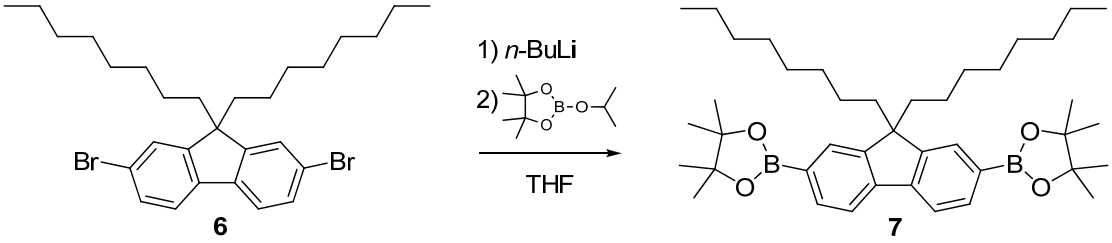

2,2'-(9,9-dioctyl-9H-fluorene-2,7-diyl)bis(4,4,5,5-tetramethyl-1,3,2-dioxaborolane) (7). **6** (5 g, 9.12 mmol) was dissolved in dry THF (70 ml). The solution was cooled to -78 °C and 1.6 M *n*-butyllithium in hexane (17 ml, 27.4 mmol) was added dropwise. The reaction mixture was stirred for 2 hour at -78 °C followed by addition of 2-isopropoxy-4,4,5,5-tetramethyl-1,3,2-dioxaborolane (7.4 ml, 36.5 mmol). The reaction mixture was allowed to warm to room temperature and stirred for 17 hours. The mixture was poured into water and extracted with ether. The combined organic phase was washed with water, brine and dried over $MgSO_4$. Concentration in vacuum gave the crude product that was recrystallized from acetone. Yield: 2.9 g (50%), white solid. ^{1}H NMR (250 MHz, $CDCl_3$): δ = 7.82 (d, J = 7.5 Hz, 2H), 7.76 (s, 2H), 7.72 (d, J = 7.5 Hz, 2H), 2.03 (m, 4H), 1.40 (s, 24H), 1.26-0.97 (m, 20H), 0.80 (t, J = 6.9 Hz, 6H), 0.55 (m, 4H). ^{13}C NMR (250 MHz, $CDCl_3$): δ = 150.2, 143.8, 133.5, 128.9, 119.4, 83.7, 55.2, 40.1, 31.7, 29.8, 29.2, 29.0, 24.8, 23.6, 22.5, 14.1.

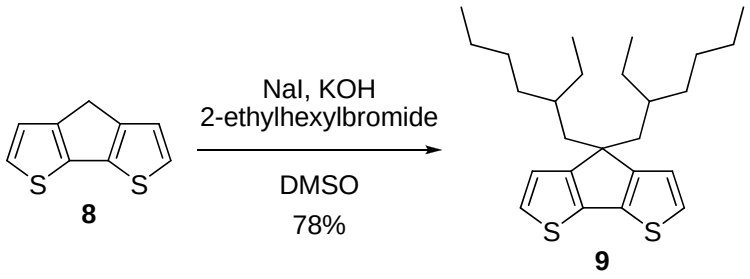

4,4-Bis(2-ethylhexyl)-4*H*-cyclopenta[2,1-*b*:3,4-*b'*]dithiophene (9). A solution of Cyclopentadithiophene (**8**) (3 g, 16.8 mmol), 2-ethylhexylbromide (6.3 ml, 35.3 mmol) and sodium iodide (1.68 mmol, 252 mg) in 100 ml DSMO was bubbled with argon for 30 minutes. Then potassium hydroxide (67.2 mmol, 3,77 g) was added and the mixture was stirred at room temperature for 17 hours. The reaction mixture was poured out in 100 ml water and extracted with heptane. The combined organic phase was washed twice with water and once with brine, after which the organic layer was dried ($MgSO_4$), filtered and concentrated in vacuum. Dry column chromatography (silica gel 15-40 μm, eluted with Heptane) afforded **9**.

Yield: 5.3 g (78 %), light yellow oil. ^{1}H NMR (250 MHz, $CDCl_3$): δ = 7.11 (d, J = 4.9 Hz, 2H), 6.96 – 6.90 (m, 2H), 1.96 – 1.79 (m, 4H), 1.07 – 0.83 (m, 18H), 0.75 (t, J = 6.7 Hz, 6H), 0.59 (t, J = 7.4 Hz, 6H). ^{13}C NMR (250 MHz, $CDCl_3$): δ = 157.6, 136.8, 123.9, 122.2, 52.9, 43.1, 35.0, 34.1, 28.4, 27.2, 22.7, 14.0, 10.5.

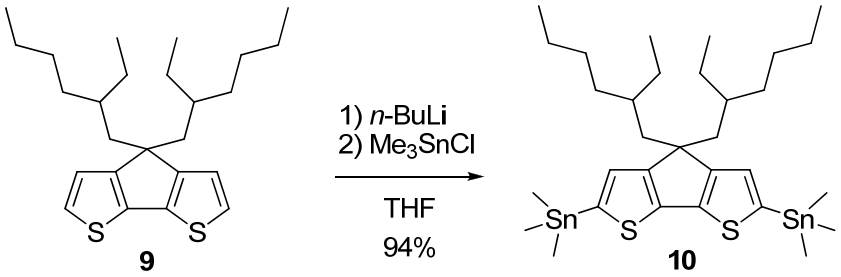

9 **10**

4,4-Bis(2-ethylhexyl)-2,6-bis(trimethylstannyl)-4*H*-cyclopenta[2,1-*b*:3,4-*b*']-dithiophene (10). **9** (3 g, 7.45 mol) was dissolved in dry THF (60 ml). The solution was cooled to -78 °C and 1.6 M *n*-butyllithium in hexane (19 ml, 29.8 mmol) was added dropwise. The reaction mixture was stirred at -78 °C for 1 hour and allowed to warm to room temperature over 2 hours. The reaction mixture was then cooled back to -78 °C and trimethyltin chloride (7.4 g, 37.1 mmol) dissolved in 15 ml dry THF was added slowly. The reaction mixture was allowed to warm to room temperature and stirred for 17 hours. 80 ml water was added to the reaction mixture followed by extraction with ether. The combined organic phase was washed with water, dried over magnesium sulfate, filtered and concentrated in vacuum. The residue was dissolved in heptane and quickly passed through a plug of aluminium oxide pretreated with triethylamine. Solvent was removed and the residue was dried under vacuum at 70 °C. Yield: 5.1 g (94 %), light yellow oil. ^{1}H NMR (250 MHz, $CDCl_3$): δ = 7.01 – 6.88 (m, 2H), 1.93 – 1.76 (m, 4H), 1.04 – 0.81 (m, 18H), 0.74 (t, J = 6.7, 6H), 0.59 (t, J = 7.3, 6H), 0.49 – 0.22 (m, 18H). ^{13}C NMR (250 MHz, $CDCl_3$): δ = 159.7, 142.6, 136.2, 130.2, 52.1, 42.8, 35.0, 34.4, 28.7, 27.5, 22.7, 13.9, 10.7, -8.3.

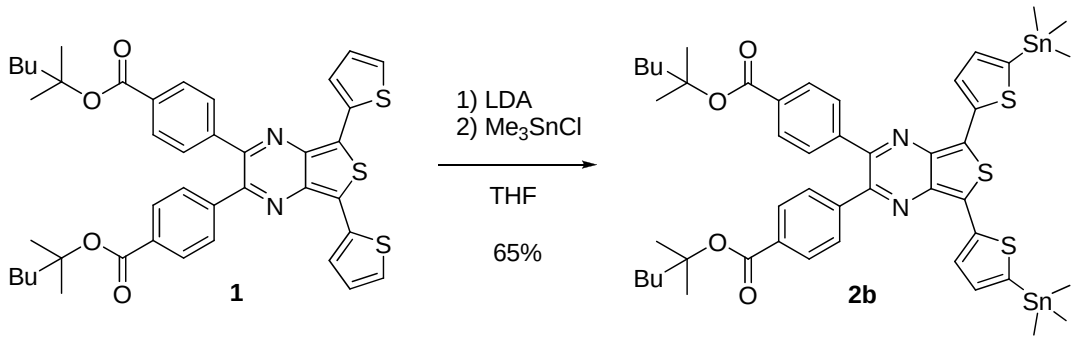

bis(2-methylhexan-2-yl)-4,4'-(5,7-bis(5-(trimethylstannyl)thiophen-2-yl)thieno[3,4-*b*]-pyrazine-2,3-diyl)dibenzoate (2b). 10 ml dry THF was cooled to -10 °C followed by addition of 10 ml *n*-butyllithium (1.6 M in hexane). Then a solution of 2.4 ml diisopropylamine and 7.6 ml dry THF was added slowly and the reaction mixture was stirred for 20 min. 20.4 ml of the freshly prepared solution of lithium diisopropylamine was added slowly to a cooled solution (-78 °C) of **1** (1.5 g, 2.04 mmol) in dry THF (60 ml). The reaction mixture was stirred for 1 hour at -78 °C followed by dropwise addition of trimethyltin chloride (2.4 g, 12.2 mmol) dissolved in 5 ml dry THF. The reaction mixture was allowed to warm to room temperature and stirred for 5 hours. Water was added to the reaction mixture followed by extraction with ether. The combined organic phase was washed with water, dried over magnesium sulfate, filtered and concentrated in vacuum. The residue was dissolved in toluene/heptane (1:2) and quickly passed through a plug of aluminium oxide pretreated with triethylamine. Solvent was removed and the residue was dried under vacuum at 70 °C. Yield: 1.4 g (65 %), dark purple solid. *Mp* = 180-181 °C. ^{1}H NMR (500 MHz, $CDCl_3$): δ = 7.98 (d, *J* = 8.5 Hz, 4H), 7.86 (d, *J* = 3.4 Hz, 2H), 7.66 (d, *J* = 8.5 Hz, 4H), 7.23 (d, *J* = 3.5 Hz, 2H), 1.99 – 1.86 (m, 4H), 1.64 (s, 12H), 1.46 – 1.34 (m, 8H), 0.95 (t, *J* = 7.0 Hz, 6H), 0.52 – 0.38 (m, 18H). ^{13}C NMR (500 MHz, $CDCl_3$): δ = 165.3, 151.5, 142.7, 140.3, 139.9, 137.3, 135.6, 132.3, 129.8, 129.2, 126.3, 125.5, 83.6, 40.8, 26.2, 26.1, 23.0, 14.1, -8.1.

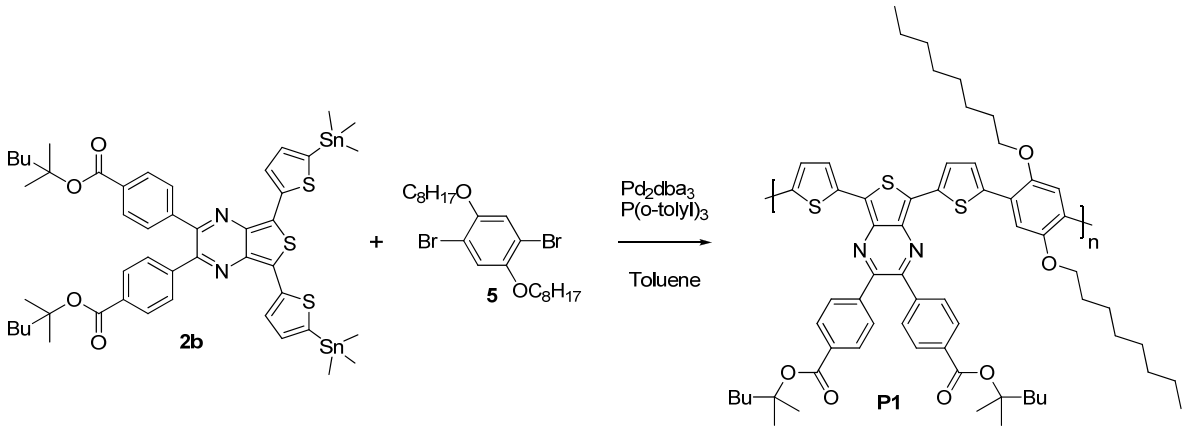

Poly(bis(2-methylhexan-2-yl)-4,4'-(5-(5-(2,5-bis(octyloxy)phenyl)thiophen-2-yl)-7-(thiophen-2-yl)thieno[3,4-*b*]pyrazine-2,3-diyl)dibenzoate) (P1). 2b (286 mg, 0.27 mmol), **5** (133 mg, 0.27 mmol), Pd_2dba_3 (12 mg, 13 µmol) and tri-(o-tolyl)phosphine (33 mg, 0.11 mmol) was mixed in dry degassed toluene (12 ml). The reaction mixture was heated to reflux for 48 hours under argon. After cooling to room temperature the mixture was poured into 100 ml methanol and the polymer was allowed to precipitate. The polymer was filtered and purified by Soxhlet extraction using methanol, hexane and chloroform. Yield: 221 mg (77 %), dark brown solid. ^{1}H NMR (500 MHz, $CDCl_3$): δ = 8.06 – 7.89 (br, 8H), 7.73 – 7.47 (br, 6H), 4.25 – 3.90 (br, 4H), 2.09 – 1.78 (br, 8H), 1.74 – 1.18 (m, 40H), 1.06 – 0.77 (m, 12H). SEC ($CHCl_3$): M_w = 7000 g/mol, PDI = 1.9.

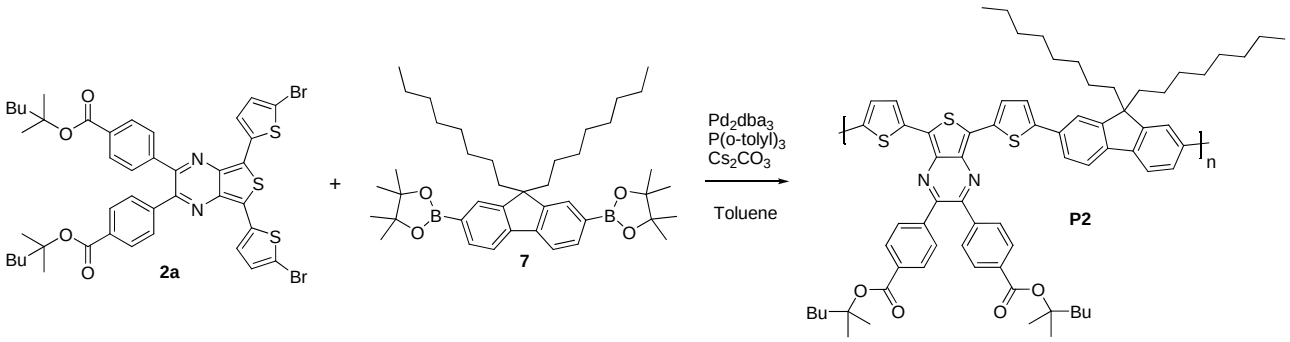

Poly(bis(2-methylhexan-2-yl)-4,4'-(5-(5-(9,9-dioctyl-9*H*-fluoren-2-yl)thiophen-2-yl)-7-(thiophen-2-yl)thieno[3,4-*b*]pyrazine-2,3-diyl)dibenzoate) (P2). 2a (300 mg, 0.34 mmol), **7** (215 mg, 0.34 mmol), Pd_2dba_3 (15 mg, 17 µmol) and tri-(o-tolyl)phosphine (41 mg, 0.13 mmol) was dissolved in dry degassed toluene (11 ml) and stirred for 15 min at room temperature under argon. Then Cs_2CO_3 (1.1 g, 3.38 mmol), degassed water (1.1 ml) and 1 drop Aliquat® 336 was added. The reaction mixture was stirred at 90 °C for 72 hours. After cooling to room temperature the mixture was poured into 100 ml methanol and the polymer

was allowed to precipitate. The polymer was filtered and purified by Soxhlet extraction using methanol, hexane and chloroform. Yield: 346 mg (90 %), green solid. ^{1}H NMR (500 MHz, $CDCl_3$): δ = 8.09 – 7.98 (br, 10H), 7.86 – 7.60 (br, 6H), 7.50 – 7.42 (br, 2H), 2.19 – 1.87 (br, 4H), 1.71 – 1.53 (m, 4H), 1.50 – 1.33 (br, 12H), 1.25 – 1.06 (br, 32H), 1.04 – 0.92 (br, 6H), 0.89 – 0.70 (br, 6H). SEC ($CHCl_3$): M_w = 42300 g/mol, PDI = 3.0.

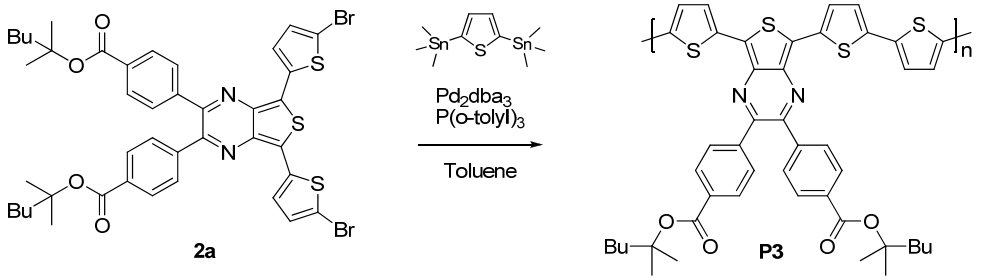

Poly(bis(2-methylhexan-2-yl)-4,4'-(5-(2,2'-bithiophen-5-yl)-7-(thiophen-2-yl)-thieno-[3,4-*b*]pyrazine-2,3-diyl)dibenzoate) (P3). Prepared with the same procedure as for **P1** using the monomers **2a** and 2,5-bis(trimethylstannyl)thiophene. Yield: 670 mg (92 %), dark green solid. ^{1}H-NMR ($CDCl_3$): δ = 8.18 – 6.37 (br, 14H), 2.30 – 0.45 (br, 30H). SEC ($CHCl_3$): M_w = 39400 g/mol, PDI = 1.9.

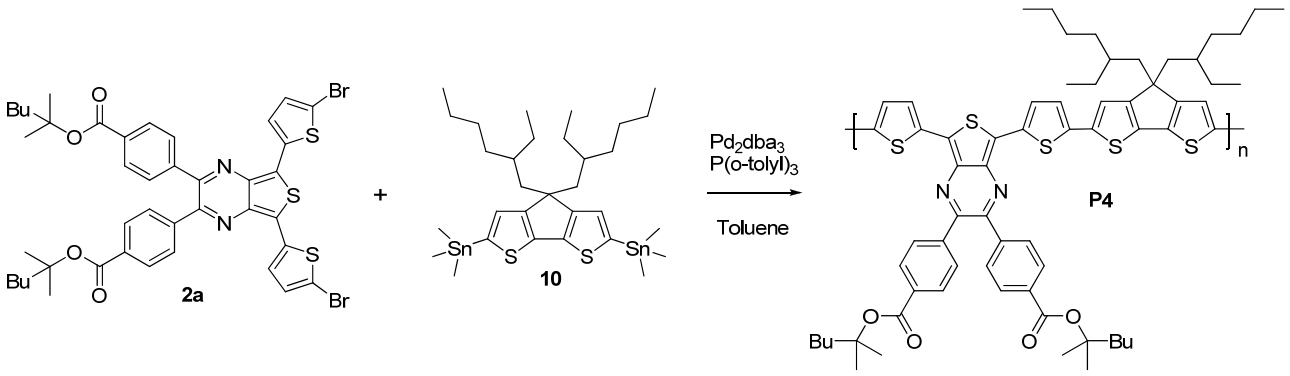

Poly(bis(2-methylhexan-2-yl)-4,4'-(5-(5-(4,4-bis-(2-ethylhexyl)-4*H*-cyclopenta-[2,1-*b*;3,4-*b'*]-dithiophene)thiophen-2-yl)-7-(thiophen-2-yl)thieno[3,4-*b*]pyrazine-2,3-diyl)dibenzoate) (P4). Prepared with the same procedure as for **P1** using the monomers **2a** and **10**. Yield: 359 mg (93 %), dark green solid. ^{1}H NMR (500 MHz, $CDCl_3$): δ = 8.04 (br, 8H), 7.72 (br, 6H), 1.95 (br, 4H), 1.75 – 1.26 (m, 22H), 1.13 – 0.86 (br, 20H), 0.84 – 0.54 (br, 18H). SEC ($CHCl_3$): M_w = 363000 g/mol, PDI = 4.8.

4.9 References

1. Petersen, M. H.; Hagemann, O.; Nielsen, K. T.; Jørgensen, M.; Krebs, F. C. *Sol. Energy Mater. Sol. Cells* **2007,** *91* (11), 996-1009.
2. Wienk, M. M.; Turbiez, M. G. R.; Struijk, M. P.; Fonrodona, M.; Janssen, R. A. J. *Appl. Phys. Lett.* **2006,** *88* (15).
3. Zhang, F. L.; Mammo, W.; Andersson, L. M.; Admassie, S.; Andersson, M. R.; Inganas, L.; Admassie, S.; Andersson, M. R.; Ingands, O. *Adv. Mater.* **2006,** *18* (16), 2169-2173.
4. Petersen, M. H.; Gevorgyan, S. A.; Krebs, F. C. *Macromolecules* **2008,** *41* (23), 8986-8994.
5. Hagemann, O.; Bjerring, M.; Nielsen, N. C.; Krebs, F. C. *Sol. Energy Mater. Sol. Cells* **2008,** *92* (11), 1327-1335.
6. Aubert, P. H.; Knipper, M.; Groenendaal, L.; Lutsen, L.; Manca, J.; Vanderzande, D. *Macromolecules* **2004,** *37* (11), 4087-4098.
7. Ranger, M.; Rondeau, D.; Leclerc, M. *Macromolecules* **1997,** *30* (25), 7686-7691.
8. Zhu, Z.; Waller, D.; Gaudiana, R.; Morana, M.; Muhlbacher, D.; Scharber, M.; Brabec, C. *Macromolecules* **2007,** *40* (6), 1981-1986.
9. Yang, X.; Loos, J. *Macromolecules* **2007,** *40* (5), 1353-1362.
10. Krebs, F. C.; Sylvester-Hvid, K. O.; Jørgensen, M. *Prog. Photovolt: Res. Appl.* **2009,** accepted.

Chapter 5

Substituted 2,1,3-benzothiadiazole- and thiophene-based polymers for solar cells – Introducing new thermocleavable precursors*

5.1 Introduction

The incorporation of aromatic heterocyclic units can greatly influence the properties of conjugated polymers based on donor and acceptor moieties. Among these, 2,1,3-benzothiadiazole has been incorporated in a growing number of low band gap materials as an acceptor unit, in large part due to the ease of preparing the monomer 4,6-dibromo-2,1,3-benzothiadiazole.[1] Conjugated materials based on 2,1,3-benzothiadiazole has been widely used in OLEDs[2-4] and bulk heterojunction polymer/PCBM solar cells where high photovoltaic performance have been reported.[5-7] In view of the popularity of the 2,1,3-benzothiazole unit, it is surprising that the synthesis of analogues or derivatives of this heterocycle and their application in organic photovoltaics only rarely have been reported.[8-10]

In this chapter the synthesis of new electron-deficient monomers based on 2,1,3-benzothiadiazole and their incorporation into conjugated polymers is presented (Figure 5.1). These new monomers bear alkoxy side chains at the 5- and 6-positions of the benzothiadiazole, resulting in improved solubility. The original idea was to compare the photovoltaic performance of polymers (**7–9**) based on these monomers with polymer analogues based on 2,1,3-benzothiadiazole bearing thermocleavable alkyl ester groups at the 5- and 6-position. However, incorporation of tertiary esters at the 5- and 6-positions of 2,1,3-benzothiadiazole turned out to be very complicated (see appendix 1) so a different polymer design was selected. The thermocleavable polymers **T1** and **T2** (Figure 5.1) is based on 2,1,3-benzothiadiazole alternating with thiophene units along the chain. In addition a branched

* Some of this work has been published: Helgesen, M.; Gevorgyan, S. A.; Krebs, F. C.; Janssen, R. A. J. *Chem. Mater.* **2009,** *21* (19), 4669-4675.

alkyl chain is attached to the polymer backbone through a labile ester bond to the thiophene segment. **T2** has enhanced donor character compared to **T1** through the incorporated planar CPDT unit. The photovoltaic performance of the five new low band gap polymers in blends with PCBM is presented.

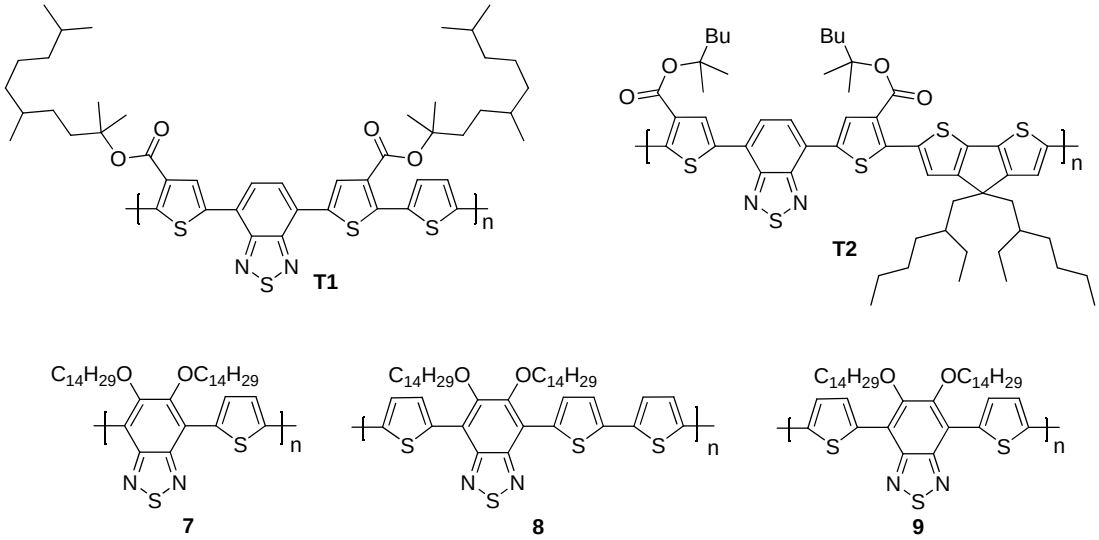

Figure 5.1. Polymers based on 2,1,3-benzothiadiazole alternating with thiophene units.

5.2 Synthesis

The synthetic steps involved in the preparation of the monomers **4** and **6** are outlined in Scheme 5.1 while detailed synthetic procedures are described in the experimental section 5.8. 1,2-Bis(tetradecyloxy)benzene (**1**) was prepared by a standard alkylation of catechol with 1-bromotetradecane in DMF at 100 °C.[11] Electrophilic aromatic nitration of **1** affords the substituted *o*-dinitrobenzene (**2**).[12] Reduction of the nitro groups with tin(II) chloride[13] gives the diamine as its hydrochloride salt which has to be used directly because of its unstable nature. Treatment of the diamine with thionyl chloride affords **3**, which is brominated with molecular bromine to give monomer **4** in excellent yield.[14] Stille coupling of **4** with 2-tributylstannylthiophene gives **5** as a yellow solid that is highly fluorescent in solution. Finally NBS bromination of **5** gives monomer **6**.

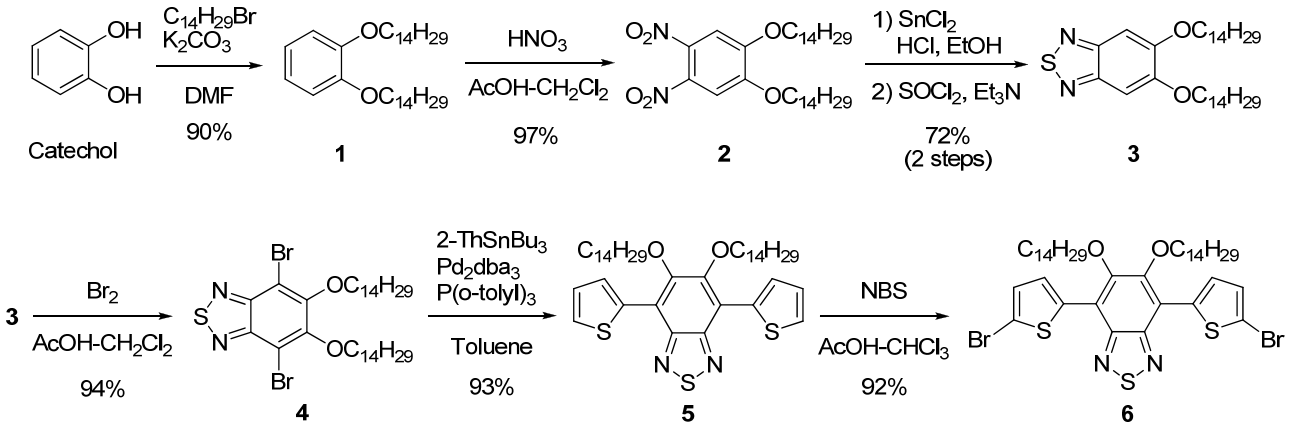

Scheme 5.1. Synthetic steps involved in the preparation of the monomers **4** and **6**

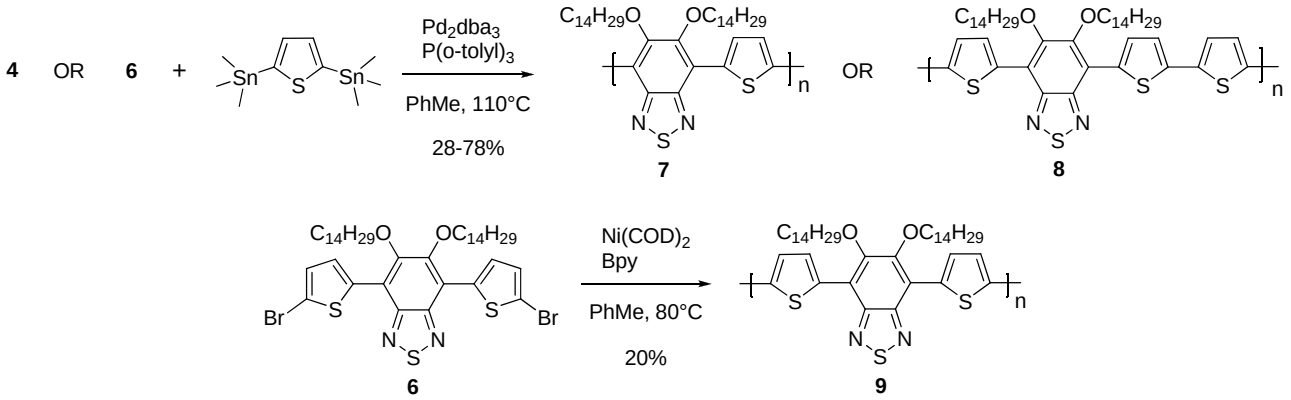

Scheme 5.2. Synthetic steps involved in the preparation of the polymers **7**, **8** and **9.**

Copolymerisation of **4** and **6** via Stille coupling with 2,5-bis(trimethylstannyl)thiophene, using the catalyst system Pd_2dba_3/P(o-tolyl)$_3$, gives polymer **7** and **8** as dark purple solids (Scheme 5.2). Yamamoto coupling of **6**, using bis(1,5-cyclooctadiene)nickel(0) ($Ni(COD)_2$) and bipyridine (Bpy) gives polymer **9** in 20 % yield (Scheme 5.2) with a molecular weight (M_w) of 7100 g/mol and a polydispersity (PDI) of 1.7. The low yield was caused by the fact that a large portion of the polymer formed was insoluble and could not be isolated by soxhlet extraction. For the same reason, a low yield of **8** was isolated (28 %) but with a higher molecular weight (M_w = 26 kg/mol, PDI = 2.9). On the contrary Polymer **7** (M_w = 16.6 kg/mol, PDI = 1.7) was isolated in good yields and are very soluble in organic solvents such as chloroform and toluene at room temperature.

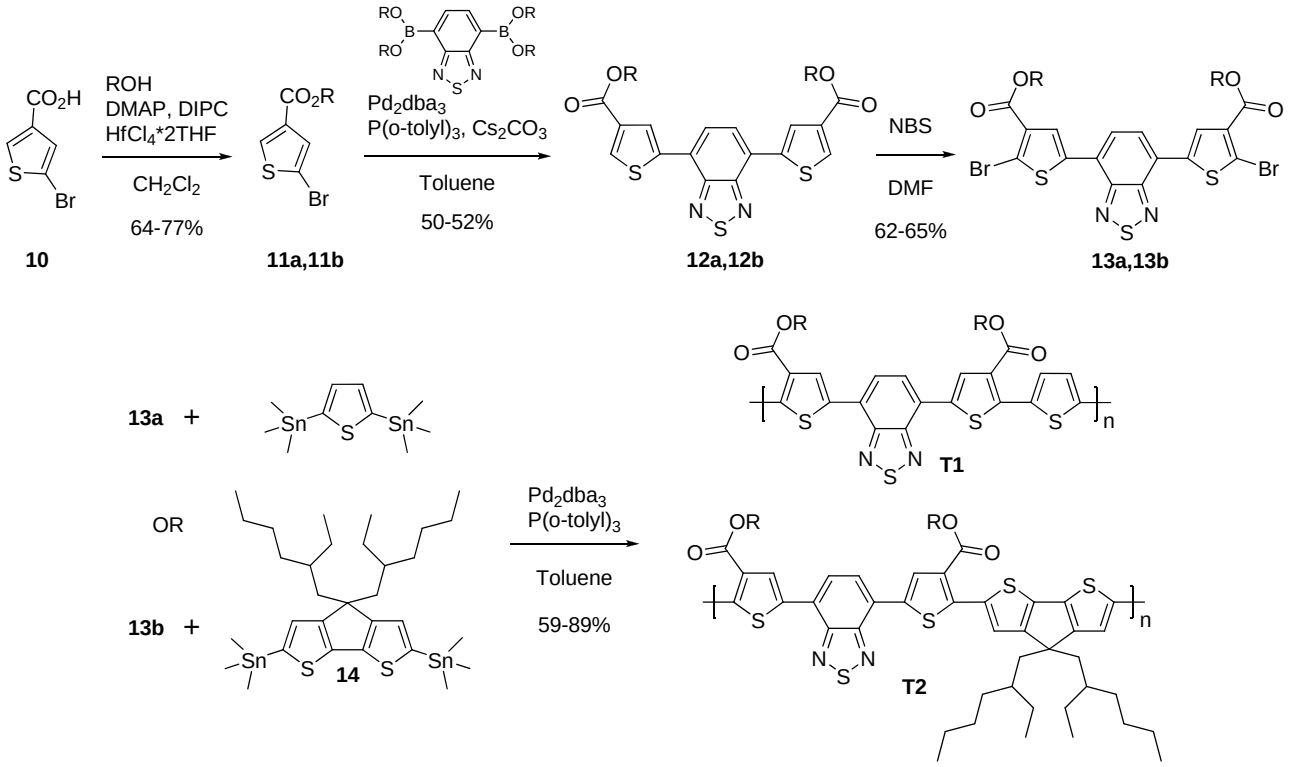

Scheme 5.3. Synthetic steps involved in the preparation of the thermocleavable polymers **T1** and **T2**.
a: R = 2,5,9-trimethyl-2-decanyl, b: R = 2-methyl-2-hexyl.

The synthetic steps involved in the preparation of the thermocleavable polymers **T1** and **T2** are outlined in Scheme 5.3. I used a slightly modified procedure, reported in our earlier work[15] (see chapter 3) for the synthesis of tertiary esters, to prepare **11**. The esterification employs a catalytic amount of hafnium(IV) chloride tetrahydrofuran complex (1:2) in combination with *N,N´*-diisopropylcarbodiimide and DMAP. The method normally employ $Sc(OTf)_3$ as the catalyst but $HfCl_4{\cdot}2THF$ is cheaper and turned out to work efficiently for the monoesterification of **10**. As discussed in chapter 3 the role of hafnium in the esterification may be to coordinate with the initially formed carbonyl oxygen of the pyridinium intermediate. Suzuki cross-coupling of **11** with the boronic ester 4,7-bis(4,4,5,5-tetramethyl-1,3,2-dioxaborolan-2-yl)benzo[*c*][1,2,5]thiadiazole affords **12** which is NBS brominated to give the monomers **13a** and **13b**. Finally copolymerisation of **13a** via Stille coupling with 2,5-bis(trimethylstannyl)thiophene affords the thermocleavable polymer **T1** in 59% yield with a M_w of 173 kg/mol and a PDI of 2.6. Using the same conditions, stille copolymerization of **13b** with the cyclopentadithiophene **14** affords **T2** as a dark purple solid (M_w = 41.6 kg/mol, PDI = 2.7). The large variation in molecular weight between **T1** and **T2** can be explained by the

different solubilizing alkyl ester groups (R) on the polymers. **T1** has a longer and more branched R group compared to **T2** which can improve solubility during the stille polymerization reaction. Another explanation can be a steric effect from the alkyl chains on **14** that may slow down the polymerization. **T1** was also prepared with the R group 2-methyl-2-hexyl but the polymer turned out to be hardly soluble and did not process acceptable well into films.

5.3 Thermal behaviour

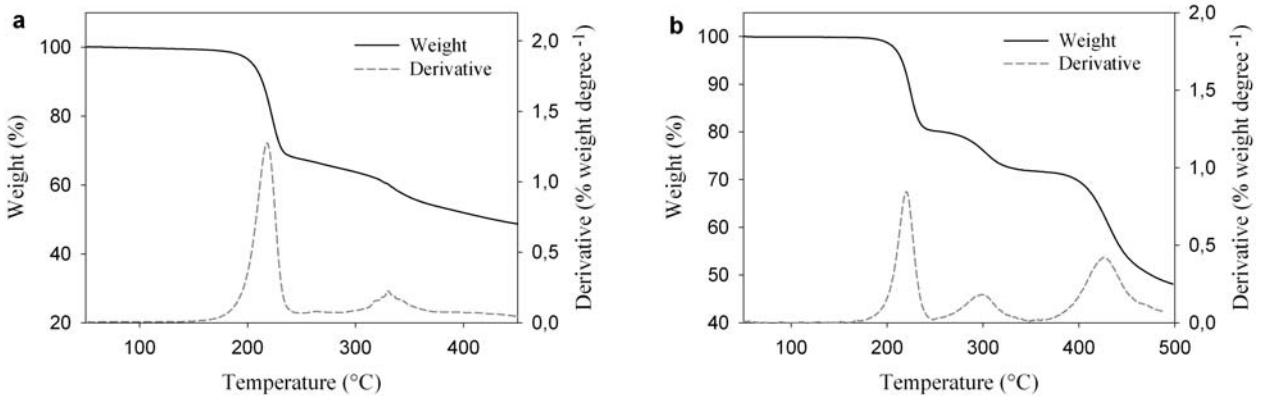

Figure 5.2. (a) TGA of **T1** and (b) **T2** in the temperature range 50-500 °C. The data were recorded at 10 °C min^{-1} under an argon atmosphere. A derivative weight loss curve has been included to tell the point at which weight loss is most apparent.

The thermal behaviour of the thermocleavable polymers was investigated by Thermogravimetric analysis (TGA). The sample holders were carefully weighed and the samples introduced. TGA was then carried out using heating rate of 10 °C min^{-1}. TGA of **T1** and **T2** in the temperature range 50-500 °C indicates that the ester bond starts to break around 200 °C (Figure 5.2) as expected from our earlier studies.[15] A second loss peak is detected at ~300-330 °C which corresponds to loss of CO_2.[15,16] According to figure 5.3b, the decarboxylation of **T2** start to happen around 265 °C whereas the transition of **T1** occurs at a somewhat higher temperature. From this point of view, the same precursor film prepared by standard solution processing of **T1** and **T2** thus gives access to three chemically different thin films (Figure 5.3). **T2** shows a third weight loss around 400 °C that is corresponding to elimination of the alkyl chains on the CPDT unit (as observed for **P4** in chapter 4).

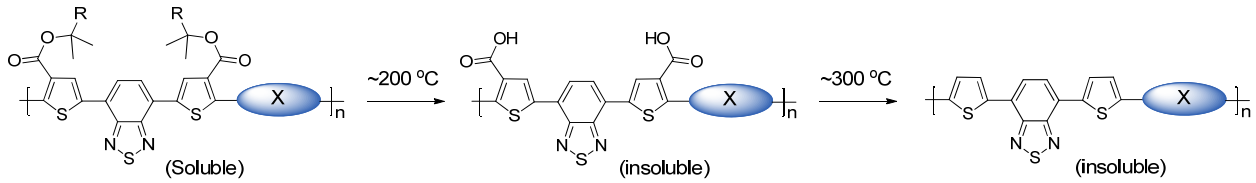

Figur 5.3. Possible chemical transitions of **T1** and **T2**

5.4 Optical Properties

The absorption spectra of the polymers in chloroform solution are shown in figure 5.4a and figure 5.5. The optical band gaps, defined by the onset of absorption, are rather similar ranging from 1.79-1.96 eV (Table 5.1). **8** exhibits a lower optical band gap in solution due to partial aggregation of the polymer in solution. **T2** has the lowest band gap of 1.79 eV caused by the incorporated CPDT unit (better donor compared to thiophene). The difference in absorption maxima (λ_{max}) is relatively small but **T1** is blue shifted compared to the other polymers (Table 5.1) indicating a more twisted backbone due to the long and branched alkyl ester side chains. The film absorption spectra for the polymers are shown in figure 5.4b and figure 5.5. Again the optical band gaps are very similar ranging from 1.66-1.75 eV (Table 5.1). The polymers, **7–9** and **T1**, have absorption maxima ranging from 525-570 nm in chloroform, and these are red shifted further to 592-654 nm when in a solid film (Table 5.1), indicating significant interchain association in the solid state. In addition polymers **7** and **8** show vibronic fine structure at 625 nm in the solid state. A weak vibronic transition may also account for the observed shoulder of **9** (Figure 5.4b). With regard to the thermocleavable polymer **T1**, a blue shift of the absorption maxima is observed when the film is heated at 250 °C for 1 min followed by a minor blue shift of the absorption maxima when the film is heated at 310 °C (Figure 5.5a). The film absorption spectra for **T2** show no significant shifts when the film is annealed (Figure 5.5b). After the thermal treatment of **T1** and **T2** the films were completely insoluble and no clear colour change was observed.

Table 5.1. GPC and spectroscopic data for polymers **T1**, **T2** and **7–9**

	solution					film		
polymer	M_w (g/mol)	PDI	λ_{max} (nm)	λ_{onset} (nm)	E_g (eV)	λ_{max} (nm)	λ_{onset} (nm)	E_g (eV)
T1	173000	2.6	525	633	1.96	593[a], 570[b]	732	1.69
T2	41600	2.7	593	691	1.79	608	746	1.66
7	16600	1.7	563	643	1.93	654	711	1.74
8	26000	2.9	570	687	1.80	644	707	1.75
9	7100	1.7	543	639	1.94	592	715	1.73

[a] 25 °C, [b] heated at 250 °C for 1 min.

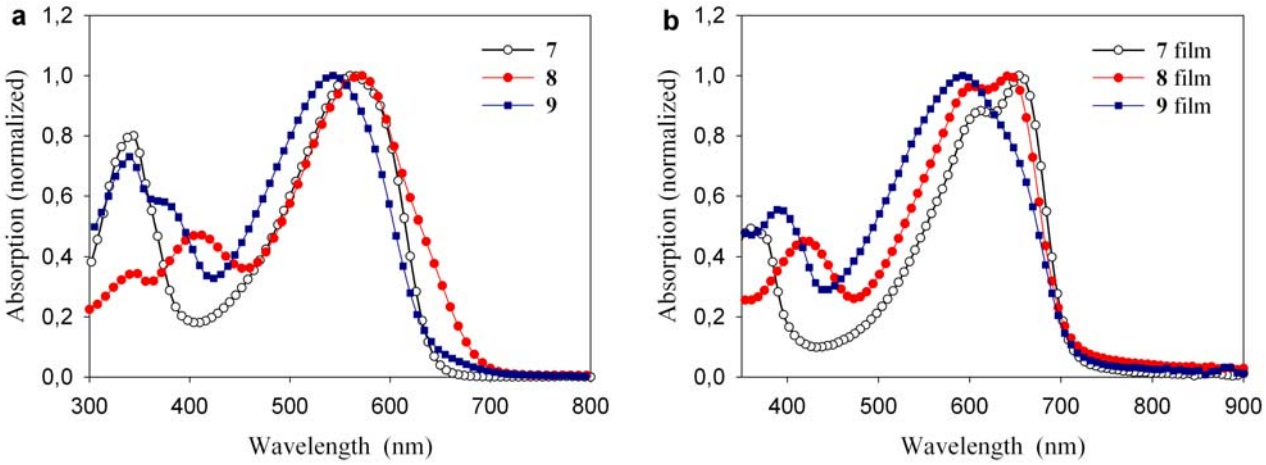

Figure 5.4. UV-vis absorption spectra of polymers **7–9** in (a) chloroform solution and (b) thin film.

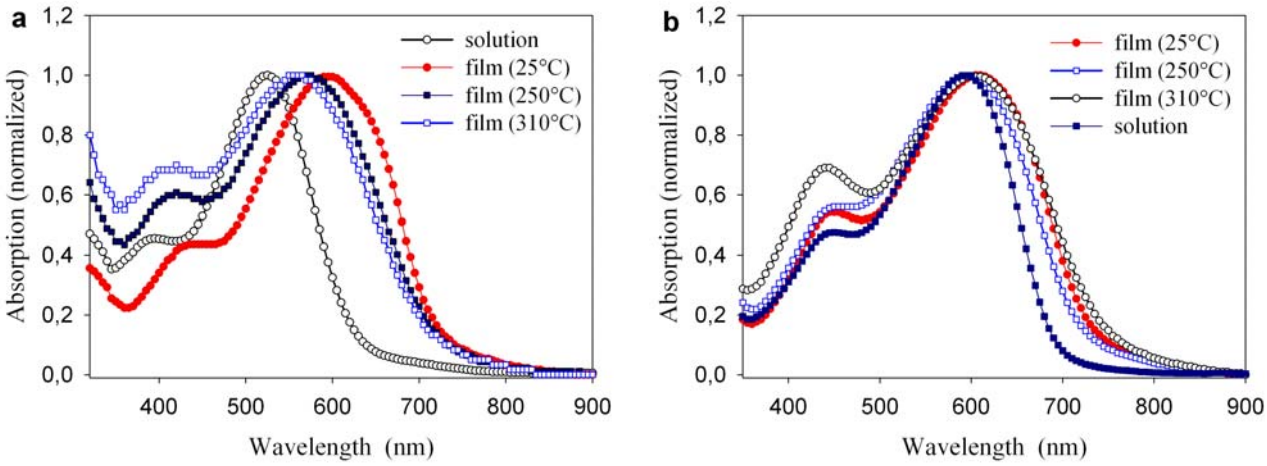

Figure 5.5. (a) UV-vis absorption spectra of **T1** and (b) **T2** in chloroform solution and in thin film before and after thermocleavage for 1 min.

5.5 Photovoltaic performance

Bulk heterojunction solar cells were fabricated on an indium tin oxide (ITO) covered glass substrate, using conventional device architecture. A thin layer of poly(3,4-ethylenedioxythiophene)–poly-(styrenesulfonate) (PEDOT-PSS) was spin coated on top of the ITO coating followed by spin coating of the active layer. The active layer contained a blend of the respective polymer and PCBM. After spin coating of the active layer the devices were either processed directly into a solar cell by evaporation of LiF (1 nm) and aluminium (100 nm) as back electrode or subjected to a thermal treatment at the temperature of thermocleavage immediately before evaporation of the back electrode (Devices based on **T2**:PCBM was prepared as described in chapter 4). The most efficient devices with **7–9** comprised a polymer/PCBM ratio of 1:2 spin-coated from chlorobenzene with a polymer concentration of 7.5 mg/ml. For **T1** and **T2** the optimal polymer/PCBM ratio was 1:4 spin-coated from o-dichlorobenzene. The optimal layer thickness was around 60-80 nm.

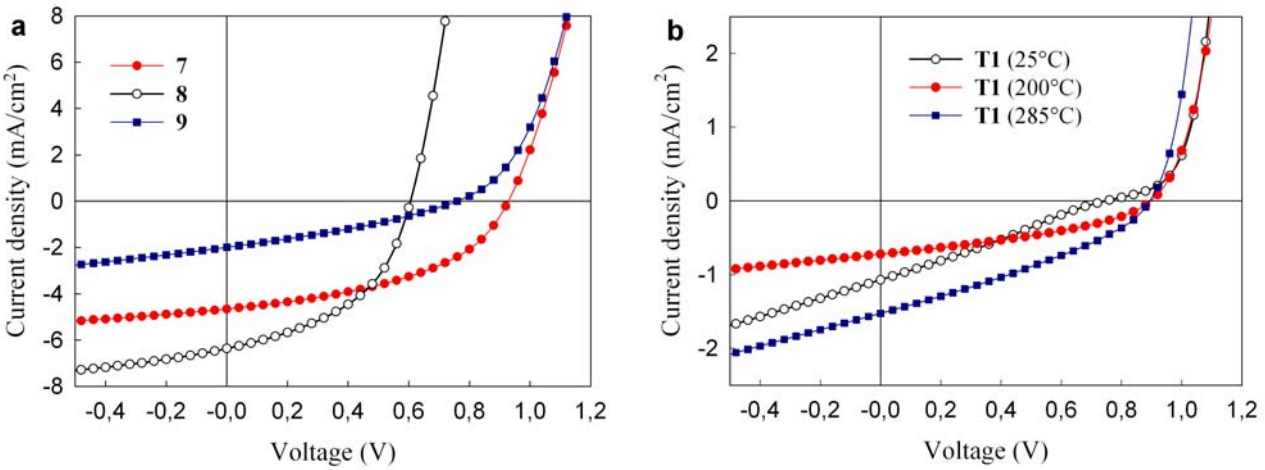

Figure 5.6. (a) *J-V* characteristics of the **7**:PCBM, **8**:PCBM and **9**:PCBM solar cells measured under 100 mW/cm² white light. (b) *J-V* characteristics of solar cells based on **T1** and PCBM measured under 100 mW/cm² white light before and after a thermal treatment.

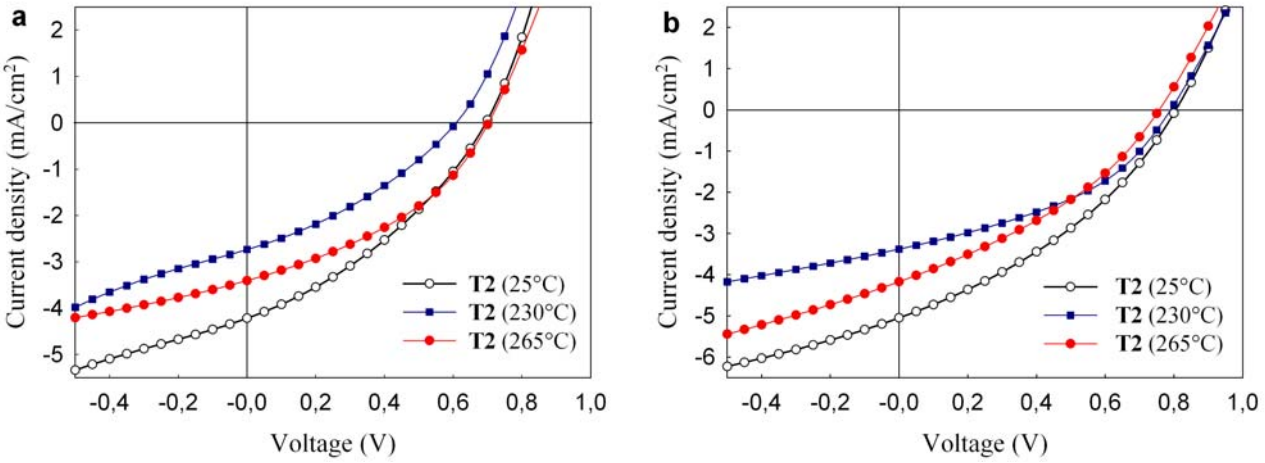

Figure 5.7. *J-V* characteristics of (a) **T2**:[60]PCBM solar cells and (b) **T2**:[70]PCBM solar cells measured under 74.3 mW/cm² white light before and after a thermal treatment.

Table 5.2. Photovoltaic performance of devices based on blends of polymer and PCBM

polymer	layer thickness (nm)	thermal treatment[a] (°C)	V_{oc} (V)	J_{sc}(SR) (mA/cm²)	FF	η (%)
T1	92	-	0.75	1.07[b]	0.26	0.21
T1	92	200	0.90	0.72[b]	0.37	0.24
T1	78	285	0.90	1.36	0.34	0.42
T2	-	-	0.69	4.22[b]	0.35	1.36
T2	-	230	0.59	2.74[b]	0.33	0,72
T2	-	265	0.70	3.40[b]	0.38	1,24
T2[c]	-	-	0.81	5.05[b]	0.35	1.93
T2[c]	-	230	0.79	3.38[b]	0.41	1.46
T2[c]	-	265	0.76	4.17[b]	0.35	1.49
7	63	-	0.93	5.18	0.46	2.22
8	80	-	0.61	6.21	0.47	1.78
9	65	-	0.76	2.56	0.32	0.62

[a] heated for 20-30 sec. [b] unestimated. [c] Devices prepared with [70]PCBM

The obtained current–voltage curves are presented in figure 5.6 and 5.7 which shows the current–voltage characteristics of the polymer:PCBM solar cells. The devices based on **7**, with only one thiophene unit alternating with benzothiadiazole, and PCBM showed power

conversion efficiencies of up to 2.22% (Table 5.2). The devices had high open-circuit voltages (V_{oc}) of 0.93 V, moderate fill factors (FF) of 0.46 and current densities (J_{sc}) of 5.18 mA/cm^2. The external quantum efficiency (EQE) for **7**:PCBM is higher than 23% in the wavelength range between 350 and 650 nm, and the maximum was found to be 35% around 370 nm where PCBM also absorbs (Figure 5.8). Polymer **8**:PCBM gives an EQE higher than 22% in the range between 400 and 680 nm with a maximum of 39% at around 600 nm. Compared to **7**:PCBM devices the EQE is enhanced by up to 10% in the range 450-720 nm which gives a current density of 6.21 mA/cm^2. The devices based on **8**:PCBM performed slightly poorer due to a lower V_{oc} of typically 0.61 V which resulted in power conversion efficiencies of up to 1.78%. Solar cells based on polymer **9**:PCBM gave significantly lower EQE with quantum efficiencies around 10-15% in the range of 350-650 nm giving current densities of 2.56 mA/cm^2. Together with a typical V_{oc} of 0.76 V and low fill factors of 0.32, power conversion efficiencies of up to 0.62% were obtained. The lower performance of **9** compared to **7** and **8** could be due to the different polymerisation procedure where excess of nickel(0) was used instead of a catalytic amount of palladium employed in the Stille coupling. The devices based on the thermocleavable polymer **T1** and PCBM showed the lowest power conversion efficiencies of up to 0.42% (Table 5.2). Without thermal treatment of **T1**:PCBM devices a typical V_{oc} of 0.75 V was obtained. Upon heating the device to 200 °C the V_{oc} increases to 0.90 V and resides there when annealing at 285 °C. The FF increased from 0.26 to 0.37 after thermal treatment at 200 °C and then drops a bit upon heating the device at 285 °C. The current density firstly drops after thermal treatment and then increases again when heating at 285 °C. The EQE of **T1**:PCBM (thermocleaved at 285 °C) is relatively low with quantum efficiencies of about 5-10% in the range 350-670 nm (figure 5.8) giving it an estimated current density of 1.36 mA/cm^2. A general observation was that the devices based on **T1**:PCBM performed better after thermocleavage due to an increase in mainly the current and fill factor. From the TGA of **T1** (Figure 5.3a) and earlier reports concerning thermocleavable materials,[16,17] it is reasonable to consider **T1** as thermocleaved to the free carboxylic acid when the devices are annealed at 200-230 °C. By annealing at 285 °C decarboxylation probably initiate leading to partial transformation. Thus, the final film then presents chemistry corresponding to both the free carboxylic acid and the native material (Figure 5.2) to varying degrees after a thermal treatment at 285 °C. Annealing at higher temperatures (310 °C) involved a drastic drop in the V_{oc} and J_{sc} thereby reducing the performance. Despite the

lower efficiency of polymer **T1** compared to the polymers **7–9** the thermocleavable polymer **T1** does show promising results with increased performance after thermocleavage. In the majority of cases where thermocleavable materials have been employed in polymer solar cells a drop in performance has been observed when thermocleaving the polymer and only one previous case has demonstrated an advantage of thermocleavage in terms of performance.[17] The lower performance of polymer **T1** compared to the polymers **7–9** can be an effect of the more electron-attracting ester groups situated on thiophene (**T1**) compared to the electron-donating alkoxy groups on benzothiadiazole (**7–9**).

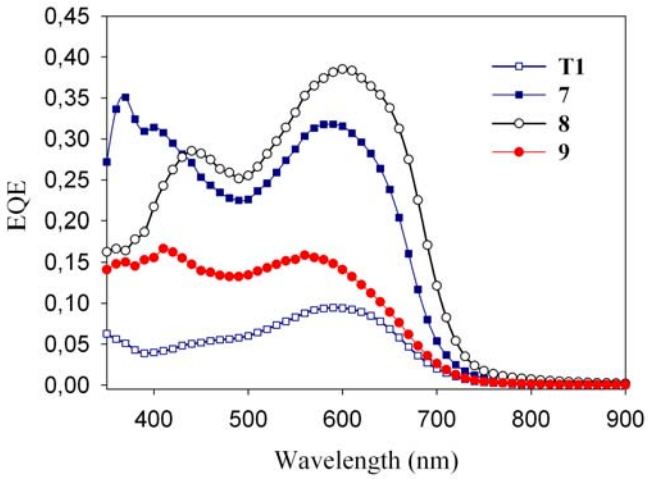

Figure 5.8. EQE spectra of polymer:PCBM solar cells. T1 were thermocleaved at 285 °C.

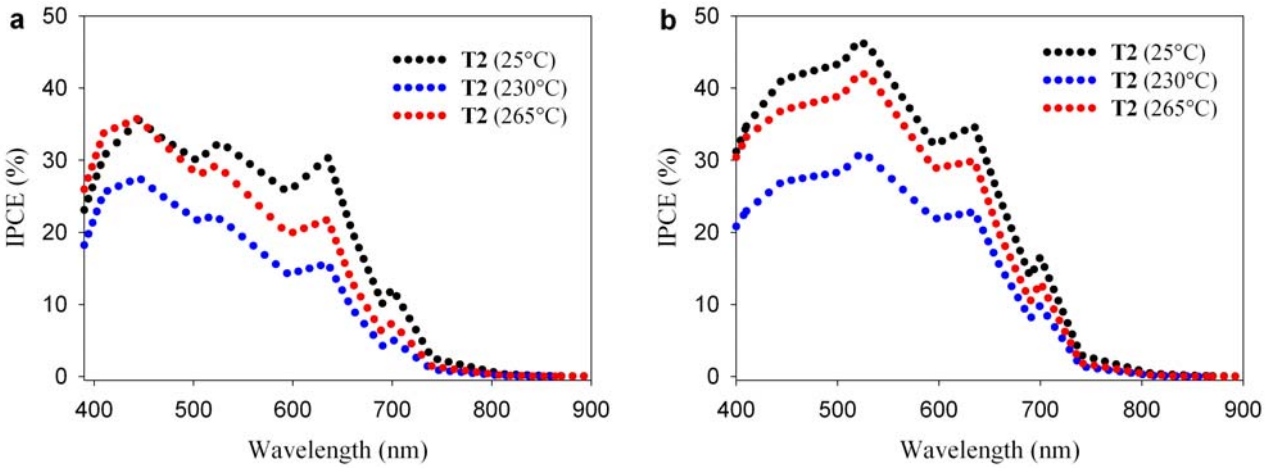

Figure 5.9. IPCE of (a) **T2**:[60]PCBM solar cells and (b) **T2**:[70]PCBM solar cells before and after a thermal treatment.

T2 has enhanced donor character compared to **T1** through the incorporated planar CPDT unit and solar cells based on **T2** demonstrate a significant improvement in performance. *J-V* curves for **T2**:PCBM devices before and after a thermal treatment are shown in figure 5.7. Devices based on **T2**:PCBM show the same trend in terms of the current density as for **T1**. Without thermal treatment of the devices a typical J_{sc} of 4.22 mA/cm^2 was obtained (Table 5.2). Upon heating the device to 230 °C the J_{sc} drops to 2.74 mA/cm^2 and then increases again to 3.40 mA/cm^2 when annealing at 265 °C. The open-circuit voltage and fill factor experience the same development where you first observe a drop upon annealing at 230 °C followed by an increase when annealing at 265 °C. This results in a nearly retained power conversion efficiency (η = 1.24%) when **T2** is thermocleaved at 265 °C compared to the un-annealed device based on the soluble precursor polymer (η = 1.36%). The effect of annealing is clearly visible in the incident photon to current efficiency (Figure 5.9a). For the un-annealed device, IPCE lies over 25% in the wavelength range 400-650 nm reaching a maximum of 36%. After annealing at 230 °C the IPCE drops up to 15% but the initial IPCE is nearly retained when annealing at 265 °C. In a try to increase the photocurrent **T2** was also tested in solar cells with [70]PCBM and the obtained *J-V* curves and IPCE are depicted in figure 5.7b and 5.9b. [70]PCBM and [60]PCBM has similar electrochemical properties but [70]PCBM absorbs more light because of its lower symmetry that allow low energy transitions.[18] The incorporation of [70]PCBM improved the performance which is clearly reflected in the IPCE which is found to be higher than 30% in the wavelength range 400-650 nm reaching a maximum of 47% (Figure 5.9b). The **T2**:[70]PCBM devices exhibit one of the best performances of any bulk heterojunction solar cell based on a thermocleavable material studied to date, with J_{sc} = 5.05 mA/cm^2, V_{oc} = 0.81 V, FF = 0.35 and η = 1.93%. As for **T1**, **T2** can be regarded as thermocleaved to the free carboxylic acid when the device films are annealed at 200-230 °C. According to TGA (Figure 5.3b), the decarboxylation of **T2** start to happen around 265 °C which is also the optimized temperature for thermocleavage of the **T2**:PCBM solar cells. It is likely that thermocleavage under the optimized conditions (265 °C), only lead to partial transformation, as discussed for **T1**, where the final film presents chemistry corresponding to both the free carboxylic acid and the decarboxylated material (Figure 5.2) to varying degrees.

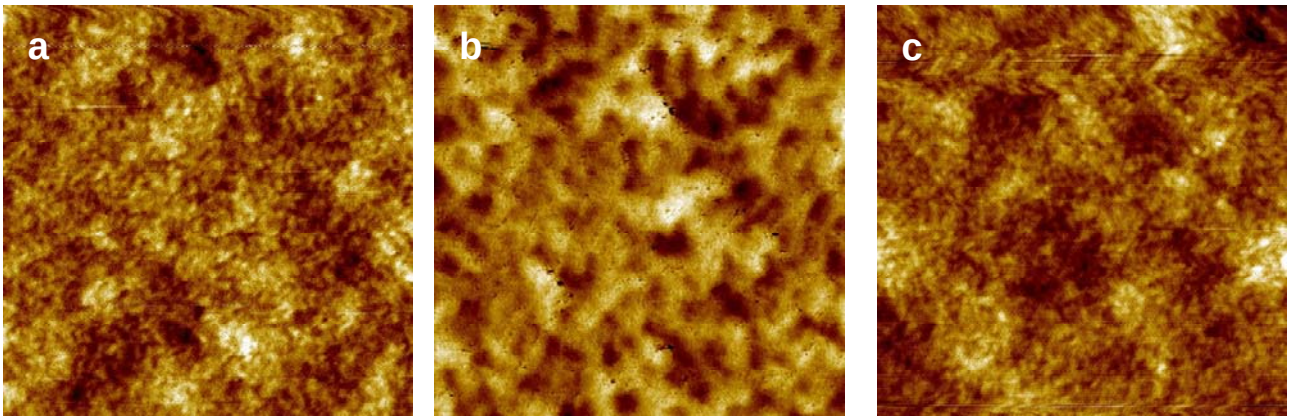

Figure 5.10. AFM topography images (2 µm×2 µm) of **T2**:[60]PCBM films. (a) un-annealed, (b) annealed at 230 °C and (c) 265 °C. The height scale is 5 nm for all images.

5.6 Morphology

The performance of bulk heterojunction solar cells based on a mixture of donor and acceptor material is known to be very dependent on the morphology of the active layer.[19-21] Creating an nanoscale interpenetrating bicontinous network of the donor and acceptor material is essential to achieve a large interfacial area ensuring quantitative charge separation. At the same time the constructed bulk heterojunction should insure a direct or percolating pathway of the charge carriers to the respective electrodes in order to effectively transport and collect the charges. Different factors have been shown to have an influence on the morphology including the donor-acceptor ratio, solvent and annealing.[22-24] Changes in the surface topography of **T2**:PCBM device films annealed at different temperatures, as measured by atomic force microscopy (AFM), are shown in figure 5.10. All films are relatively smooth showing a height difference around 5 nm. The un-annealed film and the film annealed at 265 °C (Figure 5.10a and 5.10c) reveals a rather uniform phase separation with relatively small domain sizes compared to the device film annealed at 230 °C (Figure 5.10b)**.** Figure 5.10b shows features with a size larger than 100 nm which indicate extensive phase segregation of the polymer and PCBM which is possibly limiting charge carrier generation and transport to the electrodes. The reduced current densities of the **T2**:PCBM devices annealed at 230 °C might be a direct consequence. The same effect was observed when the polymers presented in chapter 4 were thermocleaved to the free carboxylic acid.

5.7 Conclusion

In conclusion, five new low band gap polymers have been synthesized. They are based on 2,1,3-benzothiadiazole alternating with thiophene and CPDT units along the chain, bearing solubilising chains on either benzothiadiazole (**7–9**) or thiophene (**T1**, **T2**). The solubilising chain on **T1** and **T2** is a thermocleavable alkyl ester group which allows processing of three chemically different thin films from the same soluble precursor polymer. When the alkyl ester group is heated, the labile ester bond breaks, eliminating a volatile alkene and leaving the polymer component more rigid. The five polymers optical properties and photovoltaic performance in blends with PCBM have been investigated. In chloroform solution the polymers had very similar optical band gaps ranging from 1.79-1.96 eV. The optical band gaps are lowered to 1.66-1.75 eV in thin film (Table 5.1), indicating significant interchain association in the solid state. Furthermore polymer **7** and **8** showed vibronic fine structure centered at 625 nm in the solid state. The best performing polymer in a bulk heterojunction solar cell was **7** with J_{sc} = 5.18 mA/cm^2, V_{oc} = 0.93 V, FF = 0.46 and η = 2.22%. Devices based on **T1**:PCBM performed better after thermocleavage due to an increase in mainly current density and fill factor giving power conversion efficiencies up to 0.42% representing a doubling as compared to the soluble precursor polymer. Compared to **T1**, **T2** has incorporated a planar CPDT unit instead of thiophene which leads to significant improvement in solar cell performance. Bulk heterojunction solar cells based on **T2** and [70]PCBM showed very promising results for a thermocleavable material with J_{sc} = 5.05 mA/cm^2, V_{oc} = 0.81 V, FF = 0.35 and η = 1.93%.

5.8 Experimental section

^{1}H-NMR and ^{13}C-NMR spectra are included in the Supporting Information.[25]

General methods. Molecular weights were determined using size exclusion chromatography in HPLC-grade *o*-dichlorobenzene (ODCB) at 80 °C against polystyrene standards on a Polymer Laboratories-GPC 120 high temperature chromatograph, a PD 2040 high-temperature light scattering detector, and a Midas autosampler. A mixed-C 300 × 7.5 mm column was used, together with a precolumn. The flow rate was 1 mL/min and the injection

volume 100 μL. UV-vis absorption spectra were measured with a Perkin-Elmer Lambda 900 spectrometer. TGA experiments were performed with a dynamic heat rate (10 °C/min) under an argon atmosphere (50 ml/min) in the temperature range 50-500 °C. AFM images were taken on a Nanos multimode AFM (Bruker). Unless stated otherwise all reagents and solvents were obtained from Aldrich and used without further purification. Dichloromethane, DMF and toluene were dried with molecular sieves (3 Å) and used directly without filtration or distillation. NBS was recrystallised from water and dried at 70 °C in vacuum. Evaporation was performed on a rotary evaporator at 40 °C. NMR spectra were obtained on Bruker 500 MHz or 250 MHz spectrometers. Melting points were determined on an electrothermal instrument and are uncorrected. The samples were dried at 50 °C for 24 hours in a vacuum oven prior to analysis. 5-bromothiophene-3-carboxylic acid (**10**)[26] and **14**[27] was prepared according to literature procedures.

Polymer solar cell fabrication and analysis. Photovoltaic devices were made by spin coating PEDOT:PSS (Clevios P, VP Al4083) onto precleaned, patterned indium tin oxide (ITO) substrates (14 Ω per square) (Naranjo Substrates). The active layer was deposited by spin coating a blend of the polymer and [60]PCBM dissolved in chlorobenzene (20-30 mg/ml). The counter electrode of LiF (1 nm) and aluminium (100nm) was deposited by vacuum evaporation at 2-3 × 10^{-7} mbar. The active area of the cells was 0.091-0.162 cm^2 and the active layer thickness was determined with a Dektak surface profiler. *J-V* characteristics were measured under 100 mW/cm^2 white light from a tungsten-halogen lamp filtered by a Schott GG385 UV filter and a Hoya LB120 daylight filter, using a Keithley 2400 source meter. The spectral response (SR) was measured under operating conditions using bias light from a 532 nm solid state laser (Edmund Optics). Monochromatic light from a 50 W tungsten halogen lamp (Philips focusline) in combination with monochromator (Oriel, Cornerstone 130) was modulated with a mechanical chopper. The response was recorded as the voltage over a 50 Ω resistance, using a lock-in amplifier (Stanford research Systems SR830). A calibrated Si cell was used as reference. The device was kept behind a quartz window in a nitrogen filled container. Short circuit currents under AM1.5 conditions were obtained from the spectral response and convolution with the solar spectrum (J_{sc}(SR)). The value of J_{sc}(SR) was used with V_{oc} and FF from the 100 mW/cm^2 white light *J-V* characteristics to estimate the power conversion efficiency η.

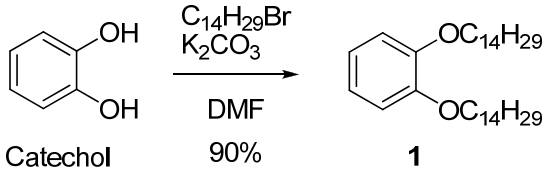

1,2-bis(tetradecyloxy)benzene (1). To a solution of catechol (10 g, 0.091 mol) in dry DMF (50 ml) was added 1-bromotetradecane (0.209 mol, 58 g, 62 mL) and K_2CO_3 (38 g, 0.27 mol). The mixture was stirred at 100 °C under a nitrogen atmosphere for 40 hours. After cooling the mixture to room temperature (RT), 100 ml of water were added. The organic layer was separated and the aqueous layer was extracted with DCM. The combined organic phase was dried over $MgSO_4$. After filtration, the mixture was concentrated under vacuum. The product was recrystallized twice from acetone. Yield: 41 g (90%), white needlelike crystals. *Mp* = 53-54 °C. ^{1}H NMR ($CDCl_3$): δ = 6.89 (s, 4H), 4.00 (t, J = 6.6 Hz, 4H), 1.88 – 1.75 (m, 4H), 1.57 – 1.22 (m, 44H), 0.89 (t, J = 6.6 Hz, 6H). ^{13}C NMR ($CDCl_3$): δ = 149.31, 121.02, 114.22, 69.33, 31.94, 29.71, 29.67, 29.65, 29.46, 29.37, 26.07, 22.69, 14.11.

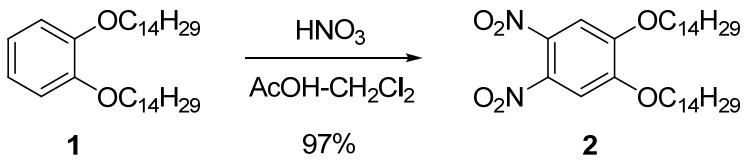

1,2-dinitro-4,5-bis(tetradecyloxy)benzene (2). To a two neck round-bottom flask containing dichloromethane (140 mL), acetic acid (140 mL), and 1,2-bisdodecyloxybenzene (10 g, 19.9 mmol) cooled to 10 °C was added dropwise 65% nitric acid (20 mL). The reaction was allowed to warm to room temperature and stirred for 1 hour. The mixture was again cooled to 10 °C and 100% nitric acid (50 mL) was added dropwise. The mixture was allowed to warm to room temperature and the mixture was stirred for 40 hours. After completion of the reaction, the reaction mixture was poured into ice-water and the dichloromethane layer separated. The water phase was extracted with dichloromethane. The combined organic phase was washed with water, sat. $NaHCO_{3\,(aq)}$, brine and dried over $MgSO_4$. Concentration in vacuum gave the crude product that was recrystallized from ethanol. Yield: 11.4 g (97%), yellow solid. *Mp* = 79-80 °C. ^{1}H NMR ($CDCl_3$): δ = 7.29 (s, 2H), 4.10 (t, J = 6.5 Hz, 4H), 1.94 – 1.81 (m, 4H), 1.56 – 1.18 (m, 44H), 0.88 (t, J = 6.6 Hz, 6H). ^{13}C NMR ($CDCl_3$): δ = 151.82, 136.49, 107.94, 70.21, 31.92, 29.70, 29.69, 29.67, 29.66, 29.57, 29.54, 29.36, 29.23, 28.71, 25.81, 22.68, 14.09.

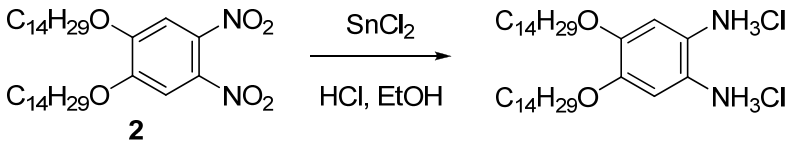

2

4,5-bis(tetradecyloxy)benzene-1,2-diaminium chloride. A mixture of 1,2-dinitro-4,5-bis-(tetradecyloxy)-benzene (2 g, 3.37 mmol) and Sn(II)Cl_2 (26.9 mmol, 5.1 g) in ethanol (50 ml) and conc. HCl (20 ml) was heated to 85 °C over the night. After cooling to room temperature the product was filtered and washed with water and methanol. Finally it was dried at RT under a stream of argon and used directly (unstable). Yield: 1.8 g (88 %), off-white solid.

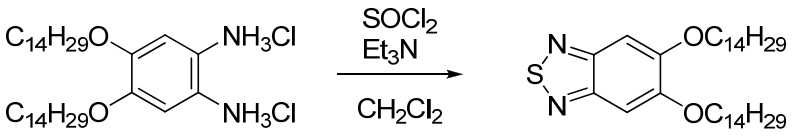

3

5,6-bis(tetradecyloxy)benzo[*c*][1,2,5]thiadiazole (3). To a mixture of 4,5-bis(tetradecyloxy)-benzene-1,2-diaminium chloride (1.54 g, 2.54 mmol) and triethylamine (25.1 mmol, 3.5 ml) in 40 ml dichloromethane was slowly added a solution of thionyl chloride (4.83 mmol, 352 µL) in 5 ml dichloromethane. After addition the mixture was heated to reflux for 6 hours. The cooled solution was concentrated in vacuum followed by trituration in water. After stirring for 30 min the product was filtered and recrystallized from ethanol. Yield: 1.1 g (77 %), off-white solid. *Mp* = 90-91 °C. ^{1}H NMR ($CDCl_3$): δ = 7.13 (s, 2H), 4.09 (t, *J* = 6.5 Hz, 4H), 2.04 – 1.79 (m, 4H), 1.58 – 1.16 (m, 44H), 0.95 – 0.81 (m, 6H). ^{13}C NMR ($CDCl_3$): δ = 154.17, 151.40, 98.44, 69.13, 31.92, 29.71, 29.69, 29.66, 29.61, 29.36, 28.75, 26.02, 22.68, 14.09.

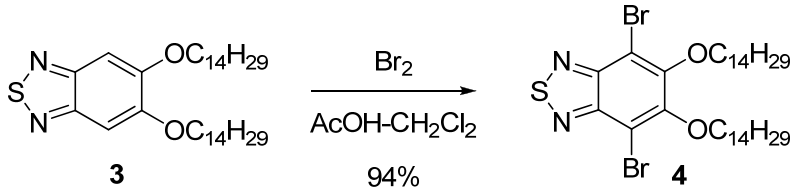

3 **4**

4,7-dibromo-5,6-bis(tetradecyloxy)benzo[*c*][1,2,5]thiadiazole (4). To a solution of **3** (8.00 g, 14.3 mmol) in a mixture of dichloromethane (400 mL) and acetic acid (175 mL) was added bromine (5 mL, 97.5 mmol), and the resulting mixture wass stirred in the dark for ca. 48 h at room temperature. The mixture was then poured in water (500 mL), extracted with dichloromethane, sequentially washed with water, saturated $NaHCO_{3\,(aq)}$, 1M $Na_2SO_{3\,(aq)}$ and the solvents are evaporated under reduced pressure. The crude product was purified by

recrystallization from ethanol twice to give fluffy needle-like microcrystals. Yield: 9.60 g (94 %). *Mp* = 65-66 °C. ^{1}H NMR ($CDCl_3$): δ = 4.16 (t, *J* = 6.6 Hz, 4H), 1.97 – 1.81 (m, 4H), 1.62 – 1.46 (m, 4H), 1.46 – 1.19 (m, 40H), 0.88 (t, *J* = 6.6 Hz, 6H). ^{13}C NMR ($CDCl_3$): δ = 154.53, 150.39, 106.25, 75.16, 31.92, 30.27, 29.71, 29.70, 29.68, 29.66, 29.63, 29.61, 29.43, 29.36, 25.99, 22.68, 14.10.

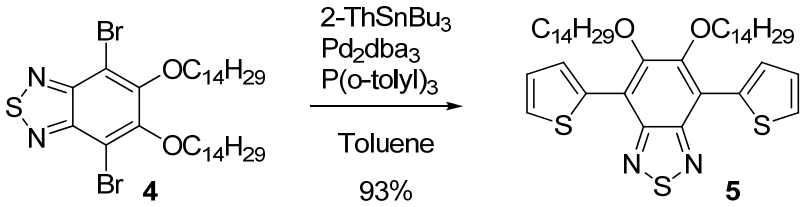

5,6-bis(tetradecyloxy)-4,7-di(thiophen-2-yl)benzo[*c*][1,2,5]thiadiazole (5). To a solution of **4** (900 mg, 1.25 mmol), Pd_2dba_3 (0.05 mmol, 46 mg) and tri-o-tolylphosphine (0.40 mmol, 122 mg) in dry toluene (10 ml) was added 2-tributylstannylthiophene (3.13 mmol, 994 µL) and the reaction mixture was heated to reflux for 16 hours under argon. The reaction mixture was concentrated directly on celit in vacuum. Dry column chromatography (silica gel 15-40 μm, eluted with Heptane/$CHCl_3$, gradient 1-10 % $CHCl_3$) afforded **5**. Yield: 848 mg (93 %), yellow solid. *Mp* = 59-60 °C. ^{1}H NMR ($CDCl_3$): δ = 8.47 (d, *J* = 2.8 Hz, 2H), 7.51 (d, *J* = 4.1 Hz, 2H), 7.26 – 7.20 (m, 2H), 4.11 (t, *J* = 7.1 Hz, 4H), 2.00 – 1.85 (m, 4H), 1.51 – 1.20 (m, 44H), 0.93 – 0.85 (m, 6H). ^{13}C NMR ($CDCl_3$): δ = 152.00, 151.02, 134.14, 130.55, 127.29, 126.74, 117.64, 74.37, 31.93, 30.33, 29.72, 29.68, 29.64, 29.55, 29.37, 25.97, 22.69, 14.10.

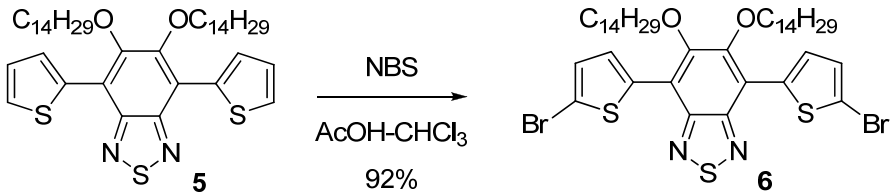

4,7-bis(5-bromothiophen-2-yl)-5,6-bis(tetradecyloxy)benzo[*c*][1,2,5]thiadiazole (6). To a solution of **5** (817 mg, 1.13 mmol) in $CHCl_3$ (40 ml) and glacial acetic acid (40 ml) was added NBS (2.26 mmol, 401 mg) in one portion. The mixture was stirred at room temperature for 20 hours in the dark. The reaction mixture was concentrated directly on celit in vacuum. Dry column chromatography (silica gel 15-40 μm, eluted with Heptane/$CHCl_3$, gradient 1-10 % $CHCl_3$) afforded **6**. Yield: 912 mg (92 %), orange solid. *Mp* = 80-81 °C. ^{1}H NMR ($CDCl_3$): δ =

8.37 (d, *J* = 4.1 Hz, 2H), 7.17 (d, *J* = 4.1 Hz, 2H), 4.12 (t, *J* = 7.2 Hz, 4H), 2.01 – 1.86 (m, 4H), 1.52 – 1.20 (m, 44H), 0.88 (t, *J* = 6.6 Hz, 6H). ^{13}C NMR ($CDCl_3$): δ = 151.52, 150.42, 135.72, 131.01, 129.67, 117.01, 115.46, 74.59, 31.93, 30.27, 29.72, 29.68, 29.63, 29.50, 29.37, 25.93, 22.69, 14.11.

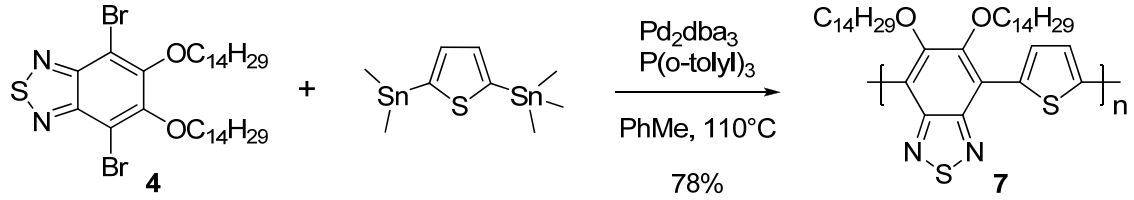

Poly(5,6-bis(tetradecyloxy)-4-(thiophen-2-yl)benzo[*c*][1,2,5]thiadiazole) (7). **4** (100 mg, 0.139 mmol), 2,5-bis(trimethylstannyl)thiophene (0.139 mmol, 57 mg), Pd_2dba_3 (6.4 mg, 6.95 µmol) and tri-(o-tolyl)phosphine (17 mg, 55.6 µmol) was mixed in dry degassed toluene (10 ml). The reaction mixture was heated to reflux for 48 hours under argon. After cooling to room temperature the mixture was poured into 100 ml methanol and the polymer was allowed to precipitate. The polymer was filtered and purified by Soxhlet extraction using methanol, hexane and chloroform. The chloroform fraction was then stirred at room temperature for 16 hours with an aqueous EDTA solution (155 mg in 5 ml H_2O). Water was added followed by separation of the phases. The chloroform phase was concentrated in vacuum and the residue was redissolved in toluene and precipitated in methanol (1:10). Filtration and drying in vacuum afforded **7**. Yield: 70 mg (78 %), dark purple solid. ^{1}H-NMR ($CDCl_3$) δ = 8.77 – 8.61 (m, 2H), 7.24 – 7.17 (m, endgroup), 4.39 – 4.18 (m, 4H), 2.60 – 2.50 (m, 4H), 2.19 – 2.04 (m, 4H), 1.67 – 1.51 (m, 4H), 1.49 – 1.20 (m, 32H), 1.14 – 1.00 (m, 4H), 0.97 – 0.85 (m, 6H). GPC (ODCB): M_w = 16600, PDI = 1.7.

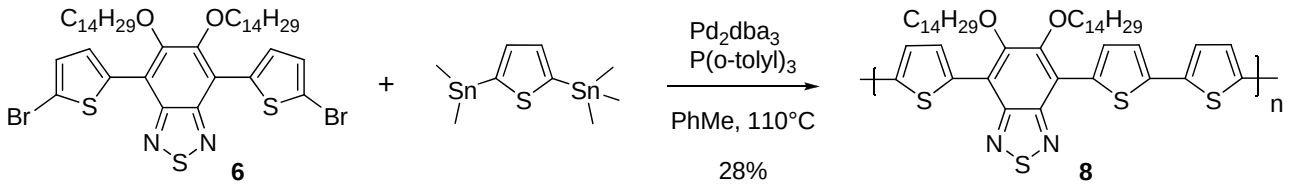

Poly(4-(2,2'-bithiophen-5-yl)-5,6-bis(tetradecyloxy)-7-(thiophen-2-yl)-benzo-[*c*]-[1,2,5]-thiadiazole) (8). **6** (195 mg, 0.221 mmol), 2,5-bis(trimethylstannyl)thiophene (0.221 mmol, 90 mg), Pd_2dba_3 (10 mg, 11.0 µmol) and tri-(o-tolyl)phosphine (27 mg, 88.3 µmol) was mixed in dry degassed toluene (20 ml). The reaction mixture was heated to reflux for 48

hours under argon. After cooling to room temperature the mixture was poured into 200 ml methanol and the polymer was allowed to precipitate. The polymer was filtered and purified by Soxhlet extraction using methanol, hexane and chloroform. The chloroform fraction was then stirred at room temperature for 16 hours with an aqueous EDTA solution (247 mg in 10 ml H_2O). Water was added followed by separation of the phases. The chloroform phase was concentrated in vacuum and the residue was redissolved in toluene and precipitated in methanol (1:10). Filtration and drying in vacuum afforded **8**. Yield: 50 mg (28 %), dark purple solid. ^{1}H-NMR ($CDCl_3$) δ = 8.66 – 8.02 (m, 4H), 7.14 – 6.66 (m, 2H), 4.36 – 4.04 (m, 4H), 2.29 – 1.93 (m, 8H), 1.80 – 1.12 (m, 40H), 1.09 – 0.79 (m, 6H). GPC (ODCB): M_w = 26000, PDI = 2.9.

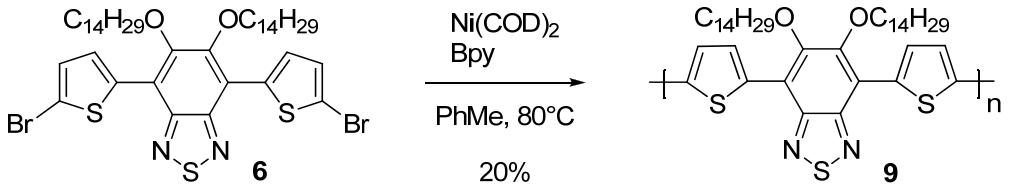

Poly(5,6-bis(tetradecyloxy)-4,7-di(thiophen-2-yl)benzo[*c*][1,2,5]thiadiazole)(9).
$Ni(COD)_2$ (187 mg, 0.681 mmol) and 2,2'-dipyridyl (0.681 mmol, 106 mg) was mixed in dry degassed toluene (30 ml). The mixture was heated to 80 ^{o}C followed by addition of **6** (200 mg, 0.227 mmol). After stirring for 9 hours under argon the mixture was poured into 300 ml methanol and the polymer was allowed to precipitate. Then the polymer was filtered and purified by Soxhlet extraction using methanol, hexane and chloroform. The chloroform fraction was then stirred at room temperature for 16 hours with an aqueous EDTA solution (760 mg in 20 ml H_2O). Water was added followed by separation of the phases. The chloroform phase was concentrated in vacuum and the residue was redissolved in toluene and precipitated in methanol (1:10). Filtration and drying in vacuum afforded **9**. Yield: 33 mg (20 %), dark purple solid. ^{1}H-NMR ($CDCl_3$) δ = 8.65 – 8.56 (m, 2H), 8.44 – 8.40 (m, endgroup), 7.49 – 7.42 (m, 2H), 7.23 – 7.19 (m, endgroup), 4.34 – 4.14 (m, 4H), 2.16 – 1.95 (m, 8H), 1.66 – 1.49 (m, 8H), 1.49 – 1.13 (m, 32H), 0.99 – 0.83 (m, 6H). GPC (ODCB): M_w = 7100, PDI = 1.7.

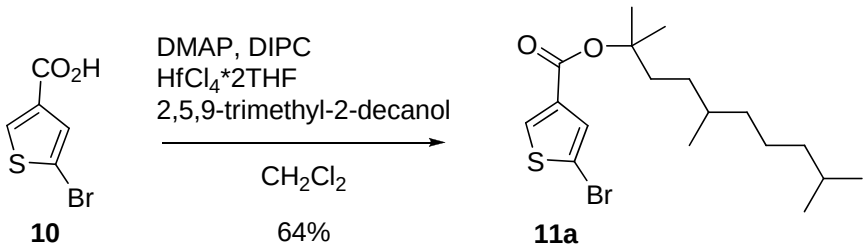

2,5,9-trimethyldecan-2-yl 5-bromothiophene-3-carboxylate (11a). A mixture of **10** (6 g, 29 mmol), DMAP (3.9 g, 32 mmol), $HfCl_4$·2THF (675 mg, 1.45 mmol) and 2,5,9-trimethyl-2-decanol (6.4 g, 32 mmol) in dry methylene chloride (100 ml) was stirred at room temperature under argon for 30 min. *N,N'*-diisopropylcarbodiimide (5 ml, 32 mmol) was added and the reaction mixture was heated to reflux and stirred for 24 hours. After cooling to RT the reaction mixture was concentrated on celite in vacuum. Dry column chromatography (silica gel 15-40 µm, eluted with EtOAc/Heptane, gradient 0-3% EtOAc) afforded **11a**. Yield: 7.2 g (64 %), colourless oil. ^{1}H NMR ($CDCl_3$): δ = 7.88 (d, J = 1.5 Hz, 1H), 7.40 (d, J = 1.5 Hz, 1H), 1.93 – 1.72 (m, 2H), 1.53 (s, 6H), 1.45 – 1.06 (m, 10H), 0.91 – 0.82 (m, 9H). ^{13}C NMR ($CDCl_3$): δ = 160.61, 135.81, 132.74, 130.13, 112.21, 83.75, 39.22, 38.33, 37.01, 32.91, 30.77, 27.89, 26.13, 26.05, 24.73, 22.65, 22.56, 19.68.

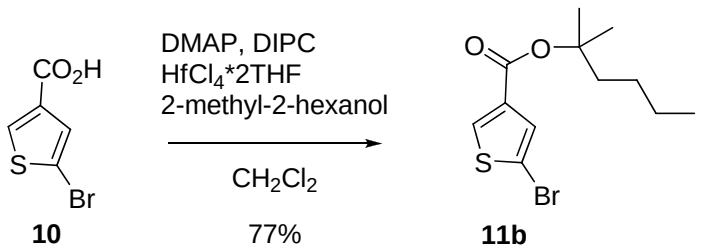

2-methylhexan-2-yl 5-bromothiophene-3-carboxylate (11b). Prepared with the same procedure as for **11a**. Yield: 4.5 mg (77 %), colourless oil. ^{1}H NMR (250 MHz, $CDCl_3$) δ = 7.89 (d, J = 1.5 Hz, 1H), 7.40 (d, J = 1.5 Hz, 1H), 1.89 – 1.79 (m, 2H), 1.53 (s, 6H), 1.39 – 1.29 (m, 4H), 0.92 (t, J = 7.0 Hz, 3H). ^{13}C NMR (250 MHz, $CDCl_3$) δ = 160.72, 135.96, 132.96, 130.34, 112.38, 83.78, 40.59, 26.10 (2 signals), 22.79, 13.97.

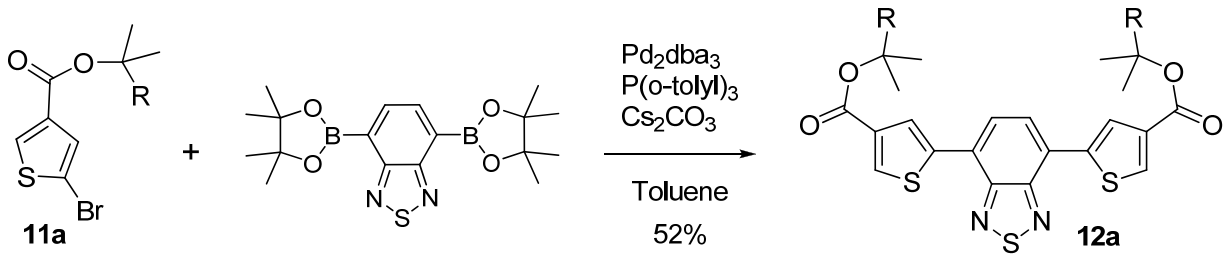

bis(2,5,9-trimethyldecan-2-yl)-5,5'-(benzo[*c*][1,2,5]thiadiazole-4,7-diyl)dithiophene-3-carboxylate (12a). 4,7-bis(4,4,5,5-tetramethyl-1,3,2-dioxaborolan-2-yl)-benzo-[*c*]-[1,2,5]-thiadiazole (1 g, 2.58 mmol), **11a** (2.3 g, 5.93 mmol), Pd_2dba_3 (94 mg, 0.1 mmol) and tri-(o-tolyl)phosphine (251 mg, 0.83 mmol) was dissolved in dry toluene (20 ml) and stirred for 15 min at RT under argon. Then Cs_2CO_3 (6.7 g, 21 mmol), degassed water (7 ml) and 1 drop Aliquat® 336 was added. The reaction mixture was stirred at 90 °C for 48 hours. The reaction mixture was allowed to cool to room temperature followed by addition of water (25 ml). The mixture was extracted with ether (3 × 25 ml) and the combined organic phase was dried ($MgSO_4$), filtered and concentrated on celit in vacuum. Dry column chromatography (silica gel 15-40 µm, eluted with EtOAc/Heptane, gradient 0-5% EtOAc) afforded **12a**. Yield: 1 g (52 %), yellow oil. ^{1}H NMR ($CDCl_3$): δ = 8.39 (d, J = 1.2 Hz, 2H), 8.11 (d, J = 1.2 Hz, 2H), 7.89 (s, 2H), 1.96 – 1.83 (m, 4H), 1.59 (s, 12H), 1.56 – 1.10 (m, 20H), 0.91 (d, J = 5.2 Hz, 6H), 0.86 (d, J = 6.6 Hz, 12H). ^{13}C NMR ($CDCl_3$): δ = 161.83, 152.39, 139.30, 136.26, 132.93, 127.70, 125.81, 125.65, 83.60, 39.29, 38.61, 37.13, 33.05, 30.95, 27.94, 26.17, 26.13, 24.77, 22.66, 22.57, 19.74.

bis(2-methylhexan-2-yl)-5,5'-(benzo[*c*][1,2,5]thiadiazole-4,7-diyl)-dithiophene-3-carboxylate (12b). Prepared with the same procedure as for **12a** using the monomer **11b**. Yield: 650 mg (50 %), yellow oil. ^{1}H NMR (250 MHz, $CDCl_3$) δ = 8.39 (d, J = 1.3 Hz, 2H), 8.11 (d, J = 1.3 Hz, 2H), 7.90 (s, 2H), 1.95 – 1.85 (m, 4H), 1.60 (s, 12H), 1.46 – 1.33 (m, 8H), 0.95 (t, J = 7.0 Hz, 6H). ^{13}C NMR (250 MHz, $CDCl_3$) δ = 161.86, 152.39, 139.30, 136.24, 132.96, 127.67, 125.81, 125.66, 83.52, 40.62, 26.18 (2 signals), 23.02, 14.06.

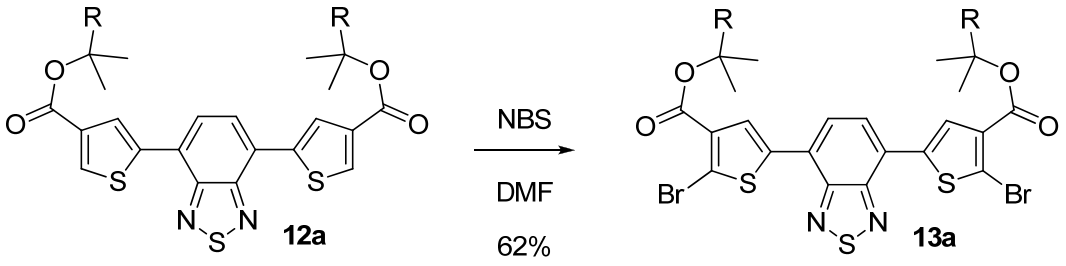

bis(2,5,9-trimethyldecan-2-yl)-5,5'-(benzo[*c*][1,2,5]thiadiazole-4,7-diyl)bis(2-bromothiophene-3-carboxylate) (13a). To a solution of **12a** (1 g, 1.33 mmol) in DMF (20 mL) was added NBS (0.52 g, 2.92 mmol). The resulting mixture was then stirred at room temperature for 24 hours. The mixture was poured into water (30 ml) and extracted several times with dichloromethane. The combined organic phase was dried ($MgSO_4$), filtered and concentrated in vacuum. The crude product was purified by column chromatography (silica gel 70-230 µm, eluted with dichloromethane/cyclohexane 1:1) to afford **13a**. Yield: 750 mg (62 %), orange oil. ^{1}H NMR ($CDCl_3$): δ = 8.15 (s, 2H), 7.80 (s, 2H), 1.99 – 1.83 (m, 4H), 1.62 (s, 12H), 1.56 – 1.08 (m, 20H), 0.92 (d, J = 6.1 Hz, 6H), 0.85 (d, J = 6.6 Hz, 12H). ^{13}C NMR ($CDCl_3$): δ = 160.94, 152.00, 138.22, 133.44, 128.50, 125.05, 124.99, 120.56, 84.77, 39.30, 38.48, 37.18, 33.09, 31.00, 27.93, 26.22, 26.19, 24.78, 22.65, 22.56, 19.75.

bis(2-methylhexan-2-yl)-5,5'-(benzo[c][1,2,5]thiadiazole-4,7-diyl)-bis-(2-bromothiophene-3-carboxylate) (13b). Prepared with the same procedure as for **13a** using the monomer **12b**. Yield: 632 mg (65 %), orange oil. ^{1}H NMR (250 MHz, $CDCl_3$) δ = 8.11 (s, 2H), 7.74 (s, 2H), 1.96 – 1.87 (m, 4H), 1.61 (s, 12H), 1.46 – 1.34 (m, 8H), 0.94 (t, J = 6.9, 6H). ^{13}C NMR (250 MHz, $CDCl_3$) δ = 160.93, 151.88, 138.16, 133.33, 128.42, 124.90 (2 signals), 120.50, 84.68, 40.69, 26.20 (2 signals), 23.03, 14.10.

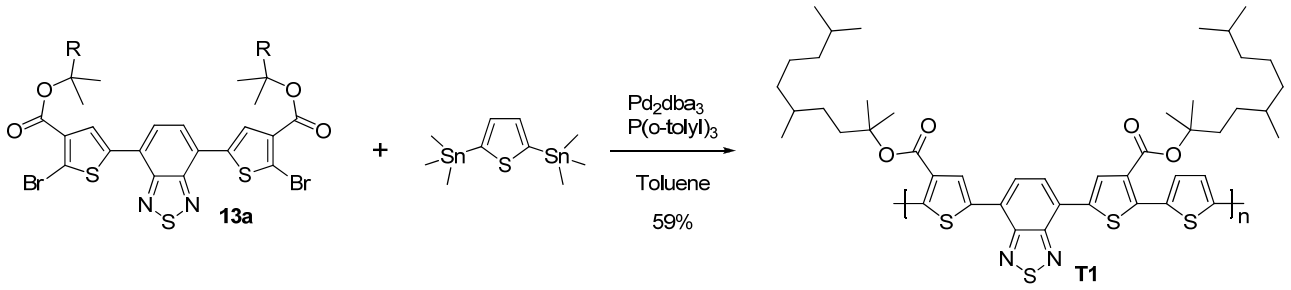

Polymer T1. 13a (323 mg, 0.355 mmol), 2,5-bis(trimethylstannyl)thiophene (0.355 mmol, 145 mg), Pd_2dba_3 (16 mg, 17.5 µmol) and tri-(o-tolyl)phosphine (43 mg, 0.141 mmol) was mixed in dry degassed toluene (25 ml). The reaction mixture was heated to reflux for 48 hours under argon. After cooling to room temperature the mixture was poured into 250 ml methanol and the polymer was allowed to precipitate. The polymer was filtered and purified by Soxhlet extraction using methanol, hexane and chloroform. The chloroform fraction was then stirred at room temperature for 16 hours with an aqueous EDTA solution (400 mg in 10 ml H_2O). Water was added followed by separation of the phases. The chloroform phase was concentrated in vacuum and the residue was redissolved in toluene and precipitated in methanol (1:10). Filtration and drying in vacuum afforded **T1**. Yield: 177 mg (59 %), dark purple-brown solid. ^{1}H-NMR ($CDCl_3$): δ = 8.52 – 8.38 (m, 2H), 8.02 – 7.86 (m, 2H), 7.65 – 7.53 (m, 2H), 2.01 – 1.81 (m, 4H), 1.63 (s, 12H), 1.60 – 1.10 (m, 20H), 0.99 – 0.81 (m, 18H). GPC (ODCB): M_w = 173000 g/mol, PDI = 2.6.

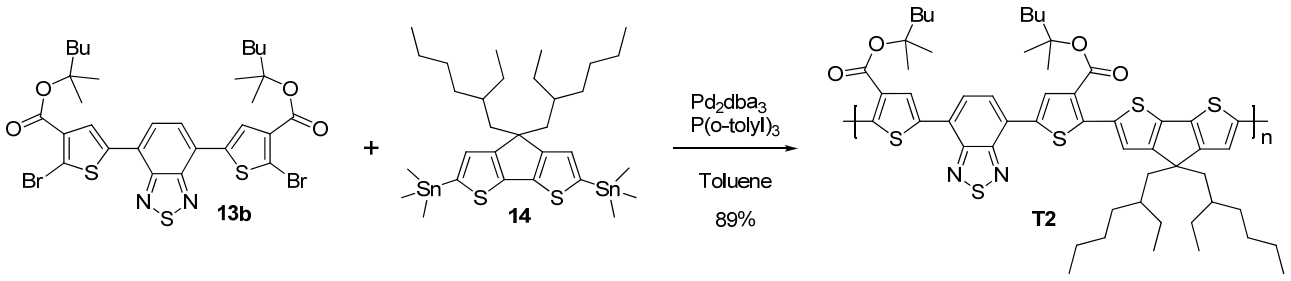

Polymer T2. Prepared with the same procedure as for **T1** using the monomers **13b** and **14**. Yield: 192 mg (89 %), dark purple solid. ^{1}H NMR (500 MHz, $CDCl_3$) δ = 8.41 (s, 2H), 7.91 (s 2H), 7.59 (s, 2H), 1.98 (br, 8H), 1.64 (s, 6H), 1.58 (s, 6H), 1.44 (br, 12H), 1.18 – 0.93 (br, 20H), 0.81 (t, J = 6.9 Hz, 6H), 0.71 (t, J = 7.3 Hz, 6H). GPC ($CHCl_3$): M_w = 41600 g/mol, PDI = 2.7.

5.9 References

1. Pilgram, K.; Zupan, M.; Skiles, R. *J. Heterocycl. Chem.* **1970,** *7* (3), 629-&.
2. Li, Z. H.; Wong, M. S.; Fukutani, H.; Tao, Y. *Chem. Mater.* **2005,** *17* (20), 5032-5040.
3. Geng, Y.; Chen, A. C. A.; Ou, J. J.; Chen, S. H.; Klubek, K.; Vaeth, K. M.; Tang, C. W. *Chem. Mater.* **2003,** *15* (23), 4352-4360.
4. Wang, J. L.; Zhou, Y.; Li, Y.; Pei, J. *J. Org. Chem.* **2009,** *74* (19), 7449-7456.
5. Hou, J. H.; Chen, H. Y.; Zhang, S. Q.; Li, G.; Yang, Y. *J. Am. Chem. Soc.* **2008,** *130* (48), 16144-16145.
6. Park, S. H.; Roy, A.; Beaupre, S.; Cho, S.; Coates, N.; Moon, J. S.; Moses, D.; Leclerc, M.; Lee, K.; Heeger, A. J. *Nat. Photonics* **2009,** *3* (5), 297-302.
7. Peet, J.; Kim, J. Y.; Coates, N. E.; Ma, W. L.; Moses, D.; Heeger, A. J.; Bazan, G. C. *Nat. Mater.* **2007,** *6* (7), 497-500.
8. Bundgaard, E.; Krebs, F. C. *Macromolecules* **2006,** *39* (8), 2823-2831.
9. Bijleveld, J. C.; Shahid, M.; Gilot, J.; Wienk, M. M.; Janssen, R. A. J. *Adv. Funct. Mater.* **2009,** *19*, 1-9.
10. Hou, J.; Chen, T. L.; Zhang, S.; Hsiang-Yu, C.; Yang, Y. *J. Phys. Chem. C* **2009,** *113* (4), 1601-1605.
11. Zhang, D.; Tessier, C. A.; Youngs, W. J. *Chem. Mater.* **1999,** *11* (11), 3050-3057.
12. Sessler, J. L.; Callaway, W. B.; Dudek, S. P.; Date, R. W.; Bruce, D. W. *Inorg. Chem.* **2004,** *43* (21), 6650-6653.
13. Far, A. R.; Shivanyuk, A.; Rebek, J. *J. Am. Chem. Soc.* **2002,** *124* (12), 2854-2855.
14. Bouffard, J.; Swager, T. M. *Macromolecules* **2008,** *41* (15), 5559-5562.
15. Petersen, M. H.; Gevorgyan, S. A.; Krebs, F. C. *Macromolecules* **2008,** *41* (23), 8986-8994.
16. Bjerring, M.; Nielsen, J. S.; Nielsen, N. C.; Krebs, F. C. *Macromolecules* **2007,** *40* (16), 6012-6013.
17. Gevorgyan, S. A.; Krebs, F. C. *Chem. Mater.* **2008,** *20* (13), 4386-4390.
18. Wienk, M. M.; Kroon, J. M.; Verhees, W. J. H.; Knol, J.; Hummelen, J. C.; van Hal, P. A.; Janssen, R. A. J. *Angew. Chem. Int. Ed.* **2003,** *42* (29), 3371-3375.
19. van Duren, J. K. J.; Yang, X. N.; Loos, J.; Bulle-Lieuwma, C. W. T.; Sieval, A. B.; Hummelen, J. C.; Janssen, R. A. J. *Adv. Funct. Mater.* **2004,** *14* (5), 425-434.

20. Yang, X.; Loos, J. *Macromolecules* **2007,** *40* (5), 1353-1362.

21. Barrau, S.; Andersson, V.; Zhang, F. L.; Masich, S.; Bijleveld, J.; Andersson, M. R.; Inganas, O. *Macromolecules* **2009,** *42* (13), 4646-4650.

22. Li, G.; Shrotriya, V.; Yao, Y.; Yang, Y. *J. Appl. Phys.* **2005,** *98* (4).

23. Nilsson, S.; Bernasik, A.; Budkowski, A.; Moons, E. *Macromolecules* **2007,** *40*, 8291-8301.

24. Martens, T.; D'Haen, J.; Munters, T.; Beelen, Z.; Goris, L.; Manca, J.; D'Olieslaeger, M.; Vanderzande, D.; De Schepper, L.; Andriessen, R. *Synth. Met.* **2003,** *138* (1-2), 243-247.

25. Helgesen, M.; Gevorgyan, S. A.; Krebs, F. C.; Janssen, R. A. J. *Chem. Mater.* **2009,** *21* (19), 4669-4675.

26. Campaigne, E.; Bourgeois, R. C. *J. Am. Chem. Soc.* **1954,** *76* (9), 2445-2447.

27. Zhu, Z.; Waller, D.; Gaudiana, R.; Morana, M.; Muhlbacher, D.; Scharber, M.; Brabec, C. *Macromolecules* **2007,** *40* (6), 1981-1986.

Appendix 1

Attempted synthesis of a monomer based on 2,1,3-benzothiadiazole bearing thermocleavable alkyl ester groups at the 5- and 6-position

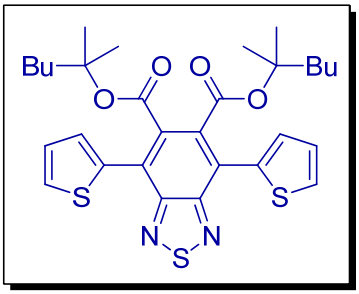

Target Monomer

The target monomer is bearing two tertiary ester groups to provide solubility and thermocleavability. Upon thermocleavage to the diacid, the benzothiadiazole unit is expected to transform into a stronger acceptor due to the electron attracting carboxylic acid groups. The attempted synthesis of this monomer is shown below.

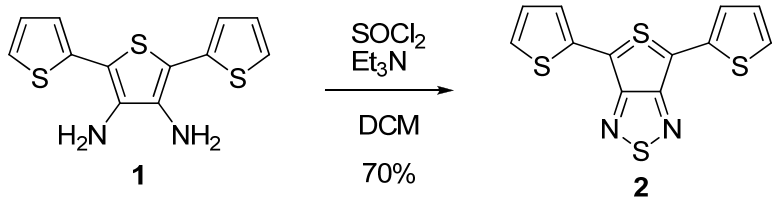

4,6-Dithienyl[3,4-*c*][1,2,5]thiadiazole (2). To a mixture of **1** (200 mg, 0.72 mmol) and triethylamine (5.75 mmol, 0.8 ml) in 5 ml dichloromethane was slowly added a solution of thionyl chloride (1.44 mmol, 105 µL) in 1 ml dichloromethane. After addition the mixture was heated to reflux for 16 hours. After cooling to room temperature the reaction mixture was concentrated on celite in vacuum. Dry column chromatography (silica gel 15-40 µm, eluted with toluene) afforded **2**. Yield: 155 mg (70 %), blue solid. ^{1}H NMR (250 MHz, $CDCl_3$) δ = 7.58 – 7.54 (m, 2H), 7.34 – 7.30 (m, 2H), 7.13 – 7.07 (m, 2H). ^{13}C NMR (250 MHz, $CDCl_3$) δ = 156.17, 134.88, 128.08, 125.30, 124.23, 112.33.

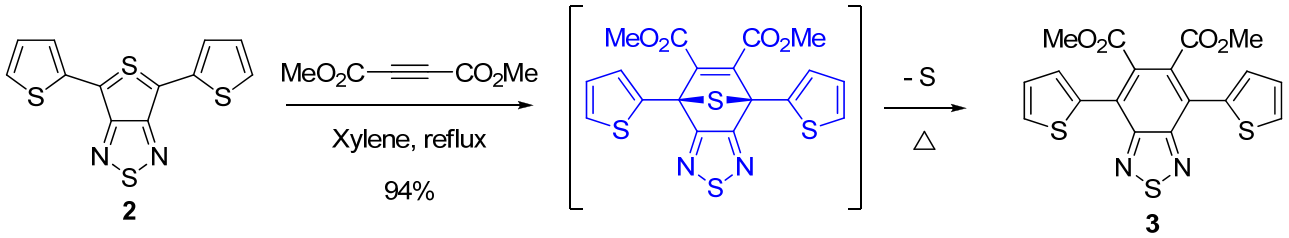

Dimethyl-4,7-di(thiophen-2-yl)benzo[*c*][1,2,5]thiadiazole-5,6-dicarboxylate (3).
A solution of **2** (1.86 g, 6.07 mmol) and acetylenedicarboxylic acid dimethyl ester (1.5 ml, 12 mmol) in xylene (40 mL) was refluxed, under argon for 6 hours. After cooling to room temperature the reaction mixture was concentrated on celite in vacuum. Dry column chromatography (silica gel 15-40 µm, eluted with Heptane/dichloromethane, gradient 0-50% dichloromethane) afforded **3**. Yield: 2.37 g (94 %), yellow/green solid. ^{1}H NMR (250 MHz, $CDCl_3$) δ = 7.62 – 7.57 (m, 2H), 7.43 (d, J = 3.6, 2H), 7.23 – 7.17 (m, 2H), 3.76 (s, 6H). ^{13}C NMR (250 MHz, $CDCl_3$) δ = 167.95, 153.61, 135.07, 132.08, 129.71, 128.81, 127.18, 126.22, 52.91.

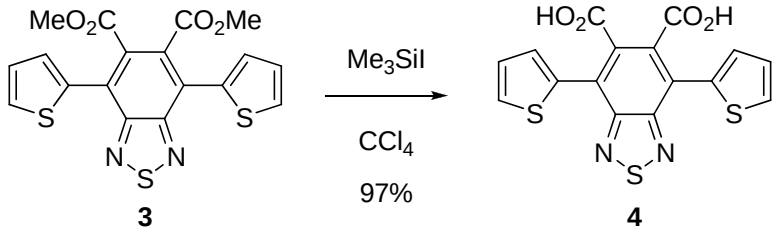

4,7-Di(thiophen-2-yl)benzo[*c*][1,2,5]thiadiazole-5,6-dicarboxylic acid (4). To a solution of **3** (300 mg, 0.72 mmol) in 5 ml CCl_4 was added trimethylsilyl iodide (2.17 mmol, 294 µL) under argon. The reaction mixture was stirred at 80 °C for 16 hours. After cooling to room temperature the mixture was poured out in 1M HCl. Filtration afforded the diacid **4**. Yield: 271 mg (97 %), red/orange solid. ^{1}H NMR (250 MHz, DMSO) δ = 13.71 (s, 2H), 7.85 (d, J = 5.0, 2H), 7.45 (d, J = 2.8, 2H), 7.26 – 7.20 (m, 2H). ^{13}C NMR (250 MHz, $CDCl_3$) δ = 168.83, 153.06, 135.28, 133.57, 130.15, 129.77, 127.62, 124.33.

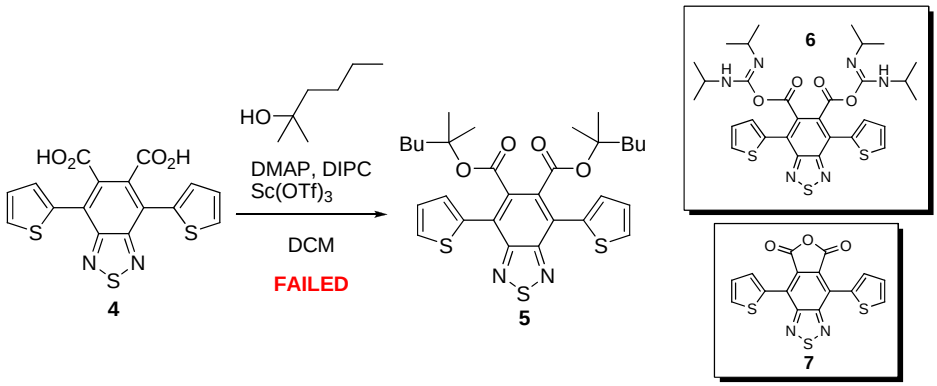

bis(2-methylhexan-2-yl)-4,7-di(thiophen-2-yl)benzo[*c*][1,2,5]thiadiazole-5,6-dicarboxylate (5). A mixture of **4** (130 mg, 0.34 mmol), DMAP (86 mg, 0.70 mmol), $Sc(OTf)_3$ (16 mg, 0.034 mmol) and 2-methyl-2-hexanol (110 µL, 0.77 mmol) in dry methylene chloride (2 ml) was stirred at room temperature under argon for 30 min. *N,N′*-diisopropylcarbodiimide (121 µL, 0.77 mmol) was added and the reaction mixture was heated to reflux. TLC and NMR after work up shows no product, only starting material and starting material that had reacted with the carbodiimide. Transformation of the diacid **4** into the diacid chloride followed by direct reaction with the tertiary alcohol was also ineffective. There can be many explanations to the failed reaction. One explanation could be that the reaction stops (slow down), due to steric factors, after conversion of the carboxylic acids to *O*-acyl isourea species (**6**) by reaction with DIPC. Another explanation could be that the anhydride (**7**) forms which is likely to be very insoluble and unreactive.

Appendix 1

Appendix 2

List of publications

A2.1 114-127

Low band gap poly-thienopyrazines for solar cells-Introducing the 11-thia-9,13-diaza-cyclopenta[b]triphenylenes

Helgesen, M.; Hagemann, O.; Nielsen, K. T.; Jørgensen, M.; Krebs, F. C. *Sol. Energy Mater.Sol.Cells* **2007,** *91* (11), 996-1009.

A2.2 128-136

Thermocleavable Low Band Gap Polymers and Solar Cells Therefrom with Remarkable Stability toward Oxygen

Helgesen, M.; Gevorgyan, S. A.; Krebs, F. C. *Macromolecules* **2008,** *41* (23), 8986-8994.

A2.3 137-143

Substituted 2,1,3-Benzothiadiazole- And Thiophene-Based Polymers for Solar Cells - Introducing a New Thermocleavable Precursor

Helgesen, M.; Gevorgyan, S. A.; Krebs, F. C.; Janssen, R. A. J. *Chem. Mater.* **2009,** *21* (19), 4669-4675.

A2.4 144-168

Advanced materials and processes for polymer solar cell devices

Helgesen, M.; Søndergaard, R.; Krebs, F. C. *J. Mater. Chem.* **2010**, *20*, 36–60

A2.5 169-176

Photovoltaic performance of polymers based on dithienylthienopyrazines bearing thermocleavable benzoate esters

Helgesen, M.; Krebs, F. C. *Macromolecules* **2010**, *43*, 1253-1260

Available online at www.sciencedirect.com
ScienceDirect
Solar Energy Materials & Solar Cells 91 (2007) 996–1009
Solar Energy Materials and Solar Cells
www.elsevier.com/locate/solmat

Low band gap poly-thienopyrazines for solar cells—Introducing the 11-thia-9,13-diaza-cyclopenta[*b*]triphenylenes

Martin H. Petersen, Ole Hagemann, Kim T. Nielsen[1], Mikkel Jørgensen*, Frederik C. Krebs

Danish Polymer Centre, Risø National Laboratory, Technical University of Denmark, P.O. Box 49, DK-4000 Roskilde, Denmark

Received 1 February 2007; received in revised form 28 February 2007; accepted 28 February 2007
Available online 11 April 2007

Abstract

The chemistry of the thienopyrazines has been explored with the aim of producing new low band gap polymers. 5,7-Di-(thiophen-2-yl)-thieno[3,4-*b*]pyrazines substituted in the pyrazine ring with alkyl groups, aryl groups and fused aromatic rings have been prepared and characterized. The electronic spectra show a great variation in the longest wavelength absorption band as a consequence of this substitution. A special case is the 11-thia-9,13-diaza-cyclopenta[*b*]triphenylene prepared by condensation of 3′,4′-diamino-[2,2′,5′,2″]terthiophene with phenanthrene-9,10-quinone. Alkyl substitution of the most promising monomers were carried out using the Kumada coupling and these were copolymerized with either 2,5-bis(trimethylstannyl)thiophene or 3-(3,7,11-trimethyl-dodecyl)-2,5-bis-trimethylstannyl-thiophene to form six new low band gap polymers: **RISO-GREEN 1–3** and **RISO-BROWN 1–3**. The band gaps of these polymers were estimated from the UV–visible absorption spectra and found to be ca. 1.3 eV. Preliminary results from photovoltaic device fabrication with mixtures of the six polymers with either [60]PCBM or [70]PCBM gave modest efficiencies of max 0.2% with open circuit voltages V_{oc} of 0.3 V and short circuit currents J_{sc} (1000 Wm^{-2} AM1.5) in the range of 2 mA cm^{-2}.

Keywords: Low band gap polymers; Organic photovoltaics

1. Introduction

In order to harvest as much as possible of the photon flux from the sun a search for new materials are presently being pursued actively. These so-called low band gap polymers ($E_g < 2.0$ eV) are designed to match the solar output better, which has a maximum in photon flux near 700 nm and an appreciable tail stretching into the infra-red region [1]. One approach is polymers with alternating electron donating and accepting groups giving rise to a material with a low-energy absorption band that may be a charge transfer band. This absorption can be tailored by adjusting the donor–acceptor strengths, or HOMO-LUMO levels, respectively. A polymer with alternating dithiophene and thienopyrazine units has been explored for this purpose by several groups [2,3]. An example of these polymers with a broad absorption maximum around 730 nm (film) and a low band gap of ca. 1.45 eV has been reported with alkyl groups on the thiophene moieties [2]. A copolymer incorporating a dithienyl-thienopyrazine with phenyl substituents together with dioctylfluorene called APFO-green 2 had an absorption maximum at 615 nm (film) [4].

In this paper, we explore a greater variation of substituents on the thienopyrazine unit tuning the absorption spectrum and band gap over a wider range. A special case is the use of phenanthrene quinone to produce the novel 11-thia-9,13-diaza-cyclopenta[*b*]triphenylene system with more extended conjugation and a further red shifted absorption. An improved method of introducing alkyl groups into these systems is also presented avoiding the troublesome synthesis of alkyl-substituted benzils. The effect of variation of the nature and number of the alkyl chains on the solubility and solar cell properties is also studied (Fig. 1).

*Corresponding author.
E-mail address: mikkel.joergensen@risoe.dk (M. Jørgensen).
[1]Present address: LEO Pharma A/S, Industriparken 55, DK-2750 Ballerup, Denmark.

0927-0248/$ - see front matter © 2007 Elsevier B.V. All rights reserved.
doi:10.1016/j.solmat.2007.02.022

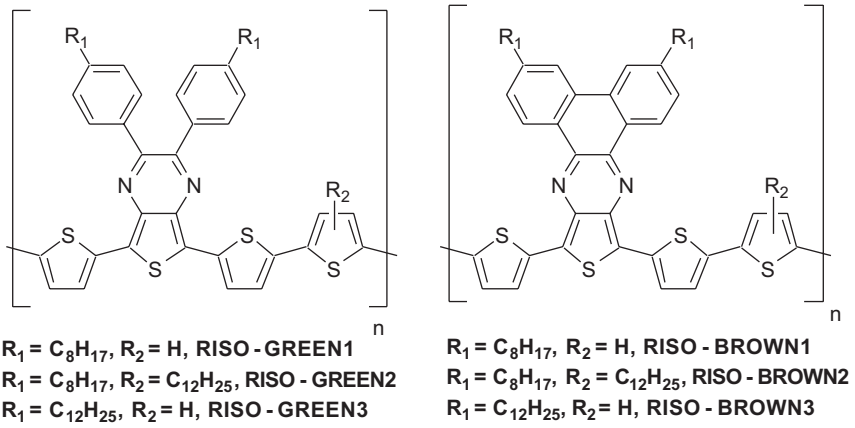

Fig. 1. The six new low band gap polymers studied based on alternating terthiophene donors and thienopyrazine acceptors.

2. Experimental

2.1. Synthesis

NMR spectra were obtained on 500 MHz Bruker Avance II or 250 MHz Bruker Avance spectrometers. 2,5-Bis(trimethylstannyl)thiophene and 3-(3,7,11-trimethyl-dodecyl)-2,5-bis-trimethylstannyl-thiophene was prepared as described in the literature [5].

3′,4′-Dinitro-[2,2′;5′,2″]terthiophene (2). 2-Tributylstannyl-thiophene (5.8 g, 16 mmol) and 2,5-dibromo-3,4-dinitro-thiophene [6] (2.6 g, 7.8 mmol) were mixed in toluene (20 mL) together with $Pd(PPh_3)_4$ (200 mg) and heated to reflux for 2 h. Toluene was removed in vacuum to give a slurry of the compound together with tributylstannyl bromide. This was taken up in chloroform (ca. 200 mL) and filtered through a layer of silica to remove a dark band. The silica was eluted with another ca. 100 mL chloroform until the washings were almost colourless. The solvent was removed from the reddish liquid in vacuum and the remaining paste mixed with petrol (50 mL) and filtered. The orange solid was washed with more petrol (ca. 50 mL) and dried in vacuum. Yield: 2.45 g, 7.2 mmol, 92%. The analytical data were in accordance with Ref. [6].

3′,4′-Diamino-[2,2′,5′,2″]terthiophene hydrochloride. 3′,4′-dinitro-[2,2′,5′,2″]terthiophene (20 g, 59 mmol) and $Sn(II)Cl_2$ (67 g, 355 mmol) were mixed in ethanol (250 mL), THF (150 mL) and concentrated HCl (100 mL). The reaction mixture was stirred at room temperature (RT) overnight. Then solvents were evaporated in vacuum and the resultant mixture was transferred into a continuous extraction apparatus and basified with concentrated NaOH (100 mL) followed by pH adjustment to ca. 8 with solid $NaHCO_3$. Continuous extraction with EtOAc overnight gave a solution that was concentrated in vacuum. Finally concentrated HCl was added (100 mL) and the product was filtered, washed with petroleum ether (200 mL) and dried at 70 °C in vacuum. Yield: 15.6 g, 84%, light brown solid. ^{1}H-NMR (CD_3OD): $\delta = 7.55$ (dd, 2H), 7.30 (dd, 2H), 7.18 (dd, 2H), 4.9 (s, amine protons and water). ^{13}C-NMR (CD_3OD): $\delta = 132.3$, 128.0, 126.54, 126.4, 126.3, 119.0. Anal. Calcd C: 51.77; H: 3.62; N: 10.06. Found C: 51.93 52.06; H: 3.41 3.38; N: 10.01 9.99.

General procedure for the condensation of 3′,4′-diamino-[2,2′5′,2″]terthiophene (4) with diketones and *o*-quinones to give the thienopyrazines 5a–5g. 3′,4′-Diamino-[2,2′,5′,2″]terthiophene hydrochloride (30% excess) and hexan-3,4-dione, benzil, 4,4′-dibromobenzil, 1,2-di-pyridin-2-yl-ethane-1,2-dione, acenaphthylene-1,2-dione, phenanthrene-9,10-dione or 3,6-dibromo-phenanthrene-9,10-dione and Et_3N (1.5 eqv) were mixed in ethanol and the resulting mixture was heated to reflux over night. Then the mixture was cooled to RT and the product was filtered, washed with ethanol and dried at 70 °C in vacuum.

2,3-Diethyl-5,7-di-thiophen-2-yl-thieno[3,4-*b*]pyrazine (5a). Recrystallized from ethanol. Yield: 53%, ^{1}H NMR ($CDCl_3$) δ: 1.49 (t, 6H, $J = 7$ Hz), 2.93 (q, 4H, $J = 7$ Hz), 7.10 (dd, 2H, $J1 = 5$ Hz, $J2 = 4$ Hz), 7.36 (dd, 2H, $J1 = 5$ Hz, $J2 = 1$ Hz), 7.61 (dd, 2H, $J1 = 4$ Hz, $J2 = 1$ Hz). ^{13}C NMR ($CDCl_3$) δ: 10.8, 28.2, 123.7, 123.9, 126.1, 127.0, 135.0, 137.6, 156.8.

2,3-Diphenyl-5,7-di-thiophen-2-yl-thieno[3,4-*b*]pyrazine (5b). Analytical data in accordance with Ref. [4].

2,3-Bis-(4-bromo-phenyl)-5,7-di-thiophen-2-yl-thieno[3,4-*b*]pyrazine (5c). M_P 253–254 °C. Yield: 79%. ^{1}H NMR ($CDCl_3$) δ: 7.12 (dd, 2H, $J1 = 5$ Hz, $J2 = 4$ Hz), 7.40 (dd, 2H, $J1 = 5$ Hz, $J2 = 1$ Hz), 7.44 (d, 4H, $J = 8$ Hz), 7.51 (d, 4H, $J = 8$ Hz), 7.63 (dd, 2H, $J1 = 4$ Hz, $J2 = 1$ Hz) ^{13}C NMR ($CDCl_3$) δ: 123.9, 124.7, 125.3, 126.9, 127.3, 131.5, 134.4, 137.3, 137.6, 151.2.

2,3-Di-pyridin-2-yl-5,7-di-thiophen-2-yl-thieno[3,4-*b*]pyrazine (5d). Recrystallized from ethanol. Yield: 67% ^{1}H NMR ($CDCl_3$) δ: 7.14 (dd, 2H, $J1 = 5$ Hz, $J2 = 4$ Hz), 7.24 (ddd, 2H, $J1 = 8$ Hz, $J2 = 5$ Hz, $J3 = 1$ Hz), 7.42 (dd, 2H, $J1 = 5$ Hz, $J2 = 1$ Hz), 7.70 (dd, 2H, $J1 = 4$ Hz, $J2 = 1$ Hz), 7.91 (dt, 2H, $J1 = 8$ Hz, $J2 = 1$ Hz), 8.3 (m, 4H). ^{13}C NMR ($CDCl_3$) δ: 122.9, 123.9, 125.0, 125.6, 127.4, 134.4, 136.8, 137.1, 147.8, 152.2, 157.7.

8,10-Di-thiophen-2-yl-9-thia-7,11-diaza-cyclopenta[*k*]fluoranthene (5e). Yield: 62%. ^{1}H NMR (*o*-$C_6D_4Cl_2$, 400 K) δ:

7.08 (t, 2H, $J = 4$ Hz), 7.33 (d, 2H, $J = 4$ Hz), 7.65 (t, 2H, $J = 8$ Hz), 7.79 (d, 2H, $J = 4$ Hz), 7.88 (d, 2H, $J = 8$ Hz), 7.21 (d, 2H, $J = 7$ Hz).

10,12-Di-thiophen-2-yl-11-thia-9,13-diaza-cyclopenta[*b*]-triphenylene (5f). Yield: 77%. ^{1}H NMR (o-$C_6D_4Cl_2$, 300 K) δ: 7.12 (t, 2H, $J = 5$ Hz), 7.37 (d, 2H, $J = 5$ Hz), 7.6–7.7 (m, 6H), 8.3 (m, 2H), 9.3 (m, 2H).

3,6-Dibromo-10,12-di-thiophen-2-yl-11-thia-9,13-diaza-cyclopenta[*b*]triphenylene (5g). Yield: 18 g, 85%, green solid. $M_p > 300$ °C ^{1}H-NMR ($(CD_3)_2SO$, 400 K): $\delta = 8.97$ (d, 2H), 8.78 (d, 2H), 7.90 (dd, 2H), 7.80 (dd, 2H), 7.70 (dd, 2H), 7.24 (dd, 2H).

2,3-Bis-(4-octyl-phenyl)-5,7-di-thiophen-2-yl-thieno[3,4-*b*]pyrazine (5h–5A). Compound **5c** (5 g, 8.2 mmol) was dissolved in diethyl ether (200 mL) together with $NiCl_2$dppp (250 mg) with stirring under Argon at RT. Octyl magnesium bromide (40 mL, ~1 M, ca. 5 eqv) was added in one portion and the reaction mixture was heated to reflux for 10 min. The reaction was followed by thin layer chromatography (silica gel, heptane-toluene 2:1). The mixture was cooled and filtered directly on a small column of silica and the purple fraction was eluted with more diethyl ether. After removal of the solvent in vacuum the residue was recrystallized from ethanol to give the product as a purple solid. Yield: 4.8 g, 86%. M_p 110–112 °C. ^{1}H NMR ($CDCl_3$) δ: 0.90 (t, 6H, $J = 7$ Hz), 1.27–1.34 (m, 20H), 1.64 (p, 4H, $J = 7$ Hz), 2.64 (t, 4H, $J = 7$ Hz), 7.13 (dd, 2H, $J1 = 5$ Hz, $J2 = 4$ Hz), 7.16 (d, 4H, $J = 8$ Hz), 7.39 (dd, 2H, $J1 = 5$ Hz, $J2 = 1$ Hz), 7.53 (d, 4H, $J = 8$ Hz), 7.69 (dd, 2H, $J1 = 4$ Hz, $J2 = 1$ Hz). ^{13}C NMR ($CDCl_3$) δ: 14.1, 22.7, 29.3, 29.5, 31.2, 31.9, 35.8, 124.5, 124.6, 126.5, 127.3, 128.1, 129.9, 134.8, 136.5, 137.5, 144.2, 153.1.

2,3-Bis-(4-[3,7,11-trimethyl-dodecyl]-phenyl)-5,7-di-thiophen-2-yl-thieno[3,4-*b*]pyrazine (5h–5B). Prepared as above for compound **5h–5A**. Yield: 5.3 g 70%; oil, ^{1}H NMR ($CDCl_3$) δ: 0.88 (t, 18H), 0.94–0.97 (m, 6H), 1.06–1.60 (m, 32H), 1.63–1.71 (m, 2H), 2.58–2.65 (m, 2H), 2.66–2.73 (m, 2H), 7.13, dd, 2H, $J1 = 4$ Hz, $J2 = 5$ Hz), 7.16 (d, 4H, $J = 8$ Hz), 7.39 (dd, 2H, $J1 = 5$ Hz, $J2 = 1$ Hz), 7.54 (d, 4H, $J = 8$ Hz), 7.69 (dd, 2H, $J1 = 4$ Hz, $J2 = 1$ Hz). ^{13}C NMR ($CDCl_3$) δ: 19.6, 19.7, 19.7, 19.8, 22.6, 22.7, 24.4 (2C), 24.8, 24.8, 28.0, 32.5, 32.5, 32.8 (2C), 33.4 (2C), 37.2 (2C), 37.3 (2C), 37.4, 37.41, 37.5, 38.6 (2C), 38.7, 39.4, 124.5, 124.6, 126.5, 127.3, 128.1, 130.0, 134.8, 136.5, 137.5, 144.4, 153.0.

3,6-Dioctyl-10,12-di-thiophen-2-yl-11-thia-9,13-diaza-cyclopenta[*b*]triphenylene (5i–5A). 3,6-Dibromo-10,12-di-thiophen-2-yl-11-thia-9,13-diaza-cyclopenta[*b*]triphenylene (10 g, 16.4 mmol, 1 eqv) and $NiCl_2$dppp (624 mg, 1.15 mmol, 0.07 eqv) was mixed in ether (400 mL) followed by the addition of 1 M octyl magnesium bromide (100 mL, 6 eqv) in ether. The reaction mixture was heated to reflux for 30 min. The mixture was then filtered through silica gel and the washing was concentrated in vacuum. The remaining solid was recrystallized from ethanol and dried at 100 °C in vacuum. Yield: 6.4 g, 58%, black solid. $M_p = 169$–170 °C. ^{1}H-NMR ($CDCl_3$): $\delta = 9.04$ (d, 2H), 8.09 (s, 2H), 7.64 (d, 2H), 7.47–7.38 (m, 4H), 7.13 (dd, 2H), 2.88–2.78 (m, 4H), 1.85–1.71 (m, 4H), 1.49–1.25 (m, 20H), 0.95–0.85 (m, 6H). ^{13}C-NMR ($CDCl_3$): $\delta = 145.9$, 143.0, 138.5, 135.2, 132.5, 128.6, 128.5, 127.1, 126.9, 126.4, 123.8, 123.5, 122.5, 36.6, 31.9, 31.5, 29.6, 29.5, 29.3, 22.7, 14.1.

10,12-Di-thiophen-2-yl-3,6-bis-(3,7,11-trimethyl-dodecyl)-11-thia-9,13-diaza-cyclopenta[*b*]triphenylene (5i–5B). Compound **5g** (1.5 g, 2.45 mmol, 1 eqv) and $NiCl_2$dppp (100 mg, 0.184 mmol, 0.075 eqv) was mixed in ether (50 mL) followed by the addition of 0.6 M 3,7,11-trimethyldodecyl magnesium bromide (25 ml, 6 eqv) in ether. The reaction mixture was heated to reflux for 30 min. The mixture was then filtered through silica gel and the washing was concentrated on celite. Dry column chromatography (toluene/cyclohexane) afforded the pure product. Yield: 938 mg, 44%, green oil. ^{1}H-NMR ($CDCl_3$): $\delta = 8.95$ (d, 2H), 8.02 (s, 2H), 7.60 (dd, 2H), 7.43–7.34 (m, 4H), 7.11 (dd, 2H), 2.89–2.72 (m, 4H), 1.87–1.70 (m, 4H), 1.66–1.07 (m, 30H), 1.05–1.01 (d, 6H), 0.90–0.84 (m, 18H). ^{13}C-NMR ($CDCl_3$): $\delta = 146.0$, 142.9, 138.4, 135.2, 132.4, 128.5, 128.4, 127.0, 126.9, 126.3, 123.7, 123.4, 122.3, 39.4, 39.0, 38.9, 37.5, 37.5, 37.4, 37.3, 34.2, 32.8, 32.7, 28.0, 24.8, 24.5, 22.7, 22.6, 19.8, 19.7, 19.75, 19.6.

5,7-Bis-(5-bromo-thiophen-2-yl)-2,3-bis-(4-octyl-phenyl)-thieno[3,4-*b*]pyrazine (6-A). Compound **5h–5A** (2.0 g, 2.95 mmol) was dissolved in dry THF (350 mL) under Argon and shielded from light by metal foil. NBS, freshly recrystallized from water (1.0 g, 5.6 mmol, 1.9 eqv) dissolved in dry THF (70 mL) was added dropwise over 30 min at RT. The reaction was followed by thin layer chromatography (silica, heptane, toluene 4:1). At the end of the reaction time a mixture of mono-, di-, and tri-brominated compound was formed (~10:85:5). Celite (10 g) was added to the mixture and the solvent was removed in vacuum. The solid mixture was applied to a flash column and separated using a gradient of heptane and toluene. The dibrominated product was eluted with 8% toluene in heptane. This fraction was collected and the solvents were removed in vacuum and the residue recrystallized from 2-propanol to remove traces of the tri-brominated material to give the product as purple flakes. Yield: 1.45 g, 59%. M_p 98–100 °C. ^{1}H NMR ($CDCl_3$) δ: 0.92 (t, 6H, $J = 7$ Hz), 1.3–1.4 (m, 20H), 1.65 (p, 4H, $J = 7$ Hz), 2.66 (t, 4H, $J = 7$ Hz), 6.99, (d, 2H, $J = 4$ Hz), 7.15 (d, 4H, $J = 8$ Hz), 7.20 (d, 2H, $J = 4$ Hz), 7.47 (d, 4H, $J = 8$ Hz). ^{13}C NMR ($CDCl_3$) δ: 14.1, 22.7, 29.3, 29.4, 29.5, 31.2, 31.9, 35.8, 114.4, 123.8, 128.1, 129.7, 130.0, 136.0, 136.1, 137.4, 144.4, 153.4.

5,7-Bis-(5-bromo-thiophen-2-yl)-2,3-bis-(4-[3,7,11-trimethyl-dodecyl]-phenyl)-thieno[3,4-*b*]pyrazine (6-B). Prepared as above for compound **6-A**. Yield: 55%, oil. ^{1}H NMR ($CDCl_3$) δ: 0.88 (t, 18H), 0.94–0.97 (m, 6H), 1.06–1.60 (m, 32H), 1.64–1.74 (m, 2H), 2.58–2.66 (m, 2H), 2.67–2.74 (m, 2H), 7.05 (d, 2H, $J = 4$ Hz), 7.18 (d, 4H, $J = 8$ Hz), 7.30 (d, 2H, $J = 4$ Hz), 7.49 (d, 4H, $J = 8$ Hz). ^{13}C NMR ($CDCl_3$) δ: 19.6, 19.7 2C), 19.8, 22.6, 22.7, 24.4

(2C), 24.8 (2C), 28.0, 32.6 (2C), 32.8 (2C), 33.4 (2C), 37,2, 37.3 (4C), 37.4, (4C), 38.6, 38.7 (2C), 39.4, 114.5, 123.9 (2C), 128.1. 129.8, 130.0, 136.1 (2C), 137.5, 144.7, 153.5.

10,12-Bis-(5-bromo-thiophen-2-yl)-3,6-dioctyl-11-thia-9,13-diaza-cyclopenta[b]triphenylene (7-A). 5i–5A (1.5 g, 2.22 mmol, 1 eqv) was dissolved in THF (300 mL). NBS (712 mg, 4.0 mmol, 1.7 eqv) dissolved in THF (100 mL) was added dropwise and the reaction mixture was stirred at RT for 10 min followed by concentration in vacuum. Column chromatography (eluted with 10% toluene/cyclohexane) afforded the pure product. Recrystallized from 2-propanol. Yield: 981 mg, 53%, green solid, $M_p = 139$–$140\,^{\circ}C$. ^{1}H-NMR ($CDCl_3$): $\delta = 8.13$ (d, 2H), 7.57 (s, 2H), 7.02 (d, 2H), 6.56 (d, 2H), 6.45 (d, 2H), 2.69–2.52 (m, 4H), 1.78–1.60 (m, 4H), 1.51–1.23 (m, 20H), 1.01–0.87 (m, 6H). ^{13}C-NMR (C_4D_8O): $\delta = 143.7$, 140.7, 135.7, 134.3, 130.4, 127.5, 126.2, 125.9, 124.8, 120.8, 120.4, 120.3, 111.9, 34.5, 30.1, 29.5, 27.8, 27.7, 27.6, 20.8, 11.7.

10,12-Bis-(5-bromo-thiophen-2-yl)-3,6-bis-(3,7,11-trimethyl-dodecyl)-11-thia-9,13-diaza-cyclopenta[*b*]triphenylene (7-B). 5i–5B (510 mg, 0.59 mmol, 1 eqv) was dissolved in THF (100 mL). NBS (177 mg, 1.0 mmol, 1.7 eqv) dissolved in THF (50 mL) was added dropwise and the reaction mixture was stirred at RT for 10 min followed by concentration in vacuum. Column chromatography (eluted with 10% toluene/cyclohexane) afforded the pure product. Yield: 388 mg, 64%, green oil. ^{1}H-NMR ($CDCl_3$): $\delta = 8.24$ (d, 2H), 7.64 (s, 2H), 7.10 (d, 2H), 6.62 (d, 2H), 6.55 (d, 2H), 2.76–2.55 (m, 4H), 1.83–1.11 (m, 34H), 1.06 (d, 6H), 0.95–0.86 (m, 18H). ^{13}C-NMR ($CDCl_3$): $\delta = 145.4$, 142.1, 137.2, 136.1, 131.9, 128.9, 128.0, 127.7, 126.7, 122.1, 122.0, 121.8, 113.7, 39.4, 39.0, 38.9, 37.7, 37.6, 37.6, 37.5, 37.4, 34.2, 33.0, 32.9, 29.7, 28.0, 25.0, 24.9, 24.7, 24.6, 22.8, 22.7, 19.9, 19.8, 19.75, 19.7.

2.1.1. Preparation of polymers

RISO-GREEN 1. Compound **6-A** (1.45 g, 1.74 mmol) and 2,5-bis(trimethylstannyl)thiophene (712 mg, 1.74 mmol) were dissolved in dry toluene under Argon and added $Pd(PPh_3)_4$ (100 mg). The reaction mixture was heated to reflux for 4 days. Most of the solvent was removed in vacuum and the residue was poured into a large amount (500 mL) methanol. The precipitate was filtered off and washed with methanol. The moist residue was transferred into a Soxhlet thimble and extracted with heptane followed by chloroform. The heptane fraction contained lower molecular weight oligomers and was discarded. The chloroform fraction was reduced in volume at reduced pressure and then precipitated by addition of methanol. The solid was filtered off and dried in vacuum overnight to give a dark green material. Yield 849 mg 47%. Characterized by SEC. Mn = 1942, Mw = 2861, Mz = 4081, PD = 1.5.

RISO-GREEN 2. Prepared as described above for **RISO-GREEN 1** from compound **6-A** (0.568 g, 0.68 mmol)) and 3-(3,7,11-trimethyl-dodecyl)-2,5-bis-trimethylstannyl-thiophene (422 mg, 0.68 mmol). Yield: 0.32 g, 37%. Characterized by SEC with $CHCl_3$ as eluent. Mn = 2598, Mw = 3295, Mz = 4149, PD = 1.3.

RISO-GREEN 3. Prepared as described above for **RISO-GREEN 1** from compound **6-B** and 2,5-bis-trimethylstannyl-thiophene. Yield: 207 mg, 49%. Characterized by SEC with $CHCl_3$ as eluent. Mn = 1568, Mw = 2284, Mz = 3738, PD = 1.6.

RISO-BROWN 1. Prepared as described above for **RISO-GREEN 1** from compound **7-A** and 2,5-bis-trimethylstannyl-thiophene. Yield: 164 mg, 78%, Characterized by SEC with $CHCl_3$ as eluent. Mn = 1964, Mw = 2284, Mz = 2696, PD = 1.6.

RISO-BROWN 2. Prepared as described above for **RISO-GREEN 1** from compound **7-A** and 3-(3,7,11-trimethyl-dodecyl)-2,5-bis-trimethylstannyl-thiophene. Yield: 167 mg, 48%, Characterized by SEC with $CHCl_3$ as eluent. Mn = 2190, Mw = 4288, Mz = 7524, PD = 1.6.

RISO-BROWN 3. Prepared as described above for **RISO-GREEN 1** from compound **7-B** and 2,5-bis-trimethylstannyl-thiophene. Yield: 134 mg 32%. Characterized by SEC with $CHCl_3$ as eluent. Mn = 1573, Mw = 3339, Mz = 5646, PD = 1.8.

2.2. Photovoltaic characterisation

Photovoltaic devices were prepared on PEDOT:PSS-coated ITO substrates as reported elsewhere [7]. The concentration of the solutions was typically 20 mg mL^{-1} in chlorobenzene or 1,2-dichlorobenzene. The film absorbencies were in the range 0.7–0.2. All manipulations were carried out in air. The samples were then transferred to the vacuum chamber of the evaporator and pumped to a pressure $< 2 \times 10^{-6}$ mBar and left for 1 h before the aluminium electrode (100 nm) was applied by thermal evaporation. After cooling the system was purged with argon and the samples were mounted with silver epoxy, Al-tape or pressure contacts. The thermosetting silver epoxy hardened in an oven at $75 \pm 5\,^{\circ}C$ for 15 min. The samples were then analysed immediately or after hardening the silver epoxy. In a second setup, the films were prepared in air and then transferred to a glove box system with a built-in metal evaporator. The devices were subsequently tested in the glove box after applying the contacts with silver epoxy, Al-tape or pressure contacts. The active area of the devices was 3 cm^{-2}. The electrical measurements were carried out using a Keithley 2400 Sourcemeter. The wavelength dependence of the photovoltaic response was measured using a high power spectrometer comprising a 150 W water-cooled Xenon lamp, a blazed diffraction grating and a movable arm with the sample. The set-up has been described earlier [8] but has been improved with a longer source to grating distance and cylindrical lenses to improve bandwidth and intensity. The photovoltaic response under simulated sunlight (AM1.5) was performed using a Solar Constant 575 from Steuernagel Lichttechnik GmBH, Germany. The spectrum of the solar simulator was determined in the wavelength range 180–1100 nm using an

optical spectrum analyser and was found to have larger abundance of UV-photons and a smaller abundance of IR photons. The use of a UV-filter was found necessary to approximate AM1.5 conditions in the wavelength range relevant for this study. The simulated sunlight was then adjusted to $1000\,W\,m^{-2}$ using a bolometric precision pyranometer from Eppley laboratories. The exact incident power was recorded during each experiment. The temperature of the devices during measurement was $72\pm2\,^{\circ}C$. The results were not corrected for mismatch of the spectral response.

2.3. X-ray crystallography

Single-crystal X-ray diffraction data of compound **4** and **5e** were collected at 100 K using a Bruker SMART Apex II diffractometer with kappa goniometer and a CCD area detector. The crystal of **4** was obtained by slowly cooling of a hot ethanol solution, while crystals of **5e** were obtained by slowly evaporation of a 1:10 acetic acid/chloroform mixture. Atomic coordinates and further crystallographic details have been deposited with the Cambridge Crystallographic Data Centre, University Chemical Laboratory, Lensfield Road, Cambridge CB21EW, England. CCDC 630780 and 630781 contains the supplementary crystallographic data for this paper. These data can be obtained free of charge from The Cambridge Crystallographic Data Centre www.ccdc.cam.ac.uk/data_request/cif.

3. Results and discussion

3.1. Synthesis of the monomers

The key steps in the synthesis of the dithienyl-thienopyrazine starting monomers are outlined in Scheme 1 and followed the original work by Kitamura et al. [9]. 2,5-Dibromo-thiophene (**1**) was nitrated in the 3 and 4 positions using the forcing conditions described by Kenning et al. [6] to give 2,5-dibromo-3,4-dinitro-thiophene **2**. A Stille-type coupling of **2** with 2-thienyl-tributylstannane afforded the dinitro-terthiophene **3**. A slight variation of the procedure by Kitamura was developed using toluene as solvent and $Pd(PPh_3)_4$ as catalyst improving the yield. Reduction to the diamino-terthiophene hydrochloride salt **4** was accomplished using tin(II) chloride in reasonable yield as previously described. [10] This step is still somewhat unsatisfactory since the product is contaminated with tin, presumably in the form of a hexachloro stannate salt. ^{119}Sn NMR show a strong signal at -799 ppm, which is in accordance with the $SnCl_6^{2-}$ ion. Careful purification by

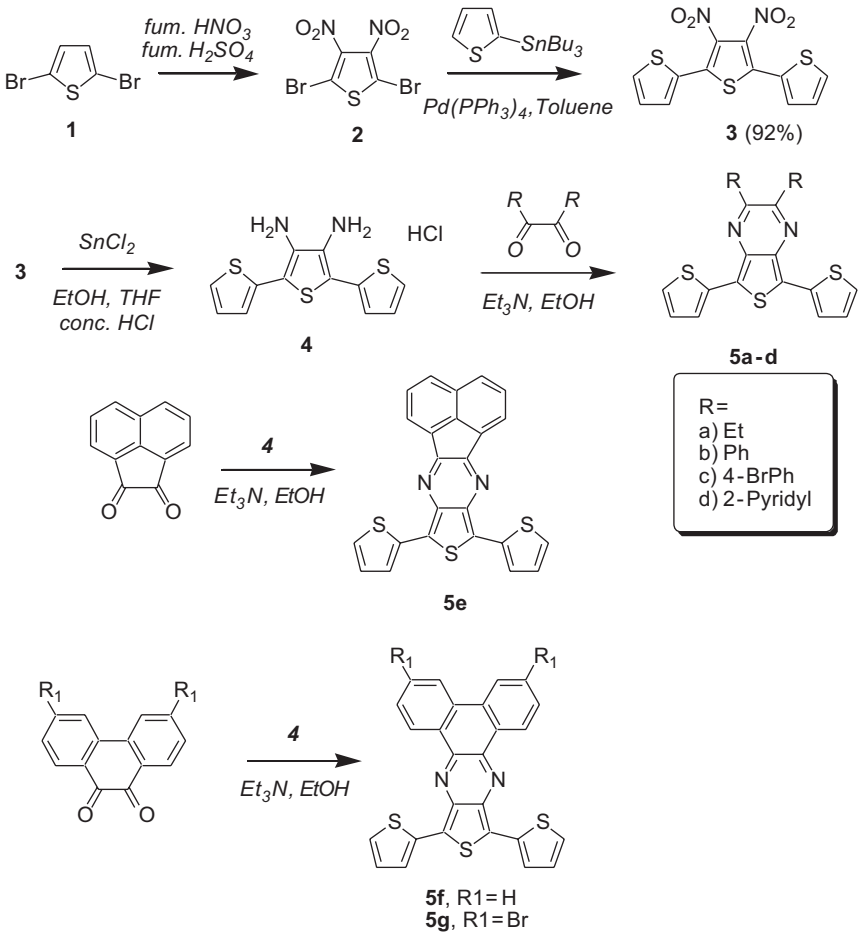

Scheme 1. Synthesis of the dithienyl-thienopyrazine monomers **5a**–**5g**.

neutralization with Na_2CO_3 followed by recrystallization, however, gave the free diamine as a pure crystalline compound that could be analysed by X-ray diffraction (see later section).

As an alternative, it is possible to reduce the dinitro-terthiophene by catalytic hydrogenation in good yield using a mixed solvent of THF, ethanol and concentrated hydrochloric acid. Large amounts of catalyst were, however, needed and had to be added at intervals during reduction, probably due to poisoning of the catalyst. This method was therefore not suited for larger-scale production of the diamine **4**.

Finally, the diamine **4** was condensed with a series of α-diketones to produce the dithienyl-thienopyrazines **5a**–**5i**. Hexan-3,4-dione gave the diethyl derivative **5a** while benzil and substituted variations gave the diaryl derivatives **5c**–**5f**. The extra phenyl rings obviously participate in the conjugated structure and red shift the absorption maximum. We have explored this further by utilizing acenaphthenequinone, 9,10-phenanthrenequinone and 3,6-dibromo-9,10-phenanthrenequinone resulting in the novel structures **5e**–**5g**. In these cases, the extended π-system is forced to be in plane with the thieno-pyrazine core. The latter two compounds belong to a new class of chromophores the 11-thia-9,13-diaza-cyclopenta[*b*]triphenylenes that give rise to an extended red shift in both the monomers and polymers. In the new chromophore, the extra bond compared to **5c**–5**f** forces the structure to be planar changing the optical properties, but it also reduces the solubility especially of the corresponding polymers. This was already a problem with the diphenyl-substituted thienopyrazine, so we decided to add alkyl groups to both systems. Our first attempt in that direction was to introduce the alkyl groups early on in the synthetic path. This approach has been utilized by Kenning et al. who prepared the simple 2,3-dialkyl substituted thieno [3,4-*b*]pyrazines. In our case, this would have required the synthesis of 4,4′-dialkyl-benzil and 3,5-dialkyl-phenanthrene quinone. Although the dialkylbenzil type of compounds have been prepared previously in a low temperature reaction of 4-alkylphenyl Grignard reagents with oxalyl chloride [11], this did not seem very suited for a larger scale production of these compounds. We therefore abandoned this route and sought an alternative. The monomers **5c** and **5g** are substituted with bromine atoms that could serve as handles for the introduction of the alkyl groups through the Kumada coupling with an alkyl Grignard reagent. At first, this did not seem promising either since an obvious side reaction is the Ziegler reaction on the pyrazine group. We found, however, that the Kumada coupling is much faster and if the reaction time is limited a good yield of the alkylated products **5h** and **5i** could be obtained (Scheme 2).

To be able to copolymerize these compounds with other monomers, it was necessary to introduce bromine atoms in the 5-positions on the thiophene units of **5h–5A**/**5h–5B** and **5i–5A**/**5i–5B**. This bromination has been successfully carried out by Zhang et al. [4] on the diphenyl thienopyrazine **5b** using NBS in a mixture of chloroform and acetic acid. We found that with these conditions the reaction proceeded very fast with our compounds, giving mixtures containing mono-, di- and tri-brominated compounds depending on among other things the amount of NBS. The unwanted bromination in the 3- or 4-positions on the thiophene rings is not always clearly seen in the crowded aromatic region of the ^{1}H NMR, while it is quite evident in

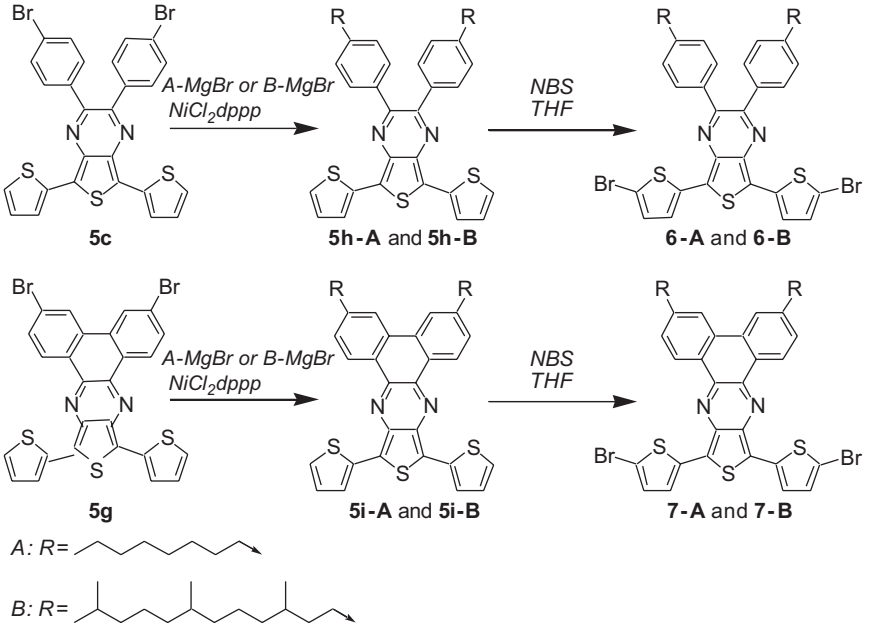

Scheme 2. Synthesis of the *n*-octyl- or 3,7,11-trimethyl-dodecyl-alkylated monomers **6-A**, **6-B**, **7-A**, **7-B**. Note that the **6** and **7** type monomers differ in the absence or presence of the bond marked in red.

the ^{13}C NMR, since the 3- or 4-bromo substituted carbon has distinct signals in the 105–110 ppm range. Bromo substitution in the 5-position on the other hand gives rise to a signal at ca. 115 ppm. Careful control of the reaction rate and addition of NBS gave mixtures, which predominantly contained the dibromo substituted monomers **6-A**, **6-B**, **7-A** and **7-B**. After quenching the reaction mixture the products were purified by flash-chromatography.

3.2. Synthesis of polymers

Bis-thienyl-thienopyrazines have been polymerized to give low band gap materials by simple homopolymerization with $FeCl_3$ or Yamamoto coupling of the 5,5′-dibromo substituted monomers with $Ni(COD)_2$ [3] Others have copolymerized the 5,5′-dibrominated thienopyrazines together with dioctyl-fluorene bis-boronic acids [4].

We have chosen to concentrate our efforts on the four monomers **6-A, 6-B** and **7-A**, **7-B** with either octyl chains or 3,7,11-trimethyl-dodecyl chains. These seemed to have a chance to make soluble and processable polymers. Stille-type copolymerization with either 2,5-bis(trimethylstannyl)-thiophene or 3-(3,7,11-trimethyl-dodecyl)-2,5-bis(trimethylstannyl)-thiophene gave polymers with alternating terthiophene donor and thienopyrazine acceptor moieties: **RISO-GREEN 1–3** and **RISO-BROWN 1–3** as shown in Scheme 3. Purification was carried out through Soxhlet extraction and gave polymers that were characterized by size exclusion chromatography and UV–visible spectroscopy. The molecular weights were in all cases not very high with Mn values between 2000 and 2500 corresponding to an average degree of polymerization of ca. 3, and the products differed somewhat in their solubility and film forming properties (*vide supra*). **RISO-GREEN 2–3** and **RISO-BROWN 2–3** were predictably more soluble than **RISO-GREEN 1** and **RISO-BROWN 1** and could be processed by spin casting to better and more uniform films.

3.3. Electronic spectra

The Absorption spectra and the band gap of the monomers **5** were recorded in chloroform solution to study the variations available for the thienopyrazine system and compiled in Table 1 and Fig. 1.

In chloroform solution the monomer **5a,** where the pyrazine is substituted with two ethyl groups, the lowest band has a maximum at 502 nm in good agreement with literature values reported by Kitamura et al. for the methyl or hexyl substituted systems (500 and 502 nm, respectively). Phenyl substituents on the pyrazine significantly red shifts the lowest absorption maximum to 552 nm (**5b**) presumably due to the more extended conjugation. Replacing the phenyl groups with 2-pyridyl groups (**5d**) has no effect on the spectra properties. One might have expected a further substantial change with the introduction of the acenaphthene group that is in plane with the thienopyrazine moiety in compound **5e**, but in this case a maximum at 548 nm is observed. On the other hand, in the new

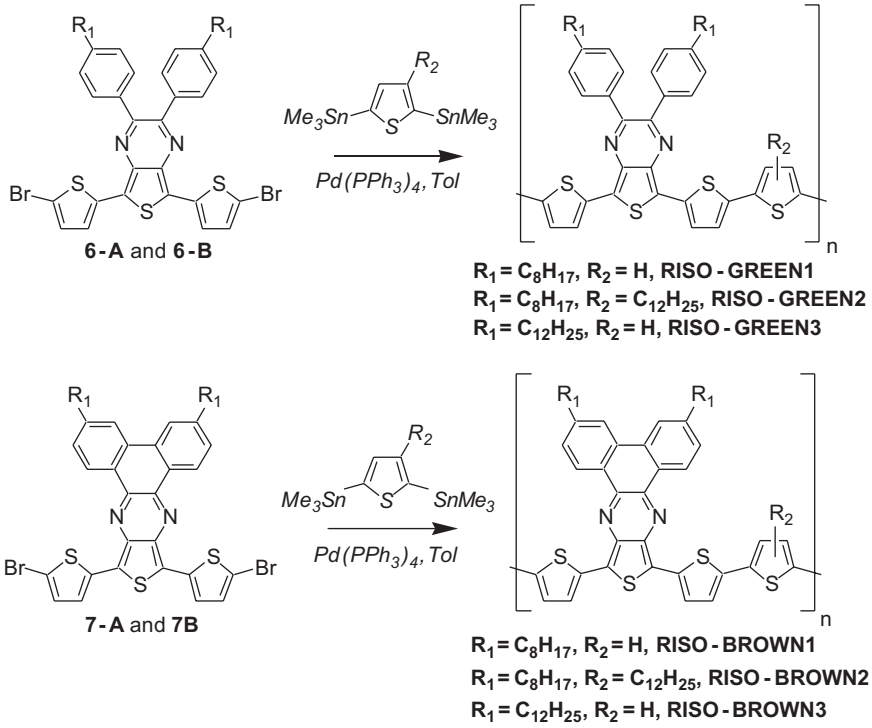

Scheme 3. Stille type polymerization of the thienopyrazines **6-A**, **6-B** and **7-A**, **7-B** with either 2,5-bis(trimethylstannyl)-thiophene or 3-(3,7,11-trimethyl-dodecyl)-2,5-bis(trimethylstannyl)-thiophene to give the six polymers **RISO-GREEN 1–3** and **RISO-BROWN 1–3** . The polymers vary in the number and nature of alkyl chains and in the extra bond in the **RISO-BROWN** series.

Table 1
Absorption maxima and extinction coefficients of the monomers **5**.

Compound	λ_{max} (nm)	log(ε_{max})
5a	343, 502	4.3, 4.1
5b	351, 552	4.6, 3.9
5c	352, 564	4.6, 3.7
5d	339, 552	4.7, 3.9
5e	353, 548	4.8, 3.8
5f	362, 641	4.8, 3.9
5g	364, 648	Not all dissolved
5h	350, 548	4.5, 3.7
5i	363, 622	4.6, 3.7

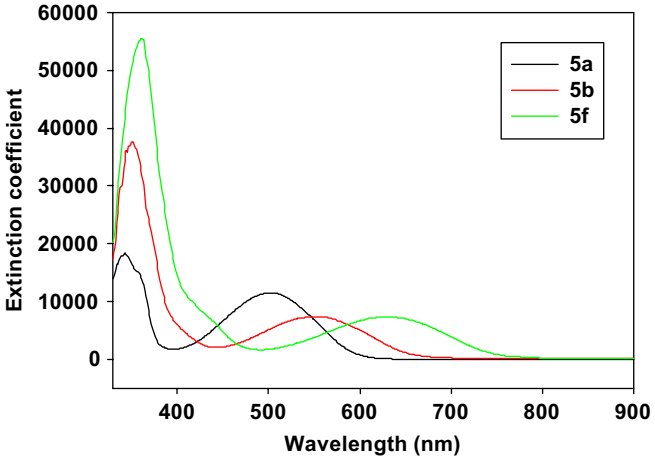

Fig. 2. Absorption spectra of the monomers **5a**, **5b** and **5f** with ethyl, phenyl or phenanthrene substitution on the pyrazine rings.

phenanthrene fused thienopyrazine system a dramatic red shift of the lowest absorption maximum to 641 nm (**5f**) is observed. This is even increased with bromine substitution of the phenanthrene to 648 nm (**5g**), but reduced somewhat with alkyl substituents (**5i**) to 622 nm. It is thus possible to tune the absorption of these monomers over at least a 150 nm range. In all cases, the longest wavelength absorption maximum also has a lower molar extinction coefficient of about $10^3\,cm^{-1}\,M^{-1}$ which is not unusual for a CT transition (Fig. 2).

The absorption spectra of the polymers **RISO GREEN 1–3** and **RISO BROWN 1–3**, in chloroform solution and cast as films, are shown in Figs. 3 and 4, respectively. The lowest energy absorption band stretching from ca. 600 to ca. 950 nm has grown in intensity relative to the band centred on 450 nm. Compared to the monomers the polymer absorption bands are thus red shifted by more than 100 nm. The solution spectra of the **RISO GREEN** type polymers are very similar with a pronounced fine structure of both the high and low energy bands. Very similar spectra of the films are obtained with some broadening of the features. The optical band gap of the **RISO GREEN**-type polymers can be estimated from the solid state spectra to be ca. 1.3 eV. The spectra of the **RISO BROWN**-type polymers differ somewhat in that no fine

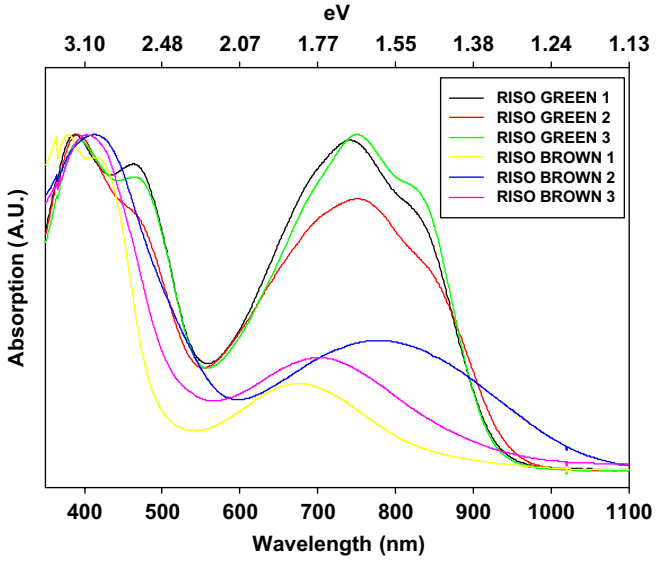

Fig. 3. Normalized absorption spectra of the polymers **RISO-GREEN 1–3** and **RISO-BROWN 1–3** in chloroform solution.

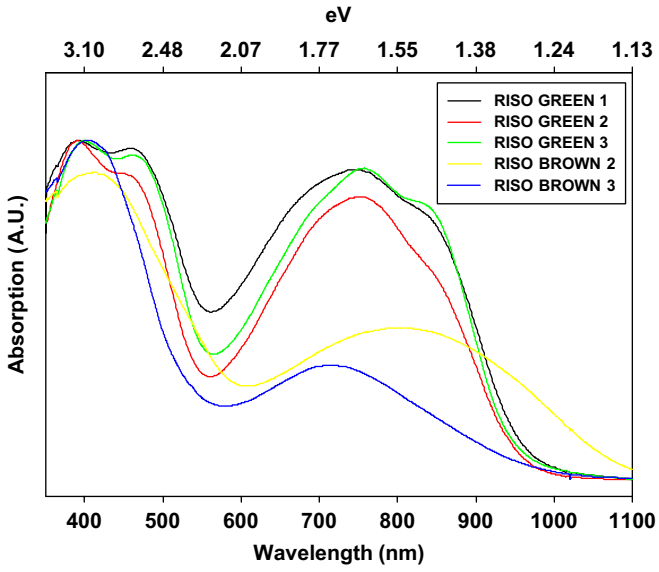

Fig. 4. Normalized absorption spectra of **RISO GREEN 1–3** and **RISO BROWN 2–3** cast as film from chloroform.

structure is observed for the high and low energy bands. It is also noteworthy that the intensity of the low energy band is considerably lower than the high-energy band. The maximum of the lowest band in solution also varies for the **RISO BROWN** series with **RISO BROWN 2** having a maximum at 779 nm, while the others have maxima at 676 and 702 nm for **RISO BROWN 1** and **RISO BROWN 3**, respectively.

3.4. Photovoltaic studies

The polymer materials were all applied in a bulk heterojunction geometry (BHJ) with either [60]PCBM or

[70]PCBM. The photovoltaic cells based on **RISO-GREEN 1–3** and **RISO-GREEN 1–3** were prepared on glass substrates with a layer of PEDOT:PSS-covered ITO. The active layer was coated on top by spin coating and the device was completed by evaporation of an aluminium electrode or by evaporation of a C_{60}-layer followed by aluminium. The devices were then tested under a sun simulator (AM1.5) with an incident power of 1000 W m^{-2} and the *IV* curves were recorded.

3.4.1. Film forming ability

There are many requirements to the materials properties of polymers for photovoltaic devices that have to be fulfilled before devices can be successfully prepared. Firstly, the polymers have to be soluble in a solvent that dissolves both the donor and the acceptor. Secondly, the solubility has to be sufficiently high for obtaining films with an absorbance of at least 0.2 and preferably higher. While these two factors are very important when it comes to preparing the thin film of the active layer, a homogenous film does automatically grant good optical, charge transport, morphological or photovoltaic properties. The polymers **RISO GREEN 1** and **RISO BROWN 1** were found to give relatively poor films due to a low solubility in solvents such as chlorobenzene and 1,2-dichlorobenzene. Earlier work [5] successfully demonstrated the use of the trimethyldodecyl sidechain to convey a better solubility and the easiest approach was to attach this side chain to the thiophene groups in the donor-part of the conjugated polymer backbone. This gave **RISO GREEN 2** and **RISO BROWN 2** that had only a slightly better solubility in chlorobenzene and 1,2-dichlorobenzene. We therefore prepared **RISO GREEN 3** and **RISO BROWN 3** with trimethyldodecyl sidechains on the acceptor-part of the conjugated polymer backbone and achieved a better solubility, good film forming ability and observed only a little effect on the optical properties. The photovoltaic properties were, however, much poorer both in terms of efficiency and stability/lifetime of the devices under illumination in the atmosphere.

3.4.2. Optimization of the acceptor-type and the polymer:acceptor ratio

All materials were tested with three different polymer:PCBM ratios (2:1, 1:1 and 1:2). Generally, a polymer:PCBM ratio of 1:2 gave the best devices with the best diode behaviour. Devices prepared with a ratio of 2:1 gave poor shunted devices. We observed lower V_{oc} and J_{sc} for devices prepared with [70]PCBM as compared to devices prepared with [60]PCBM. This is contrary to the finding that devices based on [70]PCBM are better due to the better light absorption of [70]PCBM as compared to [60]PCBM [12]. In general, the **RISO GREEN** materials were more soluble than the comparable **RISO BROWN** materials. We ascribe this to a poorer solubility of the latter as large planar systems are known to be less soluble (Table 2).

3.4.3. IPCE measurements of *RISO GREEN 1*

The photovoltaic devices prepared were relatively poor when compared to the best reports on photovoltaic devices prepared from thienopyrazine-based materials [3]. The best devices obtained from **RISO GREEN 1** did give a reasonable performance with a power conversion efficiency of 0.22% and J_{sc} values close to 2 mA cm^{-2}. A large reduction in performance is ascribed to low values for FF and V_{oc}. We recorded the IPCE curve for a device based on **RISO GREEN 1**-[60]PCBM (1:1) as shown in Fig. 5. The IPCE curve is symbatic with the absorption spectrum for the device film at the longer wavelengths. In the visible range, the large absorption at 500 nm does not lead to a large photocurrent. The devices generate a photocurrent at wavelengths up to the band gap at around 900 nm. The IPCE values obtained are quite high at the main absorption peak in the range 650–850 nm and approach 10% which

Table 2
Photovoltaic data for the materials involved

Compound	Ratio	V_{oc} (V)	J_{sc} (mA cm^{-2})	FF (%)	$RR_{\pm 1V}$	η (%)
RG1-[60]PCBM air	1:1	0.36	−1.86	33.5	61	0.22
RG1-[60]PCBM air	1:2	0.39	−1.39	35.4	540	0.19
RG1-[70]PCBM air	1:1	0.25	−0.84	34.2	25	0.07
RG1-[70]PCBM air	1:2	0.22	−1.38	36.2	245	0.11
RB1-[60]PCBM air	1:2	0.09	−0.11	25.0	8	0.002
RB1-[70]PCBM air	1:2	0.09	−0.16	25.0	1	0.003
RG2-[60]PCBM glove box	1:2	0.10	−0.44	25.0	2	0.011
RB2-[60]PCBM glove box	1:2	0.30	−0.16	29.1	60	0.014
RG3-[60]PCBM air	1:2	0.45	−0.0304	20.9	9	2.8×10^{-3}
RB3-[60]PCBM air	1:2	0.22	−0.0259	26.7	17	1.5×10^{-3}
RG3-[60]PCBM-C_{60} air	1:2	0.38	−0.195	25.2	330	1.9×10^{-2}
RB3-[60]PCBM-C_{60} air	1:2	0.14	−0.0168	25.0	5	5.9×10^{-4}

The best data under illumination are shown and were obtained with an incident light intensity of 1000 W m^{-2} (AM1.5) at a temperature of 72 ± 2 °C. The conditions were either in a glovebox (H_2O and O_2 levels < 0.1 ppm) or in the air. The active area for the devices was 3 cm^2 (RG = RISO GREEN, RB = RISO BROWN).

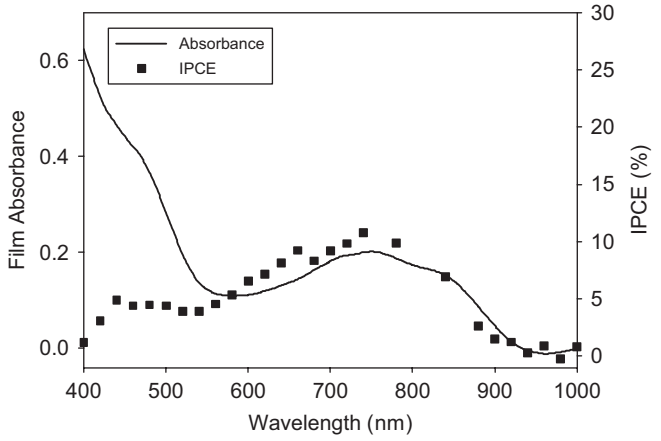

Fig. 5. The film absorbance of the device measured in transmission before evaporation of the aluminium electrode and the IPCE curve for **RISO GREEN 1**-[60]PCBM (1:1).

does show that the system has the ability to efficiently convert photons in to electrons in an external circuit.

In terms of the current density the device performs quite well. The maximum current density that is achievable with a band gap of 900 nm and an incident light intensity of $1000\,W\,m^{-2}$ @ AM1.5 is around $30\,mA\,cm^{-2}$ (see the review in this issue by Bundgaard et al. [1]). The observed J_{sc} value is $1.86\,mA\,cm^{-2}$ and from the IPCE curve an average IPCE from 400 to 900 nm of 6% is obtained that amounts to $1.8\,mA\,cm^{-2}$ which is very close to the observed J_{sc}. An optimization of the device properties in terms of FF and V_{oc} should thus enable the preparation of devices with higher efficiencies with the current IPCE profile.

3.4.4. *IV characteristics*

RISO GREEN 1 and **RISO BROWN 1** were the least tractable polymer materials from a film forming and device preparation point of view. They, however, gave the best devices and our attempts to make more soluble materials that gave better films failed. In order to understand this, we analysed the *IV* characteristics for the devices as shown in the dark and under illumination in Fig. 6. All devices exhibited comparable diode behaviour in the dark in terms of the rectification ratio that was 61 and 80, respectively, for **RISO GREEN 1**-[60]PCBM (1:1) and **RISO GREEN 3**-[60]PCBM (1:2) devices. There were obvious differences in the current densities with the latter device having much lower current densities by a factor of ~4500. This is peculiar since the device films had roughly the same absorbance. Evidently **RISO GREEN 1** has 16 carbon atoms in the sidechains and **RISO GREEN 3** has 24 carbon atoms in the alkyl side chains and some of the transport limitations can be ascribed to this dilution of the conjugated polymer backbone by side chains meaning that the films in the latter case are thicker since more side chains have been added while keeping the amount of chromophores the same. It is, however, unlikely that this can account fully for the poor transport as 66% by weight of the film is [60]PCBM. There are several other factors that may contribute to the poor transport. Firstly, the morphology of the [60]PCBM could be poor due to large crystallites as observed earlier [3] while this is not expected to fully account for the low current density. Secondly, there could be transport problems at one of the electrodes. We tested the second possibility by evaporating a layer of C_{60} before evaporation of the aluminium electrode. Aluminium is a very reactive metal and has been shown to react with soft conjugated polymer materials at the interface giving poor carrier transport properties. C_{60} also react with aluminium at the interface [13] but maintain good carrier transport properties in its reduced state and a layer of C_{60} can therefore be used as a means to stabilize a photovoltaic device. [14] We would thus expect to see an improvement in transport if this was part of the problem. As expected, the rectification ratio improved to 330 and the current density increased by a factor of 50. While some improvement was achieved the reasons for the much poorer performance are probably many. This is further substantiated when examining the *IV* curves under illumination where **RISO GREEN 1** give a moderate FF of 33.5% and a J_{sc} that is moderate. **RISO GREEN 3**, however, gave poorer efficiencies by a factor of ~100 and had very low FF's. The FF's obtained were typically below 25% and the worst case was 16.4 as shown in Fig. 6. The addition of a C_{60} layer in this case improved the efficiency by a factor of ~10 mainly due to an increased current density but also the FF. The negative curvature in the fourth quadrant of the *IV* curve has been reported earlier by Glatthaar et al. [15] that excellently linked the effect to poor transport at one of the electrodes in this case the aluminium electrode. The appearance of a negative curvature in the *IV* curve during device testing for extended periods of time has also been observed and linked to the slow corrosion of the interface between the active layer and the aluminium electrode [16].

3.4.5. *Stability considerations*

The degradation of organic photovoltaics has in isolated studies been linked to many phenomena. A more realistic picture is obtained when viewing organic/polymer photovoltaic devices as an inherently unstable technology when comparing to for instance silicon-based solar cells. The latter presents three-dimensional crystalline structures that are impervious to diffusion of small molecules such as oxygen and water and their morphology or macroscopic structure is virtually infinitely stable at or around RT. On the contrary, organic/polymer photovoltaics are soft materials with no or little crystalline order. Diffusion phenomena take place readily and the devices are not stable in chemical, physical or morphological terms. The view is thus that an organic/polymer photovoltaic starts degrading the moment it has been prepared. Many degradation processes take place simultaneously and often the most dominant under the conditions available is being

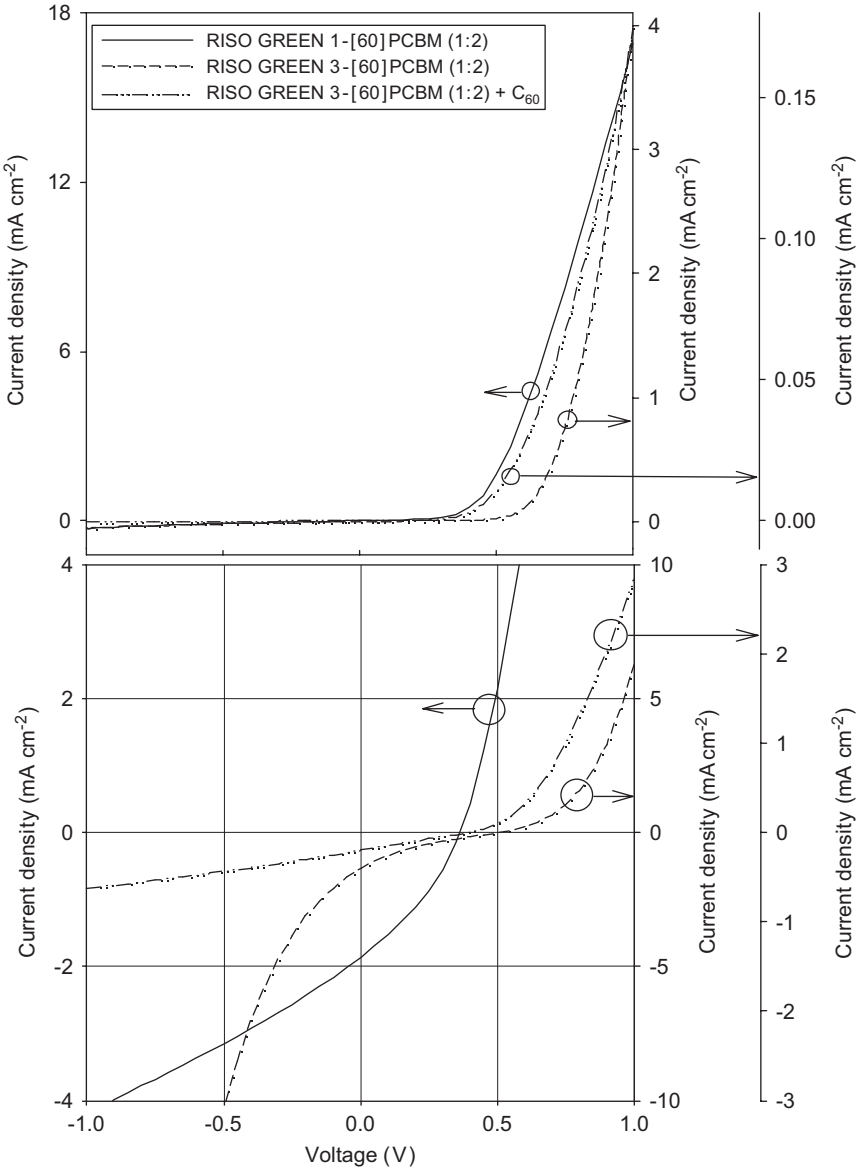

Fig. 6. *IV* curves in the dark (top) and under simulated sunlight 1000 W m^{-2} @ AM1.5 (below) for devices with an active area of 3 cm^{-2}. The dark rectification @ $|\pm 1$V$|$ was 61, 80 and 330 for **RISO GREEN 1**, **RISO GREEN 3** and **RISO GREEN 3** + C_{60}, respectively. The active layer in all devices was a 1:2 mixture of polymer:[60]PCBM (top).

observed and studied. Some of the most important mechanisms are:

(1) reaction with molecular oxygen (chemical and photochemical at the electrodes and in the bulk),
(2) reaction with water (chemical and photochemical at the electrodes and in the bulk),
(3) reaction between the electrode materials at the interfaces and diffusion,
(4) morphological changes (growth of PCBM crystallites, diffusion of ions).

Water and oxygen can be removed from the experiment but this only eliminates the degradation mechanisms where oxygen and water enter and the remaining mechanisms are still in play. One issue that is very important is the softness of the active layer and it has been shown that a tough active layer with a high glass transition temperature lead to more stable photovoltaic devices since diffusion phenomena are decelerated and a higher morphological stability is obtained [17]. Further an interface layer of C_{60} between the chemically reactive metal cathode and the active layer has been found to improve the operational stability [15] since C_{60} still conducts an electrical current when reduced by aluminium at the interface. The very poor performance of **RISO GREEN 2–3** and **RISO BROWN 2–3** is ascribed to a much poorer stability than observed for **RISO GREEN 1** and **RISO BROWN 1**.

RISO GREEN 1-[60]PCBM (1:2) devices were quite stable when operated in the atmosphere and there were no significant differences in the performance of devices prepared in air and in a glovebox. The stability in the

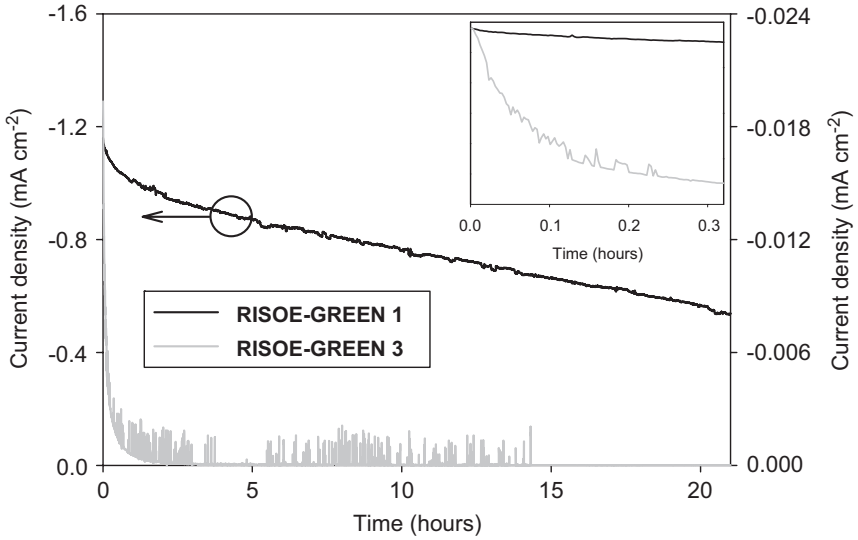

Fig. 7. A comparison of the lifetime curves for **RISO GREEN 1** and **RISO GREEN 3** as a 1:2 mixture with [60]PCBM in air. The devices were constantly illuminated at 1000 W m^{-2} @ AM1.5 at a temperature of 72±2 °C. The devices were kept at short circuit and the value for J_{sc} was recorded every 10 s. The inset shows the data of the first 20 min of the experiment.

dark was, however, better in the glovebox and devices were stable for many days whereas devices degraded in air when left in the dark. On the other hand, **RISO GREEN 3**-[60]PCBM (1:2) devices were quite unstable and degraded quickly in air but not in the glovebox. A comparison between the two types of devices is shown in Fig. 7. **RISO GREEN 1**-[60]PCBM (1:2) devices gave roughly the same values for V_{oc} and J_{sc} and FF when prepared in the glovebox and we thus rule out the possibility that the poor performance is due to device degradation before device characterization except for the special case where the device actually degrades when the aluminium electrode is evaporated.

3.5. X-ray structures

The structure of compound **4** turned out to be very difficult to solve since all crystals found were twins. The data were collected with the following orthorhombic primitive cell $Pca2_1$: $a = 10.1734$ (6), $b = 11.4904$ (7) and $c = 20.5427$ (12) with two molecules in the asymmetric unit cell. A disordered model with two conformations for one of the thiophene rings was found to satisfy the data best (see Fig. 8). The structures are characterized by that the amine groups are in plane with the central thiophene ring. The two other thiophene rings are twisted out of plane compared to the central ring. It should be noted that the rings are not twisted equally for the two molecules in the asymmetric unit. In the case of compound **5c**, the data were collected with the following triclinic primitive cell: $a = 11.5962$ (4), $b = 12.7166$ (5), $c = 16.7600$ (6), $\alpha = 71.869$ (2), $\beta = 89.983$ (2) and $\gamma = 81.526$ (2) with two molecules in the asymmetric unit cell. Again a disordered model for three of the thiophene rings was applied with distance restraints for the equivalent C–C and C–S distances together with similarity restraints. This resulted in a model (se Fig. 9) with a R_1 value of 0.106. An anomalous large thermal ellipsoid for one of the carbon atoms in one of the disordered thiophene rings was, however, observed. In the structure of **5c**, the central ring system is planar and both of the thiophenes and both phenyl rings are twisted out of plane with the thienopyrazine.

The structural disorder found for both **4** and **5c** around the bonds between the outer thiophenes and the thienopyrazine units has been noted previously [7].

4. Conclusions

The chemistry of the thienopyrazine type acceptor moiety have been explored to characterize the influence of the substituents and extended π-system on the absorption spectrum. New and improved methods for introducing alkyl groups in these systems have also been explored. It was found that adding phenyl groups to the dithienylthienopyrazine system caused a red shift of the lowest energy absorption band with ca. 50 to about 550 nm. Adding an extra bond between these two phenyl groups to form the novel and planar 11-thia-9,13-diaza-cyclopenta[*b*]triphenylene acceptor caused a further red shift of this absorption band to 640 nm.

A series of six polymers, **RISO GREEN 1–3** and **RISO BROWN 1–3**, have been prepared based on either the diphenyl-thienopyrazine or the 11-thia-9,13-diaza-cyclopenta[*b*]triphenylene acceptors together with a terthiophene donor segment. These polymers also differed in the alkyl side chains added to give solubility and processeability. The size exclusion chromatography indicated a rather low degree of polymerization of ca. 3. These materials could therefore also be considered oligomers

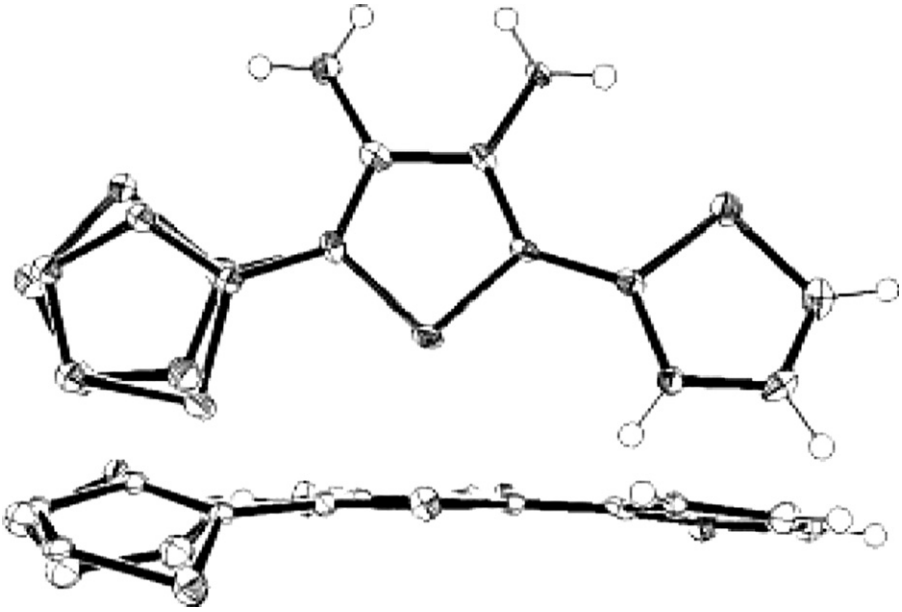

Fig. 8. The structure of compound **4**. Note that one of the thiophene rings has been modelled as a disordered system.

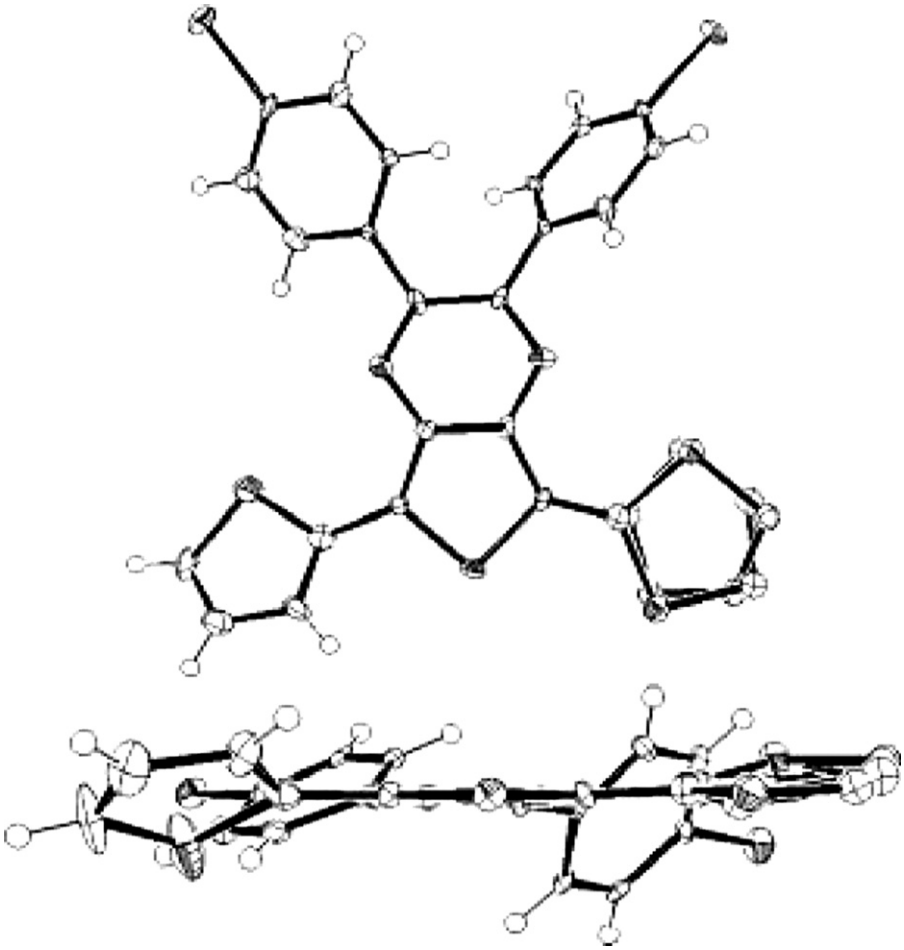

Fig. 9. The structure of compund **5c**.

rather than polymers. Absorption spectra of the polymers showed that the alternating donor acceptor motifs further red shifted the low energy transitions now extending beyond 900 nm and an optical band gap of about 1.2 eV. The lower solubility of the **RISO BROWN**-type polymers made consistent characterization difficult, but it was

apparent that the lower energy transition had a much weaker intensity compared to the **RISO-GREEN** series.

Photovoltaic devices prepared from these six polymers blended with either [60]PCBM or with [70]PCBM are as yet unoptimized and gave rather poor performances mainly due to low film absorbencies and low fill factors. Other possible causes include reaction at the reactive aluminium electrode and poor morphology. The best device was obtained with **RISO GREEN 1** mixed with [60]PCBM in the ratio 1:1 which gave an J_{sc} of $1.86\,mA\,cm^{-2}$ and an efficiency of 0.22% under simulated sunlight ($1000\,W\,m^{-2}$, AM1.5). The fill factor was 34% and the V_{oc} was 0.36 V, which is considered low and the parameters that must be improved.

Acknowledgements

This work was supported by the Danish Strategic Research Council DSF 2104-05-0052.

References

[1] E. Bundgaard, F.C. Krebs, Sol. Energy Mater. Sol. Cells 91 (2007) 1019–1025, this issue.
[2] F. Zhang, E. Perzon, X. Wang, W. Mammo, M. Anderson, O. Inganäs, Adv. Func. Mater 15 (2005) 745.
[3] M.M. Wienk, M.G.R. Turbiez, M.P. Struijk, M. Fonrodona, R.A.J. Janssen, Appl. Phys. Lett. 88 (2006) 153511.
[4] E. Perzon, X. Wang, F. Zhang, W. Mammo, J.L. Delgado, P. de la Cruz, O. Inganäs, F. Langa, M.R. Andersson, Synth. Met. 154 (2005) 53.
[5] E. Bundgaard, F.C. Krebs, Macromolecules 39 (2006) 2823.
[6] D.D. Kenning, K.A. Mitchell, T.R. Calhoun, M.R. Funfar, D.J. Sattler, S.C. Rasmussen, J. Org. Chem. 67 (2002) 9073.
[7] O. Hagemann, M. Jørgensen, F.C. Krebs, J. Org. Chem. 71 (2006) 5546.
[8] F.C. Krebs, M. Jørgensen, Rev. Sci. Instrum. 74 (2003) 3438.
[9] C. Kitamura, S. Tanaka, Y. Yamashita, J. Chem. Soc., Chem. Commun. (1994) 1585.
[10] C. Mangeney, J.-C. Lacroix, K.I. Chane-Ching, M. Jouini, F. Villain, S. Ammar, N. Jouini, P.-C. Lacaze, Chem. Eur. J. 7 (2001) 5029.
[11] H. Maeda, H. Nagomi, Y. Yamauchi, H. Ohmori, Chem. Pharm. Bull. 48 (2000) 1196.
[12] M.M. Wienk, J.M. Kroon, W.J.H. Verhees, J. Knol, J.C. Hummelen, P.A. van Hal, R.A.J. Janssen, Angew. Chem. Int. Ed. 42 (2003) 3371.
[13] K. Norrman, F.C. Krebs, Sol. Energy Mater. Sol. Cells 90 (2006) 213.
[14] F.C. Krebs, J.E. Carlé, N. Cruys-Bagger, M. Andersen, M.R. Lilliedal, M.A. Hammond, S. Hvidt, Sol. Energy Mater. Sol. Cells 86 (2005) 499.
[15] M. Glatthaar, M. Riede, N. Keegan, K. Sylvester-Hvid, B. Zimmermann, M. Niggemann, A. Hinsch, A. Gombert, Sol. Energy Mater. Sol. Cells 91 (2007) 390.
[16] F.C. Krebs, K. Norrman, Prog. Photovoltaics, submitted.
[17] F.C. Krebs, H. Spanggaard, Chem. Mater. 17 (2005) 5235.

Thermocleavable Low Band Gap Polymers and Solar Cells Therefrom with Remarkable Stability toward Oxygen

Martin H. Petersen, Suren A. Gevorgyan, and Frederik C. Krebs*

Risø National Laboratory for Sustainable Energy, Technical University of Denmark, P.O. Box 49, DK-4000 Roskilde, Denmark

Received August 26, 2008; Revised Manuscript Received October 10, 2008

ABSTRACT: Thermocleavable esters of low band gap monomers and polymers based on diphenyldithienylthienopyrazine were prepared by incorporating carboxylic acid functionalities into the system. A series of different ester groups were prepared and the temperature of elimination of the ester group was studied. The lowest temperatures of elimination obtained were in the range 220−240 °C for tertiary esters giving the free acid. The highest temperatures of elimination were found for primary esters that also lead to decomposition of the molecule. Only the tertiary esters offer a good degree of control over the chemistry in the thermocleaved product. The photovoltaic performance of the polymers prepared was tested under simulated sunlight (1000 W m^{-2}, AM1.5G, 72 °C) and the best power conversion efficiency that could be reached for devices with an active area of 3 cm^2 was up to 0.4% in an ITO/PEDOT/polymer−PCBM/aluminum device geometry. The best performing polymer material was subjected to lifetime studies in four different atmospheres (dry nitrogen, dry oxygen, humid nitrogen and the ambient atmosphere). The best stability was observed in nitrogen while the devices showed nearly the same degree of stability in dry oxygen. In both the ambient atmosphere and the humid nitrogen atmospheres the devices degraded quickly. Finally the stability was compared with two other polymer systems that are known to give stable devices, poly(3-hexylthiophene) (P3HT) and native polythiophene (PT) obtained from the thermocleavable poly(3-(2-methylhexyloxycarbonyl)dithiophene) (P3MHOCT). The performance of the materials reported here was inferior to the performance of P3HT and PT in terms of power conversion efficiency (PCE). The photovoltaic parameters as studied under continuous illumination were however much more stable than those of the reference compounds.

Introduction

The processing requirements of functional materials and polymers are key to the successful application in active devices such as polymer solar cells.[1] In addition to processing there is, in the context of polymer solar cells, increasing focus on preparation of efficient materials with low optical band gaps[1b] and materials that give stable devices. Polymer solar cell devices most often rely on a thin multilayer structure with exact requirements of the nanomorphology of the individual layers. One of the advantages of the technology is that the individual layers can be prepared by solution processing thus gaining considerably in the potential speed, simplicity and lowered cost. However, the formation of multilayer structures based on organic materials such as polymers require that the deposition of subsequent layers does not affect the previously deposited layers. In practical terms this poses a major challenge and has only been solved with some success by following one of three possible strategies or a combination thereof.

(1) Orthogonal solvents for different layers.

(2) Cross-linking after film formation.

(3) Removal of solubilizing groups by thermocleavage.

The use of orthogonal solvents is the simplest and most facile approach. While it is not generic, in the sense that one may encounter combinations of materials for which no orthogonal solvents can be devised, it is commonly employed either intentionally or because there are no other alternatives with the materials at hand. A good example is the use of a PEDOT:PSS layer spincoated from polar solvents such as water followed by another layer spincoated from an organic solvent such as dichlorobenzene.[2] Cross-linking has been employed only rarely as the possibility for cross-linkage has to be engineered into the material. One of the best known examples involved the use of solubilizing sidechains containing an oxetane group that can be cross-linked by a ring opening polymerization.[3] The last approach involving solubilizing groups that can be removed after the film is prepared is the most appealing from the solar cell point of view since all the advantages of solution processing are available up until the film has been produced. After the film has been prepared the side chains take up a considerable part of the volume of the film and are passive in terms of carrier transport and light absorption. There are obvious challenges in controlling the purity, structure and morphology of the film material after the removal of the solubilizing groups but it is reasonable to assume that these can be overcome. The most

Table 1. List of TGA Data for 6a−m, 8b−d, 8i−l

compound	ester elimination (°C)	weight loss (%) calculated	found
6a	410[a]	23.7	36
6b	333	26.7	25
6c	325	31.8	34
6d	332	26.7	25
6e	360[a]	21.1	22
6f[b]		22.4	
6g	326[a]	20.1	17
6h	300[a]	22.9	15
6i	266	27.8	18
6j	225	26.7	26
6k	197	20.1	18
6l	246	19.7	10
6m[b]		22.4	
8b	329	24.0	25
8c	325	28.9	28
8d	325	24.0	24
8i	254	25.6	15
8j	225	24.0	21
8k	206	18.0	8
8l	*c*	17.6	6

[a] Molecule decomposes at first inflection. [b] Insufficient TGA data. [c] Broad derivative peak with no maximum (see Supporting Information).

* Corresponding author. E-mail: frederik.krebs@risoe.dk.

10.1021/ma801932a CCC: $40.75
Published on Web 11/07/2008

Table 2. Photovoltaic Parameters of the Materials Reported with and without Thermocleavage[a]

polymer	J_{sc} (mA/cm^2)	V_{oc} (V)	FF	PCE (%)	cleaving temp (°C)[b]	solubility in DCB
8b	1.52	0.14	0.25	0.05	25	easy to dissolve
	0.41	0.16	0.26	0.017	310	
8c	2.1	0.4	0.29	0.25	25	hard to dissolve
	0.36	0.14	0.27	0.013	310	
8d	2.55	0.41	0.29	0.3	25	easy to dissolve
	0.24	0.08	0.26	0.005	310	
8j	2.4	0.46	0.36	0.4	25	easy to dissolve
	1.94	0.4	0.33	0.25	230	

[a] The devices had a glass/ITO/PEDOT:PSS/polymer:PCBM/Al geometry and the performance was recorded immediately after preparation in the ambient atmosphere (1000 W m^{-2}, AM1.5G, 72 ± °C, humidity 30 ± 5% rh). [b] The duration of cleaving at 230 °C was 1 min and at 310 °C was 10 min.

Scheme 1. Synthesis of the Dithienylthienopyrazines 6a−m and the Polymers 8b−d, 8i−l with Thermocleavable Benzoate Esters Substituted on the Pyrazine Ring[a]

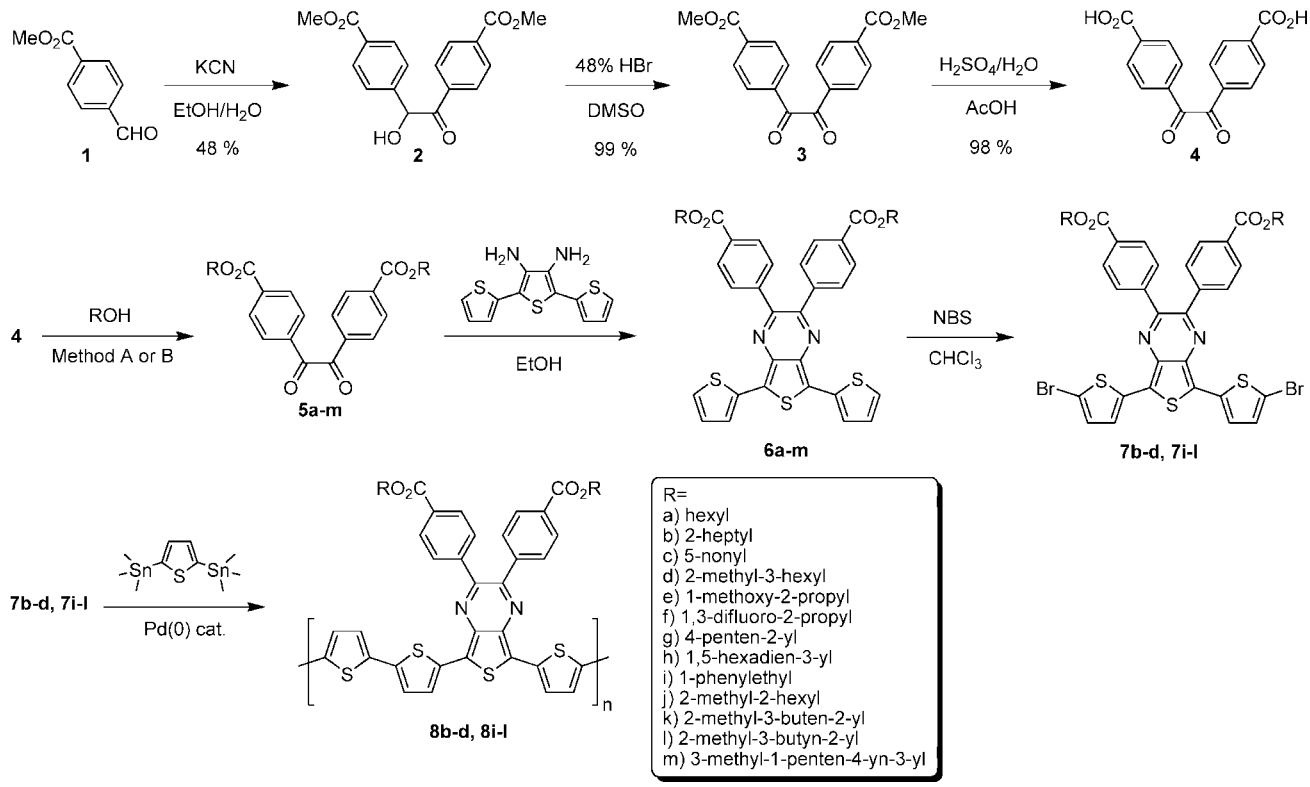

[a] Method A: 1,1′-carbonyldiimidazole, pyridine. Method B: DMAP, Sc(OTf)$_3$, *N,N*′-diisopropylcarbodiimide.

recent developments are the thermocleavable ester groups[4] and the dithiocarbamate precursor route.[5] The thermocleavable ester groups have been explored in the context of polymer solar cells giving stable operation,[6] stable nanostructures[7] and multilayer tandem cells.[8] The use of thermocleavable materials offer several advantages. Most importantly the side chains that constitute a significant proportion of the final film are alleviated and ideally the final film comprises only the active component. Furthermore, in the case of carboxylic esters attached to thiophenes the processing offer removal of the esters at lower temperatures and the acid groups at higher temperatures allowing for multistep processing.[4b] One aim is to achieve as low a temperature of elimination of the ester group as possible and the purpose of this work was to establish this in the context of choice of ester alcohol, mode of preparation of the ester using the monomers for model studies, extending this to the polymers, evaluate these materials in solar cells and finally to establish their stability performance when subjected to different conditions comprising both inert, ambient and model atmospheres presenting either water or oxygen on their own.

Experimental Section

4,4′-Bis(methyloxycarbonyl)benzoin (2). Methyl 4-formylbenzoate (**1**) (50 g, 305 mmol, 1 equiv) was stirred in 99% ethanol (150 mL) and water (50 mL). Potassium cyanide (6 g, 92.1 mmol, 0.3 equiv) was added, and the reaction mixture was stirred at room temperature for 15 min. The product was filtered, washed with water (3 × 200 mL) and dried at 70 °C in vacuum. Yield: 48 g (48%), light yellow solid. M_p = 140−141 °C. ^{1}H NMR (DMSO): δ = 8.09 (d, 2H, J = 8.6 Hz), 8.00 (d, 2H, J = 8.6 Hz), 7.90 (d, 2H, J = 8.3 Hz), 7.55 (d, 2H, J = 8.3 Hz), 6.46 (s, 1H), 6.15 (s, 1H), 3.84 (s, 3H), 3.80 (s, 3H). ^{13}C NMR (DMSO): δ = 199.0, 166.4, 165.9, 145.0, 138.8, 133.7, 129.7, 129.7, 129.6, 129.5, 127.9, 76.2, 52.9, 52.5.

4,4′-Bis(methyloxycarbonyl)benzil (3). To a stirred solution of **2** (74 g, 225 mmol) in DMSO (510 mL) was added slowly 105 mL 48% aqueous hydrobromic acid. The solution was heated to 55 °C for 24 h after which 500 mL water was added and the product was filtered, washed with water (3 × 200 mL) and dried at 70 °C in vacuum. Yield: 72.5 g (99%), yellow solid. M_p = 197−198 °C. ^{1}H NMR ($CDCl_3$): δ = 8.19 (d, 4H, J = 7.5 Hz), 8.06 (d, 4H, J = 7.5 Hz), 3.97 (s, 6H). ^{13}C NMR ($CDCl_3$): δ = 192.9, 165.8, 135.7, 135.5, 130.1, 129.9, 52.7.

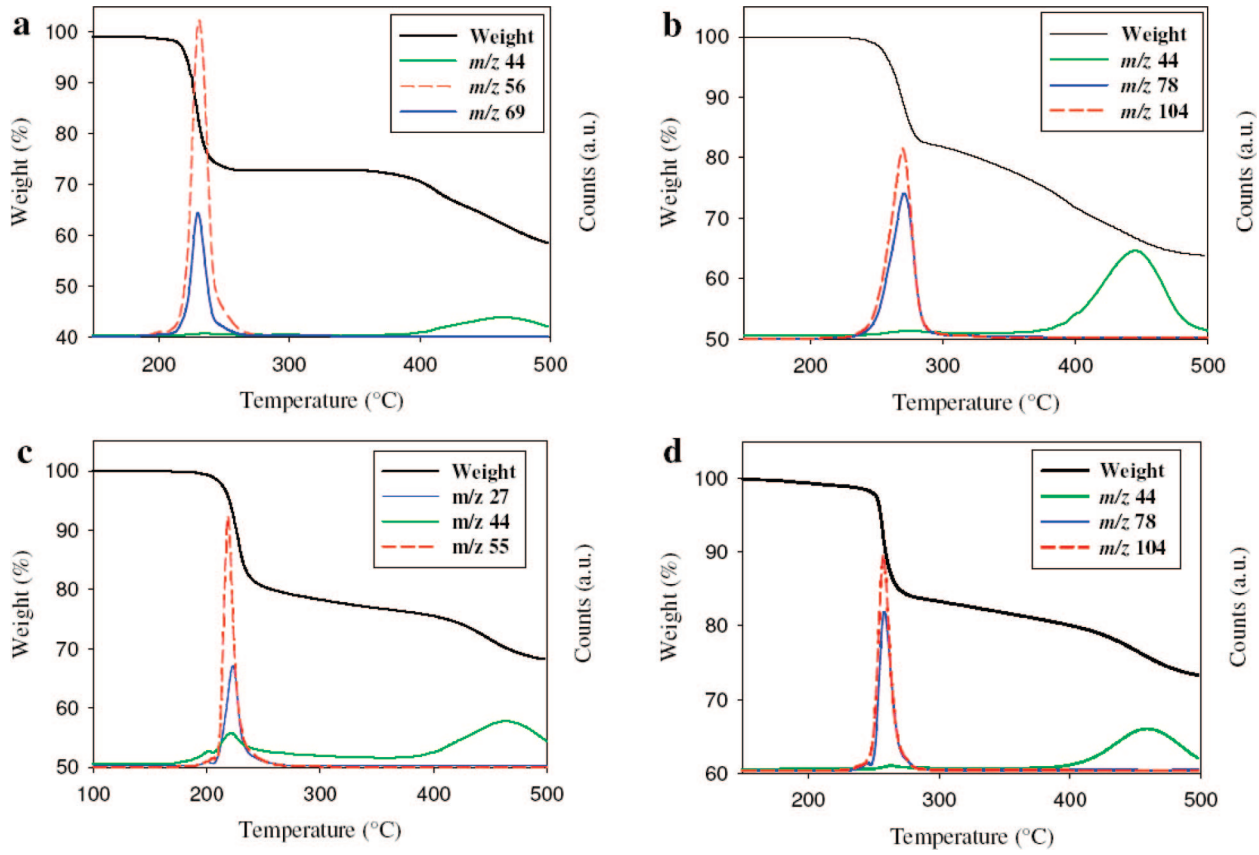

Figure 1. (a) TGA−MS of **6j**, (b) TGA−MS of **6i**, (c) TGA−MS of **8j**, and (d) TGA−MS of **8i**. The first inflection accounts for the ester elimination and the second weight loss around 400−500 °C is decomposition. The red and blue curves correspond to loss of alkenes and the green curves corresponds to loss of carbon dioxide.

4,4′-Bis(hydroxycarbonyl)benzil (4). 3 (5 g, 15.3 mmol) was mixed in acetic acid (350 mL) and a 4:1 H_2SO_4/H_2O solution (175 mL). The reaction mixture was heated to reflux and stirred for 10 h after which 250 mL water was added and the mixture was cooled on ice. After cooling the product was filtered, washed with water (3 × 20 mL) and dried at 70 °C in vacuum. Yield: 4.5 g (98%), pale yellow solid. M_p > 300 °C. ^{1}H NMR (DMSO): δ = 13.54 (s, 2H), 8.15 (d, 4H, J = 7.0 Hz), 8.08 (d, 4H, J = 7.0 Hz). ^{13}C NMR (DMSO): δ = 193.8, 166.8, 136.9, 135.5, 130.5, 130.5.

General Procedure for the Preparation of Primary and Secondary Diesters (Method A). *4,4′-Bis(hexyloxycarbonyl)benzil (***5a***).* **4** (500 mg, 1.68 mmol, 1 equiv) and 1,1′-carbonyldiimidazole (557 mg, 3.44 mmol, 2.05 equiv) were mixed in dry pyridine (5 mL) and stirred at 50 °C under argon for 1 h. 1-Hexanol (439 μL, 3.52 mmol, 2.1 equiv) was added and the reaction mixture was heated to reflux for 10 h. After TLC showed reaction completion the pyridine was evaporated in vacuum. The residue was added saturated $NaHCO_3$ (30 mL) and extracted with ether (3 × 30 mL). The combined organic phase was dried ($MgSO_4$), filtered and concentrated in vacuum. Dry column chromatography (silica gel 15−40 μm, eluted with EtOAc/Heptane, gradient 1−5% EtOAc) afforded **5a**. Yield: 625 mg (80%), yellow solid. M_p = 140−141 °C. ^{1}H NMR ($CDCl_3$): δ = 8.18 (d, 4H, J = 8.5 Hz), 8.05 (d, 4H, J = 8.5 Hz), 4.36 (t, 4H, J = 6.7 Hz), 1.83−1.74 (m, 4H), 1.49−1.39 (m, 4H), 1.39−1.29 (m, 8H), 0.95−0.86 (m, 6H). ^{13}C NMR ($CDCl_3$): δ = 192.9, 165.4, 135.9, 135.7, 130.1, 129.8, 65.9, 31.4, 28.6, 25.6, 22.5, 13.9. HRMS-FAB: m/z calcd for $C_{28}H_{35}O_6$ $[M + H]^+$, 467.2434; found, 467.2430.

General Procedure for the Preparation of Tertiary Diesters (Method B). *4,4′-Bis(2-methylhexan-2-yloxycarbonyl)benzil (***5j***).* A suspension of **4** (300 mg, 1.01 mmol, 1 equiv), DMAP (258 mg, 2.11 mmol, 2.1 equiv), scandium triflate (49.5 mg, 0,101 mmol, 0.1 equiv) and 2-methyl-2-hexanol (302 μL, 2.11 mmol, 2.1 equiv) in dry methylene chloride (5 mL) was stirred at room temperature under argon for 30 min. *N*,*N*′-Diisopropylcarbodiimide (331 μL, 2.11 mmol, 2.1 equiv) was added and the reaction mixture was heated to reflux and stirred for 24 h. The reaction mixture was concentrated on celite in vacuum. Dry column chromatography (silica gel 15−40 μm, eluted with EtOAc/Heptane, gradient 1−5% EtOAc) afforded **5j**. Yield: 388 mg (78%), yellow oil. ^{1}H NMR ($CDCl_3$): δ = 8.08 (d, 4H, J = 8.5 Hz), 7.99 (d, 4H, J = 8.5 Hz), 1.92−1.80 (m, 4H), 1.55 (s, 12H), 1.42−1.25 (m, 8H), 0.94−0.82 (m, 6H). ^{13}C NMR ($CDCl_3$): δ = 193.1, 164.2, 137.5, 135.5, 129.9, 129.6, 84.4, 40.6, 26.1, 26.0, 22.9, 13.9. HRMS-FAB: m/z calcd for $C_{30}H_{39}O_6$ $[M + H]^+$, 495.2747; found, 495.2735.

General Procedure for the Condensation. *Bis(2-methylhexan-2-yl) 4,4′-(5,7-Di(thiophen-2-yl)thieno-[3,4-b]pyrazine-2,3-diyl)dibenzoate (***6j***).* **5j** (567 mg, 1.15 mmol, 1 equiv), [2,2′;5′,2″]terthiophene-3′,4′-diamine hydrochloride (397 mg, 1.26 mmol, 1.1 equiv) and triethylamine (3.44 mmol, 0.480 mL, 3 equiv) was mixed in 99% ethanol (20 mL). The reaction mixture was heated to reflux and stirred for 15 h. After the reaction was complete the mixture was cooled on ice followed by filtration of the product. The product was washed with 99% ethanol (3 × 5 mL) and dried at 50 °C in vacuum.Yield: 730 mg (86%), dark purple solid. M_p = 197−198 °C. ^{1}H NMR ($CDCl_3$): δ = 7.97 (d, 4H, J = 8.3 Hz), 7.67−7.60 (m, 6H), 7.40 (dd, 2H, J = 5.1, 1.0 Hz), 7.11 (dd, 2H, J = 5.1, 3.7 Hz), 1.96−1.86 (m, 4H), 1.60 (s, 12H), 1.44−1.34 (m, 8H), 0.94 (t, 6H, J = 6.9, 6.9 Hz). ^{13}C NMR ($CDCl_3$): δ = 165.0, 151.3, 142.6, 137.3, 134.5, 132.4, 129.8, 129.3, 127.3, 126.9, 125.6, 124.9, 83.7, 40.8, 26.2, 26.1, 23.0, 14.0. HRMS-FAB: m/z calcd for $C_{42}H_{44}N_2O_4S_3$ $[M + H]^+$, 736.2463; found, 736.2466.

General Procedure for the NBS Bromination. *Bis(2-methylhexan-2-yl) 4,4′-(5,7-Bis(5-bromothiophen-2-yl)thieno[3,4-b]pyrazine-2,3-diyl)dibenzoate (***7j***).* **6j** (1 g, 1.36 mmol, 1 equiv) was dissolved in dry chloroform (70 mL). Then NBS (483 mg, 2.71 mmol, 2 equiv) was added slowly and the reaction mixture was stirred at room temperature in the dark for 20 min. After completed reaction

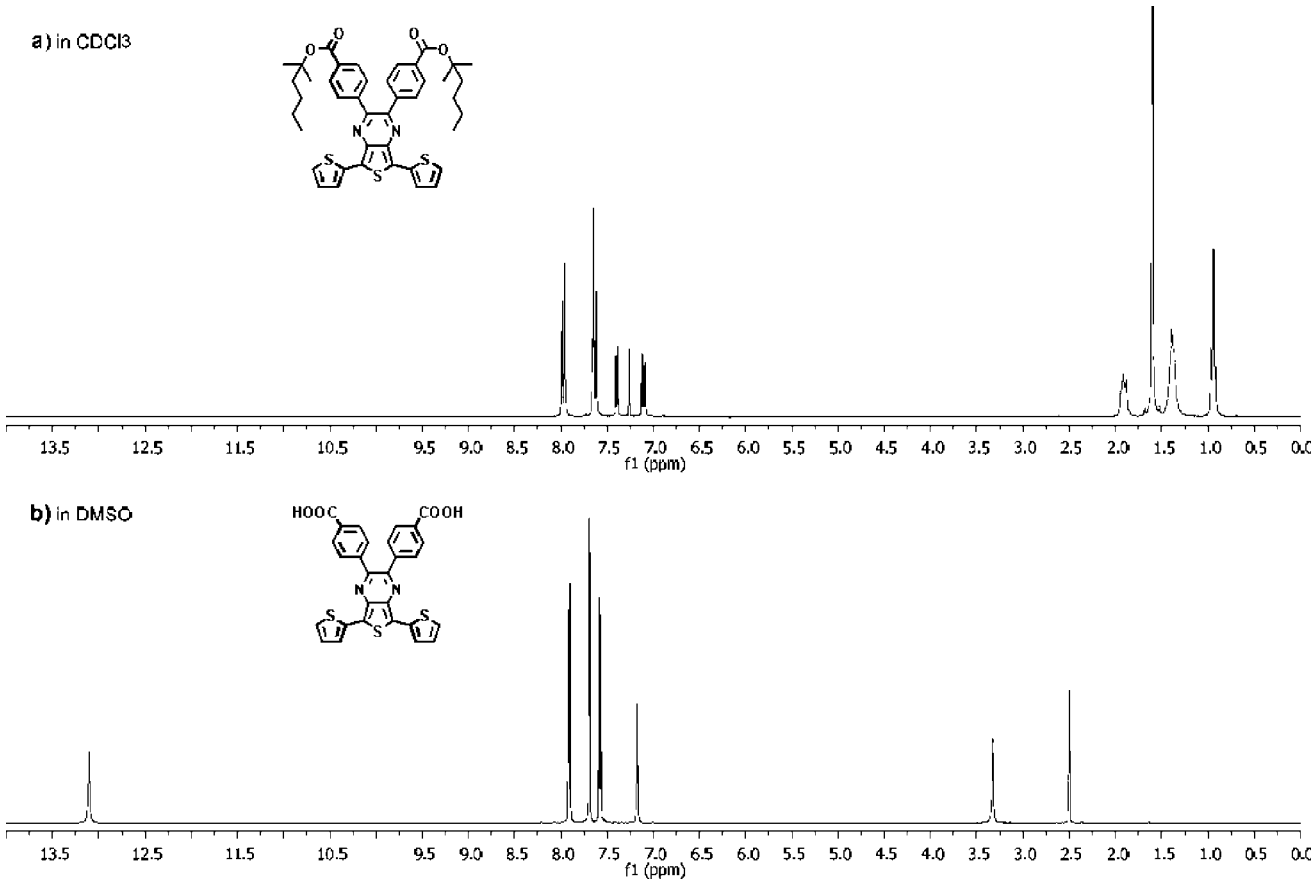

Figure 2. ^{1}H NMR spectra of **6j** (a) from before and after (b) heating to 233 °C for 30 min under argon.

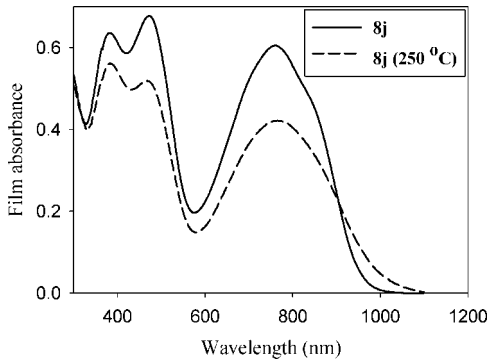

Figure 3. UV−vis for a spincoated film of **8j** on a glass substrate as measured in a transmission geometry. The spectrum for the thermocleaved film is also shown (heated to 250 °C for 1 min).

the mixture was washed with water (3 × 50 mL), dried ($MgSO_4$), filtered and concentrated in vacuum affording **7j**. Yield: 1.13 g (93%), dark purple solid. M_p = 185−186 °C.

^{1}H NMR ($CDCl_3$): δ = 7.98 (d, J = 8.4 Hz, 4H), 7.58 (d, J = 8.4 Hz, 4H), 7.22 (d, J = 4.0 Hz, 2H), 7.01 (d, J = 4.0 Hz, 2H), 1.97−1.87 (m, 4H), 1.61 (s, 12H), 1.46−1.33 (m, 8H), 0.94 (t, J = 7.0 Hz, 6H). ^{13}C NMR ($CDCl_3$): δ = 165.1, 152.0, 142.1, 137.3, 135.6, 132.7, 129.9, 129.8, 129.3, 124.8, 124.3, 115.1, 83.8, 40.8, 26.2, 26.1, 23.0, 14.0.

General Procedure for the Stille Coupling Polymerization. *Poly{bis(2-methylhexan-2-yl) 4,4′-(5-(2,2′-bithiophen-5-yl)-7-(thiophen-2-yl)thieno[3,4-b]pyrazine-2,3-diyl)dibenzoate} (8j).* **7j** (200 mg, 0.22 mmol, 1 equiv), 2,5-bis(trimethylstannyl)thiophene (92 mg, 0.22 mmol, 1 equiv), Pd_2dba_3 (20 mg, 0.022 mmol, 0.1 equiv) and tri(o-tolyl)phosphine (54 mg, 0.18 mmol, 0.8 equiv) was dissolved in dry toluene (50 mL). The reaction mixture was heated to reflux for 24 h under argon. Then the mixture was poured into 150 mL methanol and the polymer was allowed to precipitate. Finally the polymer **8j** was filtered and purified by Soxhlet extraction with MeOH,hexane and $CHCl_3$. Yield: 169 mg (92%), dark green solid. ^{1}H NMR (CD_2Cl_2): δ = 8.18−6.37 (m, 14H), 2.30−0.45 (m, 30H). SEC ($CHCl_3$): M_w = 39429, M_n = 20410, M_p = 17839, and PD = 1.932.

Thermal Analysis. The sample holders were carefully weighed and the samples introduced followed by drying for 24 h at 50 °C in vacuum. The thermogravimetric analysis was then carried out using heating rate of 10 °C min^{-1}. The carrier gas used was argon and the exhaust gases were passed through a mass spectrometer allowing for the simultaneous acquisition of mass data. A series of masses relevant to the degradation process were specifically followed such as CO_2, alkyl chain fragments and fluorine when relevant (see Supporting Information for each material).

Solar Cell Preparation. Glass substrates with pre-etched 100 nm thick layer of ITO and a sheet resistivity of 8−12 Ω square^{-1} purchased from LumTec were cleaned by consecutive ultrasonication in isopropanol and distilled water for 10 min each followed by drying immediately prior to use. A layer of PEDOT:PSS purchased from Aldrich as a 1.3 wt % aqueous solution was spin coated on top of ITO at a rotational speed of 2800 rpm and the slides were annealed at 160 °C for 5 min. Subsequently, the samples were transported into a glovebox and the active layer was applied as a blend of the polymer and [60]PCBM in a 1:1 ratio (20 mg mL^{-1} in dichlorobenzene) by spin coating onto the glass/ITO/PEDOT:PSS substrates. The samples were then dried at room temperature (25 °C) or heated to the desired cleaving temperature (see Tables 1 and 2). An aluminum metal electrode was evaporated on top after the thermal annealing to complete the devices. The devices had an active area of 3 cm^2 and were tested for photovoltaic performance and stability.

Device Characterization. The photovoltaic performance was tested under a solar simulator (KHS575) where the irradiance and emission spectrum were observed using an optical spectrum

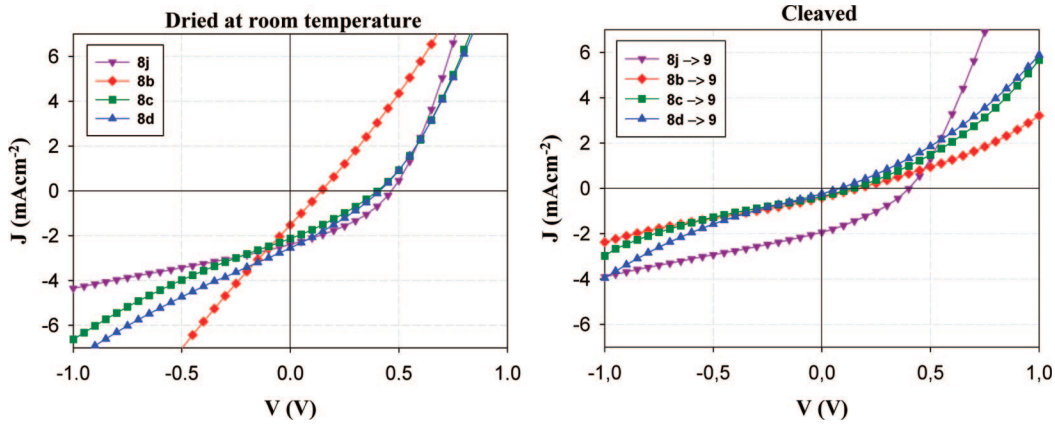

Figure 4. IV-curves for the different polymers uncleaved (left) and cleaved (right). The polymers **8b**, **8c**, and **8d** were cleaved at 310 °C for 10 min and the polymer **8j** was cleaved at 230 °C for 1 min.

Table 3. Summary of the Ranges of Performance Obtained for All Polymers (8b, 8c, 8d and 8j) in Pristine and Thermocleaved Form (1000 W m^{-2}, AM1.5G, 72 ± °C, Humidity 30 ± 5% rh)

J_{sc} (mA cm^{-2})	V_{oc} (V)	FF	PCE (%)	cleaving temp (°C)
1.52−2.55	0.14−0.46	0.25−0.36	0.05−0.4	25
0.24−1.94	0.08−0.4	0.26−0.33	0.005−0.25	230−310

Scheme 2. Thermocleavage of the the Polymer Materials 8b, 8c, 8d, or 8j All Lead to the Same Polymer Material 9

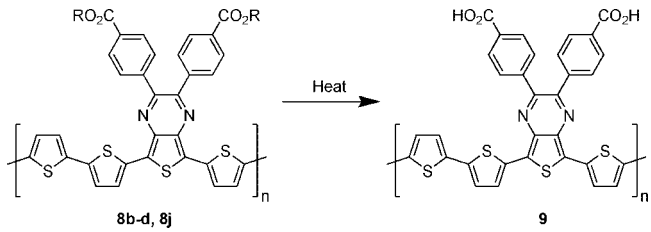

analyzer in conjunction with a precision radiometer from Eppley Laboratories. The spectrum during characterization of the solar cell efficiency was AM1.5G with an incident light power of 1000 W m^{-2}. The solar simulator is Class AAA from 400−800 nm, over the area of the cell and for the duration of the experiment. No corrections for mismatch were performed.

Stability Measurements. The stability measurements were performed in a stainless steel chamber[6f] with quartz windows and controlled atmosphere. Four different atmospheric conditions were applied to the chambers by continuously introducing the following gas mixtures: (1) nitrogen atmosphere 99.999% (oxygen <2 ppm, humidity <2 ppm); (2) dry oxygen atmosphere 99.5% (humidity <2 ppm); (3) ambient atmosphere (20 ± 5% relative humidity); (4) humid nitrogen 99.999% (oxygen <2 ppm, 95 ± 5% relative humidity). The main impurity in the 99.5% pure oxygen is nitrogen. The temperature during all experiments was 30 ± 2 °C and the incident light intensity was 330 W m^{-2}. The setup is automated and employ IV-measurements at intervals of 10 min using a Keithley 2400 through a switch matrix based on a Keithley 7705 contained in a Keithley 2700.[6f]

Results and Discussion

Synthesis. The synthetic steps involved in the preparation of the dithienylthienopyrazines with thermocleavable esters are outlined in Scheme 1. The benzils **5a**−**m** were made by a four step synthetic sequence employing a standard benzoin condensation of methyl 4-formylbenzoate (**1**) and potassium cyanide. The reaction was very fast and no heating was required. The insoluble benzoin **2** was oxidized using 48% aqueous hydrobromic acid in dimethyl sulfoxide[9] affording the benzil **3** that was then hydrolyzed in an aqueous acid to give the diacid **4**. The esterifications of the primary and secondary esters **5a**−**i** employed 1,1′-carbonyldiimidazole as the acylating agent (method A). Tertiary esters are notoriously difficult to synthesize and a series of techniques were attempted. Transformation of **4** into the diacid chloride followed by direct reaction with the tertiary alcohols (2-methyl-2-hexanol, 2-methyl-3-buten-2-ol, 2-methyl-3-butyn-2-ol, 3-methyl-1-penten-4-yn-3-ol) or by adding freshly precipitated AgCN[10] was ineffective. Other acylating agents such as 2,2′-dipyridyl disulfide/PPh$_3$,[11] 2-chloro-1-methylpyridinium iodide[12] and 2-chloro-3,5-dinitropyridine[4a] all failed. The latter method has proven useful for monoesterification albeit in low yield that makes its use impractical for diesterification. A procedure reported by Zhao et al.[13] turned out to work efficiently. The method employs a catalytic amount of scandium triflate in combination with *N*,*N*′-diisopropylcarbodiimide and DMAP (method B). Very good yields of the tertiary diesters **5j**−**m** (78−81%) were obtained. Finally, the diphenyldithienyl thienopyrazines **6a**−**m** were prepared by a known procedure[14] where the benzils **5a**−**m** were condensed with [2,2′;5′,2″]terthiophene-3′,4′-diamine.[15] The polymers of **6b**−**d** and **6i**−**l** were also made. Activation of the monomers was done by a NBS bromination and was followed by a Stille coupling polymerization with 2,5-bis(trimethylstannyl)thiophene giving **8b**−**d** and **8i**−**l**.

Thermal Behavior. The relative stability of the dithienylthienopyrazines with thermocleavable benzoate esters substituted on the pyrazine ring, **6a**−**m**, was investigated by thermogravimetric analysis (TGA) and thermogravimetric analysis in conjunction with mass spectrometry of the carrier gas (TGA−MS) in the temperature range 50−500 °C (Table 1). The thermogravimetric data in table 1 are consistent with earlier pyrolysis studies of esters.[16] As expected elimination of an alkene from the tertiary diesters **6j**−**l** take place at lower temperatures than the secondary diesters **6b**−**i**. The primary diester **6a** eliminated with decomposition at a significantly higher temperature. The presence of an inductively (σ bond) electron withdrawing β substituent on the alcohol is known to slow down the rate of ester pyrolysis.[17] **6e** eliminate at 360 °C which is 35 °C higher than the elimination temperature of **6c** that bears a β alkyl substituent.

A double bond substituent at the β carbon can reduce the elimination temperature moderately as observed by comparing **6g** with **6b** and **6d**. **6h** eliminates hexatriene at around 300 °C which is approximately 25 °C lower compared to **6c**. We ascribe this to an activation of the adjacent C$_\beta$−H bond that assist the elimination. The double bond substituents apparently contribute to other reactions (weight losses) at the higher temperatures as **6g** and **6h** decompose at the elimination temperatures. Furthermore, we observed that **6e**, **6h**, and **6m** showed a slight weight

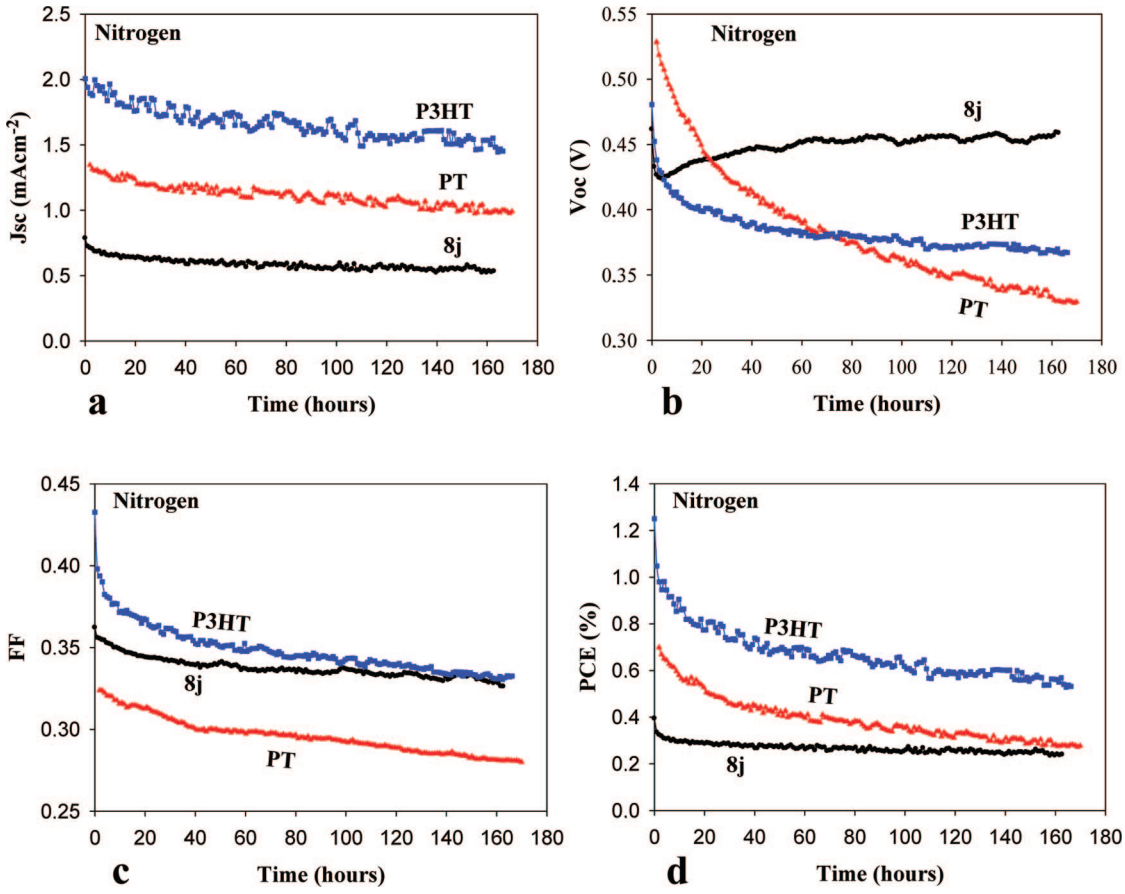

Figure 5. Comparison of the decay of the photovoltaic parameters for P3HT, PT, and **8j** polymers with a Glass/ITO/PEDOT:PSS/polymer:PCBM/Al device geometry in a nitrogen atmosphere (330 W m^{-2}, 30 °C, oxygen <2 ppm, water <2 ppm).

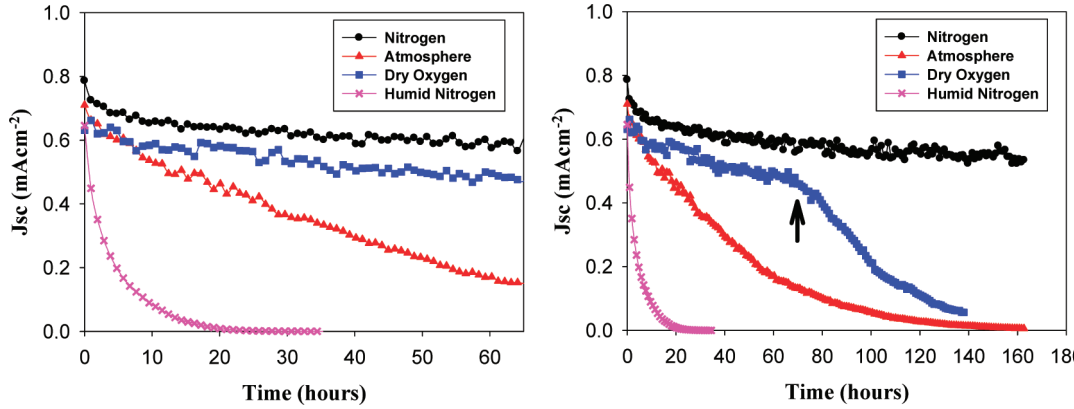

Figure 6. Decay of devices with configuration Glass/ITO/PEDOT:PSS/**8j**:PCBM/Al under conditions of: pure nitrogen atmosphere 99.999% (oxygen <2 ppm, humidity <2 ppm), dry oxygen atmosphere 99.5% (humidity <2 ppm), ambient atmosphere (20 ± 5% relative humidity), humid nitrogen 99.999% (oxygen <2 ppm, 95 ± 5% relative humidity). The temperature was 30 ± 2 °C and the incident light intensity was 330 W m^{-2} (left). The same experiment was repeated for a longer period of time while introducing ambient atmosphere after 70 h (see arrow) thus reducing the oxygen level by a factor of 5 and increasing the humidity by a factor of 10^5 whereupon rapid degradation sets in thereafter (right).

loss at low temperatures. We found no identifiable mass peaks corresponding to the solvent and also rule out the possibility for solvent loss as the samples were dried prior to analysis in a vacuum oven at 50 °C for 24 h. It is possible that these materials are subject to chemical reactions in the solid state (ie. a Cope reaction for **6h** and **6m** or elimination of methanol for **6e**). We currently have no explanation for these observations other then it being an elimination reaction or an electrocyclic reaction followed by an elimination reaction giving fragments that we did not observe in our mass spectra. **6i** has a 1-phenylethyl ester where the π bonded substituent contributes to the activation of the adjacent C_β−H. It has a simple TGA curve where the first inflection is responsible for the elimination of styrene (Figure 1). The phenyl substituent decrease the temperature for the first weight loss even further compared to **6g** and **6h.**

The tertiary diesters **6j**−**l** eliminate in the temperature range 197−246 °C. **6k** eliminates at a lower temperature compared to **6j** which may arise from the double bond activation as described above. **6l** eliminate 14 °C higher compared to **6j** and we conclude that a triple bond is not as activating as the double bond in this position (α carbon). The observed weight loss for the compounds **6g**, **6h**, **6i**, **6k**, and **6l** all show weight loss at the first inflection which is significantly lower than the calculated

value. Since all these fragments have multiple unsaturations after the elimination we ascribe this to polymerization reactions of these materials in the matrix of the material or to cross-linking. Analysis of the materials after the first weight loss by NMR was used to establish whether the ester could be used efficiently as a solubilizing group that can be removed quantitatively by a simple thermal treatment (Figure 2). NMR analysis after heating compound **6a**−**m** at the temperature of the first weight loss for 15 min. under argon showed that compounds **6a**, **6e**−**h**, **6m** could not be used for the preparation of the diacid. While the esters may eliminate liberating an alkene the materials also decompose at the given temperature. The ^{1}H NMR spectra of **6j** from before and after the pyrolysis clearly shows that the diester has been transformed into the diacid (Figure 2). Spectrum b in Figure 3 shows no aliphatic protons and the protons from the carboxylic acid appear at 13.08 ppm. From the TGA−MS data it was possible to track evolution of various small molecules and fragments as a function of the temperature. As expected the signals for the observed fragments peak in the same temperature range as the weight losses. The mass signals that we focused on were carbon dioxide and fragments for even and uneven alkenes. As shown earlier[4b] for tertiary esters of polythiophene several weight loss mechanisms may be observed and the advantage of studying the monomer was that the effects of the polymer matrix on the weight loss mechanisms were possibly eliminated.

The primary ester showed loss of both alkene and carbon dioxide starting at around 300 °C peaking at around 400 °C. For the secondary alkyl esters two loss mechanisms could be distinguished as elimination of the ester at the lower temperature (around 300 °C) and loss of carbon dioxide at a higher temperature (425 °C). The weight loss of the secondary alkyl esters corresponded well with the calculated loss while some decarboxylation was evident from a small mass peak of carbon dioxide during the first loss peak. The secondary esters with unsaturations, branching, fluorine and methoxy substituents showed more complex weight loss curves. It would seem that the only useful materials in this series are the simple secondary and tertiary esters. In terms of achieving a lower temperature for the thermocleavage this limits the choice to simple tertiary esters. The only secondary ester that works well is the ester with a phenyl group α to the alcohol and no other unsaturations. As discussed above the simplest secondary alcohol with an α-phenyl group gives styrene upon elimination and this gave an incomplete weight loss. While successfully achieving a lower temperature of elimination this alone does not grant usefulness. The elimination reaction also has to complete the weight loss and the polymer material that is the end product should be insoluble.

Polymers. The polymerization of the monomer materials was achieved through selective bromination of **6b**−**d** and **6i**−**l** using NBS to give **7b**−**d** and **7i**−**l**. These monomers were then polymerized by Stille cross coupling using bis(2,5-trimethylstannyl)thiophene. This gave the polymers **8b**−**d** and **8i**−**l** in good yield. The polymer materials had a low band gap as expected. A major requirement for processing into thin films is that the polymer materials are soluble in organic solvents. While the thermal behavior could be studied for all the polymers, not all of them had a good solubility. The molecular weights for the materials were in the 40000−70000 g mol^{-1} range and the polydispersity was around 2 as expected (see Supporting Information). The only polymers that were readily soluble, could be analyzed, processed into thin films and showed a useful thermal behavior were thus **8b**, **8c**, **8d**, and **8j**.

Only **8j** could be cleaved at an acceptably low temperature. The UV−vis spectrum of a film of **8j** spincoated from chlorobenzene is shown in figure 3. A film absorbance of 1 was easily reached with a very good film quality. The color of the film is olive green and the band gap of **8j** in the film was estimated from the crossing point of the tangent on the absorption edges[18] and was 950 nm or 1.3 eV. The observed band gap is as expected from earlier studies on the same polymer backbone[14] and similar polymers.[19] Upon thermocleavage of the film by heating it at 250 °C for 1 min a color change is observed whereby the film changes to a more brown color. The associated changes in the absorption spectrum are a less intense absorption and a smaller band gap with a band gap of 1010 nm or 1.2 eV. There may be several explanations for the lower absorption intensity.

First, the associated change in film thickness and dielectric constant may lead to changes in the reflection phenomena that also contribute to the intensities in the observed absorption spectrum for a solid film in a transmission geometry. Second, the intensity of absorption quite often decreases as the band gap is lowered. After the short thermal treatment the film maintained the optical quality and was completely insoluble in organic solvents.

Photovoltaic Performance. All of the polymer materials presented in Scheme 1 were intended for use in solar cell devices. Some of the polymer materials however were not very soluble and did not process well into films and the photovoltaic performance obtained for these were either not possible to establish or very poor. Consequently only **8b**, **8c**, **8d**, and **8j** were studied in solar cells. The devices were prepared in duplicate and were after spincoating of the active layer either processed directly into a solar cell by evaporation of the aluminum electrode or subjected to a thermal treatment at the temperature of thermocleavage immediately before evaporation of the aluminum electrode. The results obtained are shown in table 2.

A general observation was that the devices performed significantly worse after thermocleavage as indicated by a decrease in voltage and current. Some examples of IV-curves for uncleaved and cleaved devices are shown in figure 4 (see also Supporting Information). The best performing material was **8j**, which show a decreased performance upon thermocleavage, but maintained a significant performance. We chose to repeat the preparation of devices based on all polymers and obtained results in the ranges outlined in table 3.

It should be noted that polymer solar cells based on thermocleavable materials present additional complexity in terms of processing as compared to materials such as P3HT. In the case of P3HT heating of the device film leads to crystallization and changes in the morphology of the device film that significantly influences the device performance. In the case of thermocleavable materials these effects also take place, but in addition, the chemistry of the device film change and as the chemistry changes so do the processes relating to crystallization and changes in morphology. This has been observed in the case of P3MHOCT where the chemistry of the device film can be processed into three distinct forms starting from the same device film.[4b,20] This allowed for the preparation of devices with a PCE of up to 1.5%.[20]

This implies that not only the temperature of thermal annealing and the duration but also the speed of heating becomes influential. In the case of the polymers presented here the polymer esters (**8b**, **8c**, **8d**, or **8j**) are all chemically different materials. Heating them to the temperature of thermocleavage gives, in principle, the same product as polymer **9** (Scheme 2). The difference in device performance is thus not related to the molecule but rather how the final device film was obtained. Thus the same material can present different levels of performance depending on how it was processed. The chemistry of the sidechains may influence the morphology before thermocleav-

age, and if the process of thermocleavage is faster than the changes in morphology upon heating, this may also allow for the preparation of different final film morphologies. It has been shown that the morphology is stable in the final thermocleaved form when using a temperature of thermocleavage[7] below T_g and the kinetics of the film formation in such a case is important. A final issue is the completion of the thermocleavage in the final film. It is likely that thermocleavage under a given set of conditions lead only to a partially cleaved film that then present chemistry corresponding to both the uncleaved and cleaved material to varying degrees.[20] In the experiments performed here the films were completely cleaved and a detailed study of varying the degree of thermocleavage warrants further study.

In Figure 4, the performance of some of the devices are shown as IV-curves in the cleaved and uncleaved state. The drastic decrease of the performance for polymers **8b**, **8c** and **8d** is probably due to high cleaving temperature (310 °C) and long cleaving time (10 min), while thermocleavage of **8j** resulted in very little decrease of performance. In the case of earlier reported cleaving of P3MHOCT the performance dropped around 10-fold when cleaved to P3CT and then improved 15-fold when cleaved further to PT.[20]

Stability Studies. We chose to subject the best performing material **8j** to detailed stability studies. Polymer solar cells are inherently unstable under intense illumination and will degrade through a large number of coexisting paths. Some of the paths involve reactants such as water and oxygen from the atmosphere that will dominate the course of degradation if allowed to access the active layer during operation. Their efficient removal efficiently eliminates the associated degradation processes, and other slower processes become readily observable (ie. morphological changes, interlayer diffusion, reactions at interfaces, photochemistry). To get an overview of the stability of the **8j** in relation to other known polymers and as a function of atmospheric reactants we performed two studies. One comparative study in an inert atmosphere and a study where devices were subjected to different atmospheres during continuous (uninterrupted) illumination.

Figure 5 shows the degradation of devices prepared in the same manner employing respectively P3HT, PT, and **8j**. The performance of **8j** is inferior to both P3HT and PT while the photovoltaic parameters are much more stable in time. The P3HT device was annealed at 150 °C for 5 min after evaporation of the aluminum electrode. PT devices were prepared by heating P3MHOCT−PCBM films to 310 °C before evaporation of the aluminum electrode. The decay in the photovoltaic parameters were not affected significantly by the thermocleavage at 230 °C and the stability of **8j** is thus concluded to be very good without cleavage while there are processing advantages of thermocleaved **8j**. Cleaving **8j** at a higher temperature (310 °C) reduced the photovoltaic performance drastically and the decay of V_{oc} and FF was much faster.

When subjecting **8j** devices to four different atmospheres to establish the inherent stability in nitrogen and the effect of water and oxygen taken separately and finally in combination in the real atmosphere it was found that oxygen had little effect on the stability as shown in Figure 6. The interesting finding was that the presence of pure oxygen at high concentration (i.e., five times more than in the ambient atmosphere) does not seem to speed up degradation significantly and we would rate **8j** as stable toward oxygen under illumination. Humidity however was found to profoundly influence the stability leading to rapid degradation that is complete within less than 20 h whereas the absence of water leads to moderately stable operation.

Conclusion

In conclusion, the application of esters as solubilizing groups that allow for removal by a simple thermal treatment is limited to simple secondary and tertiary esters where the alcohol is saturated in order to ensure that the alkene that is eliminated is removed efficiently without undesired side reactions. The lowest temperatures of elimination were found to be achieved when employing tertiary esters as expected. In contrast to the systems where the ester reside on a thiophene ring we found that no decarboxylation takes place prior to decomposition, and it is thus not possible to access the native system without the carboxylic acid groups by a thermal treatment. We showed that a monomer relevant to low band gap polymer systems could be prepared with solubilizing groups that allow for removal by a thermal treatment of around 200−225 °C. We further prepared the polymer materials from the monomers and found that only the polymers with secondary and tertiary esters are useful and the solubility requirements make the choice of side chain functionality limited. The band gaps of the materials were in the 1.2−1.3 eV range and the operational stability was found to be very good compared to model materials such as P3HT and PT. In addition polymer solar cells in a glass/ITO/PEDOT:PSS/polymer:PCBM/Al were found to be very stable toward oxygen during operation. In pure oxygen the device decay was similar to inert conditions. This is in stark contrast to conjugated materials containing vinylene bonds that are very sensitive toward oxygen. The devices decayed rapidly in the presence of water (with and without oxygen present) and removal of water from this type of device gives devices with stability that exceeds hundreds of hours.

Acknowledgment. This work was supported by the Danish Strategic Research Council (DSF 2104-05-0052 and 2104-07-0022).

Supporting Information Available: Text giving general procedures and characterization data (including structural diagrams) and figures showing TGA and TGA−MS data, NMR spectra, IPCE curves for **8j**, and plots of the photovoltaic response as a function of incident light intensity. This material is available free of charge via the Internet at http://pubs.acs.org.

References and Notes

(1) (a) Günes, S.; Neugebauer, H.; Sariciftci, N. S. *Chem. Rev.* **2007**, *107*, 1324–1338. (b) Bundgaard, E.; Krebs, F. C. *Sol. Energy Mater. Sol. Cells* **2007**, *91*, 954–985. (c) Thompson, B. C.; Fréchet, J. M. J. *Angew. Chem. Int. Ed.* **2008**, *47*, 58–77.

(2) Hadipour, A.; de Boer, B.; Wildeman, J.; Kooistra, F. B.; Hummelen, J. C.; Turbiez, M. G. R.; Wienk, M. M.; Janssen, R. A. J.; Blom, P. W. M. *Adv. Funct. Mater.* **2006**, *16*, 1897–1903.

(3) (a) Barche, J.; Janietz, S.; Ahles, M.; Schmechel, R.; von Seggern, H. *Chem. Mater.* **2004**, *16*, 4286–4291. (b) Müller, C. D.; Falcou, A.; Reckefuss, N.; Rojahn, M.; Wiederhirn, V.; Rudati, P.; Frohne, H.; Nuyken, O.; Becker, H.; Meerholz, K. *Nature* **2003**, *421*, 829–833.

(4) (a) Liu, J. S.; Kadnikova, E. N.; Liu, Y. X.; McGehee, M. D.; Fréchet, J. M. J. *J. Am. Chem. Soc.* **2004**, *126*, 9486–9487. (b) Bjerring, M.; Nielsen, J. S.; Nielsen, N. C.; Krebs, F. C. *Macromolecules* **2007**, *40*, 6012–6013.

(5) (a) Nguyen, L. H.; Günes, S.; Neugebauer, H.; Sariciftci, N. S.; Banishoeib, F.; Henckens, A.; Cleij, T.; Lutsen, L.; Vanderzande, D. *Sol. Energy Mater. Sol. Cells* **2006**, *90*, 2815–2828. (b) Banishoeib, F.; Adriaensens, P.; Berson, S.; Guillerez, S.; Douheret, O.; Manca, J.; Fourier, S.; Cleij, T. J.; Lutsen, L.; Vanderzande, D. *Sol. Energy Mater. Sol. Cells* **2007**, *91*, 1026–1034. (c) Banishoeib, F.; Henckens, A.; Fourier, S.; Vanhooyland, G.; Breselge, M.; Manca, J.; Cleij, T. J.; Lutsen, L.; Vanderzande, D.; Nguyen, L. H.; Neugebauer, H.; Sariciftci, N. S. *Thin Solid Films* **2008**, *516*, 3978–3988.

(6) (a) Krebs, F. C.; Spanggaard, H. *Chem. Mater.* **2005**, *17*, 5235–5237. (b) Krebs, F. C.; Norrman, K. *Prog. Photovolt. Res. Appl.* **2007**, *15*, 697–712. (c) Bjerring, M.; Nielsen, J. S.; Siu, A.; Nielsen, N. C.; Krebs, F. C. *Sol. Energ. Mater. Sol. Cells* **2008**, *92*, 772–784. (d) Krebs, F. C. *Sol. Energ. Mater. Sol. Cells* **2008**, *92*, 715–726. (e) Jørgensen,

M.; Norrman, K.; Krebs, F. C. *Sol. Energ. Mater. Sol. Cells* **2008**, *92*, 686–714. (f) Gevorgyan, S. A.; Jørgensen, M.; Krebs, F. C. *Sol. Energ. Mater. Sol. Cells* **2008**, *92*, 736–745.
(7) Andreasen, J. W.; Jørgensen, M.; Krebs, F. C. *Macromolecules* **2007**, *40*, 7758–7762.
(8) Hagemann, O.; Bjerring, M.; Nielsen, N. C.; Krebs, F. C. *Sol. Energ. Mater. Sol. Cells* **2008**, *92*, 1327–1335.
(9) Floyd, M. B.; Du, M. T.; Fabio, P. F.; Jacob, L. A.; Johnson, B. D. *J. Org. Chem.* **1985**, *50*, 5022–5027.
(10) Takimoto, S.; Inanaga, J.; Katsuki, T.; Yamaguchi, M. *Bull. Chem. Soc. Jpn.* **1976**, *49*, 2335.
(11) Mukaiyama, T.; Matsueda, R.; Suzuki, M. *Tetrahedron Lett.* **1970**, 1901–1904.
(12) Mukaiyama, T.; Usui, M.; Shimada, E.; Saigo, K. *Chem. Lett.* **1975**, 1045–1048.
(13) Zhao, H.; Pendri, A.; Greenwald, R. B. *J. Org. Chem.* **1998**, *63*, 7559–7562.
(14) Petersen, M. H.; Hagemann, O.; Nielsen, K. T.; Jørgensen, M.; Krebs, F. C. *Sol. Energy Mater. Sol. Cells* **2007**, *91*, 996–1009.
(15) Mangeney, C.; Lacroix, J.-C.; Chane-Ching, K. I.; Jouini, M.; Villain, F.; Ammar, S.; Jouini, N.; Lacaze, P.-C. *Chem. Eur. J.* **2001**, *7*, 5029–5040.
(16) Houtman, J. P. W.; van Steenis, J.; Heartjes, P. M. *Recl. Trav. Chim.* **1946**, *65*, 781.
(17) Chuchani, G.; Martín, I.; Hernández, J. A.; Rotinov, A.; Fraile, G. *J. Phys. Chem.* **1980**, *84*, 944–948.
(18) Bundgaard, E.; Krebs, F. C. *Macromolecules* **2006**, *39*, 2823–2831.
(19) (a) Campos, L. M.; Toncheva, A.; Günes, S.; Sonmez, G.; Neugebauer, H.; Sariciftci, N. S.; Wudl, F. *Chem. Mater.* **2005**, *17*, 4031–4033. (b) Wienk, M. M.; Turbiez, M. G. R.; Struijk, M. P.; Fonrodona, M.; Janssen, R.A. J. *Appl. Phys. Lett.* **2006**, *88*, 153511.
(20) Gevorgyan, S. A.; Krebs, F. C. *Chem. Mater.* **2008**, *20*, 4386–4390.

MA801932A

CHEMISTRY OF MATERIALS
Article

A2.3

Chem. Mater. **2009,** *21,* 4669–4675 4669
DOI:10.1021/cm901937d

Substituted 2,1,3-Benzothiadiazole- And Thiophene-Based Polymers for Solar Cells − Introducing a New Thermocleavable Precursor

Martin Helgesen,*,† Suren A. Gevorgyan,† Frederik C. Krebs,† and René A. J. Janssen‡

†*Risø National Laboratory for Sustainable Energy, Technical University of Denmark, Frederiksborgvej 399, DK-4000 Roskilde, Denmark, and* ‡*Molecular Materials and Nanosystems, Departments of Applied Physics and Chemical Engineering & Chemistry, Eindhoven University of Technology, PO Box 513, 5600 MB Eindhoven, The Netherlands*

Received July 1, 2009. Revised Manuscript Received August 25, 2009

Alkoxysubstituted and unsubstituted 2,1,3-benzothiadiazoles were prepared and copolymerized with substituted and unsubstituted thiophenes using both Stille and Yamamoto cross-coupling reactions. One class of the materials bore thermally labile ester groups. The materials were all found to have a reduced band gap in the range of 1.69−1.75 eV and were explored in polymer photovoltaic devices as mixtures with the soluble fullerene PCBM. High open circuit voltages of up to 0.93 V and power conversion efficiencies (PCE) of up to 2.22% was observed for materials without the thermally labile groups. The thermocleavable materials have the advantage that they are insoluble after a thermal treatment, enabling a larger degree of processing freedom when preparing multilayer devices and they provide a better operational stability for the devices. So far the process of thermocleavage has led to poorer device performance than for the soluble precursor polymers; however, we found processing conditions that lead to a higher performance for the thermocleaved product, where open circuit voltages of up to 0.9 V could be obtained with power conversion efficiencies of up to 0.42%, representing a doubling as compared to the soluble precursor polymer.

Introduction

Encouraging progress has been made over the past few years in the field of photovoltaic solar cells using organic materials. Especially conjugated polymers are an attractive alternative to the traditional silicon-based solar cells because they are strong absorbers of visible light and can be deposited onto flexible substrates over large areas using wet-processing techniques such as spin-coating, printing, or roll-to-roll coating.[1−14] Compared to silicon-based solar cells, polymer photovoltaics are inferior when it comes to power conversion efficiency and stability. However, they offer low production cost, low thermal budget, and a very high speed of processing, which makes them competitive in certain applications. Many reviews and special issues on the topic of polymer solar cells have been published during the past 5 years[3,15−38] and the definitions are quite broad spanning all polymer

*Corresponding author.

(1) Dennler, G.; Lungenschmied, C.; Neugebauer, H.; Sariciftci, N. S.; Labouret, A. *J. Mater. Res.* **2005**, *20*(12), 3224–3233.
(2) Blankenburg, L.; Schultheis, K.; Schache, H.; Sensfuss, S.; Schrodner, M. *Sol. Energy Mater.* **2009**, *93*(4), 476–483.
(3) Krebs, F. C. *Sol. Energy Mater.* **2009**, *93*(4), 394–412.
(4) Krebs, F. C.; Jorgensen, M.; Norrman, K.; Hagemann, O.; Alstrup, J.; Nielsen, T. D.; Fyenbo, J.; Larsen, K.; Kristensen, J. *Sol. Energy Mater.* **2009**, *93*(4), 422–441.
(5) Krebs, F. C. *Sol. Energy Mater.* **2009**, *93*(4), 465–475.
(6) Krebs, F. C.; Alstrup, J.; Spanggaard, H.; Larsen, K.; Kold, E. *Sol. Energy Mater.* **2004**, *83*(2−3), 293–300.
(7) Krebs, F. C.; Spanggaard, H.; Kjaer, T.; Biancardo, M.; Alstrup, J. *Mater. Sci. Eng., B* **2007**, *138*(2), 106–111.
(8) Krebs, F. C. *Sol. Energy Mater.* **2009**, *93*, 1636–1641.
(9) Krebs, F. C. *Org. Electron.* **2009**, *10*, 761–768.
(10) Krebs, F. C.; Gevorgyan, S. A.; Alstrup, J. *J. Mater. Chem.* **2009**, *19*, 5442–5451.
(11) Lungenschmied, C.; Dennler, G.; Neugebauer, H.; Sariciftci, S. N.; Glatthaar, M.; Meyer, T.; Meyer, A. *Sol. Energy Mater.* **2007**, *91* (5), 379–384.
(12) Niggemann, M.; Zimmermann, B.; Haschke, J.; Glatthaar, M.; Gombert, A. *Thin Solid Films* **2008**, *516*(20), 7181–7187.
(13) Tipnis, R.; Bernkopf, J.; Jia, S.; Krieg, J.; Li, S.; Storch, M.; Laird, D. *Sol. Energy Mater.* **2009**, *93*(4), 442–446.
(14) Zimmermann, B.; Glatthaar, M.; Niggemann, M.; Riede, M. K.; Hinsch, A.; Gombert, A. *Sol. Energy Mater.* **2007**, *91*(5), 374–378.
(15) Brabec, C. J.; Hauch, J. A.; Schilinsky, P.; Waldauf, C. *Mrs Bulletin* **2005**, *30*(1), 50–52.
(16) Brabec, C. J.; Durrant, J. R. *MRS Bull.* **2008**, *33*(7), 670–675.
(17) Bundgaard, E.; Krebs, F. C. *Sol. Energy Mater.* **2007**, *91*(11), 954–985.
(18) Chen, L. M.; Hong, Z. R.; Li, G.; Yang, Y. *Adv. Mater.* **2009**, *21* (14−15), 1434–1449.
(19) Coakley, K. M.; McGehee, M. D. *Chem. Mater.* **2004**, *16*, 4533–4542.
(20) Coakley, K. M.; Liu, Y. X.; Goh, C.; McGehee, M. D. *Mrs Bulletin* **2005**, *30*, 37–40.
(21) Dennler, G.; Scharber, M. C.; Brabec, C. *J. Adv. Mater.* **2009**, *21* (13), 1323–1338.
(22) Günes, S.; Neugebauer, H.; Sariciftci, N. S. *Chem. Rev.* **2007**, *107* (4), 1324–1338.
(23) Günes, S.; Sariciftci, N. S. *Inorg. Chim. Acta* **2008**, *361*(3), 581–588.
(24) Hoppe, H.; Sariciftci, N. S. *J. Mater. Res.* **2004**, *19*(7), 1924–1945.
(25) Janssen, R. A. J.; Hummelen, J. C.; Saricifti, N. S. *Mrs Bulletin* **2005**, *30*(1), 33–36.
(26) Jørgensen, M.; Norrman, K.; Krebs, F. C. *Sol. Energy Mater.* **2008**, *92*(7), 686–714.
(27) Kippelen, B.; Bredas, J. L. *Energy Environ. Sci.* **2009**, *2*(3), 251–261.
(28) Krebs, F. C. Sol. Energy Mater. **2004**, *83* (2−3) 125−322.
(29) Krebs, F. C. *Refocus* **2005**, *6*(3), 38–39.
(30) Kroon, R.; Lenes, M.; Hummelen, J. C.; Blom, P. W. M.; de Boer, B. *Polym. Rev.* **2008**, *48*(3), 531–582.
(31) Lloyd, M. T.; Anthony, J. E.; Malliaras, G. G. *Mater. Today* **2007**, *10*, 34–41.
(32) Mayer, A. C.; Scully, S. R.; Hardin, B. E.; Rowell, M. W.; McGehee, M. D. *Mater. Today* **2007**, *10*(11), 28–33.

Published on Web 09/16/2009

solar cells, polymer-fullerene solar cells, small molecule, and hybrid solar cells. Polymer-fullerene solar cells based on composites of an electron-donating conjugated polymer and an electron-accepting fullerene have proven to be the most successful so far with power conversion efficiencies exceeding 6%.[39,40] In addition to the power conversion efficiency, there is, in the context of polymer solar cells, increasing focus on preparation of efficient materials with low optical band gaps and materials that give stable devices. Because the photon flux reaching the surface of the earth from the sun has a maximum of approximately 1.8 eV (700 nm) state-of-the-art materials for polymer solar cells like poly(3-hexylthiophene) (P3HT) is only able to harvest up to ~22% of the available solar photons.[17,30] Therefore, by decreasing the band gap of the active material it is possible to harvest a larger amount of the solar photons and thereby increase the power conversion efficiency. In terms of stability and operational lifetime polymer solar cells generally perform poorly. However, it has been demonstrated that polymer solar cells based on a blend of poly-3-(2-methylhexan-2-yl)-oxy-carbonylbithiophene (P3MHOCT) and PCBM can provide very stable behavior after thermal elimination of the solubilizing ester groups,[41−47] whereas the thermocleavage step was observed to lead to a decrease in performance.[41,42,47,48] It was found that the carboxy groups residing on the backbone after thermocleavage of the ester group could be removed by an even higher thermal treatment[49] and this could then give devices with a higher performance than the devices that had not been thermocleaved.[42] The softness provided by the solubilizing groups is related to the instability of polymer solar cells, and more rigid systems generally give devices with a better stability.[44,50,51] Furthermore, typical nonconjugated solubilizing groups reduce the density of chromophores in the polymer and do not contribute to light harvesting and charge transport. The motivation for preparing materials with thermocleavable side chains are multifold and can be summarized as the possibility to prepare materials with a higher density of chromophores leading to device films with a better operational stability and a higher level of permissible processing conditions due to the insolubility of thermocleaved films in all solvents. This has been explored with success in tandem solar cells based on thermocleavable materials.[52] It should, however, be stressed that these advantages should not come at the expense of the power conversion efficiency for the devices. So far, this has not been the case and there is an urgent need to uncover the processing conditions that are required to get high performance for devices based on thermocleavable materials.

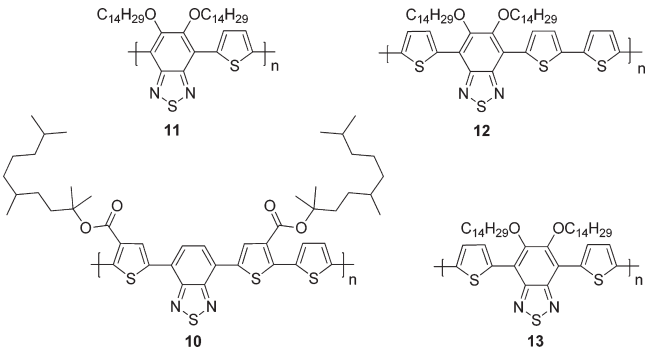

Figure 1. Low band gap polymers based on 2,1,3-benzothiadiazole and thiophene units.

Herein, we report the synthesis of four new low band gap polymers and their photovoltaic performance in blends with [6,6]-phenyl C_{61} butyric acid methyl ester (PCBM). Three of the polymers (**11**−**13**) are based on 2,1,3-benzothiadiazole, bearing solubilizing alkoxy side chains at the 5- and 6-position, alternating with thiophene units along the chain (Figure 1). The fourth polymer (**10**) is based on 2,1,3-benzothiadiazole alternating with three thiophene units along the chain. In addition, a branched alkyl chain is attached to the polymer backbone through a labile ester bond to the thiophene segment. When heated, this bond breaks, eliminating a volatile alkene and leaving the polymer component more rigid (Figure 2). The thermal treatment can be viewed as a way of performing an in situ chemical reaction, thereby allowing for the alteration of both physical and chemical properties such as solubility, hardness, hydrogen bonding, chromophore density, and ionicity after the active layer has been deposited.[42]

Experimental section

Synthetic procedures for synthesis of monomers and polymers according to Schemes 1−3 and their characterization data

(33) Rand, B. P.; Genoe, J.; Heremans, P.; Poortmans, J. *Prog. Photovoltaics* **2007**, *15*(8), 659–676.
(34) Shaheen, S. E.; Ginley, D. S.; Jabbour, G. E. *MRS Bull.* **2005**, *30*(1), 10–19.
(35) Shaheen, S. E.; Ginley, D. S.; Jabbour, G. E. MRS Bull. **2005**, *30* (Special Issue 1), 10−52.
(36) Spanggaard, H.; Krebs, F. C. *Sol. Energy Mater.* **2004**, *83*(2−3), 125–146.
(37) Thompson, B. C.; Frechet, J. M. J. *Angew. Chem., Int. Ed.* **2008**, *47* (1), 58–77.
(38) Winder, C.; Sariciftci, N. S. *J. Mater. Chem.* **2004**, *14*(7), 1077–1086.
(39) Kim, J. Y.; Lee, K.; Coates, N. E.; Moses, D.; Nguyen, T. Q.; Dante, M.; Heeger, A. J. *Science* **2007**, *317*(5835), 222–225.
(40) Park, S. H.; Roy, A.; Beaupre, S.; Cho, S.; Coates, N.; Moon, J. S.; Moses, D.; Leclerc, M.; Lee, K.; Heeger, A. J. *Nat. Photonics* **2009**, *3*(5), 297–302.
(41) Bjerring, M.; Nielsen, J. S.; Siu, A.; Nielsen, N. C.; Krebs, F. C. *Sol. Energy Mater.* **2008**, *92*(7), 772–784.
(42) Gevorgyan, S. A.; Krebs, F. C. *Chem. Mater.* **2008**, *20*(13), 4386–4390.
(43) Krebs, F. C.; Spanggaard, H. *Chem. Mater.* **2005**, *17*(21), 5235–5237.
(44) Krebs, F. C.; Norrman, K. *Prog. Photovoltaics* **2007**, *15*(8), 697–712.
(45) Krebs, F. C. *Sol. Energy Mater.* **2008**, *92*(7), 715–726.
(46) Krebs, F. C.; Thomann, Y.; Thomann, R.; Andreasen, J. W. *Nanotechnology* **2008**, *19*(42), 424013.
(47) Krebs, F. C. *Design and Applications of Polymer Solar Cells with Lifetimes Longer Than 10000 h*; Kafafi, Z. H., Lane, P. A., Eds.; SPIE: San Diego, CA, 2005; pp 59380Y−593811.
(48) Petersen, M. H.; Gevorgyan, S. A.; Krebs, F. C. *Macromolecules* **2008**, *41*(23), 8986–8994.
(49) Bjerring, M.; Nielsen, J. S.; Nielsen, N. C.; Krebs, F. C. *Macromolecules* **2007**, *40*(16), 6012–6013.
(50) Norrman, K.; Alstrup, J.; Jorgensen, M.; Lira-Cantu, M.; Larsen, N. B.; Krebs, F. C. *Proceedings of Organic Photovoltaics VII*; SPIE: Bellingham, WA, 2006; Vol. *6334*, pp U100−U111.
(51) Norrman, K.; Krebs, F. C. *Sol. Energy Mater.* **2006**, *90*(2), 213–227.
(52) Hagemann, O.; Bjerring, M.; Nielsen, N. C.; Krebs, F. C. *Sol. Energy Mater.* **2008**, *92*(11), 1327–1335.

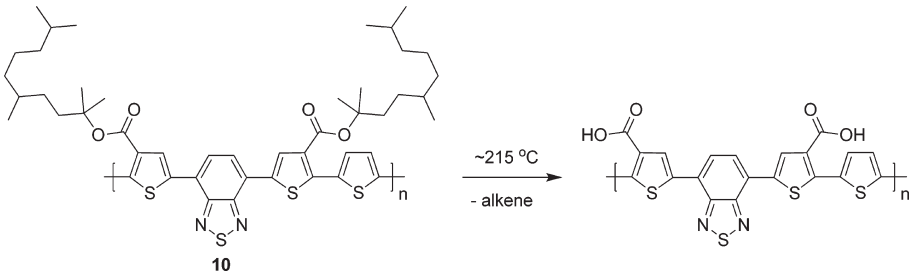

Figure 2. Thermocleavable ester groups attached to the polymer backbone of **10**. After a thermal treatment around 215 °C, the solubilizing groups are eliminated.

Scheme 1. Synthetic Steps Involved in the Preparation of the Monomers 4 and 6

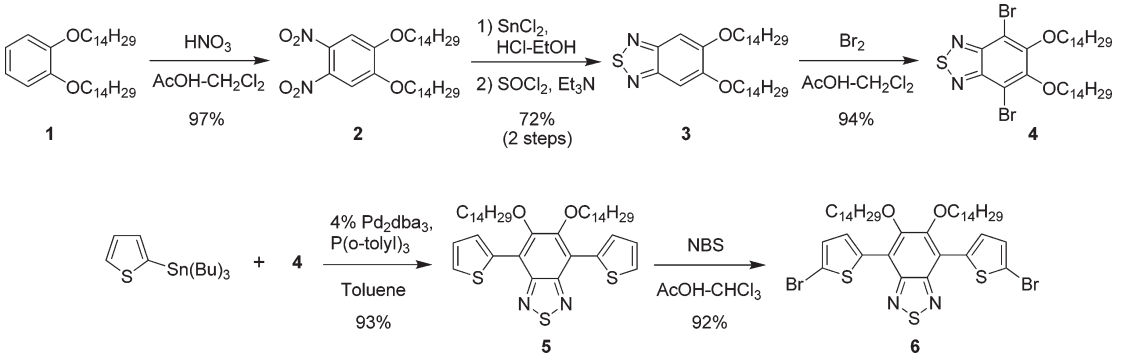

Scheme 2. Synthetic Steps Involved in the Preparation of the Thermocleavable Polymer 10; R = 2,5,9-Trimethyl-2-decanyl

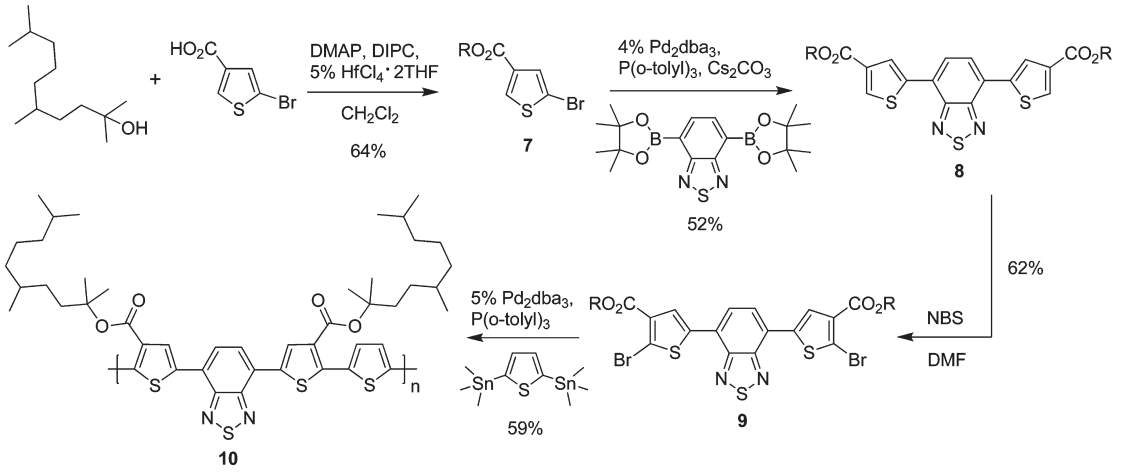

(including ^{1}H NMR and ^{13}C NMR) are described in detail in the Supporting Information, together with general experimental details.

Polymer Solar Cell Fabrication and Analysis. Photovoltaic devices were made by spin coating PEDOT:PSS (Clevios P, VP Al4083) onto precleaned, patterned indium tin oxide (ITO) substrates (14 Ω per square) (Naranjo Substrates). The active layer was deposited by spin coating a blend of the polymer and [60]PCBM dissolved in chlorobenzene (20−30 mg/mL). The counter electrode of LiF (1 nm) and aluminum (100 nm) was deposited by vacuum evaporation at $2-3 \times 10^{-7}$ mbar. The active area of the cells was 0.091−0.162 cm^2 and the active layer thickness was determined with a Dektak surface profiler. $J-V$ characteristics were measured under 100 mW/cm^2 white light from a tungsten-halogen lamp filtered by a Schott GG385 UV filter and a Hoya LB120 daylight filter, using a Keithley 2400 source meter. The spectral response (SR) was measured under operating conditions using bias light from a 532 nm solid state laser (Edmund Optics). Monochromatic light from a 50 W tungsten halogen lamp (Philips focusline) in combination with monochromator (Oriel, Cornerstone 130) was modulated with a mechanical chopper. The response was recorded as the voltage over a 50 Ω resistance, using a lock-in amplifier (Stanford research Systems SR830). A calibrated Si cell was used as reference. The device was kept behind a quartz window in a nitrogen filled container. Short circuit currents under AM1.5 conditions were obtained from the spectral response and convolution with the solar spectrum (J_{sc}(SR)). The value of J_{sc}(SR) was used with V_{oc} and FF from the 100 mW/cm^2 white light $J-V$ characteristics to estimate the power conversion efficiency η.

Results and Discussion

Approaches to Thermal Processing of Conjugated Polymers. Traditionally conjugated materials were prepared by a thermocleavable route whereby a soluble nonconjugated

Scheme 3. Synthetic Steps Involved in the Preparation of the Polymers 11, 12, and 13

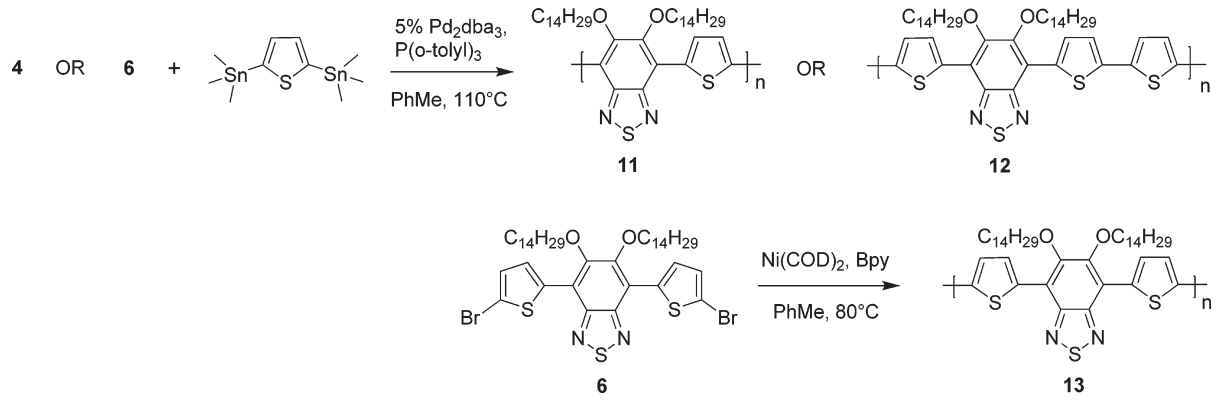

precursor was heated to provide the insoluble conjugated polymer film. Examples of this include the Wessling route to PPV[53−56] and the Durham routes to polyacetylene.[57−59] These were then replaced by efficient routes to soluble conjugated materials and it is only recently that requirements for better operational stability and processing freedom has spawned new research in this area. Generally, two approaches have been followed. The precursor route where the conjugation in the polymer film is formed upon thermocleavage after formation of a film based on the precursor polymer.[60−64] The other approach is the thermocleavable side chain route where the conjugated backbone is already present in the polymer film during formation but where the side chains are removed upon the thermal treatment to give the unsubstituted conjugated polymer backbone.[41−48,52,65−69] Common to both approaches is that the final film is insoluble and the chromophore density is high. The main difference is that the thermocleavable side chain film is functional as a photovoltaic device before being thermocleaved.

Synthesis. The synthetic steps involved in the preparation of the monomers **4** and **6** are outlined in Scheme 1. 1,2-Bis(tetradecyloxy)benzene (**1**) were prepared by a standard alkylation of catechol with 1-bromotetradecane in DMF at 100 °C.[70] Electrophilic aromatic nitration of **1** affords the substituted *o*-dinitrobenzene (**2**).[71] Reduction of the nitro groups with tin(II) chloride[72] gives the diamine as its hydrochloride salt which has to be used directly because of its unstable nature. Treatment of the diamine with thionyl chloride affords **3**, which is brominated with molecular bromine to give monomer **4** in excellent yield.[73] Stille coupling of **4** with 2-tributylstannylthiophene gives **5** as a yellow solid that is highly fluorescent in solution. Finally, NBS bromination of **5** gives monomer **6**.

The synthetic steps involved in the preparation of the thermocleavable polymer **10** are outlined in Scheme 2. A slightly modified procedure, reported in our earlier work[48] for the synthesis of tertiary esters, was used to prepare **7**. The esterification employs a catalytic amount of hafnium(IV) chloride tetrahydrofuran complex (1:2) in combination with *N,N′*-diisopropylcarbodiimide and DMAP. Suzuki cross-coupling of **7** with the boronic ester 4,7-bis(4,4,5,5-tetramethyl-1,3,2-dioxaborolan-2-yl)benzo-[*c*][1,2,5]thiadiazole affords **8** which is NBS brominated to give monomer **9**. Finally copolymerisation of **9** via Stille coupling with 2,5-bis(trimethylstannyl)thiophene affords the thermocleavable polymer **10** as a dark purple-brown solid.

Using the same conditions as for **9**, copolymerisation of **4** and **6** via Stille coupling with 2,5-bis(trimethylstannyl)-thiophene gives polymer **11** and **12** as dark purple solids (Scheme 3). Yamamoto coupling of **6**, using bis(1,5-cyclooctadiene)nickel(0) ($Ni(COD)_2$) and bipyridine (Bpy)

(53) Gagnon, D. R.; Capistran, J. D.; Karasz, F. E.; Lenz, R. W.; Antoun, S. *Polymer* **1987**, *28*(4), 567–573.
(54) Garay, R. O.; Mayer, B.; Karasz, F. E.; Lenz, R. W. *J. Polym. Sci., Part A: Polym. Chem.* **1995**, *33*(3), 525–531.
(55) Lenz, R. W.; Han, C. C.; Stengersmith, J.; Karasz, F. E. *J. Polym. Sci., Part A: Polym. Chem.* **1988**, *26*(12), 3241–3249.
(56) Wessling, R. A. *J. Polym. Sci., Polym. Symp.* **1985**, No. 72, 55–66.
(57) Bott, D. C.; Brown, C. S.; Chai, C. K.; Walker, N. S.; Feast, W. J.; Foot, P. J. S.; Calvert, P. D.; Billingham, N. C.; Friend, R. H. *Synth. Met.* **1986**, *14*(4), 245–269.
(58) Feast, W. J.; Winter, J. N. *J. Chem. Soc., Chem. Commun.* **1985**, No. 4, 202–203.
(59) Furlani, A.; Napoletano, C.; Russo, M. V.; Feast, W. J. *Polym. Bull.* **1986**, *16*(4), 311–317.
(60) Banishoeib, F.; Adriaensens, P.; Berson, S.; Guillerez, S.; Douheret, O.; Manca, J.; Fourier, S.; Cleij, T. J.; Lutsen, L.; Vanderzande, D. *Sol. Energy Mater.* **2007**, *91*(11), 1026–1034.
(61) Banishoeib, F.; Henckens, A.; Fourier, S.; Vanhooyland, G.; Breselge, M.; Manca, J.; Cleij, T. J.; Lutsen, L.; Vanderzande, D.; Nguyen, L. H.; Neugebauer, H.; Sariciftci, N. S. *Thin Solid Films* **2008**, *516*(12), 3978–3988.
(62) Girotto, C.; Cheyns, D.; Aernouts, T.; Banishoeib, F.; Lutsen, L.; Cleij, T. J.; Vanderzande, D.; Genoe, J.; Poortman, J.; Heremans, P. *Org, Electron,* **2008**, *9*(5), 740–746.
(63) Henckens, A.; Colladet, K.; Fourier, S.; Cleij, T. J.; Lutsen, L.; Gelan, J.; Vanderzande, D. *Macromolecules* **2005**, *38*(1), 19–26.
(64) Nguyen, L. H.; Gunes, S.; Neugebauer, H.; Sariciftci, N. S.; Banishoeib, F.; Henckens, A.; Cleij, T.; Lutsen, L.; Vanderzande, D. *Sol. Energy Mater.* **2006**, *90*(17), 2815–2828.
(65) Gordon, T. J.; Yu, J. F.; Yang, C.; Holdcroft, S. *Chem. Mater.* **2007**, *19*(9), 2155–2161.
(66) Gordon, T. J.; Vamvounis, G.; Holdcroft, S. *Adv. Mater.* **2008**, *20* (13), 2486–2490.
(67) Han, X.; Chen, X. W.; Holdcroft, S. *Adv. Mater.* **2007**, *19*(13), 1697–1702.
(68) Liu, J. S.; Kadnikova, E. N.; Liu, Y. X.; McGehee, M. D.; Frechet, J. M. J. *J. Am. Chem. Soc.* **2004**, *126*(31), 9486–9487.
(69) Yu, J. F.; Holdcroft, S. *Macromolecules* **2000**, *33*(14), 5073–5079.
(70) Zhang, D.; Tessier, C. A.; Youngs, W. J. *Chem. Mater.* **1999**, *11* (11), 3050–3057.
(71) Sessler, J. L.; Callaway, W. B.; Dudek, S. P.; Date, R. W.; Bruce, D. W. *Inorg. Chem.* **2004**, *43*(21), 6650–6653.
(72) Far, A. R.; Shivanyuk, A.; Rebek, J. *J. Am. Chem. Soc.* **2002**, *124* (12), 2854–2855.
(73) Bouffard, J.; Swager, T. M. *Macromolecules* **2008**, *41*(15), 5559–5562.

Table 1. GPC and Spectroscopic Data for Polymers 10−13

	solution					film		
polymer	M_w (g/mol)	PDI	λ_{max} (nm)	λ_{onset} (nm)	E_g (eV)	λ_{max} (nm)	λ_{onset} (nm)	E_g (eV)
10	173000	2.6	525	633	1.96	593,[a] 570[b]	732	1.69
11	16600	1.7	563	643	1.93	654	711	1.74
12	26000	2.9	570	687	1.80	644	707	1.75
13	7100	1.7	543	639	1.94	592	715	1.73

[a] 25 °C. [b] Heated at 250 °C for 1 min.

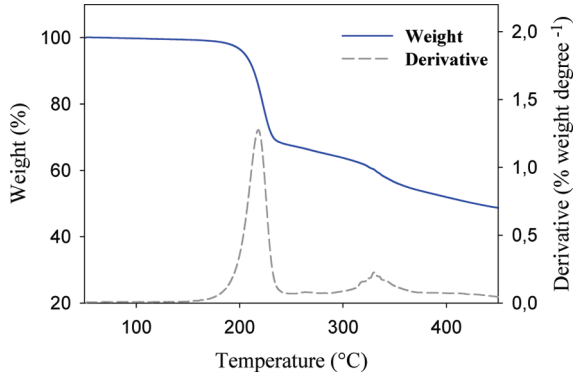

Figure 3. Thermogravimetric data for **10** in the temperature range 50−500 °C. The theoretical weight loss for the elimination process around 215 °C is 44%, whereas the observed value is ~31%. A second minor weight loss (~8%) is observed around 330 °C. The data were recorded at 10 °C min^{-1} under an argon atmosphere.

gives polymer **13** in 20% yield (Scheme 3) with a molecular weight (M_w) of 7100 g/mol and a polydispersity (PDI) of 1.7. The low yield was caused by the fact that a large portion of the polymer formed was insoluble and could not be isolated by Soxhlet extraction. For the same reason, a low yield of **12** was isolated (28%) but with a higher molecular weight (M_w = 26 000 g/mol, PDI = 2.9). On the contrary Polymer **10** and **11** were isolated in good yields and are very soluble in organic solvents such as chloroform and toluene at room temperature. The large variation in molecular weight between **10** and **11** could be explained by the difference in coupling groups, bromothiophene-stannylthiophene versus bromobenzothiadiazole-stannylthiophene.

Thermal Behavior. The sample holders were carefully weighed and the samples introduced. Thermogravimetric analysis (TGA) was then carried out using heating rate of 10 °C min^{-1}. TGA of **10** in the temperature range 50−500 °C indicates that the ester bond starts to break around 200 °C (Figure 3). The second loss peak at ~330 °C corresponds to loss of CO_2.[48,49]

Optical Properties. The absorption spectra for polymer **10**−**13** in chloroform solution are shown in Figure 4a and Figure 5. The optical band gaps, defined by the onset of absorption, are rather similar ranging from 1.8 to 1.96 eV (Table 1). **12** exhibits a lower optical band gap in solution due to partial aggregation of the polymer in solution. The difference in absorption maxima (λ_{max}) is relatively small but **10** is blue-shifted compared to polymers **11**−**13** (Table 1), indicating a more twisted backbone because of the branched ester side chains. The film absorption spectra for polymers **10**−**13** are shown in Figures 4b and

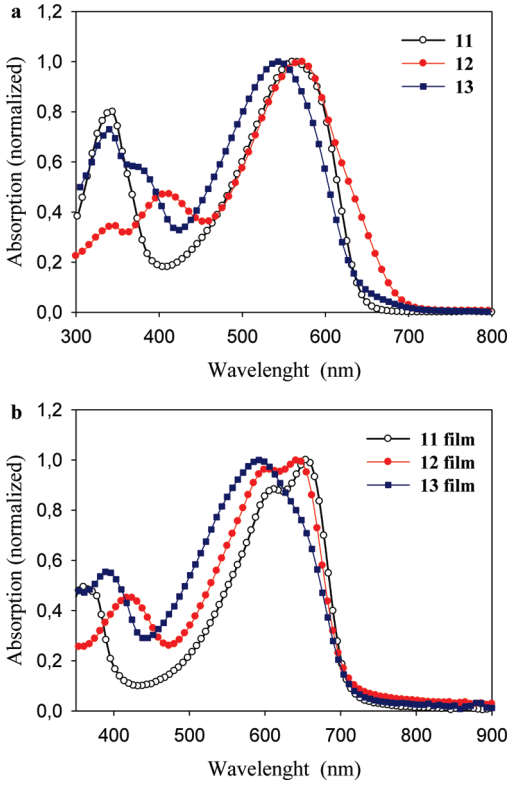

Figure 4. UV−vis absorption spectra of polymers **11**−**13** in (a) chloroform solution and (b) thin film.

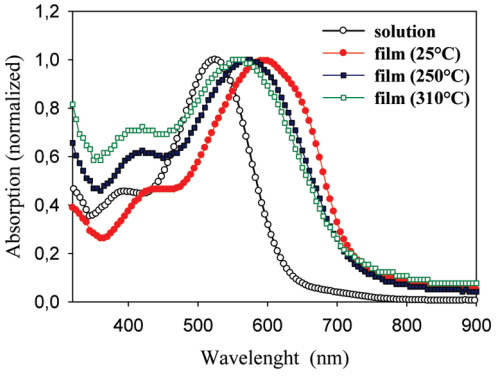

Figure 5. UV−vis absorption spectra of **10** in chloroform solution and in thin film before and after thermocleavage.

5. Again, the optical band gaps are very similar ranging from 1.69 to 1.75 eV (Table 1). The polymers have absorption maxima ranging from 525 to 570 nm in chloroform, and these are red-shifted further to 592−654 nm when in a solid film (Table 1), indicating significant interchain association in the solid state. In addition polymers **11** and **12** show vibronic fine structure

Table 2. Photovoltaic Performance of Devices Based on Blends of Polymer and PCBM

polymer	thermal treatment[a] (°C)	layer thickness (nm)	V_{oc} (V)	J_{sc}(SR) (mA/cm^2)	FF	η (%)
10		92	0.75	1.07[b]	0.26	0.21
10	200	92	0.90	0.72[b]	0.37	0.24
10	285	78	0.90	1.36	0.34	0.42
11		63	0.93	5.18	0.46	2.22
12		80	0.61	6.21	0.47	1.78
13		65	0.76	2.56	0.32	0.62

[a] Heated for 20−30 s. [b] Unestimated.

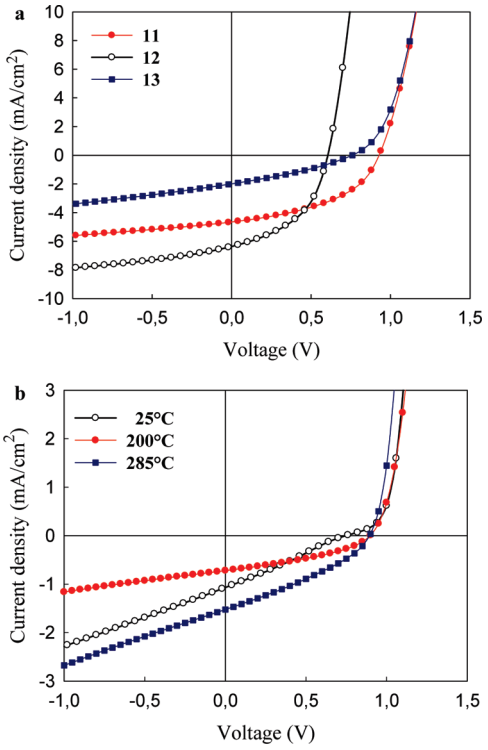

Figure 6. (a) $J-V$ characteristics of the **11**:PCBM, **12**:PCBM and **13**:PCBM solar cells measured under 100 mW/cm^2 white light; (b) $J-V$ characteristics of solar cells based on **10** and PCBM measured under 100 mW/cm^2 white light before and after a thermal treatment.

at 625 nm in the solid state. A weak vibronic transition may also account for the observed shoulder of **13** (Figure 4b). With regard to the thermocleavable polymer **10**, a blue shift of the absorption maxima is observed when the film is heated at 250 °C for 1 min (Figure 5), but no clear color change is observed. Only a minor blue shift in the absorption maxima is observed when the film is heated at 310 °C for 1 min compared to heating at 250 °C. After the thermal treatment, the film was completely insoluble.

Photovoltaic Performance. Bulk heterojunction solar cells were fabricated on an indium tin oxide (ITO) covered glass substrate, using conventional device architecture. A thin layer of poly(3,4-ethylenedioxythiophene)−poly-(styrenesulfonate) (PEDOT-PSS) was spin coated on top of the ITO coating followed by spin coating of the active layer. The active layer contained a blend of the respective polymer and [60]PCBM. After spin coating of the active layer the devices were either processed directly into a solar cell by evaporation of LiF (1 nm) and aluminum (100 nm) as back electrode or subjected to a

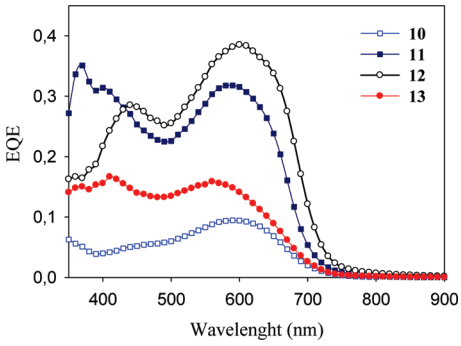

Figure 7. EQE spectra of polymer:PCBM solar cells. **10** were thermocleaved at 285 °C.

thermal treatment at the temperature of thermocleavage immediately before evaporation of the back electrode. The most efficient devices comprised a polymer/PCBM ratio of 1:2 spin-coated from chlorobenzene with a polymer concentration of 7.5 mg/mL. The optimal layer thickness was around 60−80 nm.

The obtained current−voltage curves are presented in figure 6 which shows the current−voltage characteristics of the **10**:PCBM, **11**:PCBM, **12**:PCBM and **13**:PCBM solar cells measured under 100 mW/cm^2 white light. The devices based on **11**, with only one thiophene unit alternating with benzothiadiazole, and PCBM showed power conversion efficiencies of up to 2.22% (Table 2). The devices had high open-circuit voltages (V_{oc}) of 0.93 V, moderate fill factors (FF) of 0.46 and current densities (J_{sc}) of 5.18 mA/cm^2. The external quantum efficiency (EQE) for **11**:PCBM is higher than 23% in the wavelength range between 350 and 650 nm, and the maximum was found to be 35% around 370 nm where PCBM also absorbs (Figure 7). Polymer **12**:PCBM gives an EQE higher than 22% in the range between 400 and 680 nm with a maximum of 39% at around 600 nm. Compared to **11**:PCBM, the EQE is enhanced by up to 10% in the range 450−720 nm, which gives a current density of 6.21 mA/cm^2. The devices based on **12**:PCBM performed slightly poorer due to a lower V_{oc} of typically 0.61 V, which resulted in power conversion efficiencies of up to 1.78%. Solar cells based on polymer **13**:PCBM gave significantly lower EQE with quantum efficiencies around 10−15% in the range of 350−650 nm, giving current densities of 2.56 mA/cm^2. Together with a typical V_{oc} of 0.76 V and low fill factors of 0.32, power conversion efficiencies of up to 0.62% were obtained. The lower performance of **13** compared to **11** and **12** could be due to the different polymerization procedure where excess of

nickel(0) was used instead of a catalytic amount of palladium employed in the Stille coupling. The devices based on the thermocleavable polymer **10** and PCBM showed the lowest power conversion efficiencies of up to 0.42% (Table 2). Without thermal treatment of **10**:PCBM devices a typical V_{oc} of 0.75 V was obtained. Upon heating the device to 200 °C the V_{oc} increases to 0.90 V and resides there when annealing at 285 °C. The FF increased from 0.26 to 0.37 after thermal treatment at 200 °C and then drops a bit upon heating the device at 285 °C. The current density first drops after thermal treatment and then increases again when heating at 285 °C. The EQE of **10**:PCBM (cleaved at 285 °C) is relatively low with quantum efficiencies of about 5−10% in the range 350−670 nm (figure 7) giving it an estimated current density of 1.36 mA/cm^2. A general observation was that the devices based on **10**:PCBM performed better after thermocleavage due to an increase in mainly the current and fill factor. $J-V$ curves for uncleaved and cleaved **10**:PCBM devices are shown in figure 6b. Despite the lower efficiency of polymer **10** compared to the polymers **11**-**13** the thermocleavable polymer **10** does show promising results with increased performance after thermocleavage. In the majority of cases where thermocleavable materials have been employed in polymer solar cells, a drop in performance has been observed when thermocleaving the polymer and only one previous case has demonstrated an advantage of thermocleavage in terms of performance.[42] The lower performance of polymer **10** compared to the polymers **11**−**13** can be an effect of the more electron-attracting ester groups situated on thiophene (**10**) compared to the electron-donating alkoxy groups on benzothiadiazole (**11**−**13**).

Conclusion

In conclusion, four new low band gap polymers have been synthesized. They are based on 2,1,3-benzothiadiazole alternating with thiophene units along the chain, bearing solubilizing chains on either benzothiadiazole (**11**−**13**) or thiophene (**10**). The solubilizing chain on **10** is attached to the polymer backbone through a labile ester bond which is thermocleavable around 215 °C. When heated, this bond breaks, eliminating a volatile alkene and leaving the polymer component more rigid. The four polymers optical properties and photovoltaic performance in blends with PCBM have been investigated. In chloroform solution, the polymers had very similar optical band gaps ranging from 1.8 to 1.96 eV. The optical band gaps are lowered to 1.69−1.75 eV in thin film (Table 1), indicating significant interchain association in the solid state. Furthermore polymer **11** and **12** showed vibronic fine structure centered at 625 nm in the solid state. The best performing polymer in a bulk heterojunction solar cell was **11** with J_{sc} = 5.18 mA/cm^2, V_{oc} = 0.93 V, FF = 0.46, and η = 2.22%. Devices based on **10**:PCBM performed better after thermocleavage because of an increase in mainly current and fill factor giving power conversion efficiencies up to 0.42%.

Acknowledgment. This work was supported by the Danish Strategic Research Council (DSF 2104-05-0052 and 2104-07-0022).

Supporting Information Available: General procedures and characterization data including NMR spectra; experimental procedures for the synthesis of the monomers and polymers according to Schemes 1, 2, and 3. This material is available free of charge via the Internet at http://pubs.acs.org.

Advanced materials and processes for polymer solar cell devices

Martin Helgesen, Roar Søndergaard and Frederik C. Krebs*

Received 3rd July 2009, Accepted 22nd August 2009
First published as an Advance Article on the web 14th October 2009
DOI: 10.1039/b913168j

The rapidly expanding field of polymer and organic solar cells is reviewed in the context of materials, processes and devices that significantly deviate from the standard approach which involves rigid glass substrates, indium-tin-oxide electrodes, spincoated layers of conjugated polymer/fullerene mixtures and evaporated metal electrodes in a flat multilayer geometry. It is likely that significant advances can be found by pursuing many of these novel ideas further and the purpose of this review is to highlight these reports and hopefully spark new interest in materials and methods that may be performing less than the current state-of-the-art in their present form but that may have the potential to outperform these pending a larger investment in effort.

Introduction

Encouraging progress has been made over the last few years in the field of photovoltaics using organic materials. Conventional solar cells are built from inorganic materials such as silicon. While the efficiency of such conventional solar cells is high, very expensive materials and energy consuming processing techniques are required. The main reason for the extensive interest in organic semiconducting materials is their potential for the realization of a low cost, easily processed and flexible renewable energy source. Conjugated polymers are an especially attractive alternative to the traditional silicon photovoltaics because they are strong absorbers of visible light and can be deposited onto flexible substrates over large areas using wet-processing techniques such as roll-to-roll coating or printing. Many reviews,[1–26] special issues,[27–33] and books[34–38] on the topic of polymer solar cells have been published during the past 5 years and the definitions are quite broad spanning all polymer solar cells, polymer–fullerene solar cells, small molecule and hybrid solar cells. Polymer–fullerene solar cells based on composites of an electron-donating conjugated polymer and an electron-accepting fullerene has proven to be the most successful of them so far and is advancing rapidly towards commercial viability. Although the performance of polymer solar cells has increased steadily with power conversion efficiencies (PCEs) exceeding 6%, further improvements in efficiency are required for large scale commercialization. Aside from the power conversion efficiency, processing and stability are two other important aspects that have to be addressed with equal intensity for the success of polymer and organic solar cells. To combine all three parameters into a useful technology further research in device science and new materials is needed.

Risø National Laboratory for Sustainable Energy, Technical University of Denmark, Frederiksborgvej 399, DK-4000 Roskilde, Denmark. E-mail: frkr@risoe.dtu.dk

Aim of this review

We seek to identify novel ideas in the form of materials, methods and device concepts that can potentially house the possibility to go beyond the current state-of-the-art. Armed with the identity of the potential candidates we further suggest how research might be directed towards real progress in terms of better

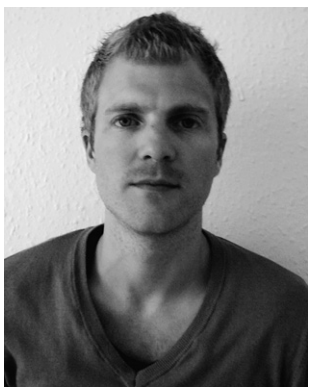

Martin Helgesen

Martin Helgesen received his Master of Science in Chemistry from The University of Copenhagen in 2006. The same year he began his PhD under the mentorship of Frederik Christian Krebs at Risø National Laboratory for Sustainable Energy, Technical University of Denmark. His research interests are in developing thermocleavable low band gap polymers and their thin films for organic photovoltaics.

Roar Søndergaard

Roar Søndergaard received his M.Sc. in 2005 from the Department of Chemistry at the University of Copenhagen. After working as a research assistant first at The University of Copenhagen and later at Risø DTU National Laboratory for Sustainable Energy he is currently pursuing his PhD at Risø DTU. His research interests include synthesis of conjugated polymers and synthesis of polymers that allow for different processing methods when preparing organic photovoltaics.

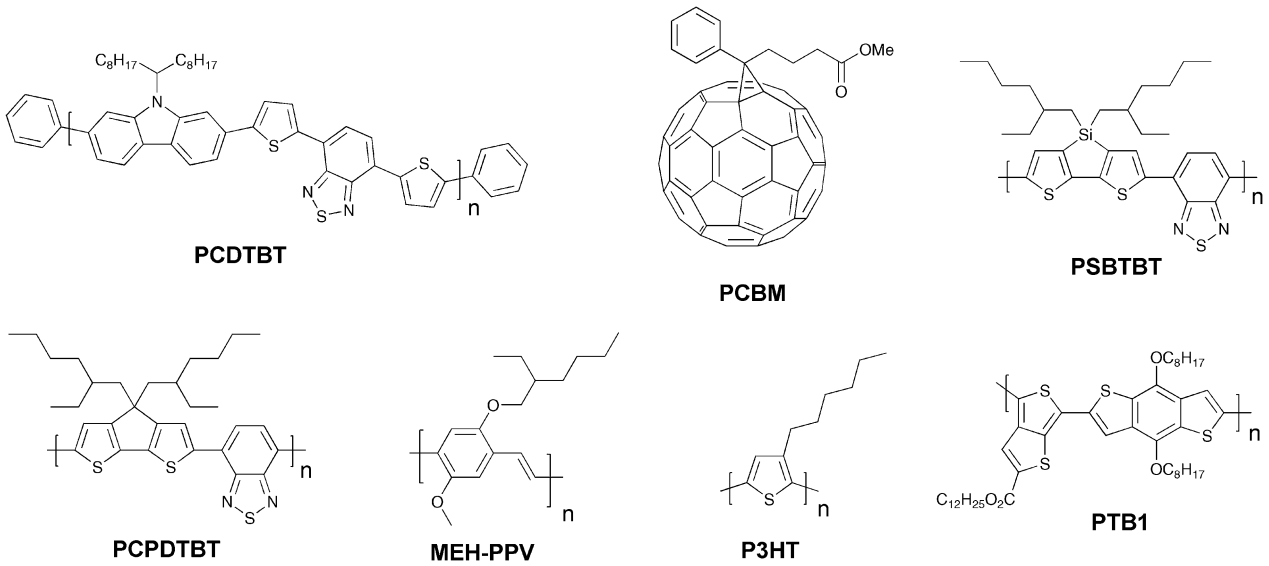

Fig. 1 Donor and acceptor materials used in polymer solar cells.

performance, higher operational stability, facile processing and easier, faster and lower cost production.

Materials

State-of-the-art

Since the first report of photoinduced charge transfer from a conjugated polymer to a buckminsterfullerene (C_{60}) in 1992 by Sariciftci *et al.*,[39] the field of polymer–fullerene solar cells has been through a dynamic development. In 1995 Yu *et al.* demonstrated a successful method to dissociate excitons and produce free charge carriers in organic semiconductors.[40] For the photoactive layer the authors used a blend of 2-methoxy-5-(2-ethylhexyloxy)-polyphenylenevinylene (MEH-PPV) as the electron donor and the soluble fullerene derivative [6,6]-phenyl C_{61} butyric acid methyl ester (PCBM) as the electron acceptor (Fig. 1).

The solar cell based on a MEH-PPV:PCBM composite or a so called bulk heterojunction (BHJ) showed an estimated efficiency of nearly 1% which was a major breakthrough for organic photovoltaics. When organic semiconductors absorb sunlight they mainly create excitons (electron–hole pairs) that are bound at room temperature. The exciton has to reach the donor–acceptor interface within its lifetime to transfer a free electron to the acceptor material and create a photovoltaic effect. Since the exciton diffusion range is limited, typically ~3–10 nm in most organic semiconductors,[41–43] which is much smaller than the necessary film thickness for effective optical absorption (50–250 nm), the key to an efficient solar cell requires that the excitons are generated in a nanoscale interpenetrating bicontinous network of donor and acceptor materials within the entire

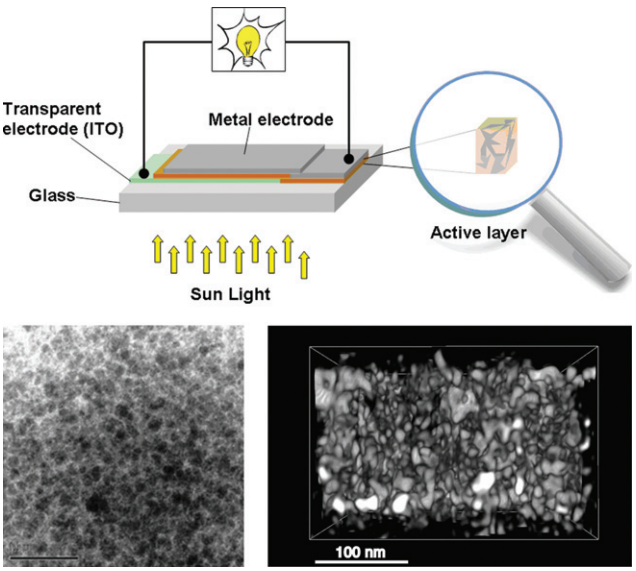

Fig. 2 A schematic illustration of a bulk heterojunction device showing electrical contacts (**top**) and a TEM image of a phase separated blend (**bottom left**. Reprinted with permission from ref. 44. © 2007 John Wiley & Sons, Ltd.) and a reconstructed tomographic 3D-image (**bottom right.** Reprinted with permission from ref. 45. © 2009 American Chemical Society).

Frederik C. Krebs

Frederik Christian Krebs received his PhD from the Technical University of Denmark in year 2000 and has since then worked in the field of polymer solar cells at Risø National Laboratory for Sustainable Energy. The areas of research include new materials with low band gap and novel processing capability, large area processing and manufacture of polymer solar cells, stability and lifetime testing, degradation mechanism studies, outside testing and demonstration.

photoactive layer. A schematic illustration of a bulk heterojunction is shown in Fig. 2.

From a materials point of view the state-of-the-art in the field of organic photovoltaics is currently represented by bulk heterojunction solar cells based on poly(3-hexylthiophene) (P3HT) and the fullerenes [60]PCBM (Fig. 1) and [70]PCBM where efficiencies in the 4–5% range have been reported.[46–50] It should be noted that the reproducibility and average efficiencies are significantly lower than these "hero" devices which is caused by the sensitivity to the fabrication process. In addition the field has seen some inconsistent reports of unrealistically high efficiencies[51–54] and this has led to the introduction of editorial procedures to avoid and/or eliminate fraud reports.[54] To improve efficiencies further towards 10% new materials are needed because the P3HT:PCBM system is approaching optimal device performance. The main disadvantage of P3HT is the poor matching of its absorption spectrum with the solar emission spectrum. The band gap of P3HT is around 1.9 eV, limiting the absorbance to wavelengths below 650 nm. Since the photon flux reaching the surface of the earth from the sun has a maximum of approximately 1.8 eV (700 nm) P3HT is only able to harvest up to 22.4% of the available solar photons.[6,20,54] Therefore, by decreasing the band gap of the active material it is possible to harvest a larger amount of the solar photons and thereby increase the power conversion efficiency. One of the most common techniques used to synthesise low band gap polymers is the donor–acceptor approach where alternating electron-rich and electron-poor units are incorporated in the polymer backbone. This causes a partial charge separation along the polymer backbone which generally gives the polymer a lower band gap.[55] New low band gap polymer:PCBM composites have already shown device efficiencies close to and even exceeding that of P3HT:PCBM with plenty of room for improvement.[56–58] One of the most efficient low band gap polymers to date is poly[2,6-(4,4-bis-(2-ethylhexyl)-4*H*-cyclopenta[2,1-b;3,4-b′]-dithiophene)-*alt*-4,7-(2,1,3-benzothiadiazole)] (PCPDTBT) (Fig. 1) which is based on a benzothiadiazole unit (acceptor) and a 4,4-bis(2-ethylhexyl)-4*H*-cyclopenta[2,1-b;3,4-b′]dithiophene unit (donor) that gives it an optical band gap around 1.46 eV. Zhu *et al.* have reported power conversion efficiencies up to 3.5% for bulk heterojunction solar cells based on PCPDTBT and [70]PCBM with a maximum EQE of 38% around 700 nm and over 25% in the wavelength range between 400 and 800 nm.[59] Moreover it was demonstrated that by incorporating a few volume per cent of alkanedithiols in the solution used to process the films of PCPDTBT and [70]PCBM, the power-conversion efficiency could be increased to 5.5% through altering the bulk heterojunction morphology.[58] This is one of the highest reported efficiencies for a low band gap polymer to date and there is still room for improvement according to the electrooptical properties of the polymer.[60–62] Recently a power conversion efficiency of 6.1% was reported for a bulk heterojunction solar cell based on a blend of the polymer poly[*N*-9″-hepta-decanyl-2,7-carbazole-*alt*-5,5-(4′,7′-di-2-thienyl-2′,1′,3′-benzothiadiazole)] (PCDTBT) and [70]PCBM.[63] The PCDTBT:[70]PCBM solar cells demonstrate the best performance of any single junction polymer solar cell studied to date. PCDTBT (Fig. 1) is based on a 4,7-dithienyl-benzothiadiazole unit and a soluble carbazole unit that gives it an optical band gap around 1.88 eV.

Polymer–polymer solar cells for potentially higher performance

It is remarkable how little effort that has been put into making novel materials that deliberately solves the problems that limit the performance, stability and processing of the existing materials into devices. From this point of view the field has been highly successful and have managed to optimize the few known materials to their best level of performance by investing most of the effort into device optimisation using mainly physical techniques. It is noteworthy that the state-of-the-art solar cell has not evolved much since 1995 from a materials point of view and still comprise a polymer such as P3HT and a fullerene such as PCBM. However, it should be mentioned that significant progress has been made in developing novel materials, of both donor and fullerene acceptors, with optimal energy levels to improve the PCE.[57,64–66]

Photovoltaic devices based on a blend of two conjugated polymers as the photoactive layer was first reported back in the 1990s,[67,68] and as with polymer–fullerene solar cells, polymer–polymer solar cells are also based on a donor–acceptor pair. The first realizations of polymer–polymer solar cells were prepared from blends of MEH-PPV and poly(2,5,2′,5′-tetrahexyloxy-7,8′-dicyano-di-*p*-phenylenevinylene) (CN-PPV) (Fig. 3). MEH-PPV

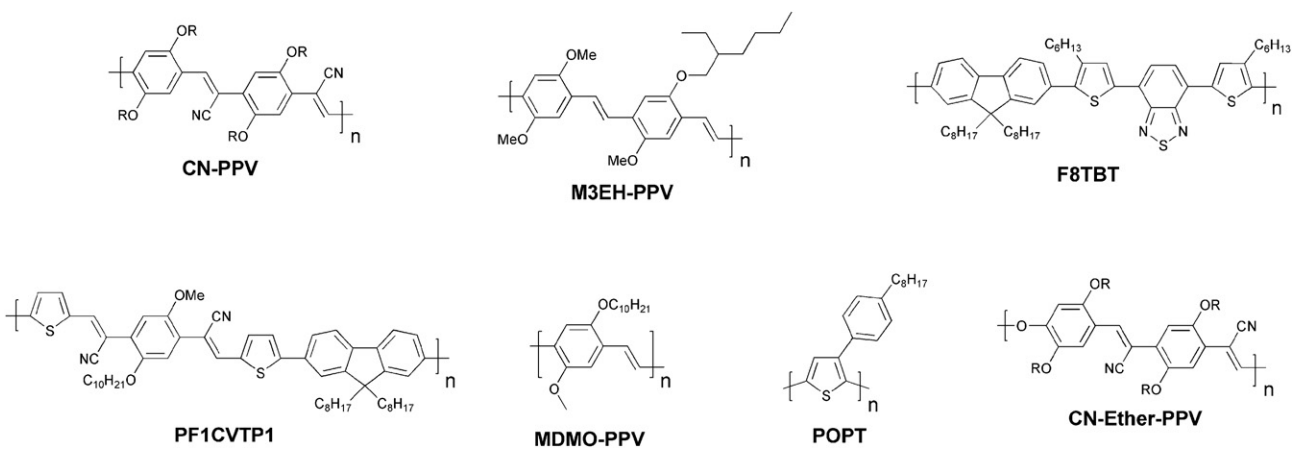

Fig. 3 Donor and acceptor materials used in polymer–polymer solar cells.

was acting as the donor and CN-PPV as the acceptor polymer. Since this initial report of polymer–polymer solar cells, they have not attracted as much attention as the polymer–fullerene solar cells. Despite their moderate performance (up to ~1.8% PCE)[69] photovoltaic devices based on polymer–polymer composites should potentially have several advantages to offer. While polymer:PCBM devices have shown efficiencies exceeding 6% it is predominantly the polymer that absorbs light since PCBM has a very weak overlap with the solar emission spectrum. Although [70]PCBM absorb more light and thus solves this problem to a limited degree, from a scientific point of view,[70] a blend of two conjugated polymers could exhibit a high optical absorption coefficient and enable absorption of solar light over a wider spectral range. Furthermore, it is relatively uncomplicated to tune the donor–acceptor energy levels when using polymers as electron acceptors because of greater flexibility in the design of the materials. Polymer–polymer solar cells have a high potential but there is a big challenge in designing conducting n-type polymers with acceptor properties up to a level that can compete with fullerenes. A problem is that polymer blends have a tendency to phase separate into domains with dimensions of several micrometres and thus is not within the exciton diffusion range. Therefore the challenge for these systems is to find a combination where the two polymers have the right morphology for efficient phase separation into an inter-penetrating network that allows for efficient charge carrier generation and transport. McNeill *et al.* have reported one of the best performing polymer–polymer solar cells to date with a PCE of 1.8%.[69] The authors used a blend of P3HT as the donor component and poly[(9,9-dioctylfluorene)-2,7-diyl-*alt*-[4,7-bis(3-hexylthien-5-yl)-2,1,3-benzothiadiazole]-2,2-diyl] (F8TBT) as the n-type polymer (Fig. 3). The efficiency is somewhat lower than the state-of-the-art polymer–fullerene solar cell by a factor of 3–4 but higher efficiencies should be reachable if spectral overlap of the two polymers could be reduced, resulting in a wider spectral coverage. High efficiencies have also been reported for the polymer–polymer composites based on POPT:CN-PPV, MDMO-PPV:PF1CVTP1 and M3EH-PPV:CN-Ether-PPV (Fig. 3).[71–73]

Thermocleavable materials for higher level processing and stability

Historically conjugated polymer materials were prepared *via* a precursor route whereby a thermal treatment was used to remove the solubilising groups and upon their elimination the conjugated and insoluble polymer formed. The best known examples are the synthetic routes leading to native poly-phenylenevinylene (PPV) and polyacetylene (PA) as exemplified by the Wessling route[74–77] and the Durham route[78–80] as shown in Fig. 4.

Initially the potential of the precursor route was not realised and it was dismissed in the middle of the 1990s[77] when soluble PPVs were made *via* the Wessling route. New methods appeared that avoided some of the problems of the early Wessling method that involved an ionic precursor polymer. This was then quickly replaced by the Gilch[81,82] and sulfinyl polymerisation types[83–85] which are similarly precursor routes to PPV but they do not involve ionic precursors. In addition transition metal catalyzed cross couplings entered the scene and were employed in polymerisations of prototypical materials such as P3HT using the Rieke[86,87] or the McCullough[88] route. Today, virtually all of the known transition metal catalyzed organic chemical reactions have been employed for the polymerisation of conjugated materials (Stille, Heck, Suzuki *etc.*). The development was at that point in time (1995–2005) driven by the desire to be able to engineer new materials and generate new chemical structures. The development did thus not pay attention to the needs for the polymer photovoltaic technology but only focussed on the materials development and employed a standard polymer solar cell scheme for materials evaluation (*i.e.* glass, ITO, PEDOT, evaporated metal back electrodes). Especially the transition metal catalyzed methods do sometimes introduce an often neglected problem of residual catalyst in the form of metallic nanoparticles in the polymer products. While it is easy to miss the presence of sub percent quantities of metallic nanoparticles (*e.g.* palladium) in a conjugated polymer product the consequences when applied in an electroactive device may be severe.[89] Methods to detect and remove the transition metal impurities have however been developed.[90–92] As the field of polymer solar cells have developed more focus has recently been placed on materials properties and purity. The interplay between the device film preparation methodology and the device performance became broadly known in 2005[47,48] and it was found that the device performance ultimately hinges on parameters such as the solvents used for film processing, the nature of the materials (molecular weight, polydispersity), the method of film formation (coating/printing technique, drying time) and treatments of the device film post formation (thermal annealing, solvent annealing). The route to a high performing device from a particular

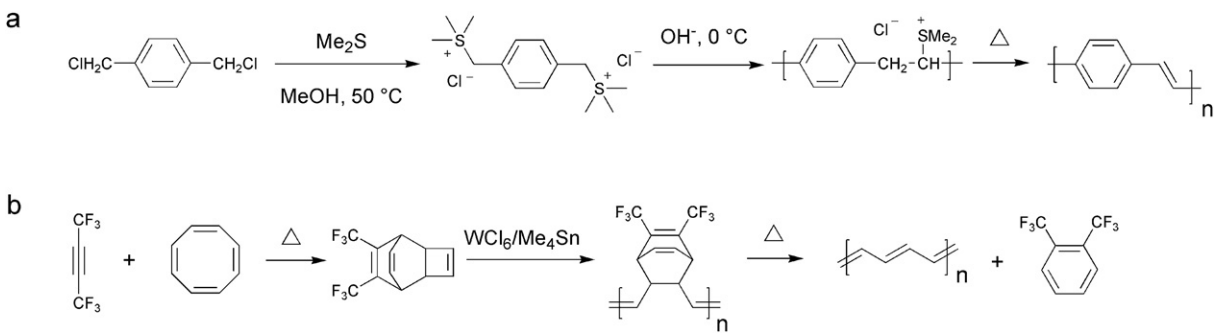

Fig. 4 The Wessling (a) and the Durham (b) route to respectively PPV and PA.

material thus follows a hair fine path where any deviation may lead to poor performance.

Thermocleavable materials (solution-processable precursors)

One route, taking the above mentioned issues into consideration, could be exploring the many possibilities in employing a conjugated material that is either reached through a precursor route or through a route where sidechains are removed *post* film formation. One can view these materials as bringing an extra dimension into the optimisation scheme where the device film in addition to thermal annealing and solvent annealing can be altered chemically. Both precursor and thermocleavable sidechain routes follow chemical reactions whereby a part of the material that constitutes the formed film is removed (sometimes up to 50% or more of the film weight or volume). The possibilities that thermocleavable materials have to offer warrant exploitation and certainly house the potential for bringing polymer solar cells to a more advanced level through materials design. To make polymer materials solution-processable, the introduction of solubilising groups is required. This is normally achieved by attaching solubilising side chains such as alkyl groups onto the conjugated polymer backbone. However, typical nonconjugated solubilising groups reduce the density of chromophores in the polymer and do not contribute to light harvesting and charge transport. Furthermore, the side chains make the material soft and allow for both morphological changes and diffusion of small molecules and constituents.[93–96] The softness provided by alkyl groups is related to the instability of polymer solar cells, and more rigid systems have proven to give devices with a better stability.[93] From this point of view, it is of some interest to prepare polymer solar cells *via* solution processing where it is possible to remove the solubilising side chains after the active layer has been deposited.

The application of thermocleavable materials fulfils this requirement. With thermocleavable materials you exploit the instability of a bond in the molecule. The labile bond functions as the linker between the solubilising group and the active material. The most recent developments are the thermocleavable ester groups and the dithiocarbamate precursor route. With regard to the thermocleavable ester groups the solubilising group is typically a branched alkyl chain attached to the active conjugated polymer backbone through an ester bond (Fig. 5). When heated this bond breaks, eliminating a volatile alkene and leaving the polymer component insoluble. The thermal treatment can be viewed as a way of performing an *in situ* chemical reaction thereby allowing for the alteration of both physical and chemical properties such as solubility, hardness, hydrogen bonding, polarity, density and ionicity after the final device film has been prepared. In terms of stability and operational lifetime polymer solar cells generally perform poorly. It was however demonstrated that heterojunction devices based on poly-3-(2-methylhexan-2-yl)-oxy-carbonylbithiophene (P3MHOCT) and C_{60} can provide very stable behaviour after thermal elimination of the solubilising groups.[93] The device film is prepared with standard solution processing methods followed by a thermal treatment around 200 °C (Fig. 6) where P3MHOCT eliminates the solubilising group as 2-methylhexene.

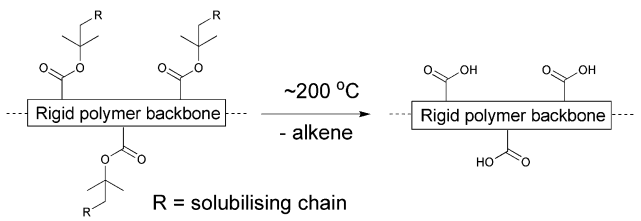

Fig. 5 Thermocleavable ester groups attached to the polymer backbone. After a thermal treatment around 200 °C the solubilising groups are eliminated.

After the thermal treatment P3MHOCT is converted to the more rigid and insoluble poly-3-carboxydithiophene (P3CT) which significantly improves the stability of the solar cell. The improved stability of this system has been linked to the rigid nature, cross-linking through a hydrogen-bonded network (Fig. 7) and a partially oxidized state.[97]

Furthermore, in the case of carboxylic esters attached to thiophenes, the processing offer removal of the esters at lower temperatures and the acid groups at higher temperatures allowing for multistep processing.[98] Thermogravimetric data for P3MHOCT in the temperature range 25–475 °C shows two distinct weight loss mechanisms. The first weight loss at ~200 °C accounts for the ester cleavage and the second weight loss at ~300 °C is decarboxylation (Fig. 8). During the annealing, it is possible to visually see the color change of the sample from red to orange (conversion from P3MHOCT to P3CT) and then from orange to purple-red (conversion from P3CT to PT) (Fig. 9a). The UV-vis absorption spectra of P3MHOCT and [60]PCBM or [70]PCBM mixtures are shown in Fig. 9b. It shows a significant change of the absorption coefficient at different temperatures. In addition a small red shift of the peaks (at 500 nm) can be seen when the samples were heated up to 310 °C.

This finding offers a route to native polythiophene (PT) by solution processing which has not been possible before. A plot of the power conversion efficiency, for P3MHOCT:PCBM devices, compared to the annealing temperature shows some interesting

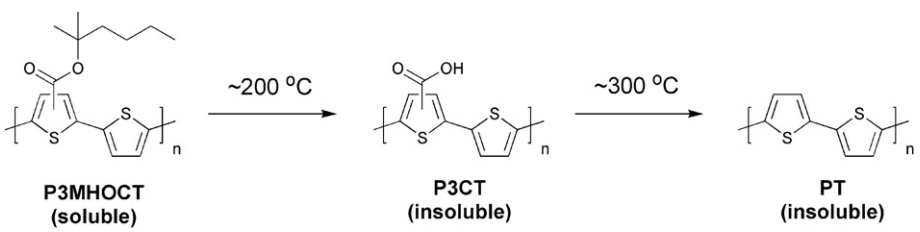

Fig. 6 Preparation of PT *via* a thermolytic reaction.

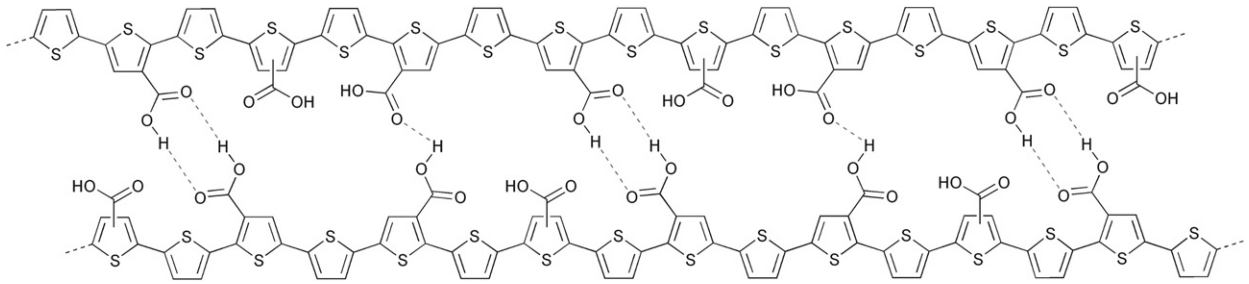

Fig. 7 Proposed cross-linked structure of P3CT through a hydrogen-bonded network.

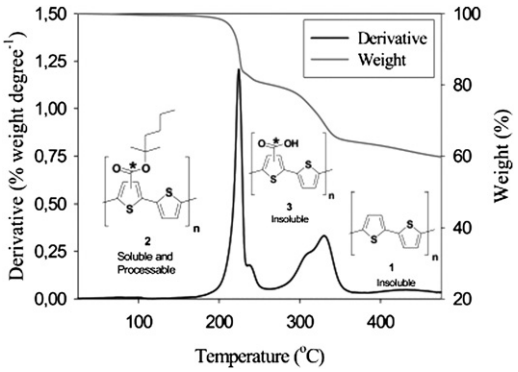

Fig. 8 Thermogravimetric data for P3MHOCT in the temperature range 25–475 °C. Reprinted with permission from ref. 98. © 2007 American Chemical Society.

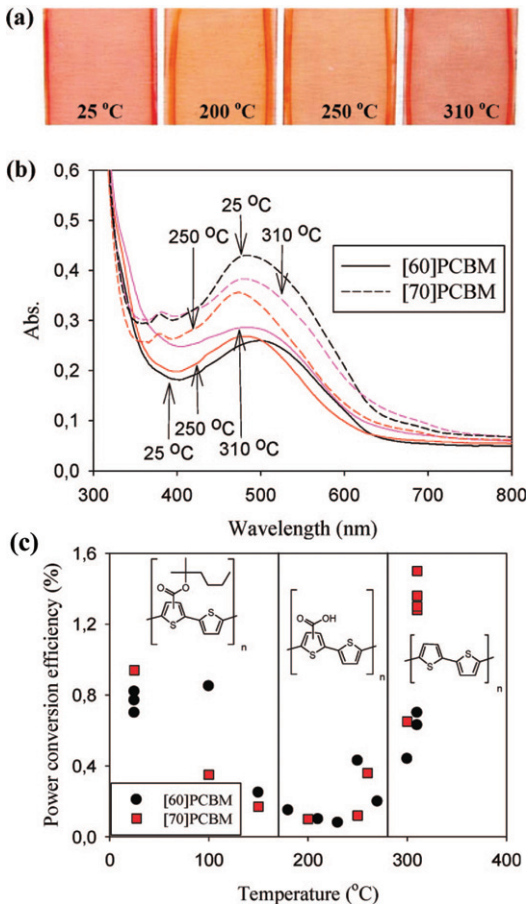

Fig. 9 (a) A photograph showing the appearance of films based on P3MHOCT:[70]PCBM when heated to different temperatures. (b) UV-vis spectra of films based on P3MHOCT and [60]PCBM or [70]PCBM mixtures spincoated on glass slides and annealed at three different temperatures (25, 250, and 310 °C). (c) Efficiency *versus* annealing temperature for bulk heterojunctions based on P3MHOCT and [60]PCBM/[70]PCBM. Reprinted with permission from ref. 99. © 2008 American Chemical Society.

results.[99] The power conversion efficiency of the bulk heterojunctions at room temperature was in the range 0.7–0.9% and was found to decrease as the device film was annealed at temperatures below the cleavage temperature (~200 °C) of P3MHOCT to P3CT. After the transformation to P3CT a broad minimum is reached with power conversion efficiencies in the range 0.1–0.4%. When reaching the temperatures of the second transformation (~300 °C) from P3CT to PT, a dramatic increase in power conversion efficiency was observed. Up to 0.6% in the case of [60]PCBM and as high as 1.5% in the case of [70]PCBM as shown in Fig. 9c. Clearly the morphology is changing with the chemical transformations and this is part of the explanation to the variable power conversion efficiency of this system. Another part of the explanation is the change in energy levels as the electron withdrawing carboxylic acid groups are removed from the conjugated polythiophene backbone. The use of thermocleavable conjugated polymer materials in polymer solar cells has been relatively limited due to the low performance observed when preparing devices from them. The preparation of efficient devices from native polythiophene *via* a thermocleavable route should be seen as the first breakthrough in the use of thermocleavable materials for polymer solar cells.[98,99] The parameter space is enormous and the added complexity of thermocleavable materials (both their synthesis and processing into devices) combined with perhaps a poor starting point have resulted in a small investment in them in terms of research effort. The fact that efficiencies approaching 2% can be reached shows that it is not impossible to prepare efficient polymer solar cell devices from thermocleavable materials and it is interesting to speculate how far thermocleavable materials could have been pushed pending the same investment of research effort that has gone into materials such as MEH-PPV or P3HT.

The use of cleavable P3MHOCT in thin film devices was first introduced by Liu *et al.*[100] The idea, besides improving the chromophore density, was to enable the interaction at the interface between the polymer and TiO_2 in a (FTO/TiO_2/P3CT/

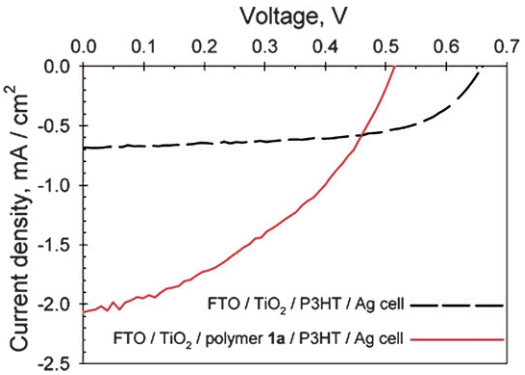

Fig. 10 *J–V* curves of a FTO/TiO_2/P3CT/P3HT/Ag cell (solid line) and a FTO/TiO_2/P3HT/Ag cell (dashed line) under 39 mW/cm^2 514 nm illumination. Reprinted with permission from ref. 100. © 2004 American Chemical Society.

P3HT/Ag) photovoltaic cell (FTO = fluorine doped tin oxide). The device showed a 3-fold improvement in photocurrent compared to a reference cell without P3CT (Fig. 10). Under illumination the FTO/TiO_2/P3CT/P3HT/Ag cell had an external quantum efficiency (EQE) of 12.6% and a power conversion efficiency of 1.10%, while the reference cell (FTO/TiO_2/P3HT/Ag) had an EQE of 4.2% and a power conversion efficiency of 0.69%. The improvement in photocurrent/performance upon introduction of the P3CT layer may be related to several factors. Cleaving the solubilising groups results in higher chromophore density and the chelation of –COOH groups in P3CT to the TiO_2 may enhance the interfacial charge-transfer efficiency.

Other thermocleavable materials exploited as semiconductors are the dithiocarbamate precursors. Poly-(2,5-thienylene vinylene) (PTV) has been synthesised *via* the dithiocarbamate precursor route which exploits the lability of the linking thiocarbamate bond in the molecule (Fig. 11).[101–105] The solution-processable non-conjugated precursor polymer is cleavable around 160 °C leaving a rigid conjugated polymer (PTV). Bulk-heterojunction solar cells based on blends of the precursor PTV and PCBM have demonstrated power conversion efficiencies of up to 0.76% after the thermal treatment.[102]

In terms of stability PTV is like PPV,[106] sensitive to oxygen due to the vinylene groups that are susceptible to photo-oxidation resulting in a short lifetime of the devices. The chemical degradation is initiated by the formation of singlet oxygen by energy transfer from the photoexcited polymer to ground state oxygen molecules.[107] The singlet oxygen can then react with the vinylene groups through a 2 + 2 cycloaddition reaction forming an intermediate dioxetane (Fig. 11) while other reactions are also possible. Finally the dioxetane can break down resulting in chain scission. As mentioned above more rigid systems generally give devices with a better stability and therefore improved stability of PTV devices prepared with the dithiocarbamate precursor route may be expected. The use of thermocleavable materials offers several advantages in the context of polymer solar cells. Most importantly the side chains that constitute a significant proportion of the final film are eliminated and ideally the final film comprises only the active component. Since bulk heterojunctions of polymer and PCBM are not directly compatible with the high temperatures acquired for elimination one aim is to achieve as low a temperature of elimination as possible. This has been investigated by Petersen *et al.* for thermocleavable esters of low band gap monomers and polymers based on diphenyldithienylthienopyrazine (Table 1).[108] The temperature of elimination of a series of different ester groups was studied with thermogravimetric analysis (Fig. 12a).

It showed that the thermal treatment is limited to simple secondary and tertiary esters where the alcohol is saturated in order to ensure that the alkene that is eliminated is removed efficiently without undesired side reactions.

As expected the tertiary esters eliminated at the lowest temperatures (200–250 °C) and even lower cleavage temperatures should be possible. The UV-vis absorption spectra of polymer **4** in thin film are shown in Fig. 12b. Upon thermocleavage of the film by heating it at 250 °C for 1 min the absorption spectrum shows a less intense absorption and a smaller band gap (1.2 eV) compared to the uncleaved film (1.3 eV). The lower absorption intensity can be explained by the associated change in film thickness and dielectric constant which may lead to changes in the reflection phenomena.[108] In addition, the intensity of absorption quite often decreases as the band gap is lowered. In contrast to P3MHOCT where the ester resides on a thiophene ring, decarboxylation does not take place ahead of decomposition for the diphenyldithienylthienopyrazines. Table 1 also shows photovoltaic parameters of polymers **1–4** before and after thermocleavage. A general observation is that the devices perform significantly worse after thermocleavage as indicated by

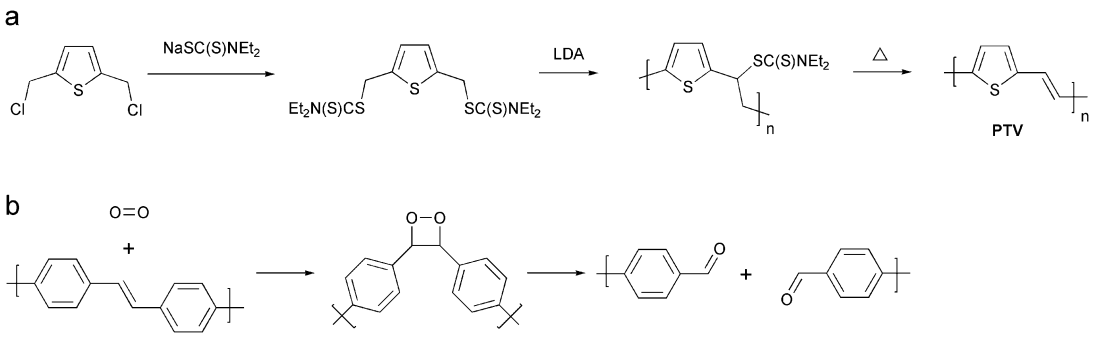

Fig. 11 (a) Preparation of PTV *via* the dithiocarbamate precursor route (b) Reaction of the vinylene bond in a PPV polymer with singlet oxygen. Singlet oxygen adds to the vinylene bond forming an intermediate dioxetane followed by chain scission. The aldehyde products shown can react further with oxygen.

Table 1 Photovoltaic parameters of polymers **1–4**

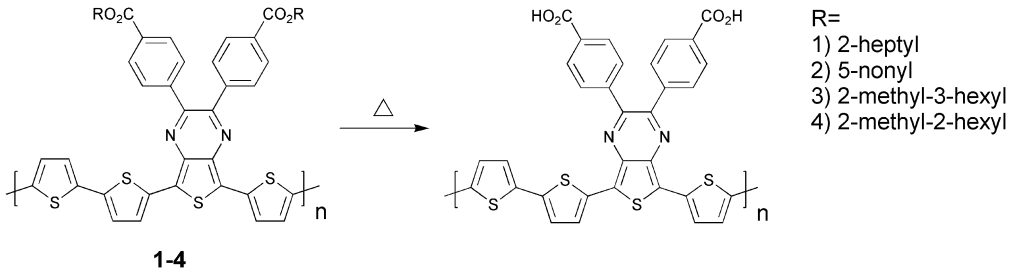

1-4

Polymer	J_{sc} (mA/cm^2)	V_{oc} (V)	FF	PCE (%)	Cleaving temp. (°C)	Solubility in DCB
1	1.52	0.14	0.25	0.05	Uncleaved	Easy to dissolve
	0.41	0.16	0.26	0.017	310	
2	2.1	0.4	0.29	0.25	Uncleaved	Hard to dissolve
	0.36	0.14	0.27	0.013	310	
3	2.55	0.41	0.29	0.3	Uncleaved	Easy to dissolve
	0.24	0.08	0.26	0.005	310	
4	2.4	0.46	0.36	0.4	Uncleaved	Easy to dissolve
	1.94	0.4	0.33	0.25	230	

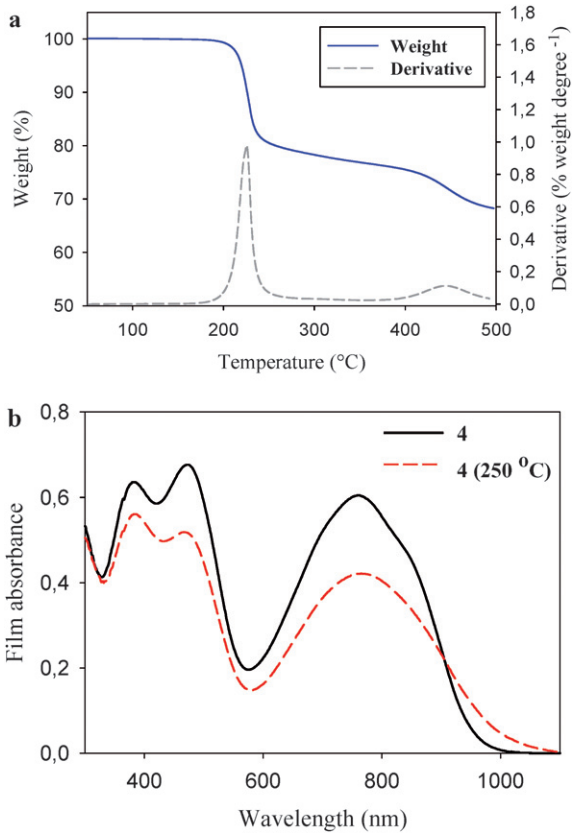

Fig. 12 (a) Thermogravimetric data for polymer **4** (see Table 1) in the temperature range 50–500 °C. (b) UV-vis absorption spectra of polymer **4** in thin film before and after thermocleavage. Reprinted with permission from ref. 108. © 2008 American Chemical Society.

a decrease in voltage and current. Polymers **1–3** require high cleaving temperatures (310 °C) which could be the reason for the drastic drop in performance compared to **4** that only shows a minor drop in performance. To compare with earlier reported photovoltaic parameters for P3MHOCT the performance dropped around 10-fold when cleaved to P3CT and then improved 15-fold when cleaved further to PT (Fig. 9). In addition to the thermocleavable materials described above other examples have been described in the literature. These are summarized in Table 2.

Cross-linking

Several investigations of the most widely used bulk heterojunction of P3HT/PCBM with a special focus on thermal stability have shown a drastic drop in performance due to morphological changes where large aggregations of PCBM appear in the films upon prolonged thermal treatment.[117–121] One way of approaching this problem has been by design of cross-linkable molecules/polymers (see Table 3) that can 'lock' the morphology and thus hinder the extensive phase separation. Zhu *et al.* and Drees *et al.* both succeeded in suppressing the aggregation by synthesising fullerene derivatives containing a glycidyl functionality (PCBG).[122,123] Bulk heterojunctions of P3HT/PCBG cross-linked by Lewis acid catalysis showed enhanced morphological stability upon thermal annealing. Nevertheless, the efficiencies of the cells dropped considerably compared to the corresponding non-cross-linked P3HT/PCBM system. Zhu *et al.* also reports some initial attempts of using cross-linkable polymers with either epoxy- or furoyl containing side chains, that are cross-linked by use of a photoacid. The films are reported to be insoluble in THF, but no devices were prepared.

A more successful approach in preparing cross-linkable polymers have recently been reported by Myanishi *et al.*[124] They have prepared a cross-linkable P3HT-analogue, poly(3-(5-hexenyl)-thiophene) (P3HNT), where the hexyl group on thiophene is substituted with a 5-hexenyl. The polymer was prepared by polymerisation of 2,5-dibromo-3-(6-bromo-hexenyl) (regioregularity above 97% plus M_n and M_w/M_n values of 32 000 and 1.30 respectively) followed by conversion of the 6-bromohexyl into the corresponding iodide. Finally basic elimination affords the desired compound (Fig. 13).

Table 2 Thermocleavable materials

Precursor	Polymer	Reference
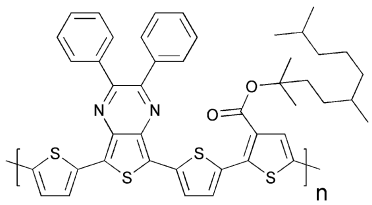	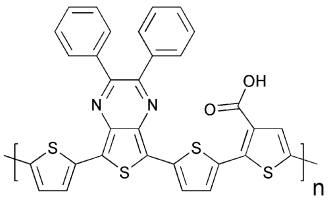	109
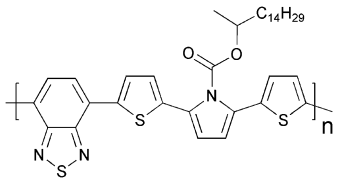	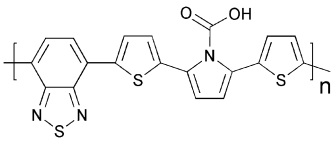	110
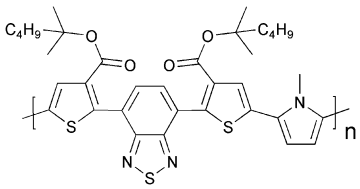	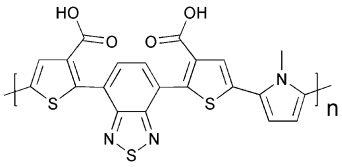	110
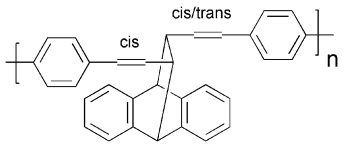	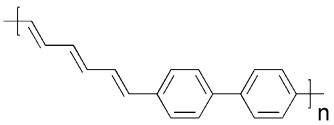	111
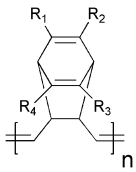	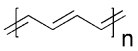	112
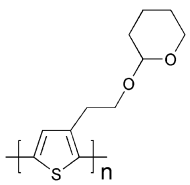	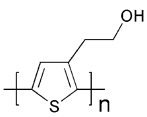	113
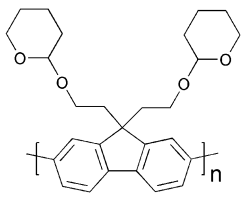	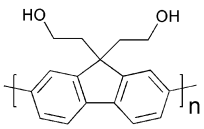	114
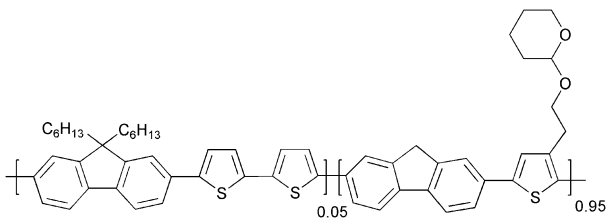	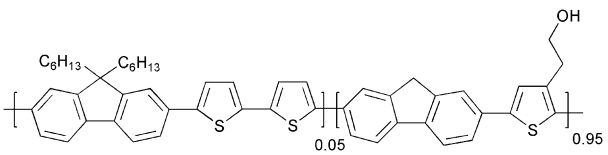	115
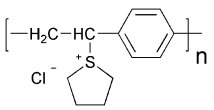	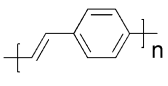	116

The cross-linking process was performed by prolonged heating of the spincast films at 150 °C. Films prepared in this way showed enhanced insolubility in chloroform, and cross-linked bulk heterojunction films (P3HNT/PCBM) showed a suppressed deterioration of PCE after annealing for 10 h (3.03% before annealing →1.74% after annealing) compared to a corresponding P3HT/PCBM device (3.11% before annealing → 1.00% after annealing).

It should be mentioned that several attempts of cross-linking conjugated polymers have been reported in the context of organic light emitting diodes (OLEDs) with various degrees of success.[125–131] Even though some of the polymers used in the OLED cross-linking experiments are different to those employed in solar cells, the methods of cross-linking the polymers could be relevant in the context of polymer photovoltaics.

Processing

The performance of polymer solar cells is intimately linked to the processing conditions during device preparation and when taking this further than the successful laboratory devices it is evident that the successful large scale preparation of polymer solar cells implies control over the interplay between process and device performance. The solutions to this puzzle for a chosen materials combination will have to be sought through the device geometry and the processing/fabrication method. Thermocleavable materials as an example have much to offer in the context of processing multilayered polymer solar cells industrially. When processing multilayer structures sequentially the processing of subsequent layers must ideally not affect the underlying layers and this is particularly important when using solution processing. The common way of solving this has been to use orthogonal solvents for adjacent layers. In the extreme case water is used as the solvent for the first layer and an organic solvent is used for the next layer. This has been the traditional way of making polymer solar cells based on a glass-ITO substrate where poly(3,4-ethylenedioxythiophene):poly(styrenesulfonate) (PEDOT:PSS) is spincoated onto the ITO from an aqueous dispersion followed by spincoating of the active layer from an organic solvent and completion of the device through evaporation of a metal back electrode. It is fortuitous that the standard laboratory polymer solar cell has only needed these two solution processed layers for several reasons. Firstly, the surface energy of a solid PEDOT:PSS film is higher than the surface tension of active materials in typical organic solvents making wetting easy. Secondly, additional layers would be faced with the problem of finding an additional solvent orthogonal to the two previously deposited layers. These two problems may seem trivial but they are at the heart of what has limited the early emergence of a low cost industrial and large scale process. The fact that the technology has evolved around fixed ingredients (*i.e.* glass, ITO, PEDOT:PSS, metal electrode) and fixed methods of application (*i.e.* spincoating, metal evaporation) implies that development has been slow towards alternative approaches such as ITO free and inverted device geometries that enables the use of printed electrodes. One way to obtain orthogonality between the processing conditions for subsequent layers is by transformation of the last processed layer into an insoluble film thus enabling free choice of processing conditions for the subsequent layers. This has been achieved unintentionally in the case of oxide layers such

Table 3 Structural representation of different molecules used in cross-linking processes in polymer photovoltaics and OLEDs

Polymer photovoltaics	Ref.
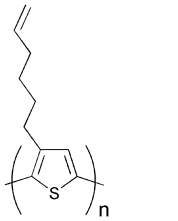	124
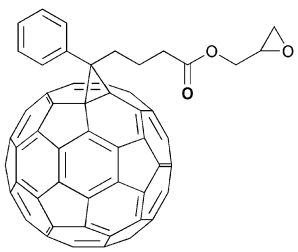	122,123
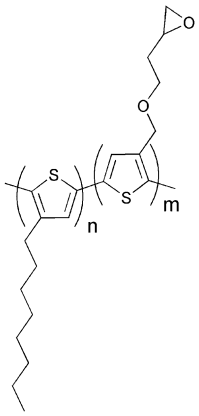	123
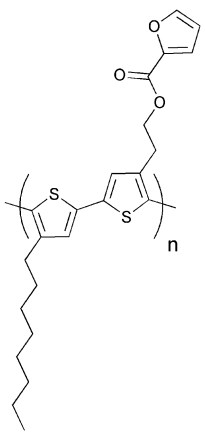	123
Organic light emitting diodes	**Ref.**
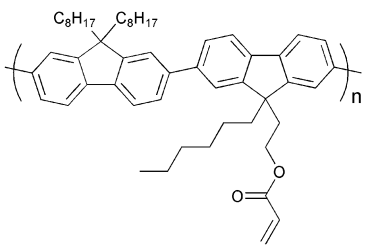	128

Table 3 (*Contd.*)

Organic light emitting diodes	Ref.
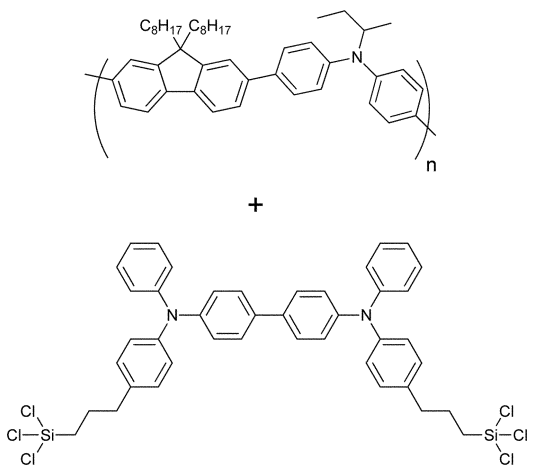	129,130
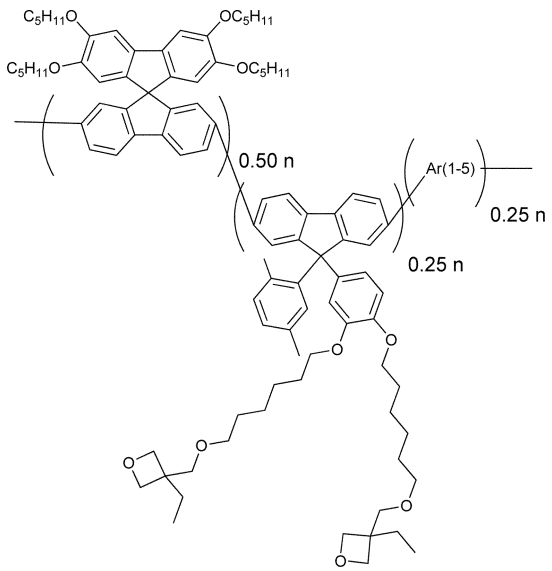	127
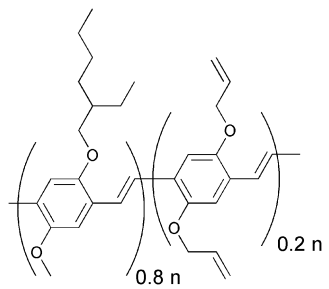	131
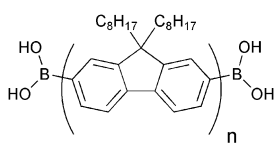 n = 2-4	126

Table 3 (*Contd.*)

Organic light emitting diodes	Ref.
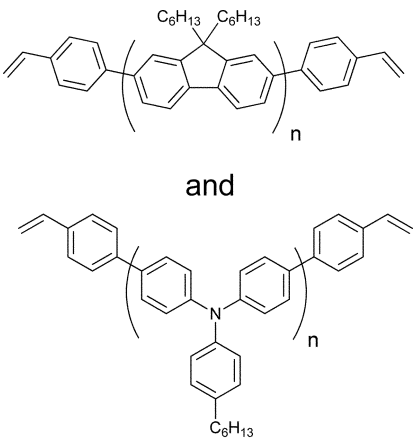 Blends (90:10 - 40:60)	125

as zinc oxide and titanium dioxide employed in hybrid solar cells and can be achieved intentionally with thermocleavable materials where insolubility arises upon thermocleavage as detailed above. Deliberate use of thermocleavable materials has been shown in one development of a process for industrially processed polymer solar cells.[132–135]

Hybrid solar cells

Hybrid solar cells (HSC) have a heterojunction consisting of both organic and inorganic materials, thus trying to combine the advantages of each of these. Polymers generally have high hole mobility but a low electron mobility, and this intrinsic carrier mobility imbalance in the polymer is overcome by incorporation of an n-type inorganic material to act as the electron acceptor and a pathway for electron transport. The efficiency of the heterojunction is limited by the exciton diffusion length as excitons formed at positions further away from an interface than the exciton diffusion length have a lower probability of efficient charge separation and harvesting. Efficient charge separation can only occur at the p–n interface and ideally the heterojunction should be constructed in a manner such that the excitons are generated in the vicinity of the interface. At the same time the constructed heterojunction should ensure a direct or percolating pathway of the charge carriers to the relevant electrodes in order to effectively transport and collect the charges. The semiconducting properties in HSC of several different inorganic materials have been examined with promising results, *i.e.* TiO_2,[136–145] ZnO,[146–158] CdSe,[159–164] CdS,[165,166] PbS,[167] PbSe,[168] SnO_2,[169] and Si,[170,171] as presented in Table 4. In recent years research has largely focused on the use of TiO_2, ZnO and Si, mainly because of the environmental harmfulness and toxicity of many of the others. The choice of polymer used in HSCs has usually been P3HT or different PPV polymers as they have shown good hole conducting properties.

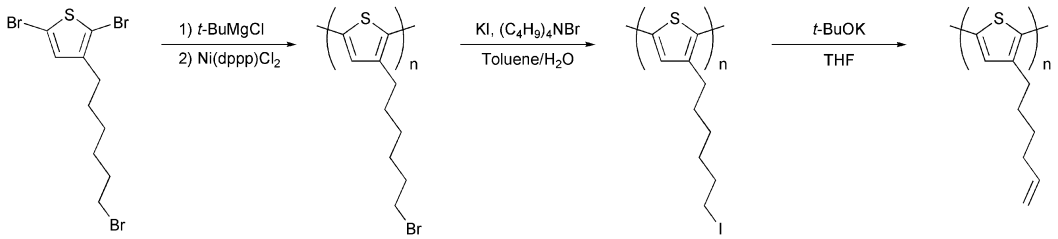

Fig. 13 Polymerisation and side chain conversion reactions for the synthesis of P3HNT.

Various approaches in HSC design have been explored and they generally fall into 4 architectural categories:

(1) planar bilayer;

(2) nanoparticle/polymer blends;

(3) *in situ* generation of the n-type inorganic in the polymer;

(4) nanostructured: infiltrating rigid nanoporous or nanorod structures with a polymer.

The schematic representation of these is shown in Fig. 14.

Covering a planar layer of inorganic semiconductor with a polymer film is the most direct approach to a hybrid solar cell, but the design has limited application as the active layer of polymer has to be very thin in order to make use of all the excitons. The simplicity of the architecture though renders it very applicable for routine evaluation of the properties of new polymers and measurement of exciton diffusion lengths.

When using nanoparticle/polymer blends the active layer is normally prepared by spincoating a solution containing dissolved polymer and suspended nanoparticles, thus enabling deposition of both semiconductors in a single step. The procedure should in principle ensure intimate mixing of the acceptor and donor, but great care must be taken in tuning the surface chemistry of the nanoparticles in order to prevent these from aggregating and at the same time ensuring a good interface for charge transfer.[172] Nanoparticle aggregation is believed to be one of the limiting factors of the efficiency in nanoparticle/polymer devices.[173]

Examples of this include the use of tetrapod, hyperbranched and nanorod CdSe nanoparticles in combination with conjugated polymers where efficiencies are approaching 3%.[159–164] Essential for the good performance is to replace the nanoparticle surface ligands with a volatile molecule (for example replacement of tri-*n*-octylphosphine oxide with pyridine), allowing for evaporation of the surface ligands during film processing. This again allows for better contact between the polymer and the nanocrystals and between the individual nanoparticles.

In one example Beek *et al.* have achieved a PCE of 1.6% and avoid the problem of surface ligands by using crystalline ZnO nanoparticles, which are soluble in organic solvents and therefore can be mixed directly with the polymer.[146,147]

An alternative approach to individual nanoparticles was introduced by van Hal *et al.* that prepared a continuous interpenetrating network of TiO_x created *in situ* within the conjugated polymer film after spincoating a mixture of MDMO-PPV and a precursor for TiO_x ($Ti(OC_3H_7)_4$).[174] Subsequent exposure of the cast film to moisture from the air led to the formation of a TiO_x network. The photoluminescence (PL) of the MDMO-PPV:TiO_x heterojunction was significantly quenched compared to a pristine MDMO-PPV film (PL is reduced by a factor 19 with a 50% w/w content of TiO_x) indicating an efficient charge separation of photoinduced excitons. These experiments were later confirmed by Slooff *et al.* where additional experiments were performed with poly(3-octyl thiophene) (P3OT) as the polymer.[175] Scanning electron microscopy (SEM) images taken after removal of the polymers by UV–ozone treatment revealed TiO_x phases with sizes on the order 100–200 nm for P3OT blends and 20–30 nm for MDMO-PPV blends. The difference is assumed to be caused by the tendency of P3OT to aggregate more easily as compared to MDMO-PPV (Fig. 15).

Despite the good interpenetrating network of TiO_x, photovoltaic devices showed rather low power conversion efficiencies which is ascribed to the fact that the inorganic phase is essentially amorphous.[147] Crystallisation of TiO_x into the anatase phase of TiO_2 would require high temperatures (>350 °C).[176]

A similar approach was taken by Beek *et al.* using MDMO-PPV and diethylzinc as a ZnO precursor.[147] ZnO is known to crystallise at much lower temperatures than TiO_2, and heating to 110 °C under nitrogen at 40% relative humidity promoted crystallisation. The final device gave a PCE of 1.1%. Moet *et al.* later reported partial degradation of the polymer during processing of MDMO-PPV and diethylzinc and that P3HT (no vinyl groups) show better stability and higher performance (PCE 1.4%).[150]

The last architectural approach involves the filling of a precreated inorganic nanostructure (vertical structured nanopores or vertically oriented nanorods/nanopillars) with a polymer (examples are given in Fig. 16). The aim is to create a structure where the separation of the phases is in the order where complete exciton harvesting and charge collection is possible and where the straight pore/channel network provides the most direct pathway for the charges to the anode and cathode. Several techniques[137,139,170,177–181] have been developed in order to create controlled structures pursuing the alleged optimal conditions. Among the published results on solar cells Olson *et al.* reported the fabrication and characterisation of heterojunctions consisting of P3HT and a mesoporous structure of ZnO nanofibers.[152] The nanofibers were grown hydrothermally on a glass/ITO substrate which was subsequently filled with P3HT by spincoating and annealed to ensure intercalation into the voids between the nanofibers. The final device showed a 3.5 times increase in PCE (to 0.53%) compared to the corresponding bilayer device of P3HT on planar ZnO.

Kuo *et al.* recently showed good results for ordered heterojunctions with vertically aligned TiO_2 nanorods and P3HT.[139] The vertical TiO_2 nanorods were prepared by spincoating a TiO_2 precursor into the pores of an aluminium anodic oxide (AAO) template pregrown on an ITO/glass substrate. After sintering, the AAO template was removed by dissolving it in aqueous

Table 4 Materials and performance parameters for a range of selected polymer–inorganic solar cells. All measurements are performed in the vicinity of AM 1.5 conditions (90–100 mW/cm^2) unless stated otherwise[a]

Inorganic semiconductor	Polymer	Architectural category	V_{OC}(V)	J_{SC} (mA/cm^2)	FF	η(%)	Comments	Ref.
CdSe	OC1C10-PPV	Tetra-pod NP	0.76	9.1	0.44	2.8	V_{OC} and J_{SC} were extracted from a figure	162
	P3HT	Nanorod P	0.62	8.79	0.50	2.6		163
	APFO-3[b]	Nanorod P	0.95	7.23	0.38	2.6		164
	P3HT	Hyperbranched P	~0.6	~7.0	—	2.2		159
	OC1C10-PPV	Tetra-pod NP	0.65	7.3	0.35	1.8		161
	P3HT	Nanorod P	0.7	5.7	0.4	1.7		160
CdS	P3HT	Surf. mod. NP	0.54	4.84	0.45	1.18	Surf. mod. with a polyacetylene containing quaternary pyridinium salts	165
	MEH-PPV	Multiarmed nanorod P	0.85	2.96	0.47	1.17		166
PbSe	P3HT	NP	0.35	1.08	0.37	0.14		168
PbS	MEH-PPV	NP	1	0.13	0.28	0.7	AM 1.5 conditions but at low power (5 mW/cm^2)	167
SnO_2	MDMO-PPV	Surf. mod. nanoporous NP layer	0.65	0.32	0.42	0.085	Surf. mod. with $C_{60}C(COOH)_2$	169
ZnO	P3HT/PCBM	Vertical nanorod array	0.58	10.4	0.65	3.9	Surf. mod. with N719	154
	P3HT/PCBM	Vertical nanorod array	0.57	9.6	0.50	2.7		153
	P3HT/PCBM	Vertical nanorod array	0.475	10	0.43	2.03		151
	P3HT/PCBM	Surf. mod. vertical nanorod array	0.57	8.89	0.41	2.0		155
	MDMO-PPV	NP	0.81	2.4	0.59	1.6		146
	P3HT	*In situ* prepared	0.83	3.3	0.50	1.4	Diethylzinc as ZnO-precurser	150
	MDMO-PPV	*In situ* prepared	1.14	2.0	0.42	1.1	Diethylzinc as ZnO-precurser	147
	P3HT	Vertical nanorod array	0.44	2.17	0.56	0.53	Surf. mod. with mercurochrome	152
	P3HT	Surf. mod. vertical nanorod array	0.46	2.45	0.46	0.52		149
	APFO-3[b]	NP	0.51	3.1	0.36	0.45		156
Si	P3HT/PCBM	Vertical nanowires	0.43	11.6	0.39	1.93		170
	P3HT	NP	0.75	3.3	0.46	1.15		171
TiO_2	P3HT	Surf. mod. nanorod P	0.78	4.33	0.65	2.20	Surf. mod. with N3-dye	141
	P3HT	Surf. mod. nanorod P	0.75	3.49	0.65	1.70	Surf. mod. with anthracene-9-carboxylic acid	140
	P3HT	Nanorod P	0.64	2.73	0.56	0.98		142
	P3HT	Nanorod P	0.52	2.97	0.54	0.83		144
	MEH-PPV	Bilayer	1	1.8	0.37	0.67		136
	P3HT/PMMA	Nanorod P	0.53	2.57	0.48	0.65		143
	P3HT	Vertical nanorod array	0.32	3.89	0.41	0.51		139
	P3HT	Surf. mod. nanofiber mat	0.57	1.27	0.40	0.29	Surf. mod. with N719-dye	145
	P3HT	Surf. mod. nanoporous NP layer	0.64	1.11	0.34	0.24	Surf. mod. with N3-dye	138
	MEH-PPV	Vertical array of hexagonal pores	0.79	0.56	0.47	0.21		137
	P3HT	Surf. mod. bilayer	0.46	0.67	0.48	0.15	Surf. mod. with black dye	138
ZnO + TiO_2	P3HT	Vertical ZnO nanorod array + TiO_2 nanorod P	0.49	2.67	0.45	0.59		148

[a] Abbreviations: **NP**: nanoparticle; **P**: particle; **Surf. mod.**: surface modified. [b] APFO-3: poly(2,7-(9,9-dioctylfluorene)-*alt*-5,5-(4′,7′-di-2-thienyl-2′,1′,3′-benzothiadiazole)).

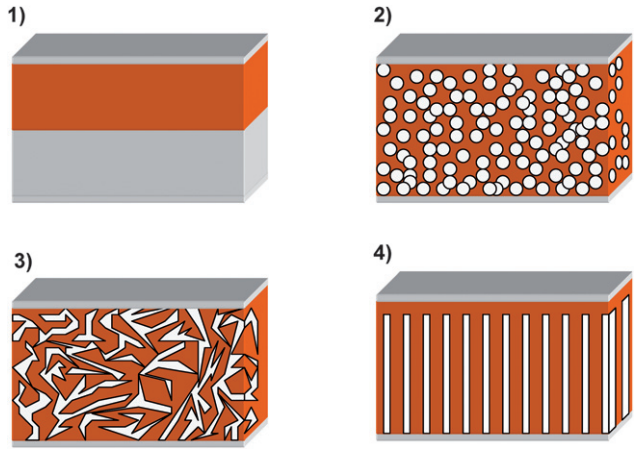

Fig. 14 The different geometries of hybrid solar cells: (1) Planar bilayer—the polymer added onto a flat inorganic surface; (2) nanoparticle/polymer blends—a mixture of the polymer and suspended inorganic particles is applied; (3) *in situ* generation of the inorganic within the polymer—a mixture of the polymer and a soluble precursor to the inorganic is applied and solidification of the inorganic is then performed after film preparation; (4) nanostructured—a rigid nanoporous or nanorod structure of inorganic is filled with the polymer.

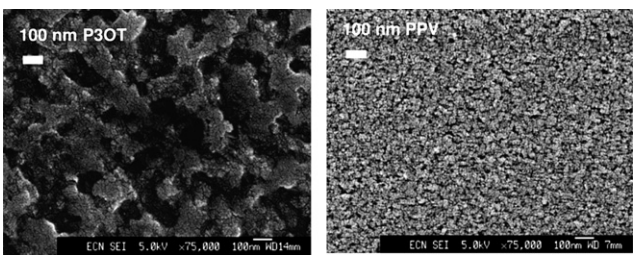

Fig. 15 SEM of the TiO_x phase after removal of the polymer by UV–ozone treatment for 10 min. Left: from a P3OT:TiO_x (12 vol% TiO_x) blend. Right: from a MDMO-PPV:TiO_x(14 vol% TiO_x) blend. Reprinted with permission from ref. 175. © 2003 Elsevier B.V.

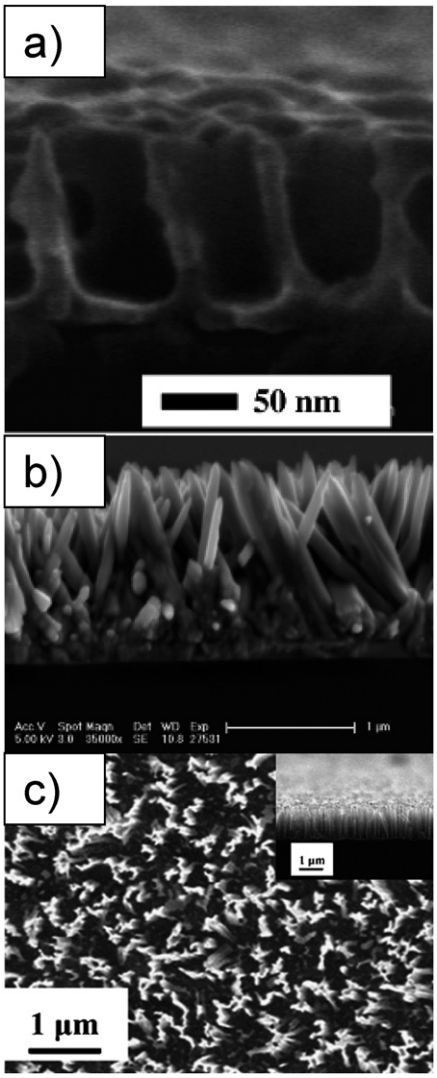

Fig. 16 SEM images of (a) cross sectional view of embossed TiO_2 structures on FTO substrate after calcinations. Reprinted with permission from ref. 178. © 2005 American Chemical Society. (b) ZnO nanorods grown on dense ZnO backing layer on ITO substrate (cross section). Reprinted with permission from ref. 181. © 2006 American Chemical Society. (c) Top view of Si-nanowires on silicon wafer prepared by wet etching, with an insert of the cross sectional view. Reprinted with permission from ref. 170. © 2008 Elsevier B.V.

NaOH. The nanorods are approximately 200 nm long and with a diameter 30–60 nm. The resulting solar cell after spincoating of P3HT and annealing showed to be 4.3 times more efficient (PCE of 0.51%) than planar TiO_2:P3HT.

As can be seen from Table 4, several of the reports with the highest efficiencies are reported for P3HT/PCBM blends and an inorganic semiconductor. The inorganic material here functions as an extra electron carrier. Takanezawa *et al.* showed that incorporation of the P3HT/PCBM bulk heterojunction into a vertical ZnO nanorod array led to an increase in PCE from 1.8% for a normal P3HT/PCBM heterojunction on top of a seed layer of ZnO to a PCE of 3.9% when growing the seed layer to nanorods with a length of 300 nm before spincoating the P3HT/PCBM solution.[153,154] As seen in Fig. 17 the ZnO rods can act as an extra electron carrier at the p–n interface with P3HT but can also operate as an intermediate between PCBM and ITO.

Another tendency in Table 4 that leads to relatively high efficiencies is the use of the surface modified inorganics, typically with a dye that can assist in charge separation and prevents back recombination. (For all results involving surface modification presented in Table 4 the concentration of the interfacial molecules is so small that they only have a minimal or negligible contribution to the light absorption, and the polymer is thus the main contributor to absorption.) Lin *et al.* have recently demonstrated that surface modification by ligand exchange of the surface ligands of freshly prepared nanorods (~20–30 nm in length and 4–5 nm in diameter) with different dyes led to improved performances compared to 'normal' ligand exchange with pyridine, a near doubling of the PCE (from 1.12% to 2.20%) was observed in a HSC with P3HT.[141] The authors ascribe the large increase in PCE to be partially an effect of enhanced charge separation but mainly to be attributed to a strong suppression of back transfer and recombination of carriers at the interfaces. In Fig. 18 the energy diagram of TiO_2, the dye ligands, and P3HT are shown. All the dyes showed improved performance when

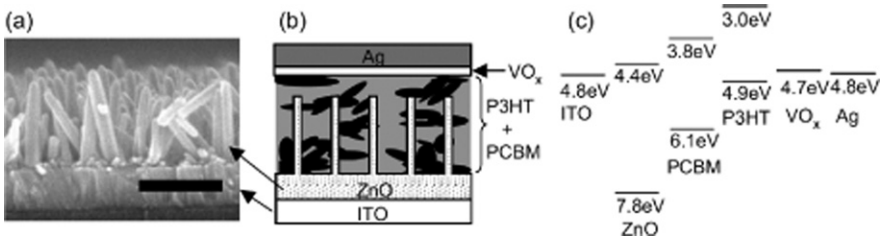

Fig. 17 (a) FE-SEM cross-section image of the ZnO nanorod arrays (scale bar: 300 nm), (b) schematic structure of a ZnO/organic hybrid device with a VO_x buffer layer, and (c) energy diagram of the ITO/ZnO/PCBM:P3HT/VO_x/Ag device. Reprinted with permission from 154. © 2008 American Institute of Physics.

used as surface modifiers in the order N3 (2.20%) > CuPc (1.80%) > ACA (1.67%).

The results for the P3HT/PCBM:n-inorganic and the use of surface modified inorganics show that 'tuning' the charge separation and back recombination by adding a third component might be a promising path for future research. The third component is typically added at the interface between the inorganic semiconductor and the polymer *vis-à-vis* the well known dye sensitized solar cells where it serves the purpose of facilitating charge injection from the polymer to the semiconductor while preventing back recombination.

Tandem cells

So far the power conversion efficiency of single bulk heterojunction solar cells has reached 6% while higher power conversion efficiencies are possible from a theoretical point of view. One drawback of single junction polymer devices is their narrow absorption window compared to the solar cells based on inorganic semiconductors. A possible approach to efficiently harvest light at both short and long wavelengths is by stacking different band gap materials/devices on top of each other. This can be done by placing the cells in series giving devices known as tandem cells.[1,13,14] By stacking different band gap materials on top of each other the tandem cell should be able to exceed the maximum theoretical efficiency of a single junction solar cell because it increases the absorption of solar light and allows exploiting the photon energy more efficiently. When two cells (in a two terminal tandem cell) are connected in series the open-circuit voltage (V_{oc}) is the sum of the V_{oc}'s of the subcells, $V_{oc1} + V_{oc2} + V_{oc3\ldots} = V_{oc\ (tandem)}$.

Fig. 19 illustrates a typical organic tandem cell architecture comprised of two distinct active layers stacked on top of each other. Both of them are based on a donor–acceptor composition and the use of materials with different band gaps enables absorption of solar light over a wider spectral range. Typically a material with a wide band gap is used for the first cell and a low band gap material is used for the second cell. In order to prevent charge build-up within the cells a transparent intermediate layer is positioned between the two active layers. The intermediate layer ensures recombination of the electrons created in the first cell with the holes created in the second cell. In addition, it can act as a protective layer to support the bottom cell during deposition of the top active layer. This can generally be accomplished with a thin inorganic layer. Several methods have been employed in the fabrication of tandem cells depending on the materials used for the active and the intermediate layer. The mode of preparation can be divided in three categories: all vacuum processing by evaporation of low molecular weight

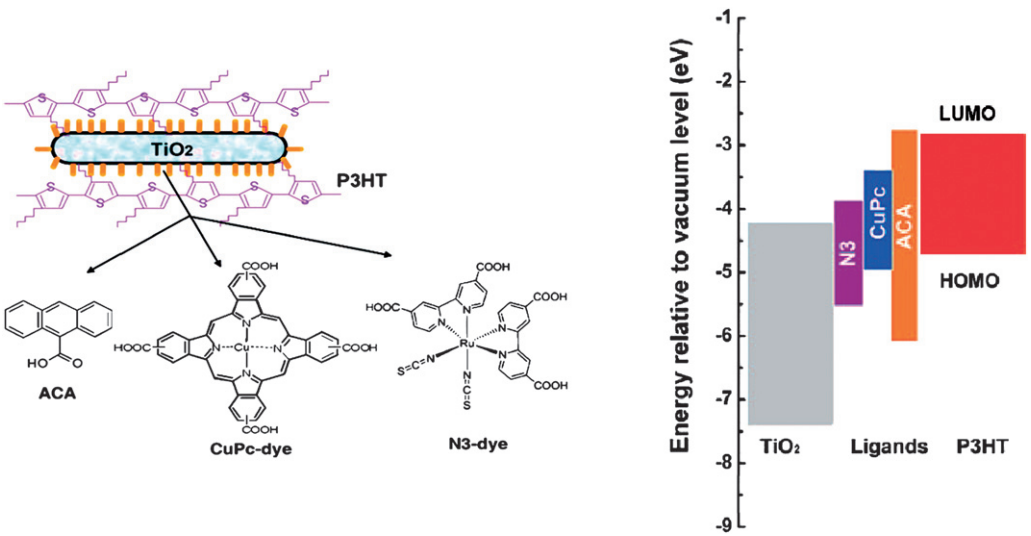

Fig. 18 **Left:** Schematic representations of P3HT/TiO_2 nanorod hybrid after interface modification and chemical structures of different interfacial molecules of ACA, CuPc-dye, and N3-dye molecules respectively. **Right:** The corresponding energy levels of the various materials. Reprinted with permission from ref. 141. © 2009 American Chemical Society.

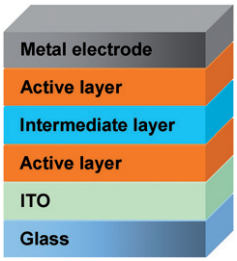

Fig. 19 Typical device setup for an organic tandem cell.

molecules, a combination of vacuum and solution processing and all solution processing. Due to the complexity of multilayer solution processing caused by interlayer mixing, the early reports of organic tandem cells are based on the vacuum deposition of small molecules and they certainly show increased V_{oc} and efficiencies.[182–186] Also a combination of vacuum and solution processing is a fine approach where the solution processed underlying layer is not disturbed during subsequent vacuum processing.[187–190] However, from an industrial point of view, all solution processing without the use of vacuum where each layer is processed from solution (including the metal electrode) is the most appealing because techniques like ink-jet printing, screen printing and roll-to-roll coating are less time and energy consuming and enable large scale organic solar cell production. Gilot *et al.* were the first to demonstrate a polymer tandem cell with each layer processed from solution (the metal electrode was evaporated).[191]

The technique relies on the choice of solvent for the different layers. They have to be complementary in the sense that the next solvent in the process is not affecting the material in the underlying layer. Fig. 20 illustrates the device setup realized by Gilot *et al.* The challenging step is the spincoating of the intermediate layer where the authors used a layer of zinc oxide nanoparticles spincoated from acetone prior to a layer of pH neutral PEDOT. The ZnO/PEDOT recombination layer was not affecting the underlying active layer of MDMO-PPV:PCBM and was also acting as a protective layer to support the bottom cell during deposition of the second active layer consisting of a P3HT:PCBM bulk heterojunction. The solution processed tandem cell has led to an efficiency of 6.5% for a polymer solar cell with an evaporated metal back electrode.[192] It was demonstrated by Kim *et al.* with a bulk heterojunction composite of PCPDTBT (Fig. 1) and PCBM for the bottom cell and a layer of P3HT:[70]PCBM for the top cell. For the intermediate layer the authors used a layer of TiO_x spincoated from a TiO_x precursor solution (sol–gel chemistry)[193] prior to a layer of PEDOT. The TiO_x precursor hydrolyses to TiO_x during 1 hour in air (Fig. 21) and the final TiO_x layer offers high mechanical stability to the tandem cell. The final polymer tandem cell showed an improvement of 38% in performance *versus* the best single cell.

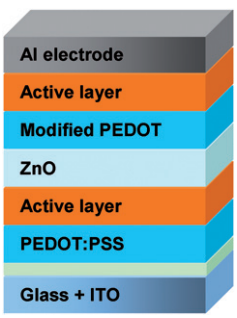

Fig. 20 Device setup for the tandem solar cell realized by Gilot *et al.*

An all solution processed tandem polymer solar cell based on thermocleavable materials has been reported by Hagemann *et al.*[109] The authors used solution-processable precursors that allow for conversion to an insoluble state by a thermal treatment. A bulk heterojunction composite of P3MHOCT and ZnO was used for the bottom cell and a blend of poly-[(3′-(2,5,9-trimethyldecan-2-yl)-oxy-carbonyl)-[2,2′;5′,2″]terthiophene-1,5″-diyl)-co-(2,3-diphenyl-thieno[3,4-b]pyrazine-5,7-diyl)] (P3TMDCTTP) and ZnO was used for the top cell (Fig. 22). Straight after each film preparation a short thermal treatment eliminated the solubilising group converting P3MHOCT to P3CT and P3TMDCTTP to P3CTTP. To separate the bottom cell from the top cell an intermediate layer of PEDOT:PSS and ZnO were used. The final tandem cell performed relatively poorly but did not involve the use of fullerenes and efficiently solved the problems associated with solubility during application of subsequent layers. In addition a solution processed metal electrode was employed. An obvious advantage of thermocleavable materials is that they offer new levels of processing after film forming. Due to the insoluble nature of the active materials after the thermal treatment there is no limit in the choice of solvents when processing the subsequent layers in the tandem cell and more research into this field appears worthwhile.

Recently a novel concept was introduced whereby the tandem solar cell is realized in a reflective geometry where the reflected light of one cell is directed towards the second one.[194–197]

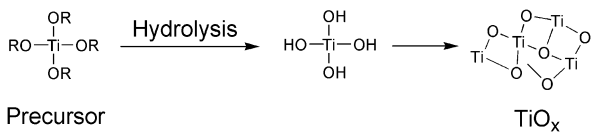

Fig. 21 Preparation of the TiO_x layer.

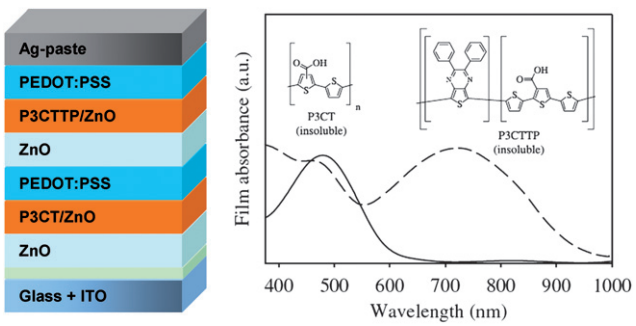

Fig. 22 Tandem solar cell based on thermocleavable materials realized by Hagemann *et al.* The active layer film absorption spectra are also shown with P3CT/ZnO plotted with a solid line and P3CTTP/ZnO plotted with a broken line. Reprinted with permission from ref. 109. © 2008 Elsevier B.V.

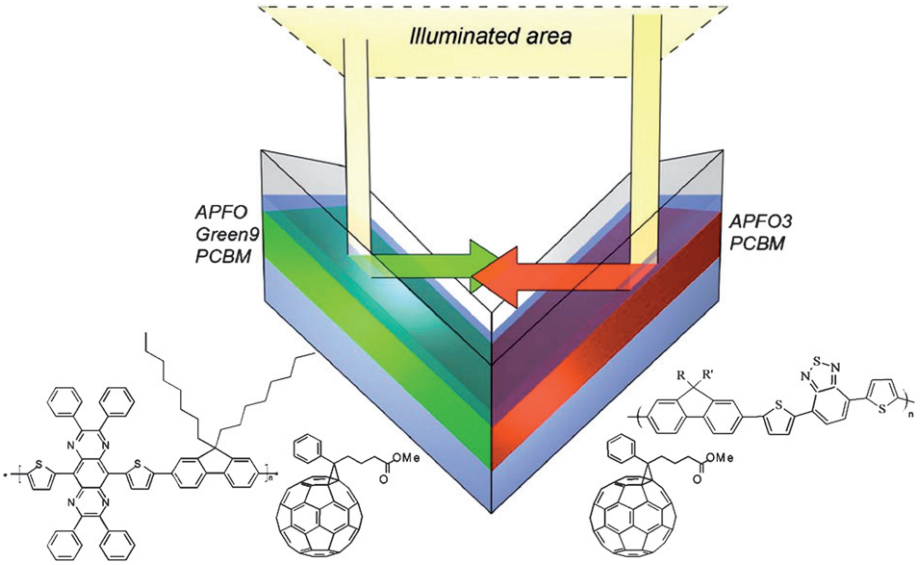

Fig. 23 Folded tandem cell realized by Tvingstedt *et al.* Sketch of the folded tandem cell and the chemical structures of the exploited alternating polyfluorenes APFO3, APFO Green-9, and the acceptor molecule PCBM. Reprinted with permission from ref. 196. © 2007 American Institute of Physics.

Tvingstedt *et al.* demonstrated that by folding two planar cells with different band gap materials toward each other, spectral broadening and light trapping are combined to give an improvement of PCE from 2% up to 3.7% upon folding from 0° to 70° (Fig. 23).[196] A bulk heterojunction composite of APFO3 and PCBM was used for one cell and APFO-Green9:PCBM for the second cell. The advantage of the folded tandem device is that it avoids complex multilayer solution processing and other problems related to multijunction stacking

Control of the nanomorphology

The nanoscale morphology is an important factor in the construction of functional organic bulk-heterojunction solar cells as it is of interest to be capable of controlling the dimension of the domains in the nanostructure such that all domain boundaries are within the exciton diffusion range in the photoactive layer. Han *et al.* have demonstrated a novel procedure to create morphologically controlled nano/microscale patterns of π-conjugated polymers.[114] An acidic mixture of polyfluorene or polythiophene bearing solubilising thermocleavable tetrahydropyranyl (THP) groups, and poly(methyl methacrylate) (PMMA) is used for the active layer. After spincoating on substrates phase separation is induced by the chemical dissimilarity of the two polymers giving rise to a nano/microscale morphology. After an acid catalyzed thermal treatment where the THP groups are eliminated the insoluble conjugated polymer remains (Fig. 24). Subsequently, PMMA is removed by treating the films with a chlorobenzene/hexane solution leaving a dot matrix of the conjugated polymer (Fig. 25).

This method, where a template is used to control the nanostructure of conjugated polymers, has been exploited by Andreasen *et al.* in a solar cell context.[198] Instead of PMMA, copper nanoparticles with an average diameter of 32 nm were used as the template to nanostructure a conjugated polymer based on P3MHOCT. Mixtures of P3MHOCT and the copper nanoparticles are processed into thin films followed by a thermal treatment whereby the solubilising side chains of the polymer were eliminated, leaving an insoluble film of conjugated P3CT with included copper nanoparticles. The copper nanoparticles could then be removed by treating the films with a THF solution of phenylazodiethylthioformamide (copper-specific solubilising agent[90,91]) leaving voids in place of the copper nanoparticles (Fig. 26). Finally the voids in the dried nanoporous films were

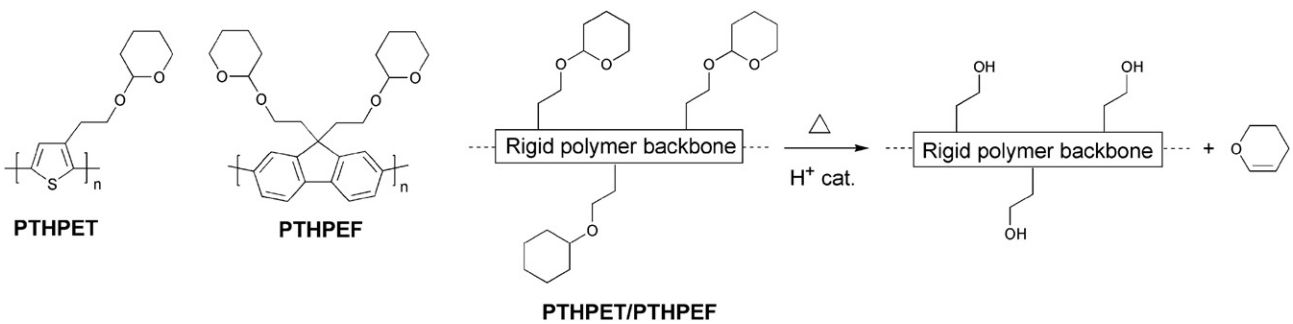

Fig. 24 Thermocleavable polymers PTHPET and PTHPEF and acid-catalyzed elimination of dihydropyran from the polymer backbone.

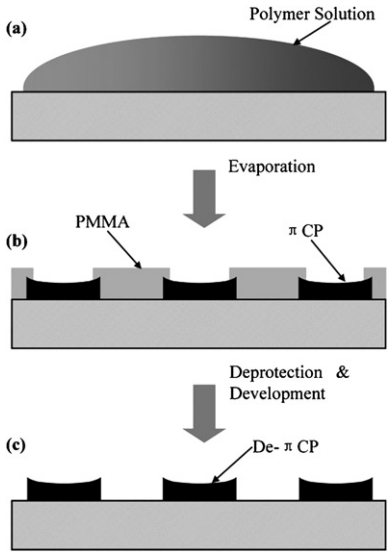

Fig. 25 Schematic illustration of the formation of a well-ordered micro and nanometre-sized π-conjugated polymer features (PTHPET or PTHPEF) by (a) solution casting, (b) self-organization, and (c) catalytic reaction and development. Reprinted with permission from ref. 114. © 2007 WILEY-VCH.

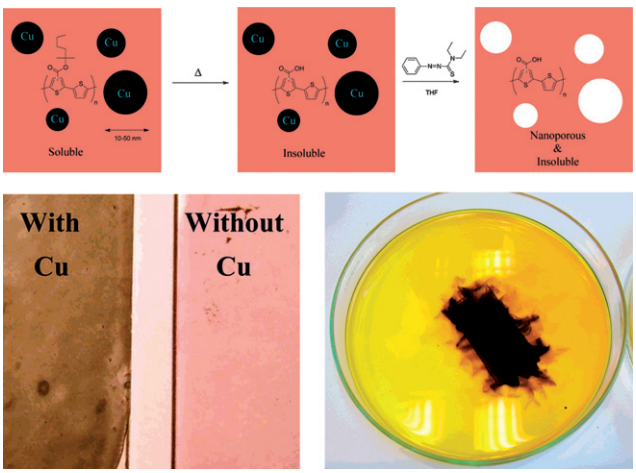

Fig. 26 Reaction scheme for the process (**above**) and pictures of the films before and after removal of the copper nanoparticles. The film loaded with copper nanoparticles has a black appearance whereas the film where the copper nanoparticles have been removed had a red color (**lower left**). The dissolution step is also shown where a device slide (50 mm × 25 mm) is covered with a THF solution of azothioformamide. The dark color is due to the formation of the copper complex of azothioformamide (**lower right**). Reprinted with permission from ref. 198. © 2007 American Chemical Society.

filled with PCBM by doctorblading forming a donor–acceptor bulk heterojunction.

However, the nanostructures had little influence on the photovoltaic effect. The best device (active area of 3 cm^2) had an open-circuit voltage of 0.43 V, a short-circuit current of 0.19 mA cm^{-2}, a fill factor of 27.4%, and a power conversion efficiency of 0.02% (0.1–0.4% for P3CT:[60]PCBM). These data are much lower than the state-of-the-art and is ascribed to the low porosity of the films (<20%) and the large size of the PCBM domains. The ideal size of the PCBM domains should be of the order of 5–10 nm, and the porosity should be closer to 50% or more. This method may find importance in the modification of nanoscale morphologies for polymer solar cell devices if it could be advanced for incorporation of larger amounts of well-distributed smaller nanoparticles (5–10 nm) into the conjugated polymer film.

Laser-induced thermal patterning is another technique to control the morphology of conjugated polymers. Gordon *et al.* have developed a method for direct thermal patterning of a thermocleavable π-conjugated polymer film containing a near-infrared (NIR) sensitive dye.[199] The NIR dye (Fig. 27) is incorporated directly into the polymer film by spincoating a NIR dye/polymer blend on a substrate.

When the film is exposed to NIR light pulses from an 830 nm laser beam the dye absorbs the irradiation and converts the NIR photons into heat by internal conversion. The polymer (PTHPET) does not absorb the NIR light. The heat produced by the dye induces thermocleavage of the THP groups. Subsequently, the NIR dye is removed by rinsing the films with methanol followed by THF leaving patterned π-conjugated polymer (Fig. 28). The patterned π-conjugated polymer shows a significant reduction in the quantum yield, compared to a pure

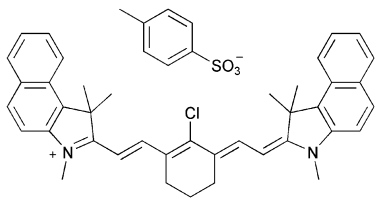

Fig. 27 NIR dye used by Gordon *et al.*[199]

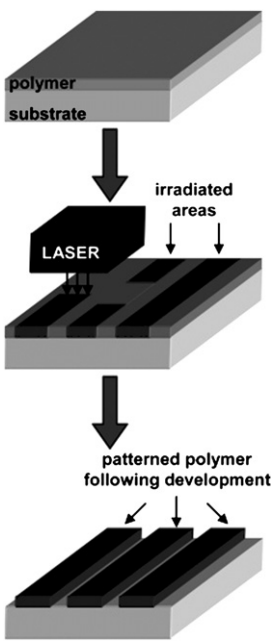

Fig. 28 Schematic diagram for the direct thermal patterning of a π-conjugated polymer using a NIR laser realized by Gordon *et al.* Reprinted with permission from ref. 199. © 2007 American Chemical Society.

PTHPET film, which is ascribed to either the presence of residual NIR dye remaining in the film after rinsing or/and coplanarisation and chain aggregation after thermocleavage of the THP groups.

To overcome this problem novel strategies have been developed where the NIR dye is not incorporated into the film. Gordon *et al.* have described a bilayer approach,[115] wherein a NIR dye is contained in a film of poly(2-hydroxyethylmethacrylate) [p(HEMA)] spincast onto a thermocleavable π-conjugated polymer film of poly(9,9-dihexylfluorene-*alt*-2-(2-thiophen-3-ethoxy)tetrahydropyran)-*co*-(9,9-dihexylfluorene-*alt*-bithiophene) (PFT-TT) (Fig. 29).

After exposure of the bilayer film to 830 nm NIR laser irradiation the p(HEMA)/NIR dye layer is removed by rinsing with methanol. Subsequent treatment of the remaining film with a THF/hexane solution removes non-cleaved PFT-TT (unexposed p(HEMA)/NIR dye regions) leaving a patterned π-conjugated polymer (Fig. 30). Using this bilayer film architecture the active conjugated polymer layer can be heated by exposure to NIR irradiation while minimizing deleterious mixing of the polymer with the NIR dye. Compared to the monolayer approach described above the π-conjugated polymer retains its photoluminescent properties showing quantum yields as high as 86% of the pristine polymer. The method is capable of imaging large surface areas, up to 1 m^2, at relatively high throughput and with micrometre size resolution (typically 5–10 μm), and thus could be valuable in the context of processing of thermocleavable polymers for solar cells.

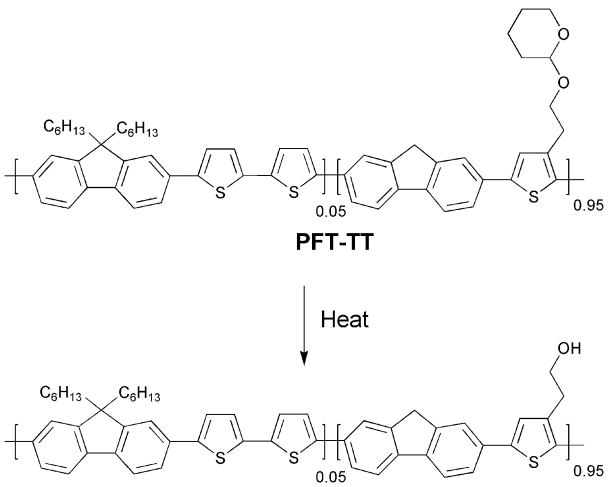

Fig. 29 PFT-TT with thermocleavable THP groups.

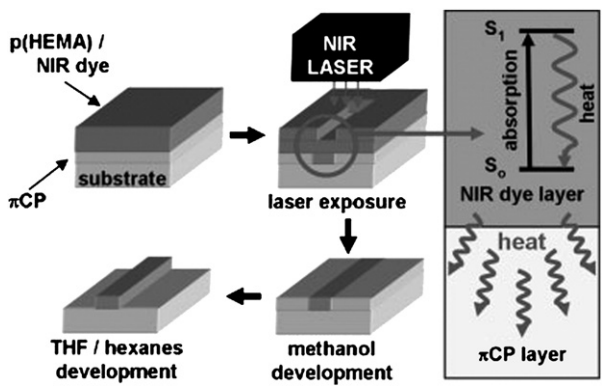

Fig. 30 Bilayer approach to laser induced direct thermal patterning of a π-conjugated polymer realized by Gordon *et al.* Reprinted with permission from ref. 115. © 2008 WILEY-VCH.

ITO-freedom and advanced device concepts

The most commonly used transparent electrode in organic photovoltaics is based on indium-tin-oxide (ITO) which has the disadvantage of being rather expensive due to the scarcity of indium which is the main material in ITO by weight. In addition, the expanding market for optoelectronic devices could create a demand so high that securing a steady supply of indium might be problematic in the near future. This generates the need of new transparent semiconducting materials with good conductivity to minimize ohmic losses or new techniques/designs of devices. There has been relatively few reports on polymer solar cells that do not employ indium.[200–208] Of these, three are directly relevant to industrial manufacturing processes.[200,201,208] The wrap through concept is well known from 1st generation photovoltaics[209] and has later been demonstrated to work well for polymer solar cells,[208] and some of the ITO free polymer solar cell module concepts have been demonstrated to work in a full roll-to-roll process.[200,201] For the latter though, the performance was significantly lower than what could be obtained using ITO based flexible substrates in a similar roll-to-roll process as shown in Fig. 31.

An alternative approach to avoid the use of indium has been introduced by Niggemann *et al.*,[210] who report the fabrication of a novel architecture in organic photovoltaic devices without the use of transparent electrodes and with extremely high voltages. Built on substrates of transparent lamellar nanostructured polymer, devices consisting of series of interconnected elementary cells (up to 1390 cells/mm) are prepared (Fig. 32). Anodes and cathodes are deposited on the vertical walls of the lamellas by thermal evaporation of titanium or MoO_3 respectively from inclined incident angles, such that anode and cathode pairs of adjacent elementary cells are interconnected at the tip of the nanolamellae. The photoactive composite (P3HT/PCBM - 3:2) is then spincoated in the final process step.

In order to suppress interconnection of adjacent cell elements by the photoactive composite, a dielectric layer of lithium fluoride was furthermore deposited at an angle on the tip of the lamellae prior to spincoating. Under AM1.5 illumination, a 17.4 mm × 7.9 mm photovoltaic nanomodule prepared in this way generated an open circuit voltage of 880 V and a short circuit current of 2×10^{-8} A. The solar power conversion efficiency is stated to be 0.008% when considering a fill factor of 25%. The concept of *wrap through* was first introduced in 1993 by Gee *et al.*[209] for silicon based solar cells and have now been implemented in polymer based photovoltaics by Zimmermann *et al.*[208] in order to avoid the use of transparent electrodes. The general idea behind wrap trough is to have both electrodes on the back side of the device, one having a traditional layered contact with the light absorber, and the other being connected to the absorber through a series of holes/channels, leading through the device, that have been filled with a highly conducting material. The holes

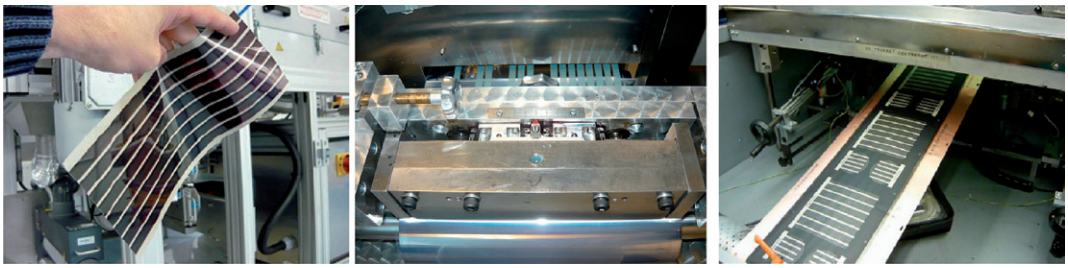

Fig. 31 Roll-to-roll coated polymer solar cells using an ITO based process (**left**) and ITO-free processes (**middle and left**).

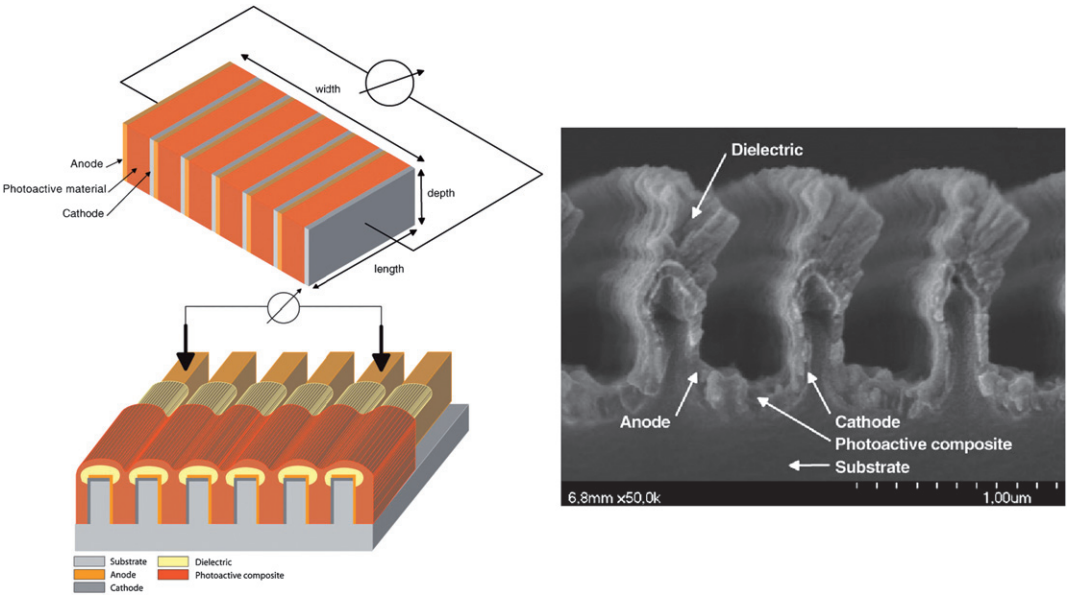

Fig. 32 High voltage devices. **Upper left**: Basic sketch of a series interconnected photovoltaic nanomodule. An elementary cell is represented by the photoactive volume sandwiched between an anode and a cathode. **Lower left**: Schematic drawing of the series interconnected photovoltaic nanomodule. Anodes and cathodes are deposited on the walls of the nanolamellae by evaporation from an inclined incident angle. The series interconnection of adjacent elementary cells is carried out by overlapping the electrodes at the tips of the lamellae. In order to suppress charge carrier recombination, the tips of the nanolamellae are coated with a dielectric layer. The electrical contact is provided *via* two contact tips positioned onto the metallised nanolamellae. **Right**: SEM cross-section of a photovoltaic nanomodule. The tips of the lamellae are coated with lithium fluoride by thermal evaporation under inclined incident angles. Reprinted with permission from ref. 210. © 2008 Wiley-VHC Verlag GmbH & Co. KGaA, Weinheim.

are placed in a pattern throughout the device that ensures good efficiency. The organic solar cell by Zimmermann *et al.* is built on a thin plastic substrate with inverted layer sequence, *i.e.* starting with the metallic electron contact. Then the active absorber layer is applied, followed by the PEDOT:PSS layer as shown in Fig. 33.

The holes/channels through the device are now created by perforation of the device with a hot needle followed by a second layer of PEDOT:PSS forming the wrap through contact. As the last step a metal (Au) back contact was evaporated thermally. Power conversion efficiencies of up to 2% were reached for parallel wrap through and 1.1% was reached for serial circuitry using simulated solar irradiation (1000 W/m^2).

Summary and outlook

From a materials point of view, the state-of-the-art in the field of organic photovoltaics has for long been represented by bulk heterojunction solar cells based on P3HT and a fullerene. Power conversion efficiencies in the 4–5% range have been reported for P3HT:PCBM devices,[46–50] but reproducibility has been difficult and average efficiencies are significantly lower than the highest reported. P3HT can only absorb light up to 650 nm, and this limited absorption of the available solar photons (up to 22.4%) has in recent years led several research teams to focus on preparation of low band gap polymers in order to be able to exploit a larger part of the solar spectrum. Recently new low band gap polymer:PCBM composites have shown device efficiencies close to and even exceeding that of P3HT:PCBM with plenty of room for improvement.[56–58,192]

Another trail deviating from the traditional P3HT:PCBM blends is the use of two different polymers to act as donor and acceptor in a polymer:polymer heterojunction. Although very little effort has been put into this area moderately good results have been achieved (~1.8%).[69] The advantages of a heterojunction consisting only of absorbing materials, allowing for absorption over a wider spectral range, together with the relative ease of tuning the donor–acceptor energy levels make the polymer:polymer solar cell a potential player in future research. Two major challenges will be the design of good n-type polymers and

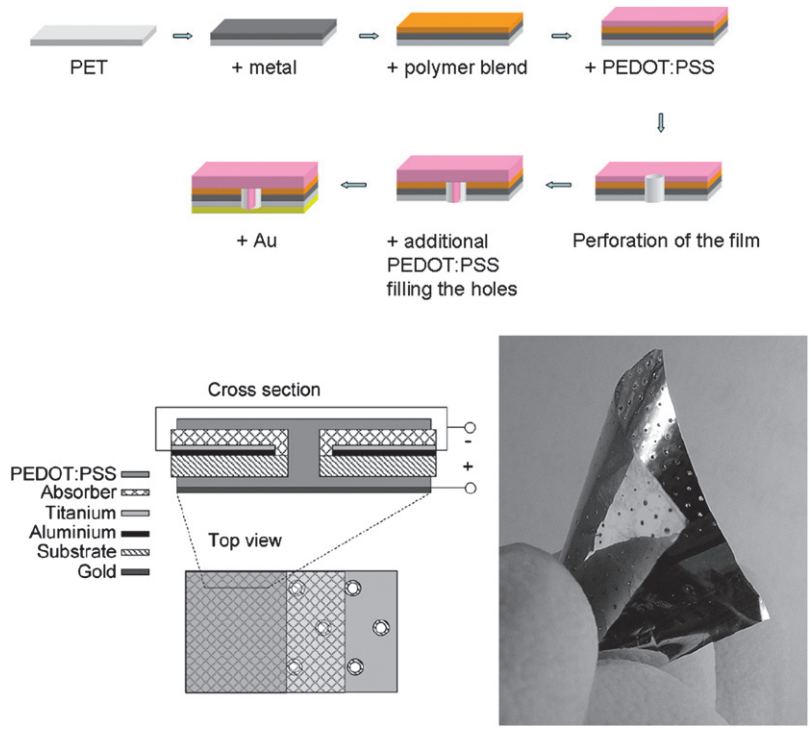

Fig. 33 Wrap through cells. **Top and lower left**: Schematic representation of the inverted layer sequence starting with the metallic contact on the plastic substrate followed by the active polymer blend and PEDOT:PSS. After perforation of the film a second layer of PEDOT:PSS is applied forming the wrap through contact and a gold back electrode is applied to finish the circuitry. **Right**: Picture of a wrap through device. The two bottom representations are reprinted with permission from ref. 211. © 2007 Elsevier B. V.

dealing with the tendency for phase separation of the polymers into larger domains instead of into a fine interpenetrating network that allows for efficient charge separation and transport.

The use of precursor or thermocleavable sidechain routes also results in a higher concentration of the photoactive participant. Heat treatment of the device film results in chemical reactions whereby removal of part of the material (sometimes up to 50% or more by weight) that constitutes the original film is achieved. Thus formed conjugated polymers have no solubilising sidechains and are insoluble in all solvents which induce stability towards degradation and furthermore allows for preparation of multilayer devices by all solution processing.[109] Light cleavage using a near-infrared (NIR) dye that is either incorporated in the polymer film or employed as a separate layer on top of the polymer is a sophisticated form of dealing with thermocleavable materials which allows for patterning as thermocleavage only occurs in areas exposed to NIR light.[114,115,199] The non-exposed areas which are still soluble can subsequently be removed.

Multilayer devices (tandem cells) allow for use of several types of polymer that each absorb light at different regions of the solar spectrum and hence render the exploitation of the incoming light more effective. The main challenge when preparing all solution processed multilayer devices is to find a way to add a new layer without destroying the underlying layer. Besides the method of rendering the polymer insoluble this can be done by careful tuning of the solvents used for each layer so that the top layer is always insoluble in the solvent used next. PCEs of up to 6.5% have been reported by the latter method.[192] An alternative approach to the already mentioned is to use a reflective geometry where the reflected light from one cell is directed towards another and *vice versa*. This again allows for the use of supplementary polymers that each absorbs light at different wavelengths.

With respect to methods trying to induce stability to the device the use of materials that can be cross-linked after film preparation and consequently a 'locking' of the morphology, should be mentioned. Limited research has been carried out within this area that has the potential of solving the problem of phase separation/aggregation that is observed for P3HT:PCBM devices upon thermal treatment. Finding ways to prepare highly cross-linked films would also make the process useful for multilayer devices.

Fabrication of hybrid solar cells is an area that has received quite a lot of attention with respect to device architecture trying to optimize charge separation and collection. Designs where the inorganic part of the heterojunction is represented as nanoparticles, are generated *in situ*, or as nanorod or -pore structures have been investigated and recently several reports of combining the traditional P3HT:PCBM setup with an inorganic into a 3-component heterojunction has been successful in improving the efficiencies compared with the corresponding P3HT:PCPM devices without the inorganic. Similar tendencies have been reported for heterojunctions of surface modified inorganics with different dyes, where the concentration of the dye is so small that its contribution to absorption is minimal to negligible. Instead the dye aids in charge separation and suppresses back recombination. The latter two examples are good indicators that combining techniques and thinking differently can lead to improvement.

The latest reports are dealing with the fact that indium, which is a major component in the most commonly used transparent electrodes (ITO), is a scarce and expensive element in a world market with a growing demand because of the development within optoelectronics. In order to approach this problem new device designs have been developed to function without ITO. High voltage devices yielding open circuit voltages up to 880 V,[210] introduction of the *wrap through* concept implemented for polymer based solar cells on thin flexible plastic substrates,[208] and some of the ITO free polymer solar cell module concepts have even been demonstrated to work in a full roll-to-roll process.[200,201] These new concepts still need optimization, but they are approaching relevant issues for industrial manufacturing processes.[134,212]

It is our opinion that, if the field of polymer solar cells is to advance to a degree where it finally succeeds in leaving the lab to go into actual production and enjoy widespread use, it will be necessary to deviate, in much larger extent than seen so far, from the tendency to just accept the flaws of the 'main road' in stead of trying to deal with them. Besides development of new device designs, new materials have to be developed. Tuning of donor–acceptor energy levels in polymer:polymer heterojunctions, in hybrid solar cells or a combination of both, attempts to minimize the amount of non-absorbing or -conducting material from the heterojunction as well as stabilising the same by use of thermocleavable materials are some of the paths where we see a large potential.

There is furthermore a need for more approaches to implement the laboratory small scale fabrication of devices into actual large scale production, in order to gain familiarity with the inevitable problems and challenges that are related to this. This will place demands on the materials properties such that they match relevant processes. This area is relatively new.

Conclusion

Materials, processes and devices that deviate significantly from the standard approach, of rigid glass substrates, indium-tin-oxide electrodes, spincoated layers of conjugated polymer/fullerene mixtures and evaporated metal electrodes in a flat multilayer geometry, that is generally used in the preparation of polymer and organic solar cells, have been presented in this review. Advanced materials such as thermocleavable polymers, for higher level processing and stability, in combination with advanced device concepts like tandem cells and ITO free roll-to-roll coating. All have the potential to go beyond the current state-of-the-art towards real progress in terms of better performance, higher operational stability, facile processing and easier, faster and lower cost production.

Acknowledgements

This work was supported by the Danish Strategic Research Council (DSF 2104-05-0052 and 2104-07-0022).

References

1 T. Ameri, G. Dennler, C. Lungenschmied and C. J. Brabec, *Energy Environ. Sci.*, 2009, **2**, 347–363.
2 J. Bouclé, P. Ravirajan and J. Nelson, *J. Mater. Chem.*, 2007, **17**, 3141–3153.
3 C. J. Brabec, N. S. Sariciftci and J. C. Hummelen, *Adv. Funct. Mater.*, 2001, **11**, 15–26.
4 C. J. Brabec, J. A. Hauch, P. Schilinsky and C. Waldauf, *MRS Bull.*, 2005, **30**, 50–52.
5 C. J. Brabec and J. R. Durrant, *MRS Bull.*, 2008, **33**, 670–675.
6 E. Bundgaard and F. C. Krebs, *Sol. Energy Mater. Sol. Cells*, 2007, **91**, 954–985.
7 L. M. Chen, Z. R. Hong, G. Li and Y. Yang, *Adv. Mater.*, 2009, **21**, 1434–1449.
8 K. M. Coakley and M. D. McGehee, *Chem. Mater.*, 2004, **16**, 4533–4542.
9 K. M. Coakley, Y. X. Liu, C. Goh and M. D. McGehee, *MRS Bull.*, 2005, **30**, 37–40.
10 G. Dennler, M. C. Scharber and C. J. Brabec, *Adv. Mater.*, 2009, **21**, 1323–1338.
11 S. Günes, H. Neugebauer and N. S. Sariciftci, *Chem. Rev.*, 2007, **107**, 1324–1338.
12 S. Günes and N. S. Sariciftci, *Inorg. Chim. Acta*, 2008, **361**, 581–588.
13 A. Hadipour, B. De Boer and P. W. M. Blom, *Org. Electron.*, 2008, **9**, 617–624.
14 A. Hadipour, B. De Boer and P. W. M. Blom, *Adv. Funct. Mater.*, 2008, **18**, 169–181.
15 H. Hoppe and N. S. Sariciftci, *J. Mater. Res.*, 2004, **19**, 1924–1945.
16 R. A. J. Janssen, J. C. Hummelen and N. S. Saricifti, *MRS Bull.*, 2005, **30**, 33–36.
17 M. Jørgensen, K. Norrman and F. C. Krebs, *Sol. Energy Mater. Sol. Cells*, 2008, **92**, 686–714.
18 B. Kippelen and J. L. Bredas, *Energy Environ. Sci.*, 2009, **2**, 251–261.
19 F. C. Krebs, *Refocus*, 2005, **6**, 38–39.
20 R. Kroon, M. Lenes, J. C. Hummelen, P. W. M. Blom and B. De Boer, *Polym. Rev.*, 2008, **48**, 531–582.
21 M. T. Lloyd, J. E. Anthony and G. G. Malliaras, *Mater. Today*, 2007, **10**, 34–41.
22 A. C. Mayer, S. R. Scully, B. E. Hardin, M. W. Rowell and M. D. McGehee, *Mater. Today*, 2007, **10**, 28–33.
23 B. P. Rand, J. Genoe, P. Heremans and J. Poortmans, *Progr. Photovolt.: Res. Appl.*, 2007, **15**, 659–676.
24 H. Spanggaard and F. C. Krebs, *Sol. Energy Mater. Sol. Cells*, 2004, **83**, 125–146.
25 B. C. Thompson and J. M. J. Frechet, *Angew. Chem., Int. Ed.*, 2008, **47**, 58–77.
26 C. Winder and N. S. Sariciftci, *J. Mater. Chem.*, 2004, **14**, 1077–1086.
27 J. Wood (Ed.), *Mater.Today*, 2007, 10, pp. 1–50.
28 S. E. Shaheen, D. S. Ginley, and G. E. Jabbour (Guest Eds.), *MRS Bull.*, 2005, 30, pp. 10–52.
29 J. Poortmans (Guest Ed.), *Prog.Photovolt.*, 2007, 15, pp. 657–754.
30 F. C. Krebs (Guest Ed.), *Sol. Energy Mater.*, 2004, 83, pp. 125–321.
31 F. C. Krebs (Guest Ed.), *Sol. Energy Mater.*, 2007, 91, pp. 953–1036.
32 F. C. Krebs (Guest Ed.), *Sol. Energy Mater.*, 2008, 92, pp. 685–820.
33 F. C. Krebs (Guest Ed.), *Sol. Energy Mater.*, 2009, 93, pp. 393–538.
34 *Organic Photovoltaics: Concepts and Realization*, ed. Brabec, C. J., Dyakonov, V., and Parisi, J., Springer, New York, 2003.
35 *Organic Photovoltaics: Mechanisms, Materials and Devices*, ed. Sun, S. S. and Sariciftci, N. S., CRC Press, Taylor & Francis Group, Florida, USA, 2005.
36 *Nanostructured Materials for Solar Energy Conversion*, ed. Soga, T., Elsevier, UK, 2006.
37 *Polymer Photovoltaics: A Practical Approach*, ed. Krebs, F. C., SPIE Press, Bellingham, 2008.
38 *Organic Photovoltaics: Materials, Device Physics and Manufacturing Technologies*, ed. Brabec, C. J., Scherf, U., and Dyakonov, V., Wiley-VCH, Weinheim, 2008.
39 N. S. Sariciftci, L. Smilowitz, A. J. Heeger and F. Wudl, *Science*, 1992, **258**, 1474–1476.
40 G. Yu, J. Gao, J. C. Hummelen, F. Wudl and A. J. Heeger, *Science*, 1995, **270**, 1789–1791.
41 Shawn R. Scully and Michael D. McGehee, *J. Appl. Phys.*, 2006, **100**, 034907.
42 D. E. Markov, J. C. Hummelen, P. W. M. Blom and A. B. Sieval, *Phys. Rev. B: Condens. Matter Mater. Phys.*, 2005, **72**, 045216.
43 P. Peumans, A. Yakimov and S. R. Forrest, *J. Appl. Phys.*, 2003, **93**, 3693–3723.
44 O. Douheret, A. Swinnen, S. Bertho, I. Haeldermans, J. D'Haen, M. D'Olieslaeger, D. Vanderzande and J. V. Manca, *Progr. Photovolt.: Res. Appl.*, 2007, **15**, 713–726.

45 B. V. Andersson, A. Herland, S. Masich and O. Inganas, *Nano Lett.*, 2009, **9**, 853–855.
46 C. J. Ko, Y. K. Lin, F. C. Chen and C. W. Chu, *Appl. Phys. Lett.*, 2007, **90**, 063509.
47 G. Li, V. Shrotriya, J. S. Huang, Y. Yao, T. Moriarty, K. Emery and Y. Yang, *Nat. Mater.*, 2005, **4**, 864–868.
48 W. L. Ma, C. Y. Yang, X. Gong, K. Lee and A. J. Heeger, *Adv. Funct. Mater.*, 2005, **15**, 1617–1622.
49 M. Reyes-Reyes, K. Kim and D. L. Carroll, *Appl. Phys. Lett.*, 2005, **87**, 083506–3.
50 M. Reyes-Reyes, K. Kim, J. Dewald, R. Lopez-Sandoval, A. Avadhanula, S. Curran and D. L. Carroll, *Org. Lett.*, 2005, **7**, 5749–5752.
51 G. Dennler, *Mater. Today*, 2007, **10**, 56.
52 J. Gilot, M. M. Wienk and R. A. J. Janssen, *Nat. Mater.*, 2007, **6**, 704.
53 M. K. Riede, T. Mueller, B. Maennig, K. Leo, K. O. Sylvester-Hvid, B. Zimmermann, M. Niggemann and A. Gombert, *Appl. Phys. Lett.*, 2008, **92**, 076101.
54 G. P. Smestad, F. C. Krebs, C. M. Lampert, C. G. Granqvist, K. L. Chopra, X. Mathew and H. Takakura, *Sol. Energy Mater. Sol. Cells*, 2008, **92**, 371–373.
55 H. A. M. van Mullekom, J. A. J. M. Vekemans, E. E. Havinga and E. W. Meijer, *Mater. Sci. Eng., R*, 2001, **32**, 1–40.
56 J. H. Hou, H. Y. Chen, S. Q. Zhang, G. Li and Y. Yang, *J. Am. Chem. Soc.*, 2008, **130**, 16144.
57 Y. Y. Liang, D. Q. Feng, Y. Wu, S. T. Tsai, G. Li, C. Ray and L. P. Yu, *J. Am. Chem. Soc.*, 2009, **131**, 7792–7799.
58 J. Peet, J. Y. Kim, N. E. Coates, W. L. Ma, D. Moses, A. J. Heeger and G. C. Bazan, *Nat. Mater.*, 2007, **6**, 497–500.
59 Z. Zhu, D. Waller, R. Gaudiana, M. Morana, D. Muhlbacher, M. Scharber and C. Brabec, *Macromolecules*, 2007, **40**, 1981–1986.
60 S. R. Forrest, *MRS Bull.*, 2005, **30**, 28–32.
61 L. J. A. Koster, V. D. Mihailetchi and P. W. M. Blom, *Appl. Phys. Lett.*, 2006, **88**, 093511.
62 M. C. Scharber, D. Wuhlbacher, M. Koppe, P. Denk, C. Waldauf, A. J. Heeger and C. L. Brabec, *Adv. Mater.*, 2006, **18**, 789.
63 S. H. Park, A. Roy, S. Beaupre, S. Cho, N. Coates, J. S. Moon, D. Moses, M. Leclerc, K. Lee and A. J. Heeger, *Nat. Photonics*, 2009, **3**, 297–302.
64 N. Blouin, A. Michaud, D. Gendron, S. Wakim, E. Blair, R. Neagu-Plesu, M. Belletete, G. Durocher, Y. Tao and M. Leclerc, *J. Am. Chem. Soc.*, 2008, **130**, 732–742.
65 J. H. Hou, M. H. Park, S. Q. Zhang, Y. Yao, L. M. Chen, J. H. Li and Y. Yang, *Macromolecules*, 2008, **41**, 6012–6018.
66 F. B. Kooistra, J. Knol, F. Kastenberg, L. M. Popescu, W. J. H. Verhees, J. M. Kroon and J. C. Hummelen, *Org. Lett.*, 2007, **9**, 551–554.
67 J. J. M. Halls, C. A. Walsh, N. C. Greenham, E. A. Marseglia, R. H. Friend, S. C. Moratti and A. B. Holmes, *Nature*, 1995, **376**, 498–500.
68 G. Yu and A. J. Heeger, *J. Appl. Phys.*, 1995, **78**, 4510–4515.
69 C. R. McNeill, A. Abrusci, J. Zaumseil, R. Wilson, M. J. McKiernan, J. H. Burroughes, J. J. M. Halls, N. C. Greenham and R. H. Friend, *Appl. Phys. Lett.*, 2007, **90**, 193506.
70 M. M. Wienk, J. M. Kroon, W. J. H. Verhees, J. Knol, J. C. Hummelen, P. A. van Hal and R. A. J. Janssen, *Angew. Chem., Int. Ed.*, 2003, **42**, 3371–3375.
71 M. Granstrom, K. Petritsch, A. C. Arias, A. Lux, M. R. Andersson and R. H. Friend, *Nature*, 1998, **395**, 257–260.
72 T. Kietzke, H. H. Horhold and D. Neher, *Chem. Mater.*, 2005, **17**, 6532–6537.
73 M. M. Koetse, J. Sweelssen, K. T. Hoekerd, H. F. M. Schoo, S. C. Veenstra, J. M. Kroon, X. N. Yang and J. Loos, *Appl. Phys. Lett.*, 2006, **88**, 083504.
74 R. A. Wessling, *J.Pol.Sci.- Pol.Symp.*, 1985, 55–66.
75 D. R. Gagnon, J. D. Capistran, F. E. Karasz, R. W. Lenz and S. Antoun, *Polymer*, 1987, **28**, 567–573.
76 R. W. Lenz, C. C. Han, J. Stengersmith and F. E. Karasz, *J. Polym. Sci., Part A: Polym. Chem.*, 1988, **26**, 3241–3249.
77 R. O. Garay, B. Mayer, F. E. Karasz and R. W. Lenz, *J. Polym. Sci., Part A: Polym. Chem.*, 1995, **33**, 525–531.
78 W. J. Feast and J. N. Winter, *J. Chem. Soc., Chem. Commun.*, 1985, 202–203.
79 D. C. Bott, C. S. Brown, C. K. Chai, N. S. Walker, W. J. Feast, P. J. S. Foot, P. D. Calvert, N. C. Billingham and R. H. Friend, *Synth. Met.*, 1986, **14**, 245–269.
80 A. Furlani, C. Napoletano, M. V. Russo and W. J. Feast, *Polym. Bull.*, 1986, **16**.
81 H. G. Gilch and W. L. Wheelwri, *J. Polym. Sci., Part A-1*, 1966, **4**, 1337–1347.
82 H. Spreitzer, H. Becker, E. Kluge, W. Kreuder, H. Schenk, R. Demandt and H. Schoo, *Adv. Mater.*, 1998, **10**, 1340–1343.
83 F. Louwet, D. Vanderzande, J. Gelan and J. Mullens, *Macromolecules*, 1995, **28**, 1330–1331.
84 F. Louwet, D. Vanderzande and J. Gelan, *Synth. Met.*, 1995, **69**, 509–510.
85 F. Louwet, D. Vanderzande and J. Gelan, *Synth. Met.*, 1992, **52**, 125–130.
86 T. A. Chen and R. D. Rieke, *J. Am. Chem. Soc.*, 1992, **114**, 10087–10088.
87 T. A. Chen, X. M. Wu and R. D. Rieke, *J. Am. Chem. Soc.*, 1995, **117**, 233–244.
88 R. D. McCullough, R. D. Lowe, M. Jayaraman and D. L. Anderson, *J. Org. Chem.*, 1993, **58**, 904–912.
89 F. C. Krebs, R. B. Nyberg and M. Jørgensen, *Chem. Mater.*, 2004, **16**, 1313–1318.
90 K. T. Nielsen, K. Bechgaard and F. C. Krebs, *Macromolecules*, 2005, **38**, 658–659.
91 K. T. Nielsen, K. Bechgaard and F. C. Krebs, *Synthesis*, 2006, 1639–1644.
92 K. T. Nielsen, P. Harris, K. Bechgaard and F. C. Krebs, *Acta Crystallogr.*, 2007, **B-63**, 151–156.
93 F. C. Krebs and H. Spanggaard, *Chem. Mater.*, 2005, **17**, 5235–5237.
94 F. C. Krebs and K. Norrman, *Progr. Photovolt.: Res. Appl.*, 2007, **15**, 697–712.
95 K. Norrman, J. Alstrup, M. Jørgensen, M. Lira-Cantu, N. B. Larsen and F. C. Krebs, *Organic Photovoltaics VII*, 2006, **6334**, U100–U111.
96 K. Norrman and F. C. Krebs, *Sol. Energy Mater.*, 23-1-2006, **90**, 213–227.
97 M. Bjerring, J. S. Nielsen, A. Siu, N. C. Nielsen and F. C. Krebs, *Sol. Energy Mater. Sol. Cells*, 2008, **92**, 772–784.
98 M. Bjerring, J. S. Nielsen, N. C. Nielsen and F. C. Krebs, *Macromolecules*, 2007, **40**, 6012–6013.
99 S. A. Gevorgyan and F. C. Krebs, *Chem. Mater.*, 2008, **20**, 4386–4390.
100 J. S. Liu, E. N. Kadnikova, Y. X. Liu, M. D. McGehee and J. M. J. Frechet, *J. Am. Chem. Soc.*, 2004, **126**, 9486–9487.
101 F. Banishoeib, P. Adriaensens, S. Berson, S. Guillerez, O. Douheret, J. Manca, S. Fourier, T. J. Cleij, L. Lutsen and D. Vanderzande, *Sol. Energy Mater. Sol. Cells*, 2007, **91**, 1026–1034.
102 F. Banishoeib, A. Henckens, S. Fourier, G. Vanhooyland, M. Breselge, J. Manca, T. J. Cleij, L. Lutsen, D. Vanderzande, L. H. Nguyen, H. Neugebauer and N. S. Sariciftci, *Thin Solid Films*, 2008, **516**, 3978–3988.
103 C. Girotto, D. Cheyns, T. Aernouts, F. Banishoeib, L. Lutsen, T. J. Cleij, D. Vanderzande, J. Genoe, J. Poortman and P. Heremans, *Org. Electron.*, 2008, **9**, 740–746.
104 A. Henckens, K. Colladet, S. Fourier, T. J. Cleij, L. Lutsen, J. Gelan and D. Vanderzande, *Macromolecules*, 2005, **38**, 19–26.
105 L. H. Nguyen, S. Gunes, H. Neugebauer, N. S. Sariciftci, F. Banishoeib, A. Henckens, T. Cleij, L. Lutsen and D. Vanderzande, *Sol. Energy Mater. Sol. Cells*, 2006, **90**, 2815–2828.
106 F. Padinger, T. Fromherz, P. Denk, C. J. Brabec, J. Zettner, T. Hierl and N. S. Sariciftci, *Synth. Met.*, 2001, **121**, 1605–1606.
107 R. D. Scurlock, B. J. Wang, P. R. Ogilby, J. R. Sheats and R. L. Clough, *J. Am. Chem. Soc.*, 1995, **117**, 10194–10202.
108 M. H. Petersen, S. A. Gevorgyan and F. C. Krebs, *Macromolecules*, 2008, **41**, 8986–8994.
109 O. Hagemann, M. Bjerring, N. C. Nielsen and F. C. Krebs, *Sol. Energy Mater. Sol. Cells*, 2008, **92**, 1327–1335.
110 C. Edder, P. B. Armstrong, K. B. Prado and J. M. J. Frechet, *Chem. Commun.*, 2006, 1965–1967.
111 G. A. Power, P. Hodge and N. B. McKeown, *Chem. Commun.*, 1996, 655–656.
112 J. H. Edwards, W. J. Feast and D. C. Bott, *Polymer*, 1984, **25**, 395–398.
113 J. F. Yu and S. Holdcroft, *Macromolecules*, 2000, **33**, 5073–5079.

114 X. Han, X. W. Chen and S. Holdcroft, *Adv. Mater.*, 2007, **19**, 1697–1702.
115 T. J. Gordon, G. Vamvounis and S. Holdcroft, *Adv. Mater.*, 2008, **20**, 2486–2490.
116 J. H. Burroughes, D. D. C. Bradley, A. R. Brown, R. N. Marks, K. Mackay, R. H. Friend, P. L. Burns and A. B. Holmes, *Nature*, 1990, **347**, 539–541.
117 S. Bertho, I. Haeldermans, A. Swinnen, W. Moons, T. Martens, L. Lutsen, D. Vanderzande, J. Manca, A. Senes and A. Bonfiglio, *Sol. Energy Mater. Sol. Cells*, 2007, **91**, 385–389.
118 S. Bertho, G. Janssen, T. J. Cleij, B. Conings, W. Moons, A. Gadisa, J. D'Haen, E. Goovaerts, L. Lutsen, J. Manca and D. Vanderzande, *Sol. Energy Mater. Sol. Cells*, 2008, **92**, 753–760.
119 K. Sivula, C. K. Luscombe, B. C. Thompson and J. M. J. Frechet, *J. Am. Chem. Soc.*, 2006, **128**, 13988–13989.
120 K. Sivula, Z. T. Ball, N. Watanabe and J. M. J. Frechet, *Adv. Mater.*, 2006, **18**, 206.
121 C. H. Woo, B. C. Thompson, B. J. Kim, M. F. Toney and M. J. Frechet, *J. Am. Chem. Soc.*, 2008, **130**, 16324–16329.
122 M. Drees, H. Hoppe, C. Winder, H. Neugebauer, N. S. Sariciftci, W. Schwinger, F. Schaffler, C. Topf, M. C. Scharber, Z. G. Zhu and R. Gaudiana, *J. Mater. Chem.*, 2005, **15**, 5158–5163.
123 Z. Zhu, S. Hadjikyriacou, D. Waller and R. Gaudiana, *J. Macromol. Sci., Part A: Pure Appl. Chem.*, 2004, **41**, 1467–1487.
124 S. Miyanishi, K. Tajima and K. Hashimoto, *Macromolecules*, 2009, **42**, 1610–1618.
125 L. D. Bozano, K. R. Carter, V. Y. Lee, R. D. Miller, R. DiPietro and J. C. Scott, *J. Appl. Phys.*, 2003, **94**, 3061–3068.
126 Y. N. Li, J. F. Ding, M. Day, Y. Tao, J. P. Lu and M. D'iorio, *Chem. Mater.*, 2003, **15**, 4936–4943.
127 C. D. Müller, A. Falcou, N. Reckefuss, M. Rojahn, V. Wiederhirn, P. Rudati, H. Frohne, O. Nuyken, H. Becker and K. Meerholz, *Nature*, 2003, **421**, 829–833.
128 G. L. Wu, C. H. Yang, B. H. Fan, B. Zhang, X. M. Chen and Y. F. Li, *J. Appl. Polym. Sci.*, 2006, **100**, 2336–2342.
129 H. Yan, P. Lee, N. R. Armstrong, A. Graham, G. A. Evmenenko, P. Dutta and T. J. Marks, *J. Am. Chem. Soc.*, 2005, **127**, 3172–3183.
130 H. Yan, M. H. Yoon, A. Facchetti and T. J. Marks, *Appl. Phys. Lett.*, 2005, **87**, 183501–1.
131 C. H. Yang, J. H. Hou, B. Zhang, S. Q. Zhang, C. He, H. Fang, Y. Q. Ding, J. P. Ye and Y. F. Li, *Macromol. Chem. Phys.*, 2005, **206**, 1311–1318.
132 M. Jørgensen, O. Hagemann, J. Alstrup and F. C. Krebs, *Sol. Energy Mater. Sol. Cells*, 2009, **93**, 413–421.
133 F. C. Krebs and M. Jørgensen., WO, 2007118850, 2007.
134 F. C. Krebs, M. Jørgensen, K. Norrman, O. Hagemann, J. Alstrup, T. D. Nielsen, J. Fyenbo, K. Larsen and J. Kristensen, *Sol. Energy Mater. Sol. Cells*, 2009, **93**, 422–441.
135 F. C. Krebs, *Sol. Energy Mater. Sol. Cells*, 2009, **93**, 465–475.
136 E. Itoh, Y. Takamizawa and K. Miyairi, *Jpn. J. Appl. Phys.*, 2008, **47**, 509–512.
137 S. S. Kim, J. Jo, C. Chun, J. C. Hong and D. Y. Kim, *J. Photochem. Photobiol., A*, 2007, **188**, 364–370.
138 N. Kudo, S. Honda, Y. Shimazaki, H. Ohkita, S. Ito and H. Benten, *Appl. Phys. Lett.*, 2007, **90**, 183513.
139 C. Y. Kuo, W. C. Tang, C. Gau, T. F. Guo and D. Z. Jeng, *Appl. Phys. Lett.*, 2008, **93**, 033307.
140 Y. Y. Lin, T. H. Chu, C. W. Chen and W. F. Su, *Appl. Phys. Lett.*, 2008, **92**, 053312.
141 Y. Y. Lin, T. H. Chu, S. S. Li, C. H. Chuang, C. H. Chang, W. F. Su, C. P. Chang, M. W. Chu and C. W. Chen, *J. Am. Chem. Soc.*, 2009, **131**, 3644–3649.
142 M. C. Wu, C. H. Chang, H. H. Lo, Y. S. Lin, Y. Y. Lin, W. C. Yen, W. F. Su, Y. F. Chen and C. W. Chen, *J. Mater. Chem.*, 2008, **18**, 4097–4102.
143 Ming-Chung Wu, Hsueh-Chung Liao, Hsi-Hsing Lo, Sharon Chen, Yun-Yue Lin, Wei-Che Yen, Tsung-Wei Zeng, Chun-Wei Chen, Yang-Fang Chen and Wei-Fang Su, *Sol. Energy Mater. Sol. Cells*, 2009, **93**, 961–965.
144 Tsung-Wei Zeng, Hsi-Hsing Lo, Chia-Hao Chang, Yun-Yue Lin, Chun-Wei Chen and Wei-Fang Su, *Sol. Energy Mater. Sol. Cells*, 2009, **93**, 952–957.
145 R. Zhu, C. Y. Jiang, X. Z. Liu, B. Liu, A. Kumar and S. Ramakrishna, *Appl. Phys. Lett.*, 2008, **93**, 013102.
146 W. J. E. Beek, M. M. Wienk and R. A. J. Janssen, *Adv. Mater.*, 2004, **16**, 1009–1013.
147 W. J. E. Beek, L. H. Slooff, M. M. Wienk, J. M. Kroon and R. A. J. Janssen, *Adv. Funct. Mater.*, 2005, **15**, 1703–1707.
148 Y. Y. Lin, C. W. Chen, T. H. Chu, W. F. Su, C. C. Lin, C. H. Ku, J. J. Wu and C. H. Chen, *J. Mater. Chem.*, 2007, **17**, 4571–4576.
149 Y. Y. Lin, Y. Y. Lee, L. W. Chang, J. J. Wu and C. W. Chen, *Appl. Phys. Lett.*, 2009, **94**, 063308.
150 D. J. D. Moet, L. J. A. Koster, B. De Boer and P. W. M. Blom, *Chem. Mater.*, 2007, **19**, 5856–5861.
151 D. C. Olson, J. Piris, R. T. Collins, S. E. Shaheen and D. S. Ginley, *Thin Solid Films*, 2006, **496**, 26–29.
152 D. C. Olson, S. E. Shaheen, R. T. Collins and D. S. Ginley, *J. Phys. Chem. C*, 2007, **111**, 16670–16678.
153 K. Takanezawa, K. Hirota, Q. S. Wei, K. Tajima and K. Hashimoto, *J. Phys. Chem. C*, 2007, **111**, 7218–7223.
154 K. Takanezawa, K. Tajima and K. Hashimoto, *Appl. Phys. Lett.*, 2008, **93**, 063308.
155 R. Thitima, C. Patcharee, S. Takashi and Y. Susumu, *Solid-State Electron.*, 2009, **53**, 176–180.
156 H. M. P. Wong, P. Wang, A. Abrusci, M. Svensson, M. R. Andersson and N. C. Greenham, *J. Phys. Chem. C*, 2007, **111**, 5244–5249.
157 F. C. Krebs, *Sol. Energy Mater. Sol. Cells*, 2008, **92**, 715–726.
158 F. C. Krebs, Y. Thomann, R. Thomann and J. W. Andreasen, *Nanotechnology*, 2008, **19**, 424013.
159 I. Gur, N. A. Fromer, C. P. Chen, A. G. Kanaras and A. P. Alivisatos, *Nano Lett.*, 2007, **7**, 409–414.
160 W. U. Huynh, J. J. Dittmer and A. P. Alivisatos, *Science*, 2002, **295**, 2425–2427.
161 B. Q. Sun, E. Marx and N. C. Greenham, *Nano Lett.*, 2003, **3**, 961–963.
162 B. Q. Sun, H. J. Snaith, A. S. Dhoot, S. Westenhoff and N. C. Greenham, *J. Appl. Phys.*, 2005, **97**, 014914.
163 B. Q. Sun and N. C. Greenham, *Phys. Chem. Chem. Phys.*, 2006, **8**, 3557–3560.
164 P. Wang, A. Abrusci, H. M. P. Wong, M. Svensson, M. R. Andersson and N. C. Greenham, *Nano Lett.*, 2006, **6**, 1789–1793.
165 W. Lee, S. Shin, S. H. Han and B. W. Cho, *Appl. Phys. Lett.*, 2008, **92**, 193307.
166 L. Wang, Y. S. Liu, X. Jiang, D. H. Qin and Y. Cao, *J. Phys. Chem. C*, 2007, **111**, 9538–9542.
167 A. A. R. Watt, D. Blake, J. H. Warner, E. A. Thomsen, E. L. Tavenner, H. Rubinsztein-Dunlop and P. Meredith, *J. Phys. D: Appl. Phys.*, 2005, **38**, 2006–2012.
168 D. H. Cui, J. Xu, T. Zhu, G. Paradee, S. Ashok and M. Gerhold, *Appl. Phys. Lett.*, 2006, **88**, 183111.
169 N. Kudo, Y. Shimazaki, H. Ohkita, M. Ohoka and S. Ito, *Sol. Energy Mater. Sol. Cells*, 2007, **91**, 1243–1247.
170 J. S. Huang, C. Y. Hsiao, S. J. Syu, J. J. Chao and C. F. Lin, *Sol. Energy Mater. Sol. Cells*, 2009, **93**, 621–624.
171 C. Y. Liu, Z. C. Holman and U. R. Kortshagen, *Nano Lett.*, 2009, **9**, 449–452.
172 N. C. Greenham, X. G. Peng and A. P. Alivisatos, *Phys. Rev. B: Condens. Matter Mater. Phys.*, 1996, **54**, 17628–17637.
173 B. R. Saunders and M. L. Turner, *Adv. Colloid Interface Sci.*, 2008, **138**, 1–23.
174 P. A. van Hal, M. M. Wienk, J. M. Kroon, W. J. H. Verhees, L. H. Slooff, W. J. H. van Gennip, P. Jonkheijm and R. A. J. Janssen, *Adv. Mater.*, 2003, **15**, 118.
175 L. H. Slooff, M. M. Wienk and J. M. Kroon, *Thin Solid Films*, 2004, **451–452**, 634–638.
176 M. Okuya, K. Nakade and S. Kaneko, *Sol. Energy Mater. Sol. Cells*, 2002, **70**, 425–435.
177 K. M. Coakley and M. D. McGehee, *Appl. Phys. Lett.*, 2003, **83**, 3380–3382.
178 C. Goh, K. M. Coakley and M. D. McGehee, *Nano Lett.*, 2005, **5**, 1545–1549.
179 V. Gowrishankar, N. Miller, M. D. McGehee, M. J. Misner, D. Y. Ryu, T. P. Russell, E. Drockenmuller and C. J. Hawker, *Thin Solid Films*, 2006, **513**, 289–294.
180 G. K. Mor, O. K. Varghese, M. Paulose, K. Shankar and C. A. Grimes, *Sol. Energy Mater. Sol. Cells*, 2006, **90**, 2011–2075.
181 P. Ravirajan, A. M. Peiro, M. K. Nazeeruddin, M. Graetzel, D. D. C. Bradley, J. R. Durrant and J. Nelson, *J. Phys. Chem. B*, 2006, **110**, 7635–7639.

182 D. Cheyns, H. Gommans, M. Odijk, J. Poortmans and P. Heremans, *Sol. Energy Mater. Sol. Cells*, 2007, **91**, 399–404.
183 B. P. Rand, P. Peumans and S. R. Forrest, *J. Appl. Phys.*, 2004, **96**, 7519–7526.
184 J. Xue, S. Uchida, B. P. Rand and S. R. Forrest, *Appl. Phys. Lett.*, 2004, **84**, 3013–3015.
185 J. Xue, S. Uchida, B. P. Rand and S. R. Forrest, *Appl. Phys. Lett.*, 2004, **85**, 5757–5759.
186 A. Yakimov and S. R. Forrest, *Appl. Phys. Lett.*, 2002, **80**, 1667.
187 A. Colsmann, J. Junge, C. Kayser and U. Lemmer, *Appl. Phys. Lett.*, 2006, **89**, 203506.
188 G. Dennler, H. J. Prall, R. Koeppe, M. Egginger, R. Autengruber and N. S. Sariciftci, *Appl. Phys. Lett.*, 2006, **89**, 073502.
189 A. Hadipour, B. De Boer, J. Wildeman, F. B. Kooistra, J. C. Hummelen, M. G. R. Turbiez, M. M. Wienk, R. A. J. Janssen and P. W. M. Blom, *Adv. Funct. Mater.*, 2006, **16**, 1897–1903.
190 H. J. Prall, R. Koeppe, R. Autengruber, M. Egginger, D. Dennler, and N. S. Sariciftci, *From Evaporation to Solution Processed Organic Tandem Solar Cells, Gombert, Andreas*, Strasbourg, France,21-4-2006.
191 J. Gilot, M. M. Wienk and R. A. J. Janssen, *Appl. Phys. Lett.*, 2007, **90**, 143512–143513.
192 J. Y. Kim, K. Lee, N. E. Coates, D. Moses, T. Q. Nguyen, M. Dante and A. J. Heeger, *Science*, 2007, **317**, 222–225.
193 J. Y. Kim, S. H. Kim, H. H. Lee, K. Lee, W. L. Ma, X. Gong and A. J. Heeger, *Adv. Mater.*, 2006, **18**, 572–576.
194 V. Andersson, K. Tvingstedt and O. Inganas, *J. Appl. Phys.*, 2008, **103**, 094520.
195 S. B. Rim, S. Zhao, S. R. Scully, M. D. McGehee and P. Peumans, *Appl. Phys. Lett.*, 2007, **91**, 243501.
196 K. Tvingstedt, V. Andersson, F. Zhang and O. Inganas, *Appl. Phys. Lett.*, 2007, **91**, 123514–3.
197 Y. H. Zhou, F. L. Zhang, K. Tvingstedt, W. J. Tian and O. Inganas, *Appl. Phys. Lett.*, 2008, **93**, 033302.
198 J. W. Andreasen, M. Jørgensen and F. C. Krebs, *Macromolecules*, 2007, **40**, 7758–7762.
199 T. J. Gordon, J. F. Yu, C. Yang and S. Holdcroft, *Chem. Mater.*, 2007, **19**, 2155–2161.
200 F. C. Krebs, *Org. Electron.*, 2009, **10**, 761–768.
201 F. C. Krebs, *Sol. Energy Mater.*, 2009, **93**, 1636–1641.
202 T. Aernouts, P. Vanlaeke, W. Geens, J. Poortmans, P. Heremans, S. Borghs, R. Mertens, R. Andriessen and L. Leenders, *Thin Solid Films*, 2004, **451–452**, 22–25.
203 A. Gadisa, K. Tvingstedt, S. Admassie, L. Lindell, X. Crispin, M. R. Andersson, W. R. Salaneck and O. Inganas, *Synth. Met.*, 2006, **156**, 1102–1107.
204 J. Y. Lee, S. T. Connor, Y. Cui and P. Peumans, *Nano Lett.*, 2008, **8**, 689–692.
205 M. Strange, D. Plackett, M. Kaasgaard and F. C. Krebs, *Sol. Energy Mater. Sol. Cells*, 2008, **92**, 805–813.
206 K. Tvingstedt and O. Inganas, *Adv. Mater.*, 2007, **19**, 2893–2897.
207 B. Winther-Jensen and F. C. Krebs, *Sol. Energy Mater. Sol. Cells*, 2006, **90**, 123–132.
208 B. Zimmermann, M. Glatthaar, M. Niggemann, M. K. Riede, A. Hinsch and A. Gombert, *Sol. Energy Mater. Sol. Cells*, 2007, **91**, 374–378.
209 J. M. Gee, W. K Schubert, and P. A. Basore, *Photovoltaic Specialists Conference, Conference Record of the Twenty Third IEEE*, 1993, 265–270.
210 M. Niggemann, W. Graf and A. Gombert, *Adv. Mater.*, 2008, **20**, 4055.
211 M. Niggemann, B. Zimmermann, J. Haschke, M. Glatthaar and A. Gombert, *Thin Solid Films*, 2008, **516**, 7181–7187.
212 F. C. Krebs, S. A. Gevorgyan and J. Astrup, *J. Mater. Chem.*, 2009, **19**, 5442–5451.

Macromolecules
ARTICLE

Macromolecules **2010**, *43*, 1253–1260 **1253**
DOI: 10.1021/ma9024812

Photovoltaic Performance of Polymers Based on Dithienylthienopyrazines Bearing Thermocleavable Benzoate Esters

Martin Helgesen* and Frederik C. Krebs

Risø National Laboratory for Sustainable Energy, Technical University of Denmark, Frederiksborgvej 399, DK-4000 Roskilde, Denmark

Received November 10, 2009; Revised Manuscript Received December 17, 2009

ABSTRACT: Thermocleavable low-band-gap polymers based on dithienylthienopyrazines were prepared and copolymerized with different donor units like dialkoxybenzene, fluorene, thiophene, and cyclopentadithiophene (CPDT) using both Stille and Suzuki cross-coupling reactions. In the solid state the band gaps are in the range of 1.17−1.37 eV. The polymers were explored as donor materials in bulk heterojunction solar cells together with PCBM as the acceptor material where they were shown to exhibit a photoresponse in the full absorption range up to 900 nm and power conversion efficiencies of up to 1.21% under 1 sun irradiation. A red shift of the absorption edge on going from solution to the solid film was observed for all the polymers. Thermogravimetric analysis of the polymers in the temperature range from 25 to 500 °C showed a weight loss at just above 200 °C, corresponding to loss of the tertiary ester groups, and a second weight loss above 400 °C, corresponding to loss of CO_2 and decomposition. Upon thermocleavage the power conversion efficiency decreased for all the polymers while the polymer films became insoluble which was desired in the context of multilayer film processing. Thermocleavable low-band-gap materials can potentially offer better light harvesting, better operational stability, and a higher level of permissible processing conditions due to the insolubility of thermocleaved films in all solvents.

Introduction

Low-band-gap polymers for photovoltaics are designed to match the solar emission spectrum better, which has a maximum in photon flux near 700 nm and an appreciable tail stretching into the infrared region.[1,2] The extended absorption by low-band-gap polymers can potentially increase the power conversion efficiency by absorbing more photons. One approach to designing these materials is by use of alternating electron-rich (donor) and electron-poor (acceptor) units giving rise to a material with a low-energy absorption band that is generally ascribed to a charge transfer band. The absorption can be tuned by adjusting the donor−acceptor strengths, or HOMO−LUMO levels, respectively. For this purpose, polymers with alternating dithiophene and thienopyrazine units have been explored by several groups[3−9] who reports band gaps in the range 1.2−1.6 eV for this type of polymer. In our earlier work,[3] we explored the chemistry of the thienopyrazine-type acceptor moiety to characterize the influence of the substituents and extended π-system on the absorption spectrum. Here we found that adding phenyl groups to the dithienylthienopyrazine system caused a red shift of the lowest energy absorption band with up to 50 nm, presumably due to the more extended conjugation. In addition, polymers based on fused aromatic thienopyrazine units can reduce the band gap even further caused by a more planar backbone between repeating units.[3,5] Low-band-gap polymers based on dithienylthienopyrazine in blends with soluble methanofullerenes have shown high power conversion efficiencies (2.2%)[9] and an extended photoresponse up to 900 nm,[7] indicating that these materials are promising for photovoltaic applications.

There has been a recent interest in the operational stability of polymer solar cells and more importantly on the understanding of why devices and materials break down.[10] By using time-of-flight secondary ion mass spectrometry (TOF-SIMS)[11] and isotopic labeling ($^{18}O_2$ and $H_2{}^{18}O$), the main finding is that oxygen and water diffuse into the various layers of the solar cell, react with the bulk of the materials and the interfaces, and thus degrade the solar cell and device performance.[12−18] Moreover, photodegradation studies of both MDMO-PPV and P3HT under illumination in the presence and absence of oxygen[19−22] have shown that widely different mechanisms are in play. Illumination of MDMO-PPV in the absence of oxygen suggests that absorption of UV−vis light by MDMO-PPV can induce the homolytic scission of the O−CH_2 bond. The generated radicals may react with the vinylene groups, which lead to loss of conjugation, or undergo photo-Fries rearrangement. Furthermore, different photochemical mechanisms have been shown to be in play, the photochemical instability of P3HT has been suggested to be mainly due to the hexyl side chains, and it has been predicted that the photochemical stability of native polythiophene should be significantly longer. Taking the above-mentioned issues into consideration, one could explore the many possibilities in employing a conjugated material that is reached either through a precursor route or through a route where side chains are removed post film formation. This can be realized with the use of thermocleavable side chains. The side chains provide solubility in organic solvents and allow film formation via solution processing. Subsequently, they can be removed by heating in a postprocessing step forming a harder insoluble material where diffusion phenomena are slowed down and in addition the photochemical reactions associated with the side chains are avoided. Ideally, the thermocleavage of the side chains leads to a high-T_g material, characterized by its high glass transition temperature, which has been demonstrated to strongly suppress morphological changes in high-T_g PPV:PCBM active layers that leads to high thermal stability of the photovoltaic characteristics.[23] Because of a high

*Corresponding author. E-mail: manp@risoe.dtu.dk.

Published on Web 01/07/2010

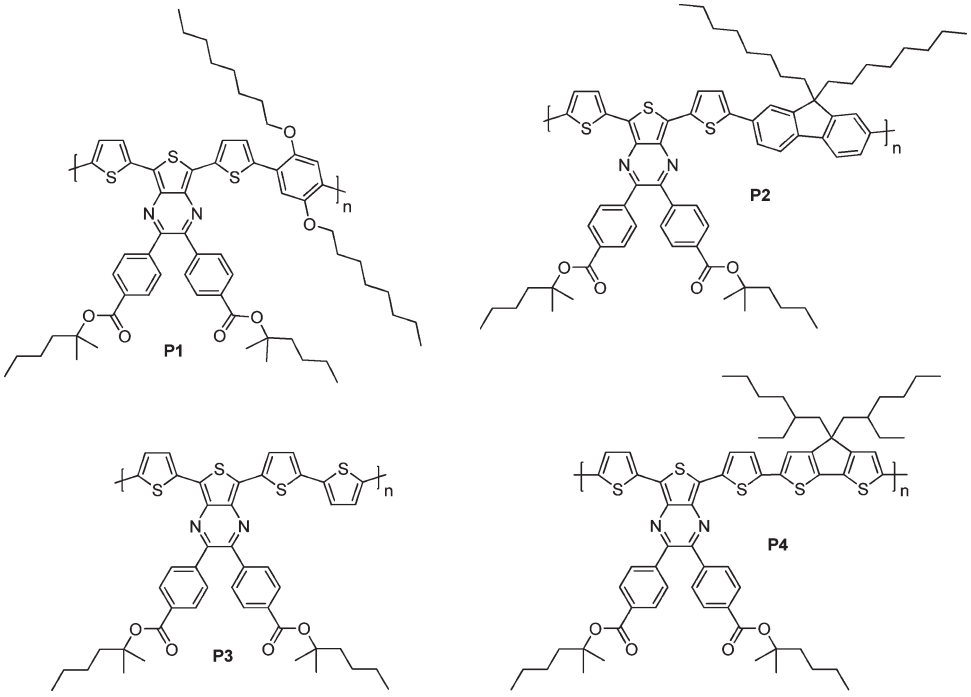

Figure 1. Low-band-gap polymers based on dithienylthienopyrazine alternating with different donor segments.

glass transition temperature, the active layer forms a more rigid and stable morphology which limit the possible migration and segregation of the PCBM molecules leading to a more stable active layer and consequently to a more stable photovoltaic behavior.[23] Alternative routes to polymer materials for polymer solar cells without side chains are precursor routes such as the dithiocarbamate route.[24−28] Lifetimes over 10 000 h have been reported for solar cells based on the thermocleavable polymer poly-3-(2-methylhexan-2-yl)oxycarbonylbithiophene (P3MHOCT) and C_{60} after thermal elimination of the solubilizing groups which transforms P3MHOCT into the more rigid and insoluble poly-3-carboxydithiophene (P3CT).[17,29]

In spite of the more complex synthetic chemistry and materials handling requirements for thermocleavable materials, the motivations for exploring those in the context of polymer solar cells include improvement of morphological, interface, and photochemical stability, improvement of the chromophore density in the device film, and significant advantages in terms of processing (solubility/insolubility switching). Thermocleavable materials remain inferior to the current state of the art in terms of power conversion efficiency while recent progress have shown power conversion efficiencies approaching 2%. It is likely that thermocleavable materials can be improved at least to the level of the current state-of-the-art pending the same investment in optimization as materials such as P3HT has received.

Herein we report our efforts in this direction through the synthesis of a series of alternating thermocleavable low-band-gap polymers and their photovoltaic performance in blends with [6,6]-phenyl C_{61} butyric acid methyl ester (PCBM). The materials are copolymers based on dithienylthienopyrazine, bearing thermocleavable benzoate esters on the pyrazine ring, alternating with different donor segments, i.e., dialkoxybenzene, fluorene, thiophene, and cyclopentadithiophene (CPDT) (Figure 1). The effects of the different donor segments on the photovoltaic performance of the polymers in blends with [60]PCBM with and without thermal treatment are presented. The alkyl benzoate ester groups make the polymer soluble in organic solvents and allow for film formation. Subsequently, they can be removed by heating in a postprocessing step forming the free acid and a volatile alkene.

Experimental Section

Synthetic procedures for synthesis of monomers and polymers according to Schemes 1 and 2 and their characterization data (including ^{1}H NMR and ^{13}C NMR) are described in detail in the Supporting Information together with general experimental details.

Polymer Solar Cell Fabrication and Analysis. Photovoltaic devices were made by spin-coating PEDOT:PSS (Aldrich, 1.3 wt % aqueous solution) onto precleaned, patterned indium tin oxide (ITO) substrates (9−15 Ω per square) (LumTec) followed by annealing at 140 °C for 5 min. The active layer was deposited, in a glovebox, by spin-coating a blend of the polymer and [60]PCBM dissolved in *o*-dichlorobenzene (40 mg/mL). After a thermal treatment (see Table 2) the counter electrode of aluminum was deposited by vacuum evaporation at $(2-3) \times 10^{-6}$ mbar. The active area of the cells was 0.5 cm^2. $I-V$ characteristics were measured under AM1.5G corresponding to 74.3 mW/cm^2 white light from a multiwavelength high-power LED array using a Keithley 2400 source meter. IPCE spectra were recorded on the same solar test platform with the LED-based illumination system.

Results and Discussion

Synthesis. The synthetic steps involved in the preparation of the monomers **2a**, **2b**, **5**, **7**, and **10** are outlined in Scheme 1. Monomer **1** was functionalized by NBS bromination and by deprotonation using lithium diisopropylamine (LDA) followed by treatment with trimethyltin chloride. This afforded **2a**[30] and **2b**[31] to be used in Suzuki- and Stille-type copolymerizations. According to a literature procedure,[32] monomer **5** can be synthesized in good yield starting with a standard alkylation of hydroquinone (**3**) followed by bromination of **4** with NBS. The diboronic acid pinacol ester **7** is prepared by lithiation of readily available 2,7-dibromo-9,9-dioctylfluorene (**6**) followed by addition of 2-isopropoxy-4,4,5,5-tetramethyl-1,3,2-dioxaborolane.[33] The synthetic route to **10**[34] initiates with a deprotonation of 4*H*-cyclopenta-[2,1-*b*:3,4-*b*′]-dithiophene (**8**) and a subsequent alkylation which affords **9** in good yield. Deprotonation of **9** using

Scheme 1. Synthetic Steps Involved in the Preparation of the Monomers

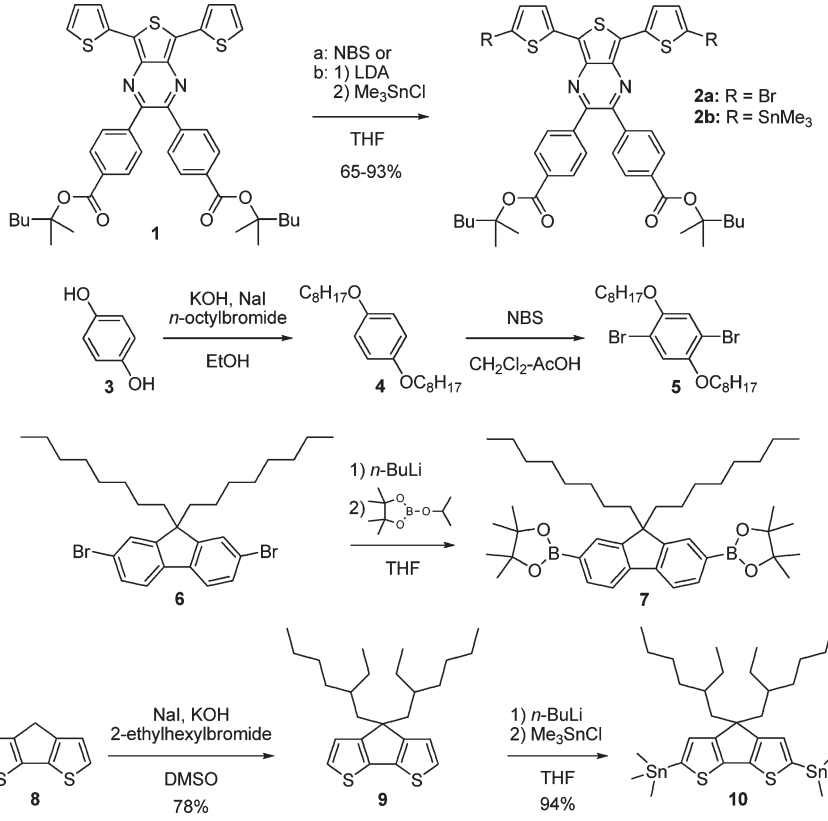

Scheme 2. Copolymerizations Leading to the Polymers P1−P4[a]

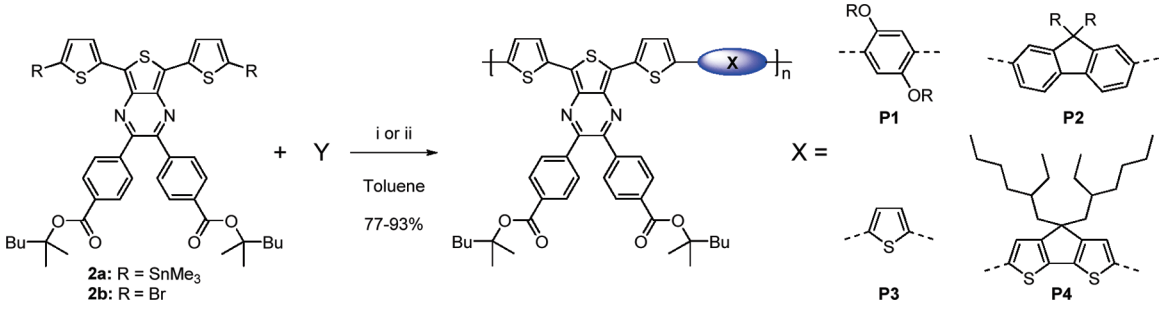

[a] Y = **5**, **7**, **10**, and 2,5-bis(trimethylstannyl)thiophene. (i) Stille coupling using Pd_2dba_3 and tri-*o*-tolylphosphine. (ii) Suzuki coupling using Pd_2dba_3, tri-*o*-tolylphosphine and Cs_2CO_3.

n-butyllithium followed by treatment with trimethyltin chloride affords monomer **10**.

Copolymerizations leading to the final polymers **P1**−**P4** are presented in Scheme 2. Copolymerization of **2b** via Stille coupling, using the catalyst system Pd_2dba_3/tri-*o*-tolylphosphine, with **5** gave polymer **P1** in 77% yield as a dark brown solid (M_w = 7 kg/mol, PDI = 1.9). Coupling of **2a** with **7** was performed with a Suzuki-type copolymerization reaction using Pd_2dba_3/tri-*o*-tolylphosphine as a catalyst and caesium carbonate as a base. The polymer **P2** was afforded in 90% yield as a green solid with a molecular weight (M_w) of 42.3 kg/mol and a polydispersity (PDI) of 3. Using the same conditions as for the preparation of **P1**, copolymerization of **2a** via Stille coupling with 2,5-bis-(trimethylstannyl)thiophene and the cyclopentadithiophene **10** gave polymer **P3** and **P4** as dark green solids in 92−93% yield. All the polymers were isolated in good yields and are soluble in organic solvents such as chloroform and toluene at room temperature.

Thermal Behavior. The thermal behavior of the thermocleavable polymers was investigated by thermogravimetric analysis (TGA). The sample holders were carefully weighed and the samples introduced. TGA was then carried out using heating rate of 10 °C min^{-1}. TGA of **P1**−**P4** are shown in Figure 2 and indicates that the tertiary ester starts to eliminate around 200 °C, in agreement with earlier results.[30] The second loss peak at ~400 °C that corresponds to loss of CO_2[30] (not prior to decomposition) can only be observed for **P3** because a greater weight loss for **P1**, **P2**, and **P4** is showing in the same temperature range. The observed value for this loss peak is ~20%, which corresponds to loss of the alkyl chains on the donor units: dialkoxybenzene, fluorene, and CPDT. The same precursor film prepared by standard solution processing of **P1**−**P4** can give access to two chemically different thin films, as shown in Figure 3.

Optical Properties. The absorption spectra for the polymers in chloroform solution are shown in Figure 4a. The copolymers **P1**−**P4** based on dithienylthienopyrazine does

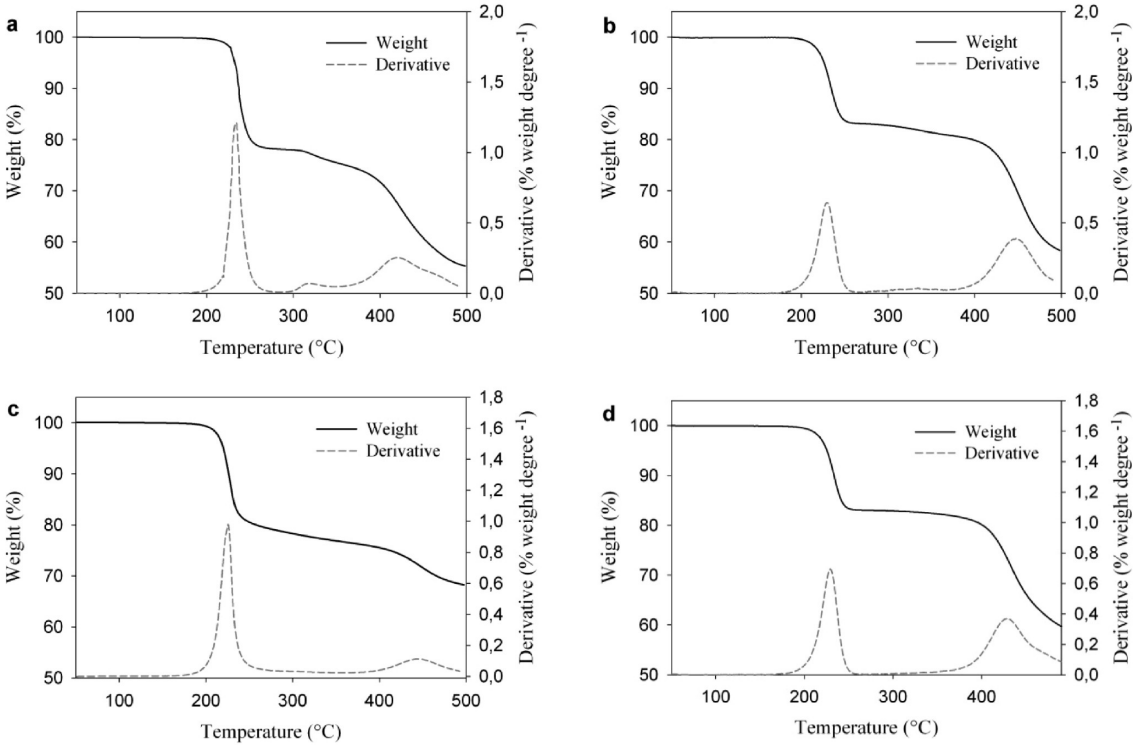

Figure 2. (a) TGA of **P1**, (b) TGA of **P2**, (c) TGA of **P3**, and (d) TGA of **P4** in the temperature range 50−500 °C. The data were recorded at 10 °C min^{-1} under an argon atmosphere. A derivative weight loss curve has been included to tell the point at which weight loss is most apparent.

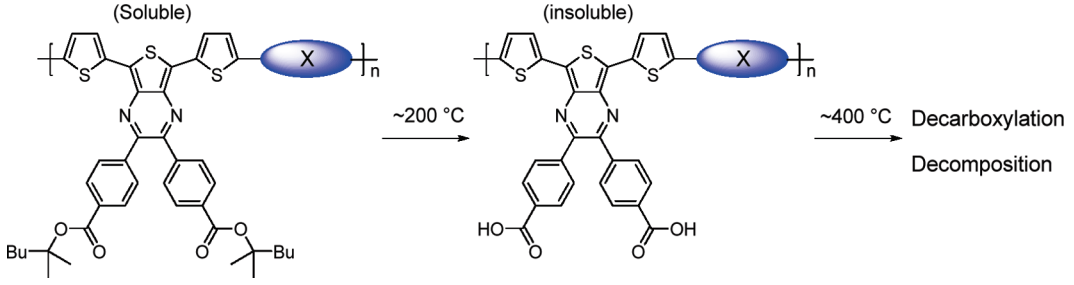

Figure 3. Possible chemical transitions of **P1**−**P4**.

indeed show a considerable spectral coverage of the solar spectrum which is varied with the different donor units. The optical band gaps, defined by the onset of absorption, are ranging from 1.22 to 1.50 eV (Table 1), which is much smaller than that of poly(3-hexylthiophene) (P3HT) homopolymer ($E_g \sim 1.9-2.1$ eV). This supports the idea that the internal charge-transfer interaction between donor and acceptor moieties in donor−acceptor copolymers is an efficient method to lower the band gap of conjugated polymers. Partial aggregation of **P1** in solution gives it the lowest optical band gap with an onset at 1015 nm. **P2** has a somewhat higher band gap of 1.5 eV because of the decreased donor strength of the fluorene unit (high degree of aromaticity) which reduce conjugation in the polymer backbone.

Three alternating thiophene units provide **P3** with a band gap of 1.3 eV in solution. Further extending the thiophene content by incorporating CPDT lowers the band gap to 1.27 eV (**P4**). Despite the improved donor character of the CPDT unit, caused by its planarity and electron-donating alkyl chains, **P3** and **P4** have rather similar band gaps though the absorption maxima (λ_{max}) of **P3** is blue-shifted compared to **P4**. The thin film absorption spectra for polymers **P1**−**P4** are shown in Figure 4b. The optical band gaps are ranging from 1.17 to 1.37 eV where only **P2** shows a significant decrease compared to in solution (Table 1). The polymers **P1** and **P2** have absorption maxima in the range from 665 to 745 nm in chloroform solution, and these are red-shifted further to 710−845 nm when in a solid film (Table 1), indicating significant interchain association in the solid state. In addition, λ_{max} for **P2** is red-shifted with 50−95 nm compared to corresponding polymers without the thermocleavable side chains.[4,9] **P3** reveals a shoulder around 800 nm in solution, and the same, but weaker, vibronic fine structure remains in the solid state. **P4** also reveals a shoulder in solution around 830 nm, but in the solid state the absorption band has broadened, caused by intermolecular interactions, and the vibronic fine structure has disappeared. Upon annealing the films only **P3** and **P4** shows a significant change in the absorption spectra (Figure 5). Upon thermocleavage of the films by heating them at 250 °C for 1 min a color change from olive green to a more brownish color is observed. The associated changes in the absorption spectrum are a less intense low-energy absorption band and a smaller band gap which is reduced to 1.23 eV for **P3** and 1.18 eV for **P4**. There may be several explanations for the lower absorption intensity. First, the associated change in film thickness,

and secondly, the dielectric constant may lead to changes in the reflection phenomena that also contribute to the intensities in the observed absorption spectrum for a solid film in transmission geometry. Thirdly, the intensity of absorption quite often decreases as the band gap is lowered. After the short thermal treatment the films maintained the optical quality and were insoluble in organic solvents.

Photovoltaic Performance. Bulk heterojunction solar cells with an active area of 0.5 cm^2 were prepared on an indium tin oxide (ITO) covered glass substrate, using conventional device architecture. A thin layer of poly(3,4-ethylenedioxythiophene)−poly(styrenesulfonate) (PEDOT−PSS) was spin-coated on top of the ITO coating followed by spin-coating of the active layer. The active layer contained a blend of the respective polymer and [60]PCBM.

After spin-coating of the active layer the devices were either processed directly into a solar cell by evaporation of aluminum as back electrode or subjected to a thermal treatment at the temperature of thermocleavage immediately before evaporation of the back electrode. The obtained current−voltage curves are presented in Figure 6 which shows the current−voltage characteristics of the polymer:PCBM solar cells measured under 74.3 mW/cm^2 white light. The unannealed devices based on **P1**, with the lowest band gap (1.15 eV), and PCBM had low open-circuit voltages (V_{oc}) of 0.36 V, moderate fill factors (FF) of 0.40, and current densities (J_{sc}) of 1.82 mA/cm^2. This resulted in power conversion efficiencies of up to 0.35% (Table 2). Devices based on the fluorine-coupled polymer **P2** and PCBM showed a somewhat higher V_{oc} up to 0.65 V (Figure 6a) as expected from earlier reports[9] with a similar system. **P2** provides a descent FF of 0.44, but the low current density (1.41 mA/cm^2) limits the performance to 0.54%. Changing the polymer backbone to be a complete thiophene segment raises the J_{sc} up to 2.22 mA/cm^2 for **P3**:PCBM devices. The V_{oc} was 0.5 V, and together with a FF of 0.38 the devices had a power conversion efficiency up to 0.57%. Solar cells based on **P4**:PCBM exhibits the best performance with the highest current density of 3.20 mA/cm^2 and a good fill factor of 0.51. Together with an open-circuit voltage of 0.55 V, the power conversion efficiency sets to 1.21%. The somewhat higher J_{sc} obtained with **P4** is also reflected in the incident photon to current efficiency (IPCE) which reaches an average IPCE of 17% with a photoresponse up to 900 nm (Figure 7a). In contrast, **P1**−**P3** have an average IPCE in the range 7−8% but also extends up to 900 nm, except **P2** in agreement with the absorption spectra (Figure 4b). Despite the extended photoresponse of **P1**−**P4**, IPCE is inferior compared to the state of the art system P3HT:PCBM (Table 2) which may be explained by limited exciton dissociation at the

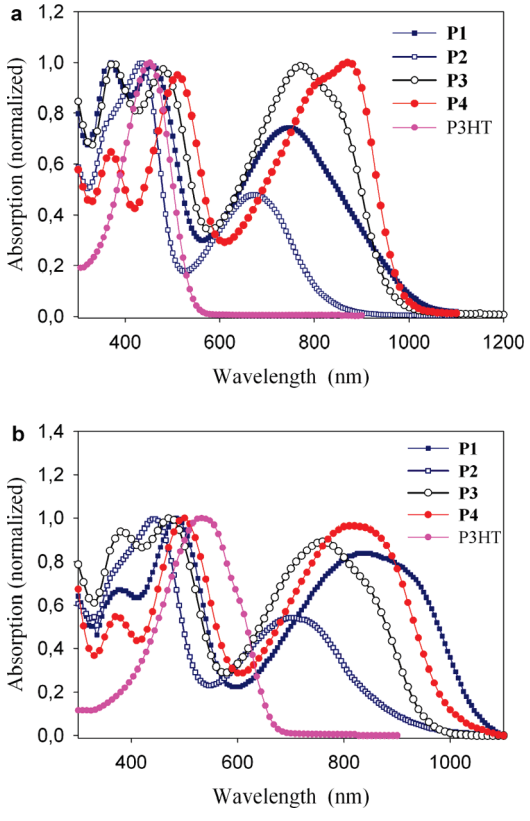

Figure 4. (a) UV−vis absorption spectra of the polymers **P1**−**P4** in chloroform solution and (b) in thin film. P3HT in chloroform solution and in thin film is also shown for comparison.

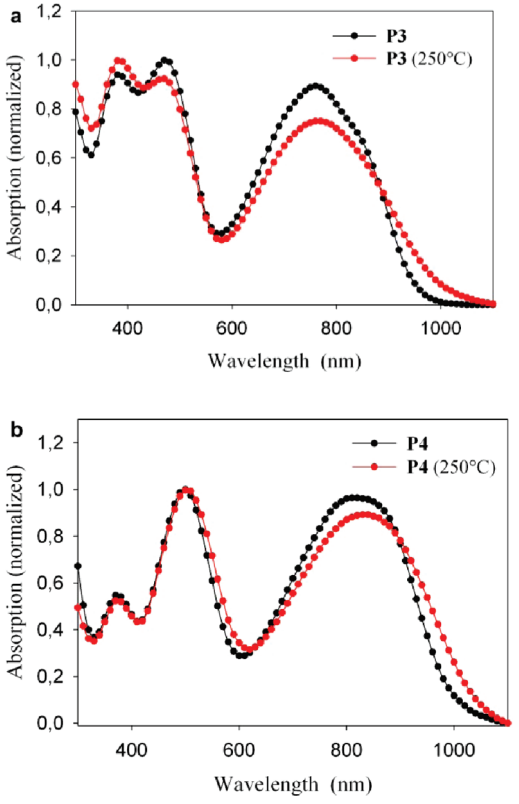

Figure 5. (a) UV−vis absorption spectra of **P3** and (b) **P4** in thin film before and after annealing for 1 min.

Table 1. GPC and Spectroscopic Data for Polymers P1−P4

			solution				film		
polymer	M_w (g/mol)	PDI	$\alpha(\lambda_{max})$ (L/(g cm))	λ_{max} (nm)	λ_{onset} (nm)	E_g (eV)	λ_{max} (nm)	λ_{onset} (nm)	E_g (eV)
P1	7 000	1.9	16	745	1015	1.22	845	1057	1.17
P2	42 300	3.0	18	665	824	1.50	710	906	1.37
P3	39 400	1.9	23	770	955	1.30	760	955	1.30
P4	363 000	4.8	29	868	980	1.27	825	1002	1.24

polymer−PCBM interface. However for **P4**, the generated charge carriers seem to be extracted relatively efficiently as is indicated by a rather good fill factor of 0.51. $J-V$ curves of the polymer:PCBM solar cells after a thermal treatment are shown in Figure 6b, and a general observation is that the performance drops after the thermocleavage. Table 2 shows a large drop in the current density for all polymers after thermocleavage together with minor drops in the V_{oc} and FF. The drop in performance is also reflected in the IPCE which is lower at all wavelengths compared to the unannealed devices (Figure 7b).

Morphology. The **P3**:PCBM and **P4**:PCBM device films annealed at different temperatures, as measured by atomic force microscopy (AFM), are shown in Figure 8. AFM reveals changes in the surface topography of the films and generally gives a good first insight into morphology of the active layer.[35] All films shows a significant roughness with a peak-to-valley difference around 15−20 nm. Comparing the films before and after thermocleavage (~200 °C) reveals that the domain sizes increases to features with dimensions larger than 100 nm which indicate extensive phase segregation of the polymer and PCBM upon annealing at high temperatures. Moreover, Figure 8c,g indicates that phase segregation commence prior to thermal cleavage of the tertiary esters. The reduced current densities of the polymer:PCBM devices after thermocleavage might be a direct consequence of the changed morphology which is possibly limiting charge carrier generation (reduced number of exitons reach the interface) and transport to the electrodes (insufficient percolating pathways). The drop in the current density after thermocleavage to the free carboxylic acid has been observed before for polymers where the thermocleavable ester resides on a thiophene unit. These polymers can undergo further transformation into the native system by decarboxylation which leads to a significant improvement in performance due to an increase in mainly the current density.[36,37] For the materials reported here heating to 300 °C resulted in significantly poorer performance. As measured by AFM, one possible explanation is that the morphology changes undesirably for this class of materials at the high temperatures, and further work on understanding the complex interplay between the

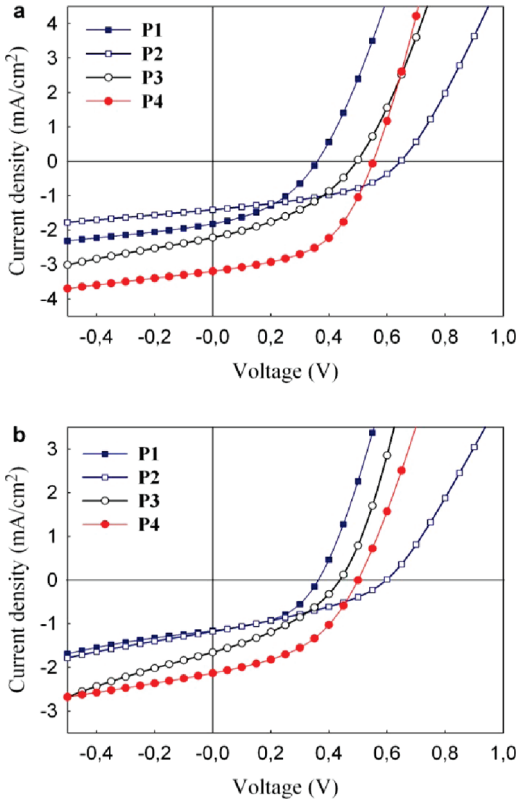

Figure 6. (a) $J-V$ characteristics of the **P1**:PCBM, **P2**:PCBM, **P3**:PCBM, and **P4**:PCBM solar cells measured under 74.3 mW/cm^2 white light before and (b) after a thermal treatment (see Table 2).

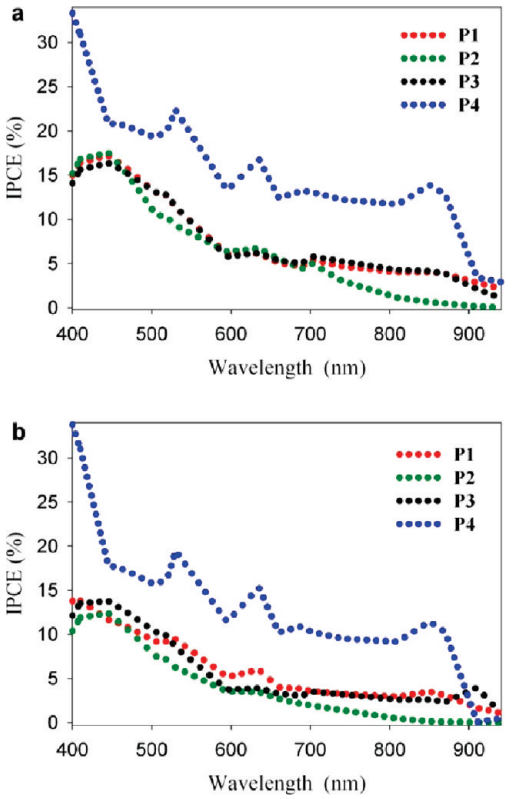

Figure 7. (a) IPCE of polymer:PCBM solar cells before and (b) after a thermal treatment.

Table 2. Photovoltaic Performance of Devices Based on Blends of Polymer and PCBM

polymer	polymer:PCBM (w/w ratio)	thermal treatment (°C)	V_{oc} (V)	J_{sc} (mA/cm^2)	FF	η (%)
P1	1:2		0.36	1.82	0.40	0.35
P1	1:2	250[a]	0.36	1.16	0.47	0.27
P2	1:3		0.65	1.41	0.44	0.54
P2	1:3	250[a]	0.60	1.18	0.35	0.33
P3	1:4		0.50	2.22	0.38	0.57
P3	1:4	230[a]	0.44	1.66	0.36	0.35
P4	1:3		0.55	3.20	0.51	1.21
P4	1:3	225[a]	0.50	2.13	0.45	0.64
P3HT	1:1	150[b]	0.62	7.69	0.48	2.3[c]

[a] Annealed for 30 s. [b] Annealed for 5 min. [c] Typical PCE reached at Risø DTU with commercially available regioregular P3HT in the same device geometry.

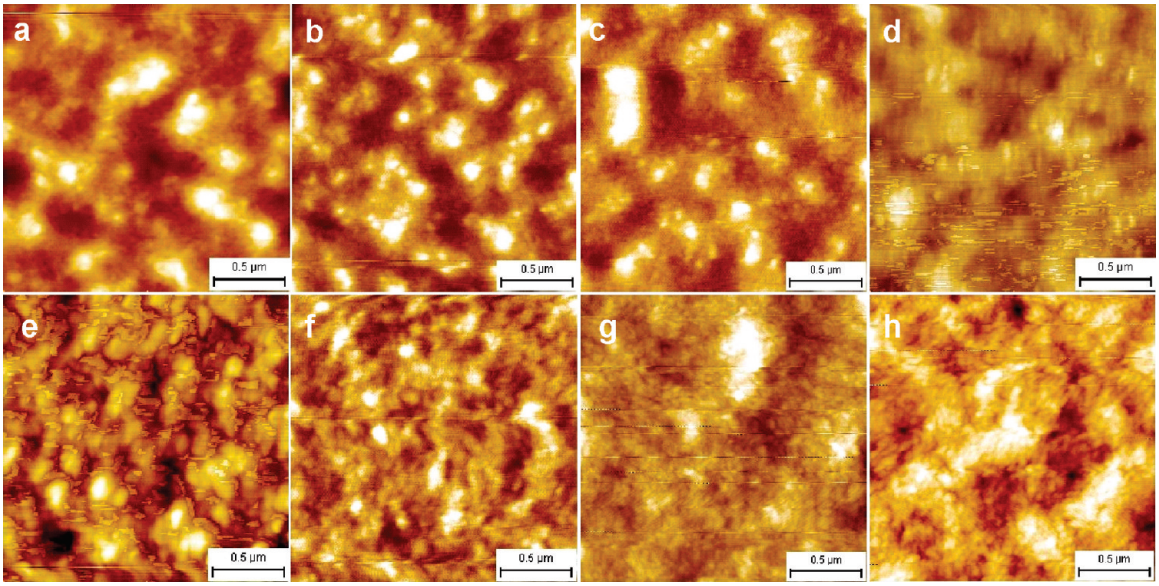

Figure 8. AFM topography images (2 μm × 2 μm) of solar cells based on blends of PCBM and (a) **P3** unannealed, height scale is 20 nm; (b) **P3** annealed at 150 °C, height scale is 15 nm; (c) **P3** annealed at 180 °C, height scale is 15 nm; (d) **P3** annealed at 230 °C, height scale is 15 nm; (e) **P4** unannealed, height scale is 15 nm; (f) **P4** annealed at 150 °C, height scale is 15 nm; (g) **P4** annealed at 180 °C, height scale is 15 nm; (h) **P4** annealed at 225 °C, height scale is 15 nm.

changes in morphology as a result of thermocleavage is warranted. This points to the importance of the difference between the temperature where changes in morphology take place and the temperature at which thermocleavage takes place. It is likely that the few examples where similar or better performance was obtained after thermocleavage of the film represent cases where the morphology does not change before thermocleavage.

Conclusion

A series of new thermocleavable low-band-gap polymers based on dithienylthienopyrazine, bearing thermocleavable benzoate esters on the pyrazine ring, alternating with different donor segments (including dialkoxybenzene, fluorene, thiophene, and CPDT) have been synthesized. The solubilizing benzoate ester groups are thermocleavable around 200 °C where a volatile alkene is eliminated, leaving the polymer component more rigid. Furthermore, it was found that no decarboxylation takes place prior to decomposition at ~400 °C where a greater weight loss for **P1**, **P2**, and **P4** is observed in the same temperature range which corresponds to loss of the alkyl chains on the donor units: dialkoxybenzene, fluorene, and CPDT. The four polymers optical properties and photovoltaic performance in blends with PCBM have been investigated. In chloroform solution the polymers had optical band gaps ranging from 1.22 to 1.50 eV. The optical band gaps are lowered to 1.17−1.37 eV in thin film, showing a considerable spectral coverage of the solar emission spectrum. Furthermore, polymers **P3** and **P4** showed a less intense low-energy absorption band and a smaller band gap after annealing the film for 1 min. The best performing polymer in a bulk heterojunction solar cell was **P4** with J_{sc} = 3.20 mA/cm^2, V_{oc} = 0.55 V, FF = 0.51, and η = 1.21%. Devices generally performed worse after thermocleavage due to a drop in mainly the current density giving power conversion efficiencies up to 0.64% for **P4**:PCBM solar cells. The drop in performance after thermocleavage can be linked to extensive phase segregation of the polymer and PCBM upon annealing as measured by AFM. We finally conclude that the interplay between temperature, morphology, and film chemistry needs to be understood before efficient thermocleavable materials can be optimally designed.

Acknowledgment. This work was supported by the Danish Strategic Research Council (DSF 2104-05-0052 and 2104-07-0022).

Supporting Information Available: General procedures and characterization data including NMR spectra; experimental procedures for the synthesis of the monomers and polymers according to Schemes 1 and 2. This material is available free of charge via the Internet at http://pubs.acs.org.

References and Notes

(1) Bundgaard, E.; Krebs, F. C. *Sol. Energy Mater. Sol. Cells* **2007**, *91*, 954–985.
(2) Kroon, R.; Lenes, M.; Hummelen, J. C.; Blom, P. W. M.; de Boer, B. *Polym. Rev.* **2008**, *48*, 531–582.
(3) Petersen, M. H.; Hagemann, O.; Nielsen, K. T.; Jørgensen, M.; Krebs, F. C. *Sol. Energy Mater. Sol. Cells* **2007**, *91*, 996–1009.
(4) Zhang, F. L.; Perzon, E.; Wang, X. J.; Mammo, W.; Andersson, M. R.; Inganas, O. *Adv. Funct. Mater.* **2005**, *15*, 745–750.
(5) Mondal, R.; Miyaki, N.; Becerril, H. A.; Norton, J. E.; Parmer, J.; Mayer, A. C.; Tang, M. L.; Brédas, J.-L.; McGehee, M. D.; Bao, Z. *Chem. Mater.* **2009**, *21*, 3618–3628.
(6) Campos, L. M.; Tontcheva, A.; Gunes, S.; Sonmez, G.; Neugebauer, H.; Sariciftci, N. S.; Wudl, F. *Chem. Mater.* **2005**, *17*, 4031–4033.
(7) Zoombelt, A. P.; Gilot, J.; Wienk, M. M.; Janssen, R. A. J. *Chem. Mater.* **2009**, *21*, 1663–1669.
(8) Wienk, M. M.; Turbiez, M. G. R.; Struijk, M. P.; Fonrodona, M.; Janssen, R. A. J. *Appl. Phys. Lett.* **2006**, *88*, 153511.
(9) Zhang, F. L.; Mammo, W.; Andersson, L. M.; Admassie, S.; Andersson, M. R.; Inganas, L.; Admassie, S.; Andersson, M. R.; Ingands, O. *Adv. Mater.* **2006**, *18*, 2169–2173.
(10) Jørgensen, M.; Norrman, K.; Krebs, F. C. *Sol. Energy Mater. Sol. Cells* **2008**, *92*, 686–714.
(11) Norrman, K.; Krebs, F. C. *Surf. Interface Anal.* **2004**, *36*, 1542–1549.
(12) Norrman, K.; Krebs, F. C. *Sol. Energy Mater. Sol. Cells* **2006**, *90*, 213–227.
(13) Lira-Cantu, M.; Norrman, K.; Andreasen, J. W.; Krebs, F. C. *Chem. Mater.* **2006**, *18*, 5684–5690.
(14) Norrman, K.; Larsen, N. B.; Krebs, F. C. *Sol. Energy Mater. Sol. Cells* **2006**, *90*, 2793–2814.
(15) Alstrup, J.; Norrman, K.; Jørgensen, M.; Krebs, F. C. *Sol. Energy Mater. Sol. Cells* **2006**, *90*, 2777–2792.
(16) Norrman, K.; Alstrup, J.; Krebs, F. C. *Surf. Interface Anal.* **2006**, *38*, 1302–1310.

(17) Krebs, F. C.; Norrman, K. *Prog. Photovoltaics* **2007**, *15*, 697–712.
(18) Norrman, K.; Gevorgyan, S. A.; Krebs, F. C. *ACS Appl. Mater. Interfaces* **2009**, *1*, 102–112.
(19) Chambon, S.; Rivaton, A.; Gardette, J. L.; Firon, M. *Sol. Energy Mater. Sol. Cells* **2008**, *92*, 785–792.
(20) Chambon, S.; Manceau, M.; Firon, M.; Cros, S.; Rivaton, A.; Gardette, J.-L. *Polymer* **2008**, *49*, 3288–3294.
(21) Manceau, M.; Rivaton, A.; Gardette, J.-L. *Macromol. Rapid Commun.* **2008**, *29*, 1823–1827.
(22) Manceau, M.; Rivaton, A.; Gardette, J.-L.; Guillerez, S.; Lemaître, N. *Polym. Degrad. Stab.* **2009**, *94*, 898–907.
(23) Bertho, S.; Janssen, G.; Cleij, T. J.; Conings, B.; Moons, W.; Gadisa, A.; D'Haen, J.; Goovaerts, E.; Lutsen, L.; Manca, J.; Vanderzande, D. *Sol. Energy Mater. Sol. Cells* **2008**, *92*, 753–760.
(24) Henckens, A.; Colladet, K.; Fourier, S.; Cleij, T. J.; Lutsen, L.; Gelan, J.; Vanderzande, D. *Macromolecules* **2005**, *38*, 19–26.
(25) Nguyen, L. H.; Günes, S.; Neugebauer, H.; Sariciftci, N. S.; Banishoeib, F.; Henckens, A.; Cleij, T. J.; Lutsen, L.; Vanderzande, D. *Sol. Energy Mater. Sol. Cells* **2006**, *90*, 2815–2828.
(26) Banishoeib, F.; Adriaensens, P.; Berson, S.; Guillerez, S.; Douheret, O.; Manca, J.; Fourier, S.; Cleij, T. J.; Lutsen, L.; Vanderzande, D. *Sol. Energy Mater. Sol. Cells* **2007**, *91*, 1026–1034.
(27) Banishoeib, F.; Henckens, A.; Fourier, S.; Vanhooyland, G.; Breselge, M.; Manca, J.; Cleij, T. J.; Lutsen, L.; Vanderzande, D.; Nguyen, L. H.; Neugebauer, H.; Sariciftci, N. S. *Thin Solid Films* **2008**, *516*, 3978–3988.
(28) Girotto, C.; Cheyns, D.; Aernouts, T.; Banishoeib, F.; Lutsen, L.; Cleij, T. J.; Vanderzande, D.; Genoe, J.; Poortmans, J.; Heremans, P. *Org. Electron.* **2008**, *9*, 740–746.
(29) Krebs, F. C.; Spanggaard, H. *Chem. Mater.* **2005**, *17*, 5235–5237.
(30) Petersen, M. H.; Gevorgyan, S. A.; Krebs, F. C. *Macromolecules* **2008**, *41*, 8986–8994.
(31) Hagemann, O.; Bjerring, M.; Nielsen, N. C.; Krebs, F. C. *Sol. Energy Mater. Sol. Cells* **2008**, *92*, 1327–1335.
(32) Aubert, P. H.; Knipper, M.; Groenendaal, L.; Lutsen, L.; Manca, J.; Vanderzande, D. *Macromolecules* **2004**, *37*, 4087–4098.
(33) Ranger, M.; Rondeau, D.; Leclerc, M. *Macromolecules* **1997**, *30*, 7686–7691.
(34) Zhu, Z.; Waller, D.; Gaudiana, R.; Morana, M.; Muhlbacher, D.; Scharber, M.; Brabec, C. *Macromolecules* **2007**, *40*, 1981–1986.
(35) Yang, X.; Loos, J. *Macromolecules* **2007**, *40*, 1353–1362.
(36) Gevorgyan, S. A.; Krebs, F. C. *Chem. Mater.* **2008**, *20*, 4386–4390.
(37) Helgesen, M.; Gevorgyan, S. A.; Krebs, F. C.; Janssen, R. A. J. *Chem. Mater.* **2009**, *21*, 4669–4675.

Risø DTU is the National Laboratory for Sustainable Energy. Our research focuses on development of energy technologies and systems with minimal effect on climate, and contributes to innovation, education and policy. Risø has large experimental facilities and interdisciplinary research environments, and includes the national centre for nuclear technologies.

Risø DTU
National Laboratory for Sustainable Energy
Technical University of Denmark

Frederiksborgvej 399
PO Box 49
DK-4000 Roskilde
Denmark
Phone +45 4677 4677
Fax +45 4677 5688

www.risoe.dtu.dk